CHARACTERIZATION OF OSTEOARTHRITIS METABOLISM:

A MASS SPECTROMETRY BASED-APPROACH

by

Hope Diane Aloha Welhaven

A dissertation submitted in partial fulfillment
of the requirements for the degree

of

Doctor of Philosophy

in

Biochemistry

MONTANA STATE UNIVERSITY
Bozeman, Montana

May 2024

DEDICATION

This dissertation is dedicated to all women. To those whose intelligence, capabilities, strength, and pure passion has been overlooked, undervalued, and underappreciated. Remember, you already have what it takes inside you. Without this reminder and the unwavering support of the women around me, I would not be where I am today. We are more powerful when we empower each other.

ACKNOWLEDGEMENTS

From the bottom of my heart, I want to thank my two advisors, Drs. Ron June and Brian Bothner, for taking me on as a student four years ago. Since, they have been much more than advisors but mentors, role models, and good friends. Without their unwavering support, I would not be half the young female investigator I am today. The lessons they have taught me about research are invaluable, but those about life and being a good human on this earth will stay with me forever. To the many mentors, professors, teachers, friends, and both blood and chosen family that have provided endless words of support, advice, a shoulder to cry on, and both an open ear and mind. You all have paved the way for me, and I aim to do the same for others.

TABLE OF CONTENTS

TABLE OF CONTENTS CONTINUED

TABLE OF CONTENTS CONTINUED

TABLE OF CONTENTS CONTINUED

TABLE OF CONTENTS CONTINUED

TABLE OF CONTENTS CONTINUED

LIST OF TABLES

LIST OF FIGURES

Figure Page

LIST OF FIGURES CONTINUED

Figure Page

LIST OF FIGURES CONTINUED

Figure Page

ABSTRACT

Osteoarthritis (OA) effects 7% of the global population, equating to more than 500 million people worldwide, and is the leading cause of disability. Its multifaceted etiology includes risk factors ranging from genetics, to aging, obesity, sex, race, and joint injury. OA manifests differently across the patient population where symptom severity, rate of progression, response to treatment, pain perception, as well as others vary person to person posing significant challenges for effective management and prevention. At the cellular level, imbalanced matrix catabolism and anabolism contribute to the breakdown of cartilage, underlying bone, and other tissues affected by OA. Leveraging mass spectrometry-based techniques, particularly metabolomics, offers a promising avenue to dissect OA metabolism across musculoskeletal tissues, while considering individual patient-specific risk factors. Therefore, the goals of this research were to: (1) comprehensively characterize OA phenotypes and endotypes and (2) explore OA pathogenesis within the context of disease-associated risk factors.

The first area of research focuses on profiling OA phenotypes and endotypes across disease development. These results provide clear evidence of OA-induced metabolic perturbations in OA cartilage and bone and elucidate mechanisms that shift as disease progresses. Several metabolites and pathways associated with lipid, amino acid, matrix, and vitamin metabolism were differentially regulated between healthy and OA tissues and within OA endotypes.

The second area of research focuses on the impact of OA risk factors – sex, injury, obesity, loading – on the metabolism of circulatory fluids (i.e., serum, synovial fluid) and chondrocytes. Identification of metabolic indicators of disease, such as cervonyl carnitine, and metabolic pathways associated with these risk factors holds potential for improving screening, monitoring disease progression, and guiding preventative strategies.

Overall, this work contributes to our current understanding of OA, its diverse metabolic landscape, risk factors and their interactions. Moreover, it lays the groundwork for personalized medicine by providing detailed insights into individualized phenotypic profiles, thereby advancing the prospect of tailored treatment strategies for OA individuals.

INTRODUCTION

Osteoarthritis Background and Diagnosis

Arthritis is the leading cause of disability worldwide with osteoarthritis (OA) being the most common form. The number of reported cases of OA since 1990 has increased by 113.25% equating to 527.81 million OA cases reported in 2019[1]. Moreover, 32.5 million US adults suffer from OA, equating to the population of Montana multiplied by 32. By 2040, this number is expected to reach approximately 46 million because of our aging population[2, 3]. The staggering number of cases comes with a significant economic burden costing the US more than $185 million annually[4, 5]. The physical burdens of OA surpass economic burdens and are ultimately carried by individuals with this disease. OA patients commonly experience increased pain, disability, decreased mobility, fatigue, and depressive moods[6]. This often results in OA individuals missing at least two days of work annually. Additionally, since individuals have varying pain tolerances, the physical burden of OA is likely to be underreported and misrepresented.

At the joint level, OA is associated with cartilage breakdown[7]. Breakdown of this near-frictionless tissue, which ultimately functions to provide smooth articulation and joint movement, is negatively influenced and physically manifests as painful bone-on-bone contact, joint stiffness, and limited mobility. OA can occur in many joints within the body, but most commonly affects hips, knees, hands, and feet[8]. Beyond cartilage breakdown, hallmarks of OA include osteophyte formation, bone sclerosis, and synovitis[9]. Thus, OA is measured and reported in two ways: symptomatically and radiographically[10]. Characteristics of symptomatic OA reported by OA individuals include joint pain, stiffness, or aching as well as limited mobility. Radiographic OA is

commonly associated with joint space narrowing, osteophyte formation, and bone sclerosis observed via x-ray[11].

OA Grading and Treatment

Currently, the Kellgren-Lawrence grading system is the most common method for classifying the severity of OA where obtained radiographs are assigned a grade 0 to 4 (Table 1.1, Figure 1.1)[10, 12]. Grade assignment correlates with increasing severity of OA with grade 0 signifying minimal to no radiographic features of OA, and 4 signifying severe OA. It is recommended that once patients reach advanced OA grades of 3 or 4, a total joint replacement is needed[6]. The cost of a total joint replacement depends on the individual's location and access to insurance. In the US, the cost of a total knee replacement is around $17,500, whereas, in European countries like Denmark the cost is equal to $14,280[13, 14]. Conversely, the cost of a total knee replacement in India and other developing countries is $961.80[15].

Table 1.1. Kellgren-Lawrence osteoarthritis grading system used to score patients from 0 to 4 based on radiographic characteristics including joint space narrowing (JSN), osteophyte formation, and sclerosis. Originally published in[10].

Osteoarthritis Grade	Description
0	None – No radiographic features of OA
1	Doubtful – Possible joint space narrowing (JSN) and osteophyte formation
2	Minimal – Definite osteophyte formation with possible JSN
3	Moderate – Multiple osteophytes, definite JSN, sclerosis, and possible bony deformities
4	Severe – Large osteophytes, marked joint space narrowing, severe sclerosis, and definite bony deformities

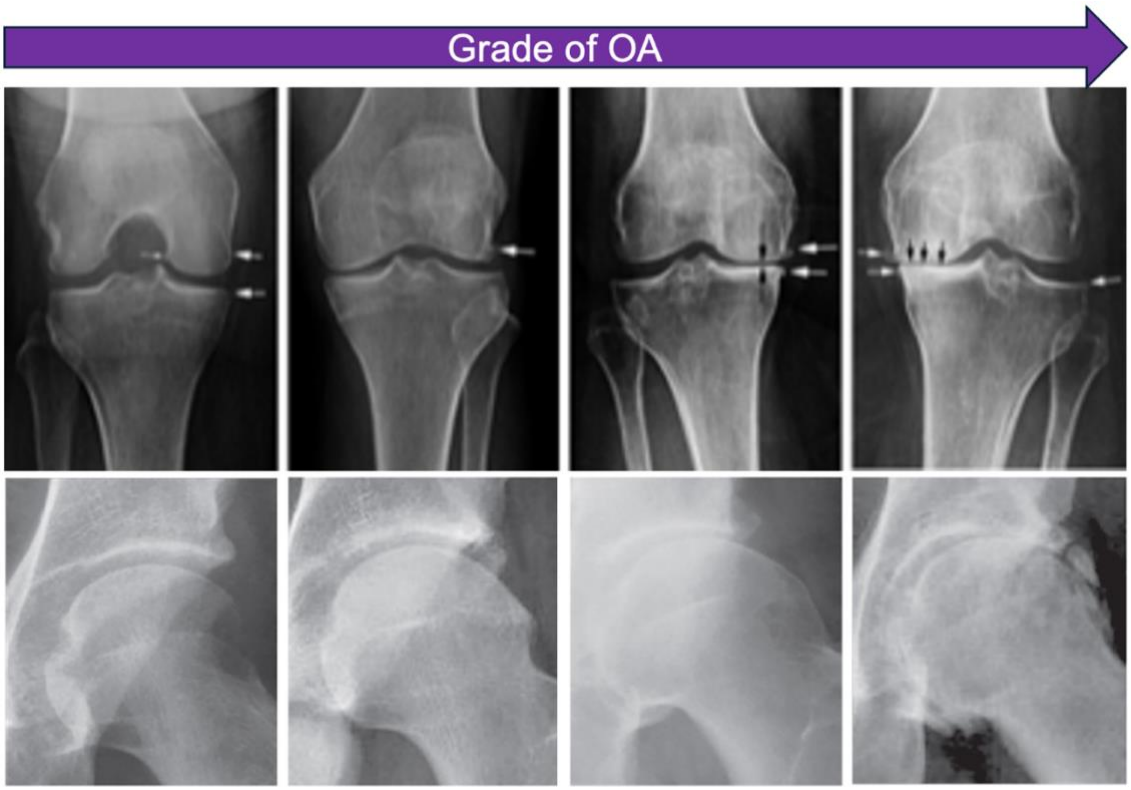

Figure 1.1. Radiographic images of Kellgren Lawrence grades of OA in both knee and hip joints. White and black arrows represent osteophytes and areas that lack joint space, respectively. Originally published in[16, 17].

Other treatment options beyond surgery include nonpharmacological and pharmacological intervention. The underlying goal across these treatment options is to manage pain, reduce disability, improve functionality and quality of life, as well as prevent OA progression. Nonpharmacological interventions typically include weight loss interventions such as diet and exercise. The effects of weight loss interventions are comparable to pharmacological interventions including analgesics like nonsteroidal anti-inflammatory drugs. Other forms of pharmacological intervention consist of intra-articular corticosteroid injections and hyaluronic acid. Unfortunately, the most effective treatment for OA is surgical intervention, which is commonly reserved for end-stage OA patients with grade III and IV OA. While joint replacements are the most common and

only effective intervention for end-stage disease, there is a great need for improved intervention measures and treatment options as this option is expensive, relatively dangerous, hinders quality of life, and is not applicable to many patients, such as obese patients.

Currently, the field has zero biomarkers for early diagnosis, disease monitoring, treatment effectiveness, and to evaluate the ability of novel treatments to slow, modify, or reverse disease. A biomarker is an objective measure that captures, or indicates, a medical state observed from outside the patient[18]. Without biomarker identification, the orthopedic field lacks this type of "red flag" detection system that signals to both the patient and clinician that something is wrong, and that this disease is in the early stages of development. Biomarker discovery for OA has gained momentum in previous years where various musculoskeletal tissues and circulator fluids have been examined at both the protein, metabolite, and circulatory RNA levels. However, none to date have been validated nor implemented in the clinical setting.

Risk Factors

While the prevalence of OA is apparent, there is no "one size fits all" approach to understanding disease onset and progression. Delving into its multifactorial nature is imperative to understand the underlying mechanisms driving disease. Risk factors for OA range far and wide including systemic factors (i.e., age, sex, genetics, race) and local factors (i.e., obesity, joint injury, and loading) (Figure 1.2). OA individuals can have any combination of systemic and local factors, all contributing to disease pathogenesis[19, 20].

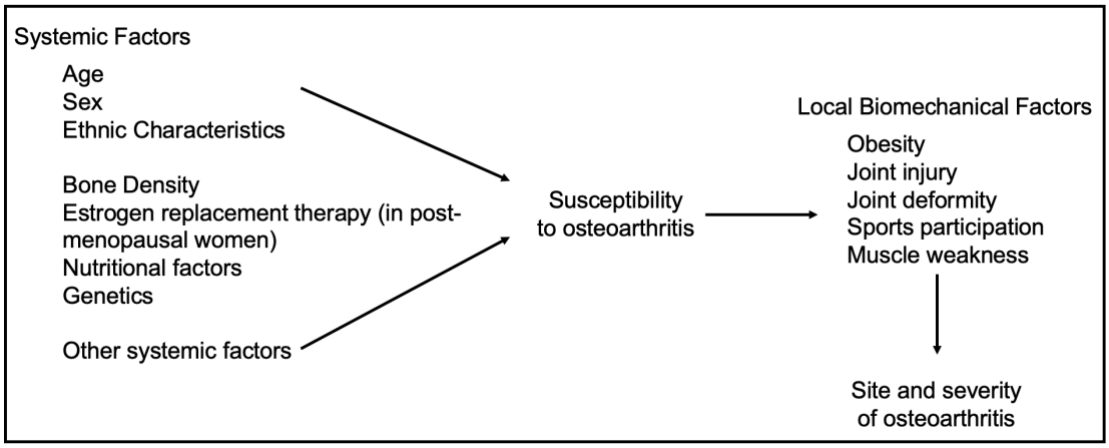

Figure 1.2. The multifactorial etiology of OA is a result of interplay between local and systemic factors. Adapted from original figure published in[19].

Obesity

Among all OA risk factors, obesity is the most common and modifiable risk factor[21]. Moreover, structural joint damage as a result of altered biomechanics and joint loading makes obesity a known accelerant of OA and is characterized by a low-grade inflammatory state. Expansion of adipose tissue leads to metabolic contributions and interactions of adipokines and leptin which have direct and downstream effects on joint tissue remodeling including chondrocytes, synoviocytes, and osteoblasts[22-25]. This is supported by increasing evidence of obesity-related OA in both weight-bearing and non-weight-bearing joints, such as the hand, suggesting circulating mediators released by adipose tissue contribute to OA development and that OA is a metabolic disease[26]. When obese patients are diagnosed with early-stage OA (KL grades I-II), weight loss is often the first line of disease management. Common ways for OA individuals to reduce weight include diet and/or exercise interventions (i.e., weightlifting, walking). Weight loss interventions improve symptomatic OA and have positive biomechanical effects[27, 28].

However, the cellular and molecular mechanisms underlying weight loss intervention and its improvements remain poorly understood.

Aging

Behind obesity, aging is the second most common risk factor for OA. Considering our aging population and increases in obesity across all ages, 67 million Americans are projected to have OA by 2030, with 50% of these individuals being 65 or older[29]. Previous studies have shown that with aging, increases in mitochondrial dysfunction, reactive oxygen species production, cell stress, autophagy, senescence, and apoptosis, as well as chronic inflammation are observed. Moreover, a hallmark of aging is a reduced repair response— likely a result of altered growth factor signaling. All of these age-related alterations combined with an emphasis on age-related mitochondrial dysfunction, play a role in age-related diseases including OA. Specific to the musculoskeletal system, cartilage thins and becomes more brittle with age due to accumulation of glycation end-products, making the tissue more susceptible to degeneration[30]. Aging also promotes imbalanced chondrocyte signaling, leading to an increase in production of matrix metalloproteinases (MMPs) and aggrecanases—both central to cartilage matrix maintenance—thus contributing to the development and progression of OA[31].

Genetics

While OA pathology is multifactorial, the genetic component is complex as it does not have a typical Mendelian pattern of inheritance and instead has been shown to have multiple gene interactions and polygenic inheritance[32]. In general, the genetic influence of OA has been estimated between 35 and 65%[33], with a 40% probability of inheritance for KOA whereas hip and hand OA have 65% probability of inheritance[34]. Previous studies have implicated specific

chromosomes to OA including 2q, 9q, 11q, 16q, and others[34-36]. At the gene level, collagen (II, IX, XI), VDR, IGF-1, TGF-B, cartilage matrix and link protein (CRTL, CRTM), AGC1, and others have been implicated in OA and have been reported to differently operate in males and females and in joint sites[34].

Race

While race is considered an OA risk factor, no study to date has explicitly examined racial differences. This glaring knowledge gap is further solidified when it comes to patient treatment and symptoms. The handful of studies that have included the factor of race in cross-sectional studies have found overweight African American and Hispanic individuals with OA were more likely to be advised to lose weight than non-Hispanic White individuals[37, 38]. A greater proportion of African Americans report both symptomatic and radiographic OA[39-41], greater pain severity[42, 43], and more pain-related disability compared to non-Hispanic White individuals[44, 45]. Racial differences are further confounded with sex where older African American females are disproportionally affected by OA and experience OA-related disability at twice the rate of non-Hispanic White females[46].

Joint Loading and Injury

It is well established that mechanical loading, too much or too little, is a risk factor for OA[19]. Historically, OA was described as a “wear-and-tear” disease where the relationship between joint health and applied mechanical load was heavily investigated. Specifically, cartilage has been closely examined because it provides near-frictionless articulation at the ends of long bones allowing for pain-free joint movement, resistance to extreme loads, and reduced stress placed on the underlying bone [47]. To maintain these functions and integrity of cartilage, physiological loading

is necessary[48, 49]. However, reduced loading (i.e., bedrest, microgravity) and overloading (i.e., loads large in duration and magnitude) can lead to imbalanced cartilage homeostasis and metabolism[50]. Once this occurs, physical manifestations at the joint level consist of cartilage degeneration and eventual OA[51].

While mechanical loading is required to maintain proper cartilage function, injurious mechanical loads are common. Within the US alone, 250,000 individuals injure their anterior cruciate ligament (ACL) annually and often damage other tissues and structures within the joint, such as the meniscus. On average, 70% of injured individuals undergo surgical repair with the majority of these individuals being between the ages of 16 and 24, and 50% of them will develop PTAO within 10 to 15 years[52]. The acute nature of ACL injury triggers an inflammatory response, activating catabolic mechanisms within the joint[53]. Consequently, ACL injury and the subsequent development of post-traumatic osteoarthritis (PTOA) stand out as notable contributors to the overarching impact of OA, with PTOA cases comprising 12% of the annual total, amounting to 5.8 million cases annually[54].

Sex

OA affects both males and females; however, knee OA (KOA) is more prevalent amongst females, particularly those over the age of 55 who often experience more severe OA[55, 56]. While the number of OA cases is projected to increase, in 2030 the projected prevalence is much higher in females (64%, ~42 million) compared to males (36%, ~25 million) (Figure 1.3)[57]. Female-specific risk factors contributing to OA encompass genetic predisposition, anatomic and hormonal differences, and injury susceptibility[58, 59]. A Finnish twin study indicates a higher heritability of OA among females when compared to their male twin[60]. Anatomically, females have narrower

pelves, smaller femurs, thinner cartilage at the distal femur, a smaller ACL, and a narrower intercondylar notch (i.e., the groove the ACL travels through) compared to males[61-63].

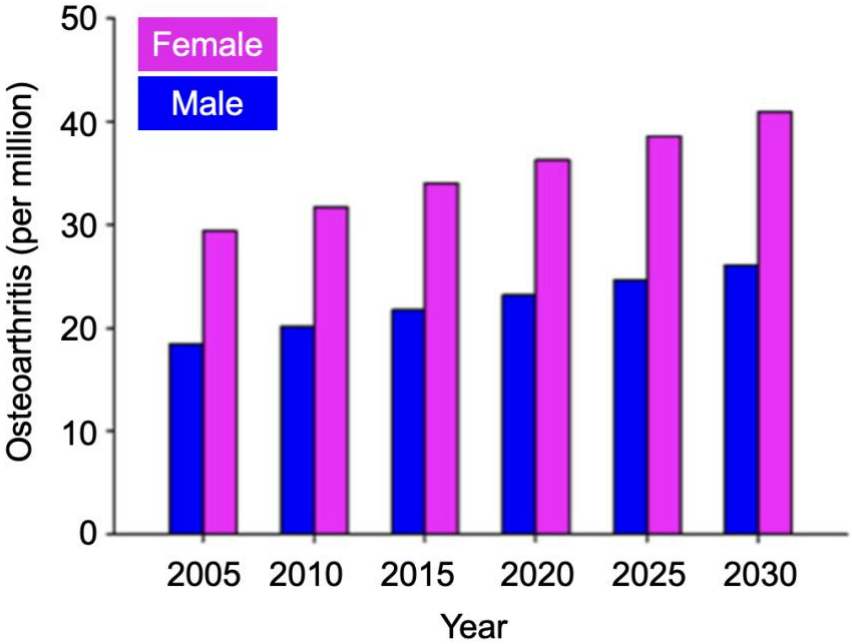

Figure 1.3. Prevalence of OA among males (blue) and females (pink) in the past (2005-2025) and the projected prevalence of arthritis by 2030 with females accounting for approximately 64% of OA cases. Adapted from original figure published in[57].

These anatomical differences amplify the propensity for ACL injuries or ruptures, a phenomenon observed more frequently in females. Annually, 15% of knee injuries are among high-school athletes with young female athletes composing the majority of these injuries as they are 2-6 times more likely to sustain a knee injury that requires surgical repair compared to male athletes[64, 65]. Once injured, females report poorer outcomes post-repair where they experience greater joint instability and distress and have a 25% reduced chance of returning to their sport within 5 years compared to male athletes[66, 67]. Moreover, most studies investigating injury and PTOA's association with sports are primarily studied in male-dominated sports[66].

Despite the recognition of sex differences in OA dating back to 1956, little to no attention has been given to this issue[68]. Particularly concerning is the underrepresentation of both male and female subjects in many human and animal studies. Using the search terms “knee OA” and “sex” for the clinical population of interest, only 9% and 6% identified sex and gender, respectively, out of the total 2,968 clinical studies on KOA[57]. In 1993, the National Institutes of Health mandated the enrollment of women in human clinical trials, however, no comparable initiatives have been established for animal trials, resulting in a disproportionate ratio of 5:1 male to female subjects in animal studies[69]. In a review summarizing all animal OA studies published between 2002 and 2012 (n=1043) revealed that only 32 studies identified the sex of animals, with only one study comparing results between males and females[57].

Beyond human and animal models, OA is investigated at smaller length scales, such as cell culture studies, where the sex of the cell source is often overlooked or regarded as asexual[57]. Few studies report this because non-reproductive tissue is used, however, genes expressed on the X and Y sex chromosomes have a strong impact on the biology of diverse tissues, including biochemical pathway regulation and cellular physiology, beyond reproductive tissues[70, 71]. While many journals have implemented policies that the source of cells utilized, including species and sex, should be indicated, such reporting remains sporadic[71]. A notable exception to this trend is the HeLa cell line, derived without consent from Henrietta Lacks, which has emerged as one of the oldest and most widely used cell lines in scientific history[72]. HeLa cells have been central to numerous biomedical and general scientific breakthroughs[71], underscoring the debt owed to patients like Henrietta Lacks by scientists and individuals worldwide. Beyond the HeLa cell line, sex information is often lacking or poorly documented, necessitating further investigation, which very

few undertake. In the realm of OA research, for instance, SW1353 cells, derived from a 72-year-old white female with chondrosarcoma, are commonly used for chondrocyte experiments, yet the significance of sex in this context remains underexplored.

Lastly, the influence of hormonal modulation extends beyond reproductive organs and tissues and impacts many joints affected by OA, including the knee and hand. Sex hormones undergo cyclic fluctuations throughout the lifespan, with females experiencing monthly cycles lasting approximately 30 days, while males undergo daily hormonal cycling. Furthermore, post-menopausal women exhibit increased OA severity, a phenomenon that cannot solely be attributed to systemic estrogen levels[73], but possibly elucidated by variations in receptor number and type[74]. Even before menopause, higher levels of circulating estrogen in females compared to males have been associated with increased expression of beta-oxidation pathways and mechanisms like adenosine monophosphate-activated protein kinase (AMPK)[75, 76]. AMPK, a key energy sensor that regulates ATP production, can be activated by estrogen. Despite these nuanced differences, the recognition of sex-related distinctions remains limited across various scales. Consequently, discussions often stop at hormonal differences, resulting in disproportionate research emphasis on females, thereby adversely affecting the development and implementation of clinical care, preventative strategies, and therapies.

Mass Spectrometry

Mass spectrometry is a powerful analytical tool capable of identifying and quantifying the mass-to-charge ratio (m/z) of one or more molecules in a sample. In our daily lives, we use mass spectrometers without realizing it. For instance, Transportation Security Administration agents utilize mass spectrometers to test swabs from passengers' hands and items to detect bomb-related

materials like TNT. Additionally, when a baby is born, a heel-prick blood sample is obtained and then subjected to mass spectrometry analysis in search of biomarkers indicative of disease. More recently, mass spectrometers have been used in the operating room during surgical procedures where the iKnife aids surgeons in real-time tissue-type identification to discriminate cancerous tissues from normal tissues[77]. Beyond these real-world applications, mass spectrometry has widespread applications across diverse fields of research, including the musculoskeletal domain.

Instrumentation

At the core of all three of these examples are the three fundamental components of a mass spectrometry instrument: the ion source, mass analyzer, and mass detector (Figure 1.4)[78]. In a sequential process, the sample is introduced into the system and becomes positively or negatively charged through ionization methods, such as electrospray ionization (ESI). Once charged, ions traverse the mass analyzer via generated electromagnetic fields. The mass analyzer is the heart of the mass spectrometer and is crucial for downstream analyses as it separates ions based on m/z and filters out uncharged molecules. Upon reaching the mass detector, charged ions produce a measurable current. At both the mass analyzer and mass detector, the size of the ion dictates its velocity, with smaller ions reaching the detector before larger ions. Combined, the measured time and velocity aid in determining the ion's specific mass. The functional readout from standard mass spectrometers includes m/z, relative abundance or intensity, and retention time. Since its inception in the early 1900s, mass spectrometry has undergone profound instrument development, leading to the emergence of numerous ion sources, mass analyzers, and mass detectors with various combinations of all three components have been utilized. Furthermore, the integration of

chromatography techniques has significantly enhanced the coverage of molecules within a complex sample.

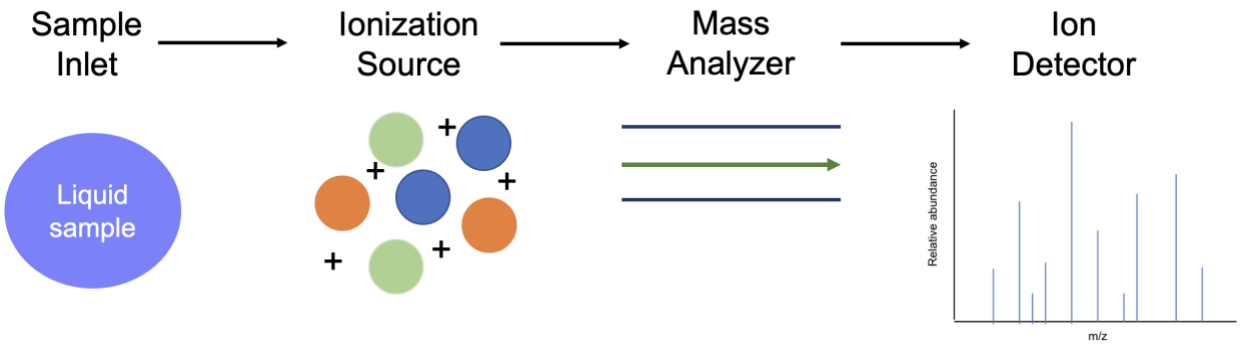

Figure 1.4. Overview of the analytical framework of mass spectrometers where samples are introduced to the system, molecules become ionized, traverse through the mass analyzer, then hit the ion detector where the time to traverse is interpolated to a m/z value in an MS spectrum.

Ionization

The introduction of samples into the mass spectrometer occurs through two primary routes: direct insertion and direct infusion. Direct infusion involves a continuous flow of the sample into the mass analyzer, while direct insertion employs a lock system for static sample introduction[78]. Both routes produce ions, with ionization playing a crucial role in mass spectrometry as molecules lacking a charge are unable to traverse the mass analyzer. Examples of direct infusion include electron ionization, chemical ionization, and ESI while direct insertion techniques include fast atom/ion bombardment, electron ionization via probe, and matrix-assisted laser desorption ionization (MALDI).

ESI is a widely used method due to its ability to provide a continuous sample introduction into the mass analyzer and its compatibility with chromatographic techniques. ESI produces singly charged molecules, either positive or negative, using electrical energy, heat, and gas (i.e., nitrogen)

to transfer ions from solution into the gaseous phase (Figure 1.5). This process involves three main steps: (1) the dispersion of a fine spray of charged droplets, (2) solvent evaporation, and (3) ion ejection from the highly charged droplets[79]. Advantages of ESI include a practical mass range of up to 70,000 Da, high sensitivity, soft ionization, easily adapted to liquid chromatography (LC) and various mass analyzers, and minimal matrix interference. However, a drawback includes potential multiple charging and incompatibility with salts due to sample dehyration[78].

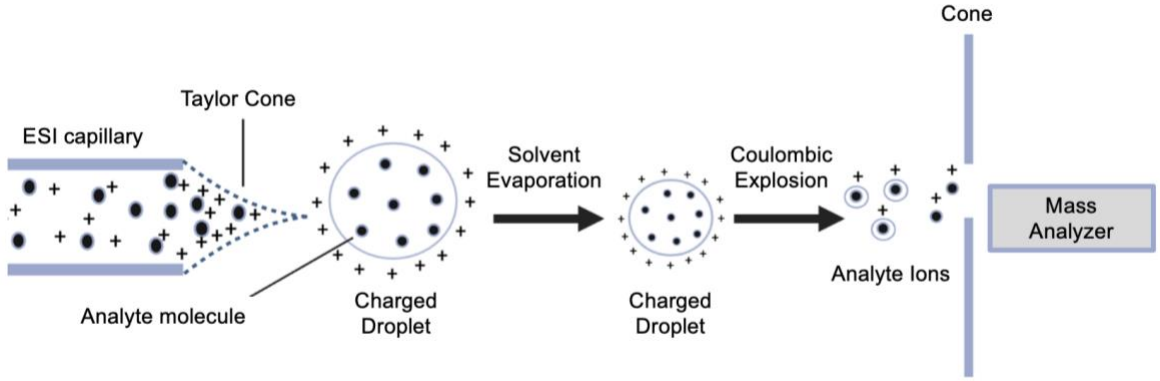

Figure 1.5. Schematic of electrospray ionization (ESI) which is a common ionization method used in mass spectrometry. To generate ions, a Taylor cone is formed at the tip of the ESI capillary, creating a large droplet. Through solvent evaporation, charged droplets get smaller and smaller while the charge intensity on the surface gradually increases. This charge concentration culminates in a Coulombic explosion where many smaller droplets, or ions, are formed which can then enter the mass analyzer.

MALDI, a type of direct insertion ionization technique, utilizes matrix and laser ablation to generate ions. In this process, a sample is first coated with a matrix where the sample is co-crystallized with the matrix compound. Many matrices have been utilized for MALDI, where most contain aromatic rings capable of absorbing UV light. The matrix is very important as it helps facilitate desorption and irradiation by absorbing laser radiation and energy, thereby protecting the sample. Upon laser irradiation, vaporization of the matrix containing analytes occurs, with analytes subsequently ionized by protonation or deprotonation in the hot plume of ablated gas before being

accelerated into the mass detector[80] (Figure 1.6). Advantages to MALDI ionization include a practical range of 300,000 Da exceeding ESI, high sensitivity, minimal fragmentation, and is highly suited for the analysis of complex mixtures. However, disadvantages include high matrix background, potential photodegradation from the laser, and the requirement for substantial amounts of matrix[78, 81].

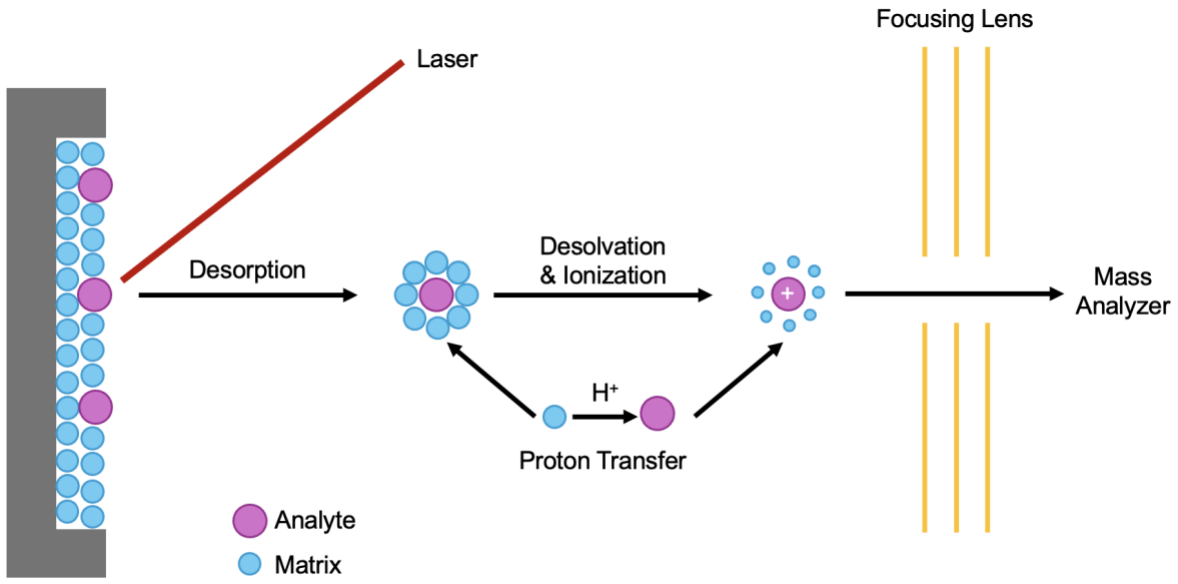

Figure 1.6. Schematic of matrix-assisted laser desorption ionization (MALDI) where co-crystalized matrix (blue) and sample analytes (pink) undergo laser ablation to ionize analytes while protecting the sample.

Recently, MALDI ionization has catalyzed spatial imaging. Specifically, MALDI-mass spectrometry imaging (MALDI-MSI) is utilized to spatially locate metabolites within biological samples (Figure 1.7). This powerful tool offers advantages beyond standard histological imaging where molecular information is correlated with localization in a label-free and multiplexed way offering high sensitivity, high throughput, and a high degree of molecular specificity. In 1997, the first study that employed MALDI-MSI to image biological tissues was published[82], and was

quickly implemented in the study of cancer, neurological disorders, and drug distribution and metabolism[83]. A noteworthy application of MALDI-MSI demonstrating its diagnostic potential is in the differentiation of tissues like tumors and the degree of metastasis[84, 85].

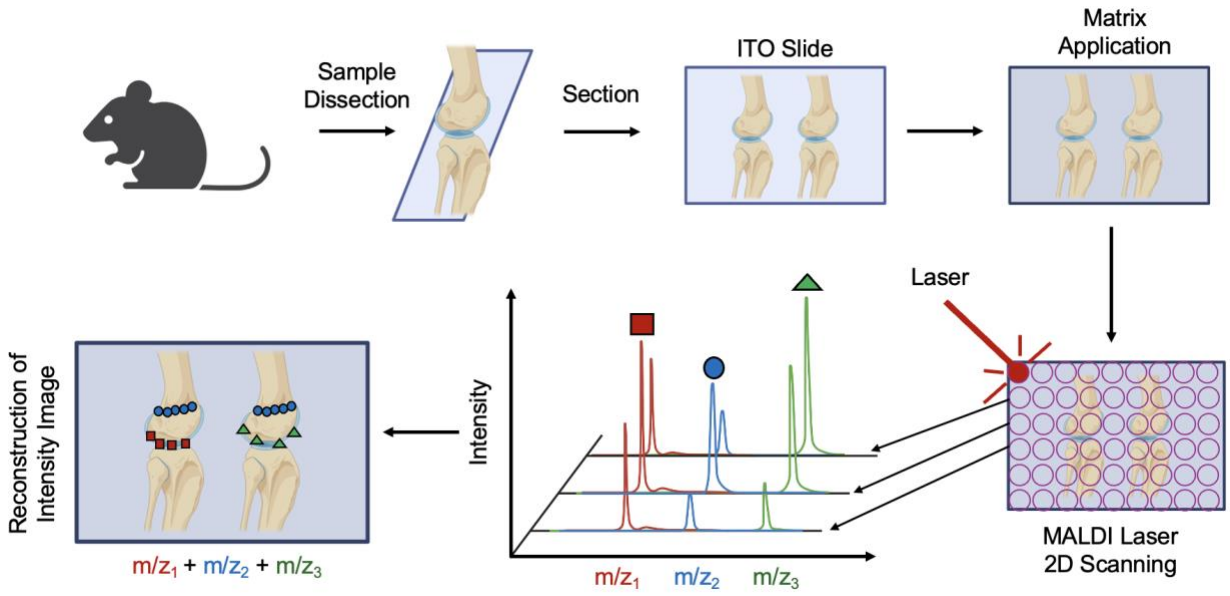

Figure 1.7. Schematic of matrix assisted laser desorption ionization-mass spectrometry imaging (MALDI-MSI) where the tissue of interest is dissected and sectioned. Next, sections are transferred to indium tin oxide (ITO) slides where matrix is applied. Co-crystallized matrix and sample are then ablated using a laser to spatially locate metabolites within a biological sample using a reconstructed intensity image.

Mass Analyzers

Following ionization, the ions generated by various techniques are then measured by the mass analyzer. Central to many of the mass analyzers on the market is the quadrupole, an element first reported in the mid-1950s, utilizing radiofrequency and direct current potential to separate ions based on their m/z. Since, advancements have led to the development of triple quadrupoles (QQQ), quadrupole time of flight (QTOF), quadrupole ion traps, and orbitraps. The selection of a specific mass analyzer depends on the same type and research hypothesis at hand. For instance,

QTOF instruments offer high accuracy and are well-suited for comprehensive global analyses, while QQQ serves as the gold standard for more targeted analyses.

Chromatography

Chromatography first entered the realm of mass spectrometry in the late 1950s, establishing itself as a standard method for isolating and purifying substances. Specifically, in the context of mass spectrometry, chromatography serves the vital function of resolving complex samples allowing more analytes to be detected. Peak separation, also referred to as resolution, hinges on retention (elution time for analytes), selectivity (indicating how effectively analytes are separated), and efficiency (the column's capacity to separate analytes within a complex mixture).

At the core of chromatographic separation lies the column, which is instrumental in achieving peak resolution. In essence, the column is packed with a stationary phase, and as the mobile phase, either gas or liquid, moves through the column various analytes elute over a set period. The observed separation is influenced by many factors such as the injected sample, polarity, electrical characteristics, and molecular size. Additionally, the polarity of both the stationary and mobile phases can be adjusted to optimize the separation of complex mixtures.

Chromatography Techniques

The two primary chromatography techniques are liquid chromatography (LC) and gas chromatography (GC). In 1952, the utilization of gas chromatography-mass spectrometry (GC-MS) was first documented. Due to the utilization of a gas mobile phase and the elution of analytes from the column as a gas, the technical complexity of these systems was relatively lower, delaying the emergence of liquid chromatography-mass spectrometry (LC-MS) systems until the late 1960s.

Key distinctions between GC-MS and LC-MS are the type of mobile phase (gas vs. liquid), shape of column (circular vs. linear), and consideration of sample polarity and content.

Polarity-based separation consists of normal- and reverse-phase chromatography (Figure 1.8). In normal-phase chromatography, the stationary phase is polar, and the mobile phase is nonpolar, leading to the retention of polar analytes by the column while nonpolar analytes elute quickly. Conversely, reverse-phase chromatography operates in the reverse, where the stationary phase is nonpolar, and the mobile phase is polar, resulting in quick elution of weakly retained polar analytes and strong retention of nonpolar analytes to the column.

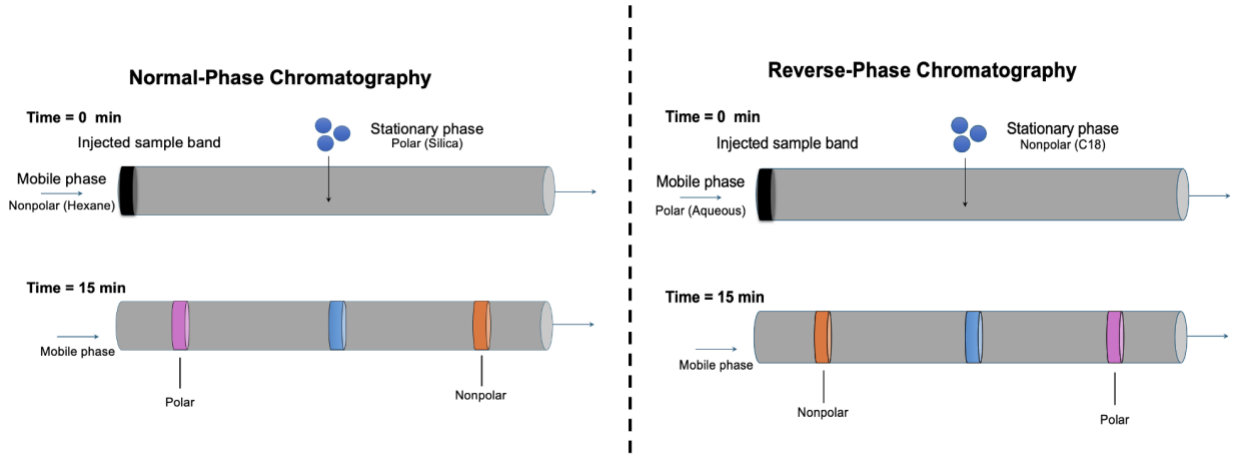

Figure 1.8. Schematic of both normal- (left) and reverse-phase (right) chromatography depicting differences in stationary and mobile phases and elution and retention of analyte bands based on polarity (pink = polar, orange = nonpolar).

More complex chromatography exists for both normal- and reverse-phase consisting of hydrophilic-interaction chromatography (HILIC) and hydrophobic-interaction chromatography (HIC). HILIC falls under the umbrella of normal-phase chromatography where a gradient elution mode consisting of organic and inorganic mobile phase. This approach allows initially retained polar compounds on the column to be eluted as the polarity of the mobile phase increases.

Similarly, HIC relies on optimizing hydrophobic interactions to elute analytes to increase hydrophobicity. Depending on sample type and complexity, HILIC is favored for complex mixtures and HIC is preferred for separation of proteins and the removal of salts. Overall, the selection of a chromatographic method and column type should consider factors such as sample type, the polarity of the analyte(s) of interest, and the underlying research hypothesis (Figure 1.9).

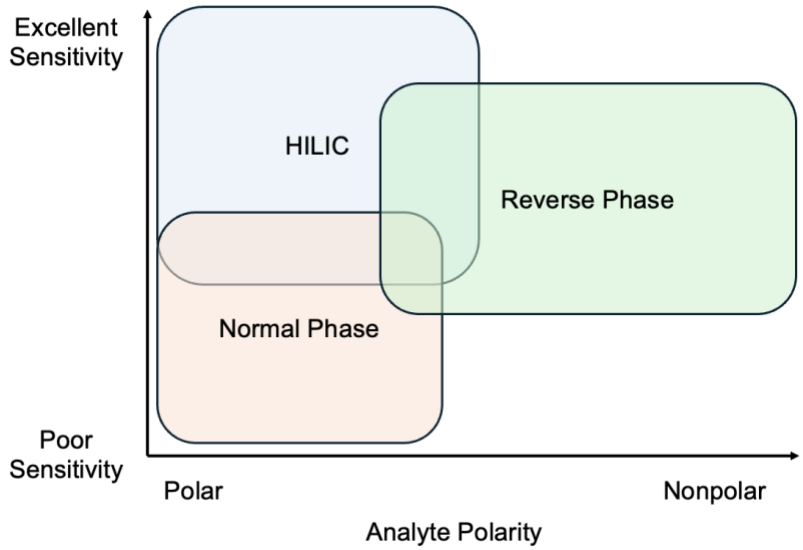

Figure 1.9 Schematic depicting different chromatographic methods based on sensitivity and analyte polarity. Hydrophilic-interaction chromatography (HILIC) is highly sensitive and well-suited for complex mixtures where it has success in eluting polar as well as some nonpolar analytes. Normal phase chromatography has poorer sensitivity compared to HILIC and is most compatible for polar analytes. Lastly, reverse-phase chromatography is most compatible with nonpolar analytes and has moderate sensitivity. Schematic was adapted from Dr. Brian Bothner's BCH 524 lecture slides.

Metabolomics

Metabolomics, a relatively new member of the '-omics' family and systems biology, focuses on the comprehensive analysis of small molecule intermediates known as metabolites. These metabolites, present within cells, tissues, and biofluids, provide a direct snapshot of biochemical activity occurring at the cellular level, offering insight beyond genes and proteins as they are not subject to epigenetic regulation and post-translational modifications[87-89] (Figure 1.10). This global approach allows researchers to gain an unbiased view of dynamic metabolic regulation influenced by various factors such as genetic architecture, environment, and internal and external factors.

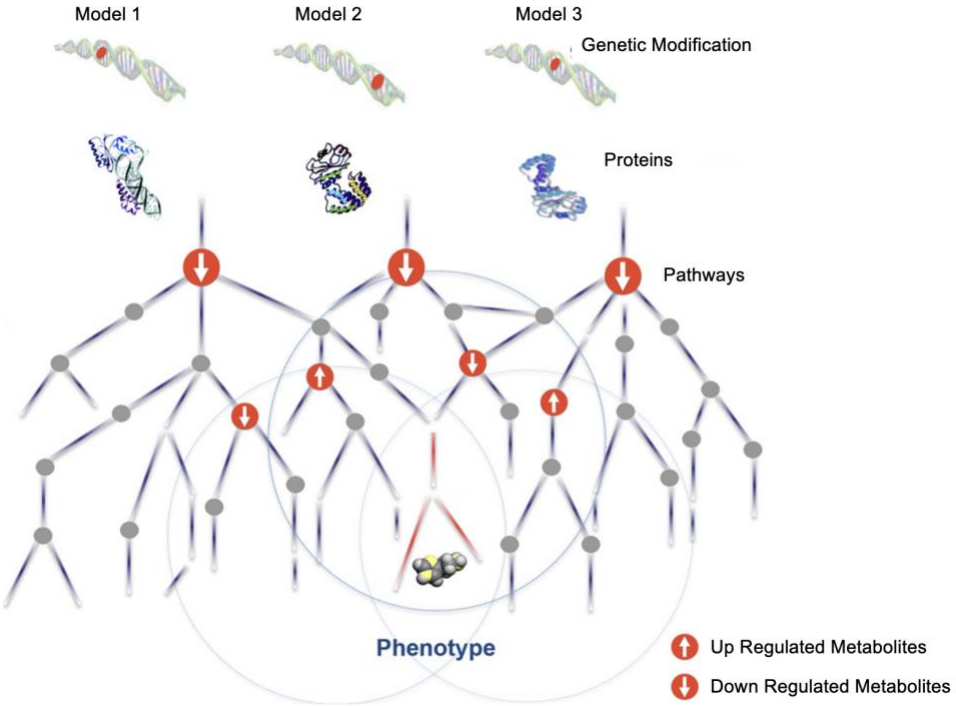

Figure 1.10. Multi-omic cascade representing the gene, protein, and metabolite levels. Combined, profiling at each level, especially at the metabolite level, phenotypes can be identified using this systems biology approach. Schematic originally published in[87].

Metabolomics History and Profiling Techniques

Historically, the two most common profiling methods in metabolomics are mass spectrometry and nuclear magnetic resonance (NMR). NMR, first utilized in 1974 for detecting metabolites in biological samples[90], requires substantial sample volume and offers limited sensitivity and metabolite coverage. In contrast, mass spectrometry, initially employed via GC-MS to measure metabolites in human urine in 1971[91, 92], requires minimal sample volume, provides higher sensitivity, and identifies a wide range of metabolites. The pivotal work by Siuzdak and Lerner, who were some of the first to perform LC-MS-based metabolomics in 1995[93, 94], leading to many other studies and development of databases like METLIN (2005)[95], XCMS (2006)[96], and the Human Metabolome Database (2007)[97], solidifying metabolomics as an emerging field by 2010.

When searching PubMed using the search term “metabolomics”, 82,293 papers spanning from 1993 to the present day are yielded. Notably, in 2023 alone, 13,270 papers that leveraged metabolomics were published, highlighting it has become a powerful approach and is widely adopted by many fields of research. Metabolomics has emerged as a potent tool in clinical research, particularly for biomarker discovery to identify metabolic indicators of disease[87]. These biomarkers hold promise as potential drug targets or markers to monitor disease progression over time. Crucially, metabolomics advances the trajectory toward personalized medicine by providing detailed snapshots of individuals’ phenotypes and endotypes, thus facilitating tailored therapeutic interventions.

Metabolomics encompasses two main approaches: untargeted and targeted (Figure 1.11). Untargeted metabolomics aims to comprehensively analyze all detectable metabolites within a given sample, thus providing an unbiased global view of the metabolic landscape without bias.

This approach, often performed using LC-MS, is extremely valuable as it is "hypothesis-generating" and valued for exploring novel biomarkers and uncovering metabolic alterations that may have gone unnoticed on targeted and hypothesis-directed studies[87, 98].

Conversely, targeted metabolomics aims to measure a predefined set, or panel, of metabolites often selected based on known relevance to a particular biological process or pathway[99]. This approach enables precise measurement of specific metabolites and is "hypothesis driving" and valued for biomarker validation, pharmacokinetics, and is employed in the clinical setting[100]. Moreover, targeted metabolomics, often performed using a QQQ, has been applied to perform selected reaction monitoring in a relatively high throughput way[87, 101]. Both approaches are paramount to metabolomics as a whole and advance our understanding of complex biological systems as they provide complimentary insight into disease mechanisms, therapeutic interventions, and personalized medicine. Leveraging both approaches synergistically has the potential to unravel the intricate interplay of biochemical activity at multiple length scales paving the way for patient-tailored medicine for a brighter future.

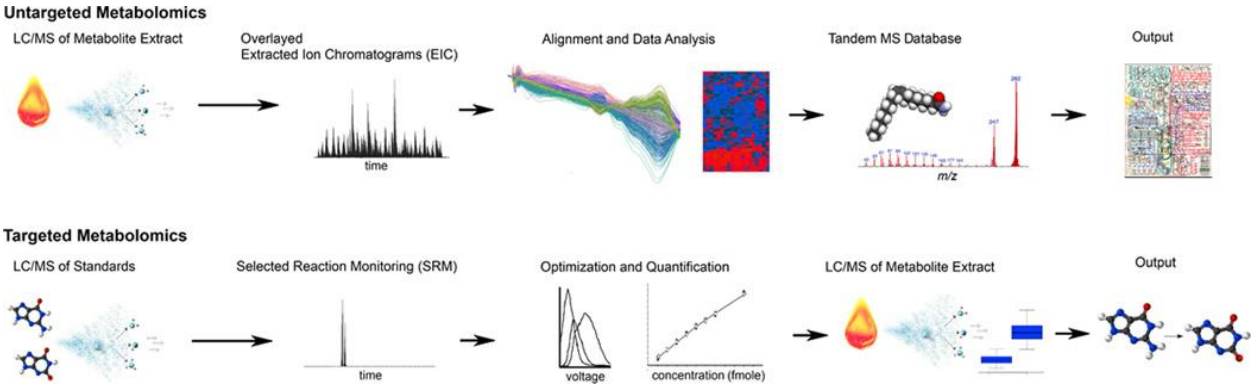

Figure 1.11. Untargeted and targeted metabolomic workflows. In untargeted metabolomics, a global approach typically employing LC-MS, all detected metabolites in a sample are analyzed. In contrast, targeted metabolomics focuses on a predefined panel of metabolites of interest, enabling specific detection within predetermined pathways through reaction monitoring (bottom). Originally published in[87].

Data Analysis

Metabolomic datasets, particularly untargeted, are extremely large and complex files due to the detection of thousands of metabolites combined with the high-resolution of the data. Because of this, manual inspection of data is complicated, incredibly time-intensive and subject to bias. Considering this, numerous open-access platforms, such as XCMS96, have been developed to first perform peak detection, sample and retention time alignment, and process raw signals into feature abundances. With this output consisting of m/z, relative abundance or intensity, and retention time, bioinformatic tools like MetaboAnalyst can be used to visualize metabolomic data and perform statistical and pathway analyses. Common visualization analyses to observe metabolic dissimilarities or similarities include hierarchical clustering analysis (HCA), principal component analysis (PCA), partial least squares-discriminant analysis (PLS-DA), and heatmaps. Statistical tests like fold change, volcano plot, student's t-test, and ANOVA analyses can be performed to distinguish and identify populations of metabolites that are differentially regulated between experimental groups of interest. Next, populations distinguished by these analyses can be subjected

to pathway enrichment analyses using the *Mummichog* algorithm where metabolites are projected onto biological pathways to infer or predict networks of functional activity and regulation.

Research Goals and Outline

While OA has been extensively researched, little progress has been made at the patient level and many gaps in knowledge remain. Key challenges persist including (1) the lack of optimal treatment options beyond expensive and invasive total joint replacement, (2) the absence of biomarkers for early detection, and (3) an incomplete understanding of the complex interactions between OA risk factors and musculoskeletal tissues. Consequently, my research sought to address these critical gaps by undertaking two overarching objectives: (1) comprehensively characterize OA phenotypes and endotypes, and (2) explore OA pathogenesis through the lens of disease-associated risk factors, leveraging advanced mass spectrometry-based approaches.

Osteoarthritis Phenotypes, Endotypes, and Targets

As a true crime fan, I enjoy learning about how various scientific discoveries have taken the field of forensics by storm. Among these, fingerprinting analysis stands out as a cornerstone method in identifying suspects by analyzing prints found at the scene of the crime. The complexity of fingerprints renders this technique invaluable to investigators. The idea of fingerprinting can be applied to OA where individuals around the globe have their own distinct “OA fingerprint” representing their disease status, susceptibility, and specific risk factors. Another term for these fingerprints are phenotypes and endotypes where these can be investigated and characterized to better understand the complex nature of OA metabolism and how they evolve in healthy and

diseased individuals. OA is not a “one-size-fits-all” disease, and treatment and interventions should reflect that.

A phenotype is defined by a single or collection of disease characteristics that describe differences between patients and outcomes[102]. In the context of OA, these physical and measurable outcomes include symptom severity, radiographic grade, and progression, mobility, and function. Characterization of phenotypes has the potential to improve treatment stratification and identify individuals who would benefit most from currently available treatments[102]. In contrast, an endotype is a subtype of disease defined functionally and pathologically by a molecular mechanism where different mechanisms lead to the same manifestation[103], such as end-stage OA. Characterization of endotypes is pivotal for implementing targeted therapies and advancing biomarker and drug discovery efforts. Thus, elucidating both OA phenotypes and endotypes is essential for understanding disease epidemiology, monitoring progression, tailoring preventative, and personalized treatments, and identifying prognostic and diagnostic biomarkers and drug targets.

Previous studies have investigated the role of metabolism and metabolic alterations across joint tissues in response to disease and specific risk factors. In Chapter 2, musculoskeletal tissue metabolism during times of health and how it changes with disease is reviewed at length. Many of the studies discussed applied metabolomics as it as has emerged as a powerful tool for OA research. Specific to my research, metabolomics can help us delineate OA phenotypes and endotypes, offering insight into the metabolic alterations occurring across various musculoskeletal tissues and circulatory fluids during health and disease. While previous studies have explored OA biomarkers in fluids like blood[104-111], urine[112, 113], and synovial fluid[114-122] using metabolomics,

tissues such as cartilage and bone remain relatively uncharted territory. Given the pivotal role of these tissues in OA pathology and their role in the Kellgren-Lawrence grading system, there is a compelling need to investigate bone and cartilage. Thus, two specific aims were generated: (1) characterize the metabolome of osteoarthritic cartilage and bone considering disease progression and (2) classify disease-associated and pathological mechanisms underlying OA metabolism in healthy and diseased cartilage.

The first aim, addressed in Chapter 3, employed a tissue-centric approach combined with LC-MS metabolomics to understand OA metabolism in end-stage disease. By extracting metabolites from end-stage OA bone and cartilage, this study sought to distinguish and define metabolic phenotypes of cartilage and bone, grades of OA, and spatially map metabolic shifts across the diseased joint. The results of this study provide compelling evidence that end-stage tissues from OA individuals differ by both grade and tissue, with pronounced metabolic perturbations observed in regions experiencing greater mechanical stress.

The second aim, addressed in Chapter 4, built upon the phenotypes and endotypes generated in Chapter 3 and incorporated healthy samples to shed light on disease-associated mechanisms. Moreover, OA participants alone were examined at length to characterize endotypes of OA. Unique to this study, tandem LC-MS (LC-MS/MS) was performed to unveil metabolic indicators of disease that could function as biomarkers and drug targets to slow, halt, or reverse OA. Combined, the results of this study unveiled specific metabolic endotypes and metabolites reflective of disease status, shedding light on the multifaceted landscape of OA metabolism and offering potential avenues for therapeutic intervention.

Osteoarthritis Risk Factors

In Chapters 5-8, my research delves into the multifaceted landscape of OA risk factors, with a great focus on sex and joint injury. To enhance the current understanding of how various risk factors influence the development and progression of OA, both human and mouse studies were conducted. Moreover, investigation into treatment and various interventions associated with these risk factors was also performed.

In Chapter 5, LC-MS metabolomics was employed to examine the influence of risk factors, sex, and injury, on the synovial fluid metabolome. Synovial fluid, located within the joint cavity and in direct contact with joint tissue and structures, is an optimal sample type for assessing metabolic changes post-injury. Thus, the goals of this study were to capture local, systemic, and metabolic changes within the joint following different types of injuries in both male and female individuals. The results of this study highlight distinct metabolic phenotypes associated with different injuries and sexes, offering insights into potential markers that could be monitored overtime to oversee disease progression.

Similarly, Chapter 6 employs a mouse injury model to investigate the effects of injury and sex on metabolic signatures in synovial fluid, whole joint tissue, and serum. By profiling multiple tissues using this LC-MS metabolomic approach, a greater understanding of how the joint responds to injury across multiple tissues may lead to the identification of a panel of metabolites, or pathways, that is easily detected in circulatory fluids like serum. Additionally, MALDI imaging was performed to spatially locate and detect differences in osteochondral metabolites that compose the mouse knee joint. By strategically combining metabolomic and imaging data, the effects of injury and sex can be comprehensively examined at multiple length scales–metabolically and structurally–to gain a full picture of activity acutely following injury.

Chapter 7 shifts the focus to obesity, the most major and modifiable OA risk factor, and investigates the effects of currently prescribed weight loss interventions, including diet and exercise, on the serum metabolome of OA patients. The Intensive Diet and Exercise for Arthritis (IDEA) trial was conducted to closely investigate the effects of diet and exercise intervention on OA symptoms and radiographic progression. In collaboration with the leaders of the IDEA trial, serum samples were obtained from 30 participants to examine (1) changes in metabolism over 18 months of assigned intervention, (2) distinguish pathways associated with specific intervention types, and (3) identify phenotypes that are sex-dependent using LC-MS and LC-MS/MS. The findings of this study suggest that intensive weight loss offers metabolic benefits for OA individuals and motivates further research to closely examine interventions and treatments currently prescribed to patients.

Lastly, Chapter 8 explores the effects of mechanical loading on chondrocyte metabolism, the primary cell type of cartilage. Motivation for this study lies in cartilage degradation which manifests as decreased mobility, increased pain, and overall, reduced quality of life. To better understand the effects of overloading and cartilage homeostasis, a common model system, pioneered by past June lab members, was utilized. Specifically, SW1353 chondrocyte cells were exposed to cyclical mechanical stimuli – shear and compression – for different durations of time (0, 15, 30 minutes). Using LC-MS metabolomics, metabolites that differentiate between the type and duration of loading were investigated. The findings of this study showcase that different mechanical stimuli differentially influence metabolism expanding our knowledge on chondrocyte metabolism and the effects of loading.

In summary, these chapters contribute to our understanding of OA phenotypes and endotypes, risk factors and their interactions, and offer insights into potential biomarkers, treatment strategies, and mechanisms underlying disease pathogenesis.

Abbreviations List

OA = osteoarthritis; MMPs = matrix metalloproteinases, ACL = anterior cruciate ligament; PTOA = post-traumatic osteoarthritis; KOA = knee osteoarthritis; AMPK = adenosine monophosphate-activated protein kinase; m/z = mass-to-charge ratio; ESI = electrospray ionization; MALDI = matrix assisted laser desorption ionization; LC = liquid chromatography; MALDI-MSI = matrix assisted laser desorption ionization-mass spectrometry imaging; QQQ = triple quadrupole; QTOF = quadrupole time of flight; GC = gas chromatography; GC-MS = gas chromatography-mass spectrometry; LC-MS = liquid chromatography-mass spectrometry; HILIC = hydrophilic-interaction chromatography; HIC = hydrophobic-interaction chromatography; NMR = nuclear magnetic resonance; HCA = hierarchical clustering analysis; PCA = principal component analysis; PLS-DA = partial least squares-discriminant analysis; LC-MS/MS = liquid chromatography tandem mass spectrometry

References

1. Long H, Liu Q, Yin H, Wang K, Diao N, Zhang Y, et al. Prevalence trends of site-specific osteoarthritis from 1990 to 2019: findings from the Global Burden of Disease Study 2019. Arthritis Rheumatol 2022.

2. Barbour KE, Helmick CG, Boring M, Brady TJ. Vital Signs: Prevalence of Doctor-Diagnosed Arthritis and Arthritis-Attributable Activity Limitation - United States, 2013-2015. MMWR Morb Mortal Wkly Rep 2017; 66: 246-253.

3. Hootman JM, Helmick CG, Barbour KE, Theis KA, Boring MA. Updated Projected Prevalence of Self-Reported Doctor-Diagnosed Arthritis and Arthritis-Attributable

Activity Limitation Among US Adults, 2015-2040. Arthritis Rheumatol 2016; 68: 1582-1587.

4. Neogi T. The epidemiology and impact of pain in osteoarthritis. Osteoarthritis Cartilage 2013; 21: 1145-1153.

5. Bitton R. The economic burden of osteoarthritis. Am J Manag Care 2009; 15: S230-235.

6. Sinusas K. Osteoarthritis: diagnosis and treatment. Am Fam Physician 2012; 85: 49-56.

7. Goldring MB. Articular cartilage degradation in osteoarthritis. HSS J 2012; 8: 7-9.

8. Woolf AD, Pfleger B. Burden of major musculoskeletal conditions. Bull World Health Organ 2003; 81: 646-656.

9. Poulet B, Staines KA. New developments in osteoarthritis and cartilage biology. Curr Opin Pharmacol 2016; 28: 8-13.

10. Kellgren JH, Lawrence JS. Radiological assessment of osteo-arthrosis. Ann Rheum Dis 1957; 16: 494-502.

11. Kevorkova O, Martineau C, Martin-Falstrault L, Sanchez-Dardon J, Brissette L, Moreau R. Low-bone-mass phenotype of deficient mice for the cluster of differentiation 36 (CD36). PLoS One 2013; 8: e77701.

12. Kohn MD, Sassoon AA, Fernando ND. Classifications in Brief: Kellgren-Lawrence Classification of Osteoarthritis. Clin Orthop Relat Res 2016; 474: 1886-1893.

13. Gandhi N, Qadeer AS, Meher A, Rachel J, Patra A, John J, et al. Costs and models used in the economic analysis of Total Knee Replacement (TKR): A systematic review. PLoS One 2023; 18: e0280371.

14. Skou ST, Roos E, Laursen M, Arendt-Nielsen L, Rasmussen S, Simonsen O, et al. Cost-effectiveness of total knee replacement in addition to non-surgical treatment: a 2-year outcome from a randomised trial in secondary care in Denmark. BMJ Open 2020; 10: e033495.

15. George J, Gautam D, Devasenapathy N, Malhotra R. Is It Worth Delaying Total Knee Replacement as Late as Possible? A Cost-Effectiveness Analysis Using a Markov Model in the Indian Setting. Value Health Reg Issues 2021; 24: 173-180.

16. Guntur AR, Le PT, Farber CR, Rosen CJ. Bioenergetics during calvarial osteoblast differentiation reflect strain differences in bone mass. Endocrinology 2014; 155: 1589-1595.

17. Hayashi D, Roemer FW, Guermazi A. Imaging for osteoarthritis. Ann Phys Rehabil Med 2016; 59: 161-169.

18. Strimbu K, Tavel JA. What are biomarkers? Curr Opin HIV AIDS 2010; 5: 463-466.

19. Felson DT, Lawrence RC, Dieppe PA, Hirsch R, Helmick CG, Jordan JM, et al. Osteoarthritis: new insights. Part 1: the disease and its risk factors. Ann Intern Med 2000; 133: 635-646.

20. Zhang Y, Jordan JM. Epidemiology of osteoarthritis. Clin Geriatr Med 2010; 26: 355-369.

21. King LK, March L, Anandacoomarasamy A. Obesity & osteoarthritis. Indian J Med Res 2013; 138: 185-193.

22. Figenschau Y, Knutsen G, Shahazeydi S, Johansen O, Sveinbjornsson B. Human articular chondrocytes express functional leptin receptors. Biochem Biophys Res Commun 2001; 287: 190-197.

23. Garnero P, Rousseau JC, Delmas PD. Molecular basis and clinical use of biochemical markers of bone, cartilage, and synovium in joint diseases. Arthritis Rheum 2000; 43: 953-968.

24. Karsenty G. Convergence between bone and energy homeostases: leptin regulation of bone mass. Cell Metab 2006; 4: 341-348.

25. Simopoulou T, Malizos KN, Iliopoulos D, Stefanou N, Papatheodorou L, Ioannou M, et al. Differential expression of leptin and leptin's receptor isoform (Ob-Rb) mRNA between advanced and minimally affected osteoarthritic cartilage; effect on cartilage metabolism. Osteoarthritis Cartilage 2007; 15: 872-883.

26. Sellam J, Berenbaum F. Is osteoarthritis a metabolic disease? Joint Bone Spine 2013; 80: 568-573.

27. Messier SP, Loeser RF, Miller GD, Morgan TM, Rejeski WJ, Sevick MA, et al. Exercise and dietary weight loss in overweight and obese older adults with knee osteoarthritis: the Arthritis, Diet, and Activity Promotion Trial. Arthritis Rheum 2004; 50: 1501-1510.

28. Messier SP, Mihalko SL, Legault C, Miller GD, Nicklas BJ, DeVita P, et al. Effects of intensive diet and exercise on knee joint loads, inflammation, and clinical outcomes among overweight and obese adults with knee osteoarthritis: the IDEA randomized clinical trial. JAMA 2013; 310: 1263-1273.

29. Hootman JM, Helmick CG. Projections of US prevalence of arthritis and associated activity limitations. Arthritis Rheum 2006; 54: 226-229.

30. Verzijl N, DeGroot J, Ben ZC, Brau-Benjamin O, Maroudas A, Bank RA, et al. Crosslinking by advanced glycation end products increases the stiffness of the collagen network in human articular cartilage: a possible mechanism through which age is a risk factor for osteoarthritis. Arthritis Rheum 2002; 46: 114-123.

31. Loeser RF. The Role of Aging in the Development of Osteoarthritis. Trans Am Clin Climatol Assoc 2017; 128: 44-54.

32. Fernandez-Moreno M, Rego I, Carreira-Garcia V, Blanco FJ. Genetics in osteoarthritis. Curr Genomics 2008; 9: 542-547.

33. Cicuttini FM, Spector TD. Genetics of osteoarthritis. Ann Rheum Dis 1996; 55: 665-667.

34. Spector TD, MacGregor AJ. Risk factors for osteoarthritis: genetics. Osteoarthritis Cartilage 2004; 12 Suppl A: S39-44.

35. Demissie S, Cupples LA, Myers R, Aliabadi P, Levy D, Felson DT. Genome scan for quantity of hand osteoarthritis: the Framingham Study. Arthritis Rheum 2002; 46: 946-952.

36. Ingvarsson T, Stefansson SE, Gulcher JR, Jonsson HH, Jonsson H, Frigge ML, et al. A large Icelandic family with early osteoarthritis of the hip associated with a susceptibility locus on chromosome 16p. Arthritis Rheum 2001; 44: 2548-2555.

37. Fontaine KR, Haaz S, Bartlett SJ. Are overweight and obese adults with arthritis being advised to lose weight? J Clin Rheumatol 2007; 13: 12-15.

38. Reyes AM, Katz JN. Racial/Ethnic and Socioeconomic Disparities in Osteoarthritis Management. Rheum Dis Clin North Am 2021; 47: 21-40.

39. Dillon CF, Rasch EK, Gu Q, Hirsch R. Prevalence of knee osteoarthritis in the United States: arthritis data from the Third National Health and Nutrition Examination Survey 1991-94. J Rheumatol 2006; 33: 2271-2279.

40. Jordan JM, Helmick CG, Renner JB, Luta G, Dragomir AD, Woodard J, et al. Prevalence of knee symptoms and radiographic and symptomatic knee osteoarthritis in African Americans and Caucasians: the Johnston County Osteoarthritis Project. J Rheumatol 2007; 34: 172-180.

41. Nelson AE, Renner JB, Schwartz TA, Kraus VB, Helmick CG, Jordan JM. Differences in multijoint radiographic osteoarthritis phenotypes among African Americans and Caucasians: the Johnston County Osteoarthritis project. Arthritis Rheum 2011; 63: 3843-3852.

42. Creamer P, Lethbridge-Cejku M, Hochberg MC. Determinants of pain severity in knee osteoarthritis: effect of demographic and psychosocial variables using 3 pain measures. J Rheumatol 1999; 26: 1785-1792.

43. Parmelee PA, Harralson TL, McPherron JA, DeCoster J, Schumacher HR. Pain, disability, and depression in osteoarthritis: effects of race and sex. J Aging Health 2012; 24: 168-187.

44. Burns R, Graney MJ, Lummus AC, Nichols LO, Martindale-Adams J. Differences of self-reported osteoarthritis disability and race. J Natl Med Assoc 2007; 99: 1046-1051.

45. Vaughn IA, Terry EL, Bartley EJ, Schaefer N, Fillingim RB. Racial-Ethnic Differences in Osteoarthritis Pain and Disability: A Meta-Analysis. J Pain 2019; 20: 629-644.

46. Song J, Chang HJ, Tirodkar M, Chang RW, Manheim LM, Dunlop DD. Racial/ethnic differences in activities of daily living disability in older adults with arthritis: a longitudinal study. Arthritis Rheum 2007; 57: 1058-1066.

47. Sophia Fox AJ, Bedi A, Rodeo SA. The basic science of articular cartilage: structure, composition, and function. Sports Health 2009; 1: 461-468.

48. Jaalouk DE, Lammerding J. Mechanotransduction gone awry. Nat Rev Mol Cell Biol 2009; 10: 63-73.

49. Orr AW, Helmke BP, Blackman BR, Schwartz MA. Mechanisms of mechanotransduction. Dev Cell 2006; 10: 11-20.

50. Guilak F. Biomechanical factors in osteoarthritis. Best Pract Res Clin Rheumatol 2011; 25: 815-823.

51. Racunica TL, Teichtahl AJ, Wang Y, Wluka AE, English DR, Giles GG, et al. Effect of physical activity on articular knee joint structures in community-based adults. Arthritis Rheum 2007; 57: 1261-1268.

52. Brophy RH, Silvers HJ, Mandelbaum BR. Anterior cruciate ligament injuries: etiology and prevention. Sports Med Arthrosc Rev 2010; 18: 2-11.

53. Hahn AK, Wallace CW, Welhaven HD, Brooks E, McAlpine M, Christiansen BA, et al. The microbiome mediates epiphyseal bone loss and metabolomic changes after acute joint trauma in mice. Osteoarthritis Cartilage 2021; 29: 882-893.

54. Brown TD, Johnston RC, Saltzman CL, Marsh JL, Buckwalter JA. Posttraumatic osteoarthritis: a first estimate of incidence, prevalence, and burden of disease. J Orthop Trauma 2006; 20: 739-744.

55. Blaker CL, Ashton DM, Doran N, Little CB, Clarke EC. Sex- and injury-based differences in knee biomechanics in mouse models of post-traumatic osteoarthritis. J Biomech 2021; 114: 110152.

56. Srikanth VK, Fryer JL, Zhai G, Winzenberg TM, Hosmer D, Jones G. A meta-analysis of sex differences prevalence, incidence and severity of osteoarthritis. Osteoarthritis Cartilage 2005; 13: 769-781.

57. Boyan BD, Tosi LL, Coutts RD, Enoka RM, Hart DA, Nicolella DP, et al. Addressing the gaps: sex differences in osteoarthritis of the knee. Biol Sex Differ 2013; 4: 4.

58. Loughlin J. Familial inheritance of osteoarthritis: documented family subsets. Clin Orthop Relat Res 2004: S22-25.

59. O'Connor MI. Sex differences in osteoarthritis of the hip and knee. J Am Acad Orthop Surg 2007; 15 Suppl 1: S22-25.

60. Kaprio J, Kujala UM, Peltonen L, Koskenvuo M. Genetic liability to osteoarthritis may be greater in women than men. BMJ 1996; 313: 232.

61. Faber SC, Eckstein F, Lukasz S, Muhlbauer R, Hohe J, Englmeier KH, et al. Gender differences in knee joint cartilage thickness, volume and articular surface areas: assessment with quantitative three-dimensional MR imaging. Skeletal Radiol 2001; 30: 144-150.

62. Hitt K, Shurman JR, 2nd, Greene K, McCarthy J, Moskal J, Hoeman T, et al. Anthropometric measurements of the human knee: correlation to the sizing of current knee arthroplasty systems. J Bone Joint Surg Am 2003; 85-A Suppl 4: 115-122.

63. Poilvache PL, Insall JN, Scuderi GR, Font-Rodriguez DE. Rotational landmarks and sizing of the distal femur in total knee arthroplasty. Clin Orthop Relat Res 1996: 35-46.

64. Ingram JG, Fields SK, Yard EE, Comstock RD. Epidemiology of knee injuries among boys and girls in US high school athletics. Am J Sports Med 2008; 36: 1116-1122.

65. Hewett TE, Myer GD, Ford KR. Anterior cruciate ligament injuries in female athletes: Part 1, mechanisms and risk factors. Am J Sports Med 2006; 34: 299-311.

66. Bruder AM, Culvenor AG, King MG, Haberfield M, Roughead EA, Mastwyk J, et al. Let's talk about sex (and gender) after ACL injury: a systematic review and meta-analysis of self-reported activity and knee-related outcomes. Br J Sports Med 2023; 57: 602-610.

67. Tan SH, Lau BP, Khin LW, Lingaraj K. The Importance of Patient Sex in the Outcomes of Anterior Cruciate Ligament Reconstructions: A Systematic Review and Meta-analysis. Am J Sports Med 2016; 44: 242-254.

68. Sokoloff L. Natural history of degenerative joint disease in small laboratory animals. I. Pathological anatomy of degenerative joint disease in mice. AMA Arch Pathol 1956; 62: 118-128.

69. Beery AK, Zucker I. Sex bias in neuroscience and biomedical research. Neurosci Biobehav Rev 2011; 35: 565-572.

70. Miller VM. In pursuit of scientific excellence: sex matters. Adv Physiol Educ 2012; 36: 83-84.

71. Shah K, McCormack CE, Bradbury NA. Do you know the sex of your cells? Am J Physiol Cell Physiol 2014; 306: C3-18.

72. Jones HW, Jr., McKusick VA, Harper PS, Wuu KD. George Otto Gey. (1899-1970). The HeLa cell and a reappraisal of its origin. Obstet Gynecol 1971; 38: 945-949.

73. Boyan BD, Hart DA, Enoka RM, Nicolella DP, Resnick E, Berkley KJ, et al. Hormonal modulation of connective tissue homeostasis and sex differences in risk for osteoarthritis of the knee. Biol Sex Differ 2013; 4: 3.

74. Kinney RC, Schwartz Z, Week K, Lotz MK, Boyan BD. Human articular chondrocytes exhibit sexual dimorphism in their responses to 17beta-estradiol. Osteoarthritis Cartilage 2005; 13: 330-337.

75. Oosthuyse T, Bosch AN. The effect of the menstrual cycle on exercise metabolism: implications for exercise performance in eumenorrhoeic women. Sports Med 2010; 40: 207-227.

76. Purdom T, Kravitz L, Dokladny K, Mermier C. Understanding the factors that effect maximal fat oxidation. J Int Soc Sports Nutr 2018; 15: 3.

77. Tzafetas M, Mitra A, Paraskevaidi M, Bodai Z, Kalliala I, Bowden S, et al. The intelligent knife (iKnife) and its intraoperative diagnostic advantage for the treatment of cervical disease. Proc Natl Acad Sci U S A 2020; 117: 7338-7346.

78. Siuzdak G. The Expanding Role of Mass Spectrometry in Biotechnology. 2nd Edition Edition, MCC Press 2006.

79. Ho CS, Lam CW, Chan MH, Cheung RC, Law LK, Lit LC, et al. Electrospray ionisation mass spectrometry: principles and clinical applications. Clin Biochem Rev 2003; 24: 3-12.

80. Karas M, Kruger R. Ion formation in MALDI: the cluster ionization mechanism. Chem Rev 2003; 103: 427-440.

81. Hillenkamp F, Karas M, Beavis RC, Chait BT. Matrix-assisted laser desorption/ionization mass spectrometry of biopolymers. Anal Chem 1991; 63: 1193A-1203A.

82. Caprioli RM, Farmer TB, Gile J. Molecular imaging of biological samples: localization of peptides and proteins using MALDI-TOF MS. Anal Chem 1997; 69: 4751-4760.

83. Norris JL, Caprioli RM. Analysis of tissue specimens by matrix-assisted laser desorption/ionization imaging mass spectrometry in biological and clinical research. Chem Rev 2013; 113: 2309-2342.

84. Aichler M, Walch A. MALDI Imaging mass spectrometry: current frontiers and perspectives in pathology research and practice. Lab Invest 2015; 95: 422-431.

85. Casadonte R, Kriegsmann M, Zweynert F, Friedrich K, Baretton G, Otto M, et al. Imaging mass spectrometry to discriminate breast from pancreatic cancer metastasis in formalin-fixed paraffin-embedded tissues. Proteomics 2014; 14: 956-964.

86. Fujimura Y, Miura D. MALDI Mass Spectrometry Imaging for Visualizing In Situ Metabolism of Endogenous Metabolites and Dietary Phytochemicals. Metabolites 2014; 4: 319-346.

87. Patti GJ, Yanes O, Siuzdak G. Innovation: Metabolomics: the apogee of the omics trilogy. Nat Rev Mol Cell Biol 2012; 13: 263-269.

88. Gieger C, Geistlinger L, Altmaier E, Hrabe de Angelis M, Kronenberg F, Meitinger T, et al. Genetics meets metabolomics: a genome-wide association study of metabolite profiles in human serum. PLoS Genet 2008; 4: e1000282.

89. Jewett MC, Hofmann G, Nielsen J. Fungal metabolite analysis in genomics and phenomics. Curr Opin Biotechnol 2006; 17: 191-197.

90. Hoult DI, Busby SJ, Gadian DG, Radda GK, Richards RE, Seeley PJ. Observation of tissue metabolites using 31P nuclear magnetic resonance. Nature 1974; 252: 285-287.

91. Horning EC, Horning MG. Metabolic profiles: gas-phase methods for analysis of metabolites. Clin Chem 1971; 17: 802-809.

92. Teranishi R, Mon TR, Robinson AB, Cary P, Pauling L. Gas chromatography of volatiles from breath and urine. Anal Chem 1972; 44: 18-20.

93. Cravatt BF, Prospero-Garcia O, Siuzdak G, Gilula NB, Henriksen SJ, Boger DL, et al. Chemical characterization of a family of brain lipids that induce sleep. Science 1995; 268: 1506-1509.

94. Lerner RA, Siuzdak G, Prospero-Garcia O, Henriksen SJ, Boger DL, Cravatt BF. Cerebrodiene: a brain lipid isolated from sleep-deprived cats. Proc Natl Acad Sci U S A 1994; 91: 9505-9508.

95. Smith CA, O'Maille G, Want EJ, Qin C, Trauger SA, Brandon TR, et al. METLIN: a metabolite mass spectral database. Ther Drug Monit 2005; 27: 747-751.

96. Smith CA, Want EJ, O'Maille G, Abagyan R, Siuzdak G. XCMS: processing mass spectrometry data for metabolite profiling using nonlinear peak alignment, matching, and identification. Anal Chem 2006; 78: 779-787.

97. Wishart DS, Tzur D, Knox C, Eisner R, Guo AC, Young N, et al. HMDB: the Human Metabolome Database. Nucleic Acids Res 2007; 35: D521-526.

98. Jonsson P, Bruce SJ, Moritz T, Trygg J, Sjostrom M, Plumb R, et al. Extraction, interpretation and validation of information for comparing samples in metabolic LC/MS data sets. Analyst 2005; 130: 701-707.

99. Dudley E, Yousef M, Wang Y, Griffiths WJ. Targeted metabolomics and mass spectrometry. Adv Protein Chem Struct Biol 2010; 80: 45-83.

100. Nicholson JK, Connelly J, Lindon JC, Holmes E. Metabonomics: a platform for studying drug toxicity and gene function. Nat Rev Drug Discov 2002; 1: 153-161.

101. Buescher JM, Moco S, Sauer U, Zamboni N. Ultrahigh performance liquid chromatography-tandem mass spectrometry method for fast and robust quantification of anionic and aromatic metabolites. Anal Chem 2010; 82: 4403-4412.

102. Deveza LA, Nelson AE, Loeser RF. Phenotypes of osteoarthritis: current state and future implications. Clin Exp Rheumatol 2019; 37 Suppl 120: 64-72.

103. Anderson GP. Endotyping asthma: new insights into key pathogenic mechanisms in a complex, heterogeneous disease. Lancet 2008; 372: 1107-1119.

104. Surowiec I, Arlestig L, Rantapaa-Dahlqvist S, Trygg J. Metabolite and Lipid Profiling of Biobank Plasma Samples Collected Prior to Onset of Rheumatoid Arthritis. PLoS One 2016; 11: e0164196.

105. Zhang W, Likhodii S, Aref-Eshghi E, Zhang Y, Harper PE, Randell E, et al. Relationship between blood plasma and synovial fluid metabolite concentrations in patients with osteoarthritis. J Rheumatol 2015; 42: 859-865.

106. Zhang W, Sun G, Likhodii S, Liu M, Aref-Eshghi E, Harper PE, et al. Metabolomic analysis of human plasma reveals that arginine is depleted in knee osteoarthritis patients. Osteoarthritis Cartilage 2016; 24: 827-834.

107. Sitton NG, Dixon JS, Bird HA, Wright V. Serum and synovial fluid histidine: a comparison in rheumatoid arthritis and osteoarthritis. Rheumatol Int 1986; 6: 251-254.

108. Tootsi K, Vilba K, Martson A, Kals J, Paapstel K, Zilmer M. Metabolomic Signature of Amino Acids, Biogenic Amines and Lipids in Blood Serum of Patients with Severe Osteoarthritis. Metabolites 2020; 10.

109. Wallace CW, Hislop B, Hahn AK, Erdogan AE, Brahmachary PP, June RK. Correlations between metabolites in the synovial fluid and serum: A mouse injury study. J Orthop Res 2022.

110. Zhai G, Wang-Sattler R, Hart DJ, Arden NK, Hakim AJ, Illig T, et al. Serum branched-chain amino acid to histidine ratio: a novel metabolomic biomarker of knee osteoarthritis. Ann Rheum Dis 2010; 69: 1227-1231.

111. Zhang Q, Li H, Zhang Z, Yang F, Chen J. Serum metabolites as potential biomarkers for diagnosis of knee osteoarthritis. Dis Markers 2015; 2015: 684794.

112. Abdelrazig S, Ortori CA, Doherty M, Valdes AM, Chapman V, Barrett DA. Metabolic signatures of osteoarthritis in urine using liquid chromatography-high resolution tandem mass spectrometry. Metabolomics 2021; 17: 29.

113. Loeser RF, Pathmasiri W, Sumner SJ, McRitchie S, Beavers D, Saxena P, et al. Association of urinary metabolites with radiographic progression of knee osteoarthritis in overweight and obese adults: an exploratory study. Osteoarthritis Cartilage 2016; 24: 1479-1486.

114. Carlson AK, Rawle RA, Adams E, Greenwood MC, Bothner B, June RK. Application of global metabolomic profiling of synovial fluid for osteoarthritis biomarkers. Biochem Biophys Res Commun 2018; 499: 182-188.

115. Carlson AK, Rawle RA, Wallace CW, Adams E, Greenwood MC, Bothner B, et al. Global metabolomic profiling of human synovial fluid for rheumatoid arthritis biomarkers. Clin Exp Rheumatol 2019; 37: 393-399.

116. Carlson AK, Rawle RA, Wallace CW, Brooks EG, Adams E, Greenwood MC, et al. Characterization of synovial fluid metabolomic phenotypes of cartilage morphological changes associated with osteoarthritis. Osteoarthritis Cartilage 2019; 27: 1174-1184.

117. Cui Z, Liu K, Wang A, Liu S, Wang F, Li J. Correlation between sialic acid levels in the synovial fluid and the radiographic severity of knee osteoarthritis. Exp Ther Med 2014; 8: 255-259.

118. Kim S, Hwang J, Kim J, Ahn JK, Cha HS, Kim KH. Metabolite profiles of synovial fluid change with the radiographic severity of knee osteoarthritis. Joint Bone Spine 2017; 84: 605-610.

119. Kim S, Hwang J, Kim J, Lee SH, Cheong YE, Lee S, et al. Metabolic discrimination of synovial fluid between rheumatoid arthritis and osteoarthritis using gas chromatography/time-of-flight mass spectrometry. Metabolomics 2022; 18: 48.

120. Kim S, Hwang J, Xuan J, Jung YH, Cha HS, Kim KH. Global metabolite profiling of synovial fluid for the specific diagnosis of rheumatoid arthritis from other inflammatory arthritis. PLoS One 2014; 9: e97501.

121. Mickiewicz B, Heard BJ, Chau JK, Chung M, Hart DA, Shrive NG, et al. Metabolic profiling of synovial fluid in a unilateral ovine model of anterior cruciate ligament reconstruction of the knee suggests biomarkers for early osteoarthritis. J Orthop Res 2015; 33: 71-77.

122. Nieminen P, Hamalainen W, Savinainen J, Lehtonen M, Lehtiniemi S, Rinta-Paavola J, et al. Metabolomics of Synovial Fluid and Infrapatellar Fat Pad in Patients with Osteoarthritis or Rheumatoid Arthritis. Inflammation 2022; 45: 1101-1117.

CHAPTER TWO

OSTEOARTHRITIS AND METABOLISM: WHAT YOU KNEE-D TO KNOW

Contribution of Authors and Co-Authors

Manuscript in Chapter 2

Author: Hope D. Welhaven

Contributions: Conceptualization, Literature Assessment, Curation, Writing – original draft, review, and editing.

Co-Author: Avery H. Welfley

Contributions: Conceptualization, Literature Assessment, Curation, Writing – original draft, review, and editing.

Co-Author: Brian Bothner

Contributions: Writing – review and editing.

Co-Author: Ronald K. June

Contributions: Validation, Writing – review and editing, Supervision, Funding Acquisition.

Manuscript Information

Hope D. Welhaven, Avery H. Welfley, Brian Bothner, Ronald K. June

Status of Manuscript:
☐ Prepared for submission to a peer-reviewed journal
X Officially submitted to a peer-reviewed journal
☐ Accepted by a peer-reviewed journal
☐ Published in a peer-reviewed journal

Abstract

Osteoarthritis (OA) is a disease of the whole joint where degeneration of various tissues including cartilage, bone, synovium, and others manifests as pain, loss of function, and ultimately joint failure. Most current treatments and interventions are not proactive in nature, ranging from nonpharmacological to total joint arthroplasty. To positively influence prevention measures, treatment options, and advance biomarker identification, recent studies investigated the role of metabolism and metabolic alterations across joint tissues in response to disease and risk factors such as injury. Therefore, the aim of this review is to elucidate musculoskeletal tissue metabolism during times of health and disease and to shed light on the biochemical crosstalk between tissues that contribute to OA development and progression.

Introduction

Osteoarthritis (OA), characterized by the breakdown of cartilage and other tissues, is the leading cause of disability worldwide. Since 1999, prevalent cases of OA have increased by 114.5%[1]. This disease has culminated in extensive economic toil, costing the US approximately $185 billion annually[2]. Increased pain and limited mobility result in reduced quality of life for those suffering with OA. Despite the immense economic and physical burdens of OA, most treatments remain costly and frequently do not lead to complete resolution of symptoms. These typically include encompassing pain management, physical therapy, and ultimately total joint replacement[3].

While OA research has predominantly centered around cartilage, the pathological and metabolic perturbations of OA encompass a significantly broader spectrum of tissues. Beyond

cartilage degeneration, pathological hallmarks of OA include osteophyte formation, bone sclerosis, synovitis, and changes in synovial fluid (SF) viscosity, among many others[4]. At the heart of these pathological changes lies imbalanced metabolism, which plays a pivotal role in driving the observed changes in affected tissues and fluids.

Metabolism, consisting of anabolic and catabolic activity, is composed of thousands of interconnected reactions. Central metabolism involves cellular energy where adenosine-monophosphate (ATP) is the most common energy currency in biological systems. The extraction of this energy involves metabolic pathways including glycolysis, the TCA cycle, oxidative phosphorylation, and closely related pathways like the pentose phosphate pathway, fatty acid oxidation, and many others. In brief, large molecules are broken down into smaller ones, such as glucose, which can then be metabolized to simpler fuel molecules, like acetyl-CoA, and then completely oxidized to generate ATP via the TCA cycle and oxidative phosphorylation (Fig. 2.1). Dependent on cellular needs and demands, metabolic regulation is fluid where it functions to provide ATP as well as building blocks for important biomolecules like nucleotide bases and proteins.

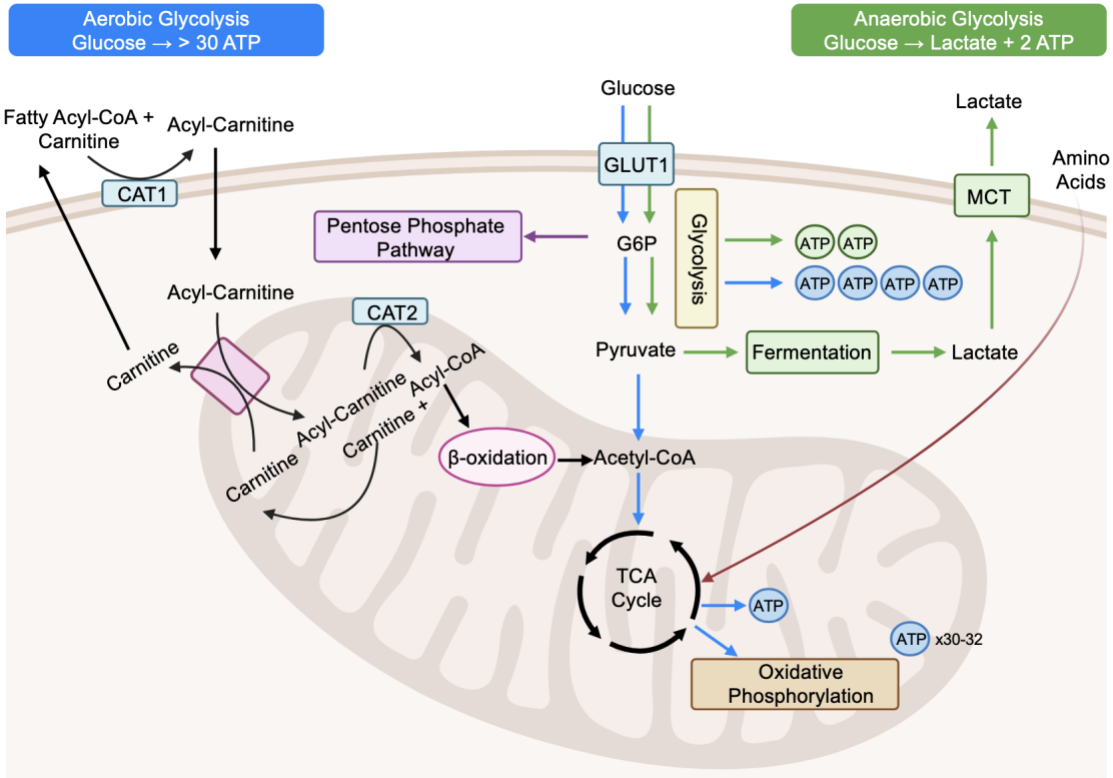

Figure 2.1. Overview of central energy metabolic pathways. Adenosine-triphosphate (ATP) serves as the primary energy currency in various biological systems and tissues such as muscloskeletal tissues. Key energy metabolic regulation centers around bioenergetic fuels such as glucose, lipids, and amino acids. Glucose is able to enter the cell via glucose transporter 1 (GLUT1) where it is converted to glucose-6-phosphate (G6P). This intermediate is interconnected to multiple metabolic pathways like the pentose phosphate pathway and depending on the hosts needs and demands, aerobic or anaerobic glycolysis can be executed each yielding different amounts of ATP. Anaerobic glycolysis, also known as the Warburg Effect, involves the conversion of pyruvate to lactate via fermentation, which is then transported out of the cell via monocarboxylate transporters (MCT). This type of respiration yields one lactate and two ATPs per glucose. In comparison, aerobic glycolysis involves the conversion of G6P to pyruvate, and is further metabolize through the TCA cycle and oxidative phosphorylation to yield 30-32 molecules of ATP per glucose molecule. Beyond glycolysis, fatty acids can be utilized to yield ATP through transportation into the cell via the carnitine shuttle, then oxidized via β-oxidation. Moreover, numerous lipid-related metabolic pathways contribute to the bioenergetic state of the cell and production of ATP. The interconnectedness and orchestration these pathways contribute to the extraciton of energy and are paramount to homeostatic regulation, adapating to the hosts needs and demands. Adenosine-triphosphate – ATP; Glucose transporter 1 – GLUT1; glucose-6-phosphate – G6P; monocarboxylate transporter – MCT; triboxylic acid cycle – TCA cycle; carnitine-acyl transferse 1 – CAT1; carnitine-acyl transferse 2 – CAT2.

Recent studies examine the heterogenous pathology of OA and emphasize the significance of metabolism in disease progression. Specifically, the disruption of metabolic activity and intricate biochemical crosstalk among various tissues and cell types are key contributors to the disease process. Examining the metabolism of musculoskeletal tissues in both healthy and diseased states, coupled with uncovering the intricate biochemical interactions between tissues, provides deep insight into understanding the complexities underlying the onset and progression of OA (Fig. 2.2). A comprehensive understanding of OA metabolism from a whole-joint perspective may aid in identifying biomarker or pathway targets to slow, halt, or reverse disease. This review aims to summarize musculoskeletal tissue metabolism spanning cartilage, bone, synovium, SF, and circulatory fluids while discussing potential biochemical regulation and crosstalk that contributes to advancing our knowledge of OA.

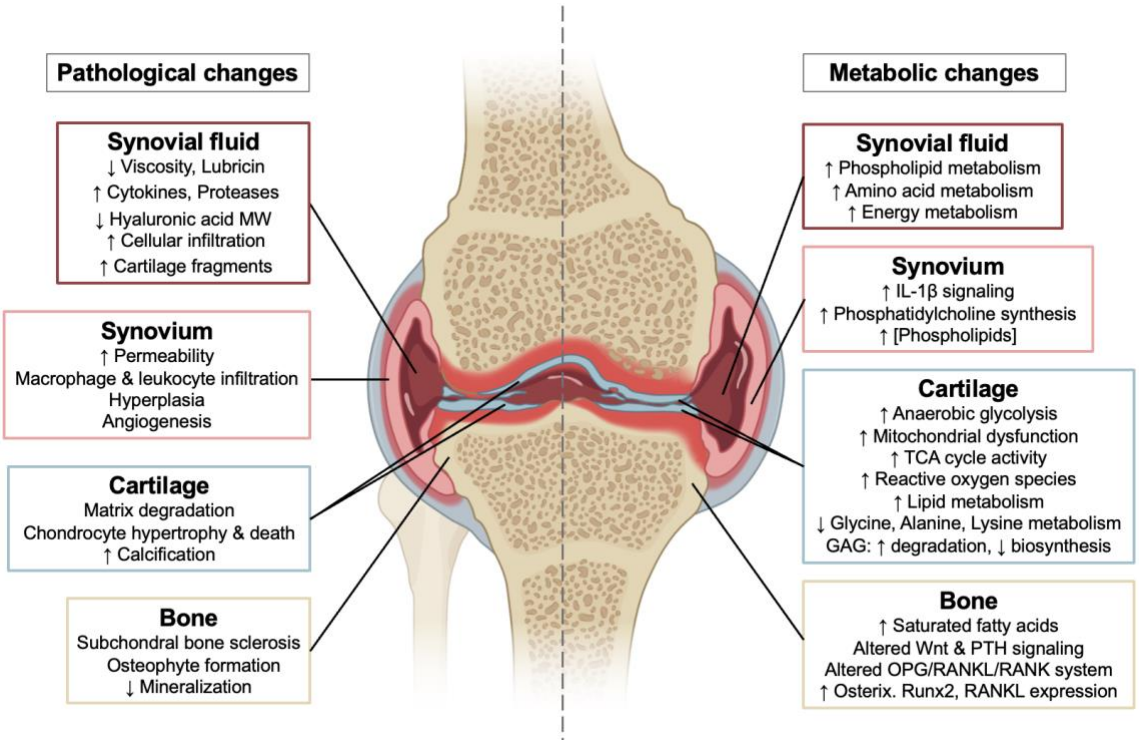

Figure 2.2. Pathological and metabolic changes manifest across musculoskeletal tissues in the wake of osteoarthritis (OA) onset. Within osteoarthritic bone, cartilage, synovium, and synovial fluid, diverse metabolic pathways including phospholipid, amino acid, and energy pathways, undergo discernible changes. Notably, broader metabolic activities such as Wnt and PTH signaling are altered in OA bone. It is hypothesized that these metabolic shifts physically manifest as pathological changes. These alterations encompass a decrease in synovial fluid viscosity and joint lubrication, increased permeability and hyperplasia of synovium, degradation of cartilage matrix, and sclerosis with heightened mineralizing in bone. Collectively, OA extends its impact beyond cartilage, exerting negative influences metabolically and pathologically on various joint tissues, structures, and fluids.

Cartilage

Articular cartilage, the soft tissue that lines the end of long bones, provides a smooth surface that allows low-friction articulation, reduces stress on underlying bone, and ultimately allows for pain-free locomotion[5]. This essential tissue is composed of an extracellular matrix (ECM) that surrounds local cartilage cells called chondrocytes. The ECM is composed of 3 main constituents: collagen, proteoglycans, and water— with water making up the majority (80%) of

cartilage mass[5]. Additionally, cartilage is avascular, aneural, and relies on other joint tissues such as underlying subchondral bone and synovial fluid for nutrients and oxygen supply via diffusion[5]. Because oxygen supply is reduced and cells function in a hypoxic state, chondrocytes are sensitive to oxygen influencing metabolism.

Cartilage primarily depends on glucose as its primary energy source to rapidly generate ATP via glycolysis and mitochondrial respiration[6]. Previous studies show that cartilage possesses functional mitochondria that undergo mitochondrial respiration, and that glucose and lipids are both relied on as energy sources[7]. However, OA perturbs mitochondrial homeostasis and activity, causing mitochondria to rely more on lipids leading to lipid accumulation[8]. This marked sign of perturbed mitochondrial homeostasis leads to elevated reactive oxygen species, increased nitric oxide production, and a compromised stress-response[9-11]. Additionally, several other key pathways and metabolic mechanisms are dysregulated and have been implicated in OA-induced cartilage degeneration including increased oxidative stress, cytokine-induced inflammation, matrix catabolism, and calcification— which compound to trigger chondrocyte hypertrophy and death[12]. Contrary to the historical view of dominant anaerobic glycolysis in chondrocytes, recent studies provide evidence that chondrocytes adapt to undergo aerobic glycolysis, also known as the Warburg effect (Figure 1). Here, the rate of glucose uptake is increased, lactate is preferentially produced even in when oxygen is present, reducing the cell's reliance on mitochondrial respiration as a result of dysfunction[6].

The impact of these metabolic mechanisms during OA progression is substantial. As chondrocytes increase glycolytic dependence on ATP production, TCA cycle activity also increases[13-15]. These TCA activity increases may produce amino acids as precursors for the

synthesis of proteins, such as collagen, to either repair the damaged matrix or to serve as an alternate source for ATP generation to mitigate oxidative damage[16] (Fig. 2.3). Amino acid metabolism changes in human OA cartilage, where glycine and alanine are downregulated as OA progresses[17]. Many studies of synovial fluid also detect perturbed levels of amino acids and associated metabolic pathways in OA. These metabolic changes are hypothesized to exist in joint tissues other than cartilage. We will explore this relationship later in the review.

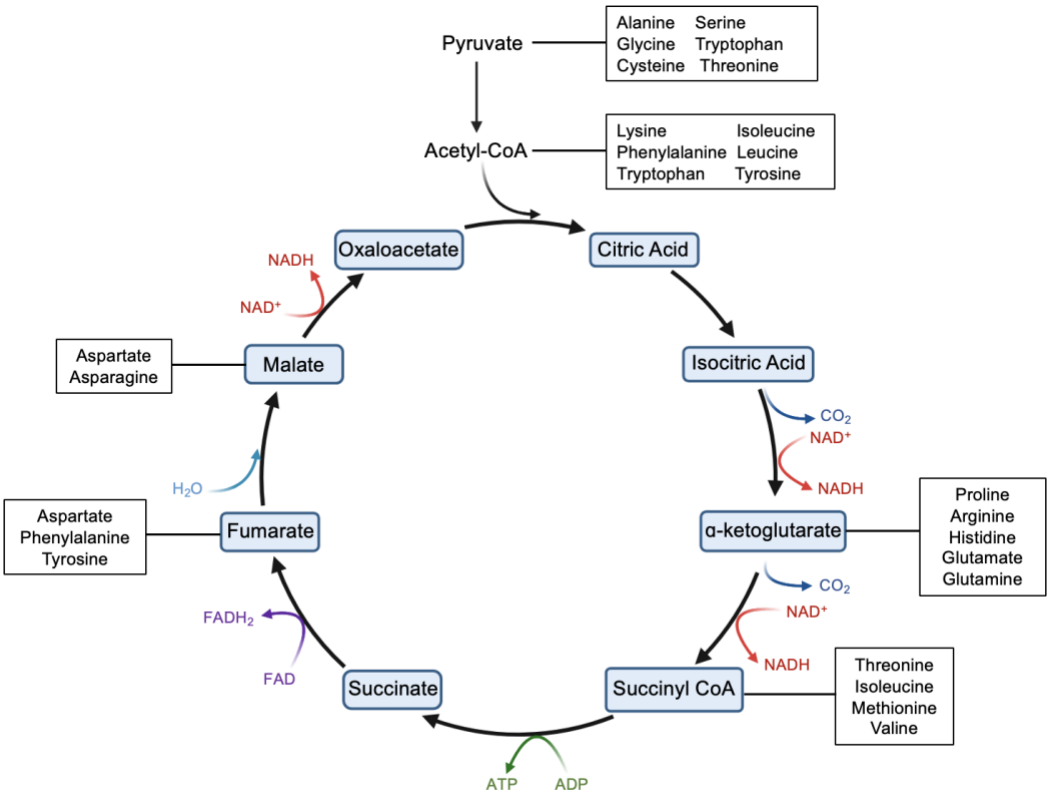

Figure 2.3. Metabolic entry points where amino acids can serve as alternative sources for energy generation. Generation of the major energy currency, adenosine-triphosphate (ATP), is reliant on the tricarboxylic acid (TCA) cycle. Here, amino acids can enter directly through TCA cycle intermediates and be further oxidized and converted into energy. Moreover, when amino acids enter, substrates required for the electron transport chain – NADH, $FADH_2$ – are generated.

Unlike many cells, chondrocytes have ample lipid stores, with linoleic, oleic, and palmitic acids representing 85% of the total stored fatty acids[18]. Furthermore, cartilage has two potential sources of lipid transport from SF and subchondral bone[19] making lipid metabolism an important, but relatively unstudied, avenue of investigation related to cartilage homeostasis and OA pathophysiology. Previous studies find that lipid-associated metabolic changes precede histopathological changes[20]. Arachidonic acid (AA), a type of ω-6 polyunsaturated fatty acid (PUFA), is typically low in concentration in healthy cartilage but increases as OA progresses. Accumulation of AA in diseased cartilage has strong proinflammatory and catabolic effects which further exacerbates metabolic imbalances and cartilage damage[21]. This is further supported by the positive association between levels of AA and cartilage degeneration[22].

In summary, the landscape of OA involves a complex interplay of metabolic shifts within articular cartilage. These shifts encompass elevated glycolysis, mitochondrial alterations, and an increase in TCA cycle activity. Additional investigation into the use of different bioenergetic fuels, like amino acids and lipids, may improve our understanding of metabolic dysfunction in early- and late-stage OA. Collectively, these multifaceted changes contribute to the intricate progression of OA at the cartilage level and highlight the need for additional experiments studying how cartilage metabolism is affected during OA pathogenesis.

Bone

Bone, an integral and dynamic component of synovial joints, not only supports cartilage but also maintains joint homeostasis. However, the role of bone in OA has only recently been recognized. Anomalies in mineralization commonly result in OA-defining characteristics, including sclerosis, osteophyte formation, and bone marrow lesions[23, 24]. At the cellular level, OA

pathogenesis in bone is associated with altered morphology, disrupted metabolic regulation, and apoptosis of bone cells. Coordination of osteoclast, osteoblast, and osteocyte bioenergetics is paramount to maintaining healthy bone. When this coordination is disrupted, there are broad systemic implications that contribute to the development of skeletal diseases like OA.

Osteocytes, the most abundant cell type in bone, are crucial for maintaining bone integrity and homeostasis by supporting bone remodeling, mechanotransduction, and mineralization. Their pivotal role is key to the dysfunction in OA-affected bone, resulting in abnormalities spanning multiple levels: altered lacunae morphology at the tissue level, irregular osteocyte activity, and changes in protein expression at the molecular level[25]. Despite this, relatively few studies have been directed toward understanding osteocyte metabolism in the context of OA. Recent studies illuminate the connection between lipid metabolism, general mitochondrial function, and osteocytes[26-28]. After the liver, bone serves as the second primary organ for lipid uptake. It is plausible that osteocytes are heavily fueled by lipids. Therefore, any disruption could potentially contribute to OA pathogenesis. Notably, saturated fatty acids consumed via diet (i.e., lauric, myristic, palmitic, stearic acid) are associated with osteocyte apoptosis, potentially suggesting a role in OA-related osteocyte death[28]. Furthermore, mitochondrial respiration is greater in osteocytes compared to other bone cell types, with variations in content and activity that depend on regional bone location[27]. Specifically, osteocytes near the periosteal surface have more mitochondria with high activity levels compared to those near the endocortical surface that are less active[26]. Taken together, the diverse role of lipids and changes in mitochondrial dynamics may be important to OA-induced metabolic disturbances.

Osteoclasts— responsible for bone resorption— contribute to whole-body calcium homeostasis and are regulated by numerous molecular signaling pathways like the OPG/RANKL/RANK system[29]. Like osteocytes, osteoclasts depend on mitochondrial respiration for differentiation and function. OPG/RANKL/RANK stimulates mitochondrial biogenesis through the upregulation of Ppar-γC and NF-KB signaling[30-32]. Moreover, the observed upregulation of osteoclastic activities in OA is believed to be modulated by sclerostin and the OPG/RANKL/RANK system[25, 29]. Beyond mitochondria, glucose is also a critical energy source and plays a pivotal role in osteoclast activity by facilitating resorptive functions through aerobic glycolysis[31, 33, 34]. The combination of both glycolytic and oxidative energetic routes is essential, yet further research is needed to unveil the specific details between these mechanisms and OA development.

Osteoblasts—responsible for bone tissue formation—play a critical role in bone pathology. These cells primarily utilize aerobic glycolysis, where lactate production is favored over pyruvate oxidation despite sufficient oxygenation. Data suggest that as much as 80% of osteoblast energy is produced from this pathway[31]. Pathways like parathyroid hormone (PTH) and Wnt/b-catenin signaling influence glucose metabolism, impacting both glycolysis and mitochondrial respiration[35]. Specifically, using an *Igf1* receptor knockout model, PTH stimulates glucose consumption, lactate production, and alters glucose flux through induction of Igf signaling which activates mTORC2 to enhance glycolytic enzyme abundance[36]. PTH can also divert glucose-6-phosphate to the pentose phosphate pathway for potential nucleotide synthesis and to limit pyruvate entry into the TCA cycle (Figure 1). Bypassing the TCA cycle by converting glucose to lactate is not energetically efficient. However, aerobic glycolysis offsets reactive oxygen species

generated when performing oxidative phosphorylation and reduces TCA cycle intermediates (citrate, acetyl-CoA) that influence epigenetic modifications during osteoblast differentiation[31].

Wnt/B-catenin signaling coordinates osteoblast metabolism to meet energy demands required for bone formation and affects fatty acid utilization through receptors like LRP5, LRP6[35, 37], and C36[38, 39]. Importantly, C36 is crucial for lipid transport into osteoblasts. Receptor mutations disrupt downstream fatty acid utilization, later impacting bone volume and fat mass--highlighting their importance in coordinating bone metabolism. Additionally, Wnt/B-catenin signaling modulates the expression of essential genes for bone matrix proteins, like osterix and Runx2, which are increased in OA, indicating intense osteoblastogenesis[40, 41]. Moreover, OA progression shifts bone homeostasis: increased remodeling is observed in early OA compared to a combination of decreased resorption and increased formation later OA[41, 42]. These abnormalities, coupled with reduced mineralization, contribute to the altered bone architecture observed in OA.

Synovial Fluid

The synovial joint cavity is filled with SF that directly contacts many joint tissues (i.e., cartilage, ligaments, meniscus, synovium) that secrete assorted compounds and intermediates into the cavity. The mechanical role of SF is to support low friction between articular cartilage surfaces by lubricating the joint. Three main components of SF that promote lubrication include lubricin[43], hyaluronic acid (HA)[44], and phospholipids (PL)[45]. Alterations in composition and concentration of these molecules lead to insufficient boundary lubrication and cartilage damage[46, 47]. Considering the important role of SF, its proximity to other joint tissues, and the diverse pool of compounds it includes, the molecular content of this fluid directly reflects local changes within the joint. As such, it is a useful sample for investigating joint homeostasis and pathophysiology.

Several human and animal studies examine both healthy and diseased SF metabolism to better understand overall joint health, pinpoint disease-associated changes, and disentangle the effects of common OA risk factors. Of these, metabolic differences and mechanisms commonly detected between osteoarthritic and healthy SF are associated with amino acid, energy, inflammatory, steroid, and lipid-related pathways.

Perturbed SF metabolism serves as an indicator of OA-induced metabolic changes in neighboring joint tissues. Lubricin depletion highlights the catabolic activity of OA and how it reduces chondroprotection[43, 47]. Additionally, HA molecular weight in SF is greatly reduced in OA. This is attributed to enzymatic breakdown and synovial membrane changes consequently impacting SF viscosity[48]. Numerous studies link a range of diverse fatty acids to OA progression and inflammation. ω-3-PUFAs reduce inflammatory markers and cartilage degeneration, while ω-6-PUFAs increase these markers[49]. ω-3 and ω-6 PUFA serum levels correlate with clinical features of OA like synovitis and histological disease severity[18, 50]. Arachidonic Acid (AA), a type of ω-6 PUFA, decreases as OA advances[51], yet metabolites and pathways associated with AA are higher in OA SF than healthy SF[52]. Moreover, these same regulation patterns have been detected in OA cartilage and bone, suggesting that SF reflects metabolic status of nearby joint tissues.

Synovial fluid contains the principal phospholipid classes: phosphatidylcholines (PC), lysophosphotidylcholines (LPC), and sphingomyelins (SM)[46]. These PL species help build and support cell membrane function, offer protection, and impact metabolic function. The relationships between SF, cartilage, and PLs are paramount to joint health. Cartilage has a ~20-um superficial layer that attracts outward-oriented PLs, creating a hydrophobic surface[53] that enhances lubricated, pain-free movement[45, 47]. Previous studies find elevated PL levels in OA SF compared to controls

and between early and late-stage OA SF[46, 47, 54, 55]. These changes likely relate to damaged cartilage and worsened joint disease and may indicate the need to replenish this surface layer. Fibroblast-like synoviocytes (FLS) may contribute, but further research is needed to understand the cellular sources of increased PL levels in OA SF and how lubrication safeguards cartilage. Additionally, the transport of fatty acids into the mitochondria for beta-oxidation, a process mediated by carnitines and associated metabolites, is perturbed during disease progression. Dysregulation of fatty acids, acylcarnitines, and the carnitine shuttle are found in both rheumatoid arthritis (RA) and OA[56-58].

Amino acids, including proline, arginine, serine, and asparagine have been detected in SF and linked to OA. Dysregulation of these amino acids and related pathways may reflect energy usage and protein synthesis in tissues like cartilage and bone to counteract OA-related degradation (Figure 3). Notably, SF asparagine is higher in human OA compared to RA[59]. In a sheep study of post-injury SF changes, serine and asparagine were initially detected but decreased over time. Proline, derived from arginine, contributes to collagen synthesis and both have been implicated in OA development through analysis of human SF[56, 59] and cartilage[60] from OA patients. Similarly, a mouse model of post-injury SF changes found both amino acids at high concentrations initially, tapering over time. Hence, arginine and proline levels in SF may (1) indicate disrupted joint tissue metabolism and (2) offer protective effects due to their relationship with collagen synthesis.

Synovium

The synovium is a thin connective tissue separating the joint capsule and cavity. It contains 1-3 layers of specialized columnar fibroblast-like synoviocytes (FLS) and macrophages. This dynamic tissue serves as a major source of SF components like lubricin and HA[61]. It provides

essential nutrients, MMPs, and maintains anabolic and catabolic activities for proper joint function. Synovial membrane permeability controls the flow of metabolites between the joint capsule and cavity, allowing growth factors and cytokines to diffuse through while retaining HA and lubricin[62, 63]. OA-associated inflammation alters synovium permeability, causing the release of joint tissue breakdown products into the cavity. Lining cells activate endothelial cells promoting the formation of new blood vessels and infiltration of cytokines and leukocytes. This influx of immune cells results in synovial hyperplasia, fibrosis, angiogenesis, and downstream phenotypic shifts in other joint tissues and chondrocyte-related cell types[64, 65]. Consequently, synovial inflammation (i.e., synovitis) is common in OA patients and correlates with radiographic progression of knee OA[66].

Under normal conditions, the synovium primarily uses both glycolysis and oxidative phosphorylation for ATP production. However, inflammatory stimuli and other stresses alter glucose metabolism via glucose transporter 1 to accommodate the increased demand for ATP. Comparing OA and RA fibroblast-like synoviocytes, fatty and organic acid-related metabolites were elevated in OA, influencing glycolysis, pentose phosphate pathway, and amino acid metabolism[67]. Such changes likely reflect inflammation and hyperplasia experienced during OA, but further investigation is required.

Cytokines and different lipid species are altered in OA synovium and are proposed to regulate synovial inflammation. Levels of AA, stearic acid, and oleic acid are elevated in OA synovium compared to healthy controls suggesting altered fatty acid metabolism which could explain fatty acid accumulation observed in OA cartilage[68]. Prostaglandins, a type of eicosanoid derived from AA, are released in the early stages of inflammation resulting in the recruitment and activation of immune cells and other lipid species like PLs[69]. Comparing hyperplastic synovial

tissue between OA and healthy patients, PCs were the most variable between diseased states and were notably enriched in OA samples[70]. The activation and regulation of PC synthesis is influenced by IL-1β signaling in the FLS in OA synovium[71]. Moreover, synovial IL-1β signaling decreases aggrecan expression[72], collagen synthesis in chondrocytes[73], and regulation of proteolytic enzymes like MMP-13[74] and ADAMTS-4[75]. Other studies find enriched PC concentration in OA SF[46]. Taken together, the increased levels of PCs due to IL-1β signaling-driven PC synthesis in OA synovium highlights the complex interplay between the synovium, SF, and the entire joint.

Plasma/Others

In recent years, extensive efforts sought biomarkers of OA that serve as indicators of pathogenesis and disease progression. Among these, only a few studies explored the association between plasma and SF in OA. Identification of SF surrogates in plasma would be a major advance because SF harvest is challenging. To validate this, one study obtained blood plasma and SF from OA patients to investigate associations and correlations between metabolites in each sample type[76]. Highly correlated metabolites and pathways between plasma and SF may indicate systemic metabolic regulation. These involve various PC and SM species and general lipid metabolism. Moderately correlated metabolites and pathways between sample types include amino acid metabolism, urea cycle, TCA cycle, energy metabolism, and carbohydrate metabolism that suggest localized metabolism within the SF joint space[76].

Lipid profiles of both serum and SF are potential predictors of OA progression including synovitis and OA severity[77]. Specifically, serum ω-6 PUFAs positively correlate with joint degeneration and systemic inflammatory cytokines, while saturated fatty acids negatively correlate

with joint degradation. Plasma ω-3 and ω-6 PUFAs are positively associated with synovitis[77], suggesting these lipid species plays a role in structural changes during OA.

In plasma alone, a handful of studies examine the relationship between amino acid concentration and OA. There are low levels of anti-inflammatory amino acids, like asparagine and arginine, in serum from OA patients[78, 79]. Arginine's metabolic versatility allows it to be metabolized either in the urea cycle, serving as a precursor to nitric oxide[76, 80] — an OA-related catabolic factor— or catabolized to produce other intermediates like ornithine, a crucial precursor for collagen that also increases in OA patients. Hence to repair damaged cartilage, arginine may also be catabolized during OA progression, giving rise to ornithine via the ornithine pathway to foster downstream collagen production. In addition to amino acid metabolism, lipid metabolism and concentrations of AA and PLs (i.e., LPCs, PCs) are altered in plasma from OA patients. Notably, lipid concentration further differentiates OA patients with more moderate disease from those in the early stages of OA[81].

Future Directions

While many studies provide a knowledge base for the metabolism of musculoskeletal tissues affected by OA, additional research is needed to compare multiple tissues synchronously and better understand OA as a disease of the whole joint. Moreover, it is crucial to recognize that numerous OA risk factors, such as age, obesity, diet, joint loading, and others, influence metabolism. Obesity, the most modifiable OA risk factor, affects OA pathogenesis through excessive loading, altered biomechanics, and cytokine dysregulation[82]. Previous studies explored the relationship between obesity and OA in both weight-bearing and non-weight bearing joints, suggesting metabolism contributes to OA development in obese individuals[83, 84]. Thus, weight loss

interventions, including both physical activity and dietary changes, are recommended as they have demonstrated efficacy in alleviating OA symptoms. Beyond obesity, females often experience more severe OA, potentially attributed to hormonal differences[85]. Collectively, patient-specific risk factors and lifestyle significantly influence metabolism, underscoring the need for further investigation into the intricate relationship between OA, its development, and metabolism.

Conclusions

OA is a whole joint disease that affects articular cartilage, bone, synovium, and other crucial tissues and structures. Metabolic homeostasis of each component is paramount to maintaining joint health and when perturbed, the joint is negatively influenced throughout. Dissecting musculoskeletal tissue metabolism and unraveling the complex biochemical interplay between tissues, provides a profound perspective for comprehending the intricacies of OA's development and progression (Figure 2). Moreover, exploring novel metabolic perturbations within and between tissues provides novel avenues for preventative measures and interventions to improve the quality of life of OA patients. While this review provides a broad perspective of OA metabolism, expansion of these studies may provide additional mechanistic insight to better characterize the metabolic landscape of osteoarthritis.

Abbreviation List

OA = osteoarthritis; SF = synovial fluid; ECM = extracellular matrix, ATP = adenosine triphosphate; TCA = tricarboxylic acid; AA = arachidonic acid; PUFA = polyunsaturated fatty acid; ALK = activin receptor-like kinase; SBP = subchondral bone plate; HA = hyaluronic acid;

PL = phospholipid; PC = phosphatidylcholine; LPC = lysophosphotidylcholine; SM = sphingomyelin; FLS = fibroblast-like synoviocytes; RA = rheumatoid arthritis

References

1. Long H, Liu Q, Yin H, Wang K, Diao N, Zhang Y, et al. Prevalence trends of site-specific osteoarthritis from 1990 to 2019: findings from the Global Burden of Disease Study 2019. Arthritis Rheumatol 2022.

2. Bitton R. The economic burden of osteoarthritis. Am J Manag Care 2009; 15: S230-235.

3. Sinusas K. Osteoarthritis: diagnosis and treatment. Am Fam Physician 2012; 85: 49-56.

4. Poulet B, Staines KA. New developments in osteoarthritis and cartilage biology. Curr Opin Pharmacol 2016; 28: 8-13.

5. Sophia Fox AJ, Bedi A, Rodeo SA. The basic science of articular cartilage: structure, composition, and function. Sports Health 2009; 1: 461-468.

6. June RK, Liu-Bryan R, Long F, Griffin TM. Emerging role of metabolic signaling in synovial joint remodeling and osteoarthritis. J Orthop Res 2016; 34: 2048-2058.

7. Coleman MC, Ramakrishnan PS, Brouillette MJ, Martin JA. Injurious Loading of Articular Cartilage Compromises Chondrocyte Respiratory Function. Arthritis Rheumatol 2016; 68: 662-671.

8. Dalmao-Fernandez A, Lund J, Hermida-Gomez T, Vazquez-Mosquera ME, Rego-Perez I, Blanco FJ, et al. Impaired Metabolic Flexibility in the Osteoarthritis Process: A Study on Transmitochondrial Cybrids. Cells 2020; 9.

9. Lane RS, Fu Y, Matsuzaki S, Kinter M, Humphries KM, Griffin TM. Mitochondrial respiration and redox coupling in articular chondrocytes. Arthritis Res Ther 2015; 17: 54.

10. Smith RL, Soeters MR, Wust RCI, Houtkooper RH. Metabolic Flexibility as an Adaptation to Energy Resources and Requirements in Health and Disease. Endocr Rev 2018; 39: 489-517.

11. Wu L, Liu H, Li L, Liu H, Cheng Q, Li H, et al. Mitochondrial pathology in osteoarthritic chondrocytes. Curr Drug Targets 2014; 15: 710-719.

12. Blanco FJ, Rego I, Ruiz-Romero C. The role of mitochondria in osteoarthritis. Nat Rev Rheumatol 2011; 7: 161-169.

13. Jutila AA, Zignego DL, Hwang BK, Hilmer JK, Hamerly T, Minor CA, et al. Candidate mediators of chondrocyte mechanotransduction via targeted and untargeted metabolomic measurements. Arch Biochem Biophys 2014; 545: 116-123.

14. Welhaven HD, McCutchen CN, June RK. Effects of mechanical stimulation on metabolomic profiles of SW1353 chondrocytes: shear and compression. Biol Open 2022; 11.

15. Zignego DL, Hilmer JK, June RK. Mechanotransduction in primary human osteoarthritic chondrocytes is mediated by metabolism of energy, lipids, and amino acids. J Biomech 2015; 48: 4253-4261.

16. Li Y, Xiao W, Luo W, Zeng C, Deng Z, Ren W, et al. Alterations of amino acid metabolism in osteoarthritis: its implications for nutrition and health. Amino Acids 2016; 48: 907-914.

17. Shet K, Siddiqui SM, Yoshihara H, Kurhanewicz J, Ries M, Li X. High-resolution magic angle spinning NMR spectroscopy of human osteoarthritic cartilage. NMR Biomed 2012; 25: 538-544.

18. Lippiello L, Walsh T, Fienhold M. The association of lipid abnormalities with tissue pathology in human osteoarthritic articular cartilage. Metabolism 1991; 40: 571-576.

19. Wang Y, Wei L, Zeng L, He D, Wei X. Nutrition and degeneration of articular cartilage. Knee Surg Sports Traumatol Arthrosc 2013; 21: 1751-1762.

20. Park S, Baek IJ, Ryu JH, Chun CH, Jin EJ. PPARalpha-ACOT12 axis is responsible for maintaining cartilage homeostasis through modulating de novo lipogenesis. Nat Commun 2022; 13: 3.

21. Ioan-Facsinay A, Kloppenburg M. Bioactive lipids in osteoarthritis: risk or benefit? Curr Opin Rheumatol 2018; 30: 108-113.

22. Attur M, Krasnokutsky S, Statnikov A, Samuels J, Li Z, Friese O, et al. Low-grade inflammation in symptomatic knee osteoarthritis: prognostic value of inflammatory plasma lipids and peripheral blood leukocyte biomarkers. Arthritis Rheumatol 2015; 67: 2905-2915.

23. Chiba K, Nango N, Kubota S, Okazaki N, Taguchi K, Osaki M, et al. Relationship between microstructure and degree of mineralization in subchondral bone of osteoarthritis: a synchrotron radiation microCT study. J Bone Miner Res 2012; 27: 1511-1517.

24. Hunter DJ, Gerstenfeld L, Bishop G, Davis AD, Mason ZD, Einhorn TA, et al. Bone marrow lesions from osteoarthritis knees are characterized by sclerotic bone that is less well mineralized. Arthritis Res Ther 2009; 11: R11.

25. Zhang L, Wen C. Osteocyte Dysfunction in Joint Homeostasis and Osteoarthritis. Int J Mol Sci 2021; 22.

26. Frikha-Benayed D, Basta-Pljakic J, Majeska RJ, Schaffler MB. Regional differences in oxidative metabolism and mitochondrial activity among cortical bone osteocytes. Bone 2016; 90: 15-22.

27. Schilling K, Brown E, Zhang X. NAD(P)H autofluorescence lifetime imaging enables single cell analyses of cellular metabolism of osteoblasts in vitro and in vivo via two-photon microscopy. Bone 2022; 154: 116257.

28. Sekar S, Shafie SR, Prasadam I, Crawford R, Panchal SK, Brown L, et al. Saturated fatty acids induce development of both metabolic syndrome and osteoarthritis in rats. Sci Rep 2017; 7: 46457.

29. Palumbo C, Ferretti M. The Osteocyte: From "Prisoner" to "Orchestrator". J Funct Morphol Kinesiol 2021; 6.

30. Datta HK, Ng WF, Walker JA, Tuck SP, Varanasi SS. The cell biology of bone metabolism. J Clin Pathol 2008; 61: 577-587.

31. Long F. Glucose metabolism in skeletal cells. Bone Rep 2022; 17: 101640.

32. Zeng R, Faccio R, Novack DV. Alternative NF-kappaB Regulates RANKL-Induced Osteoclast Differentiation and Mitochondrial Biogenesis via Independent Mechanisms. J Bone Miner Res 2015; 30: 2287-2299.

33. Li B, Lee WC, Song C, Ye L, Abel ED, Long F. Both aerobic glycolysis and mitochondrial respiration are required for osteoclast differentiation. FASEB J 2020; 34: 11058-11067.

34. Williams JP, Blair HC, McDonald JM, McKenna MA, Jordan SE, Williford J, et al. Regulation of osteoclastic bone resorption by glucose. Biochem Biophys Res Commun 1997; 235: 646-651.

35. Alekos NS, Moorer MC, Riddle RC. Dual Effects of Lipid Metabolism on Osteoblast Function. Front Endocrinol (Lausanne) 2020; 11: 578194.

36. Esen E, Lee SY, Wice BM, Long F. PTH Promotes Bone Anabolism by Stimulating Aerobic Glycolysis via IGF Signaling. J Bone Miner Res 2015; 30: 1959-1968.

37. Teufel S, Hartmann C. Wnt-signaling in skeletal development. Curr Top Dev Biol 2019; 133: 235-279.

38. Glatz JF, Luiken JJ, Bonen A. Membrane fatty acid transporters as regulators of lipid metabolism: implications for metabolic disease. Physiol Rev 2010; 90: 367-417.

39. Kevorkova O, Martineau C, Martin-Falstrault L, Sanchez-Dardon J, Brissette L, Moreau R. Low-bone-mass phenotype of deficient mice for the cluster of differentiation 36 (CD36). PLoS One 2013; 8: e77701.

40. Dragojevic J, Logar DB, Komadina R, Marc J. Osteoblastogenesis and adipogenesis are higher in osteoarthritic than in osteoporotic bone tissue. Arch Med Res 2011; 42: 392-397.

41. Maruotti N, Corrado A, Cantatore FP. Osteoblast role in osteoarthritis pathogenesis. J Cell Physiol 2017; 232: 2957-2963.

42. Findlay DM, Atkins GJ. Osteoblast-chondrocyte interactions in osteoarthritis. Curr Osteoporos Rep 2014; 12: 127-134.

43. Jay GD, Torres JR, Warman ML, Laderer MC, Breuer KS. The role of lubricin in the mechanical behavior of synovial fluid. Proc Natl Acad Sci U S A 2007; 104: 6194-6199.

44. Schmidt TA, Gastelum NS, Nguyen QT, Schumacher BL, Sah RL. Boundary lubrication of articular cartilage: role of synovial fluid constituents. Arthritis Rheum 2007; 56: 882-891.

45. Schwarz IM, Hills BA. Surface-active phospholipid as the lubricating component of lubricin. Br J Rheumatol 1998; 37: 21-26.

46. Kosinska MK, Liebisch G, Lochnit G, Wilhelm J, Klein H, Kaesser U, et al. A lipidomic study of phospholipid classes and species in human synovial fluid. Arthritis Rheum 2013; 65: 2323-2333.

47. Kosinska MK, Ludwig TE, Liebisch G, Zhang R, Siebert HC, Wilhelm J, et al. Articular Joint Lubricants during Osteoarthritis and Rheumatoid Arthritis Display Altered Levels and Molecular Species. PLoS One 2015; 10: e0125192.

48. Fraser JR, Laurent TC, Laurent UB. Hyaluronan: its nature, distribution, functions and turnover. J Intern Med 1997; 242: 27-33.

49. Bagga D, Wang L, Farias-Eisner R, Glaspy JA, Reddy ST. Differential effects of prostaglandin derived from omega-6 and omega-3 polyunsaturated fatty acids on COX-2 expression and IL-6 secretion. Proc Natl Acad Sci U S A 2003; 100: 1751-1756.

50. Baker KR, Matthan NR, Lichtenstein AH, Niu J, Guermazi A, Roemer F, et al. Association of plasma n-6 and n-3 polyunsaturated fatty acids with synovitis in the knee: the MOST study. Osteoarthritis Cartilage 2012; 20: 382-387.

51. Van de Vyver A, Clockaerts S, van de Lest CHA, Wei W, Verhaar J, Van Osch G, et al. Synovial Fluid Fatty Acid Profiles Differ between Osteoarthritis and Healthy Patients. Cartilage 2020; 11: 473-478.

52. Carlson AK, Rawle RA, Wallace CW, Brooks EG, Adams E, Greenwood MC, et al. Characterization of synovial fluid metabolomic phenotypes of cartilage morphological changes associated with osteoarthritis. Osteoarthritis Cartilage 2019; 27: 1174-1184.

53. Sarma AV, Powell GL, LaBerge M. Phospholipid composition of articular cartilage boundary lubricant. J Orthop Res 2001; 19: 671-676.

54. Antonacci JM, Schmidt TA, Serventi LA, Cai MZ, Shu YL, Schumacher BL, et al. Effects of equine joint injury on boundary lubrication of articular cartilage by synovial fluid: role of hyaluronan. Arthritis Rheum 2012; 64: 2917-2926.

55. Brouwers H, von Hegedus J, Toes R, Kloppenburg M, Ioan-Facsinay A. Lipid mediators of inflammation in rheumatoid arthritis and osteoarthritis. Best Pract Res Clin Rheumatol 2015; 29: 741-755.

56. Carlson AK, Rawle RA, Adams E, Greenwood MC, Bothner B, June RK. Application of global metabolomic profiling of synovial fluid for osteoarthritis biomarkers. Biochem Biophys Res Commun 2018; 499: 182-188.

57. Surowiec I, Arlestig L, Rantapaa-Dahlqvist S, Trygg J. Metabolite and Lipid Profiling of Biobank Plasma Samples Collected Prior to Onset of Rheumatoid Arthritis. PLoS One 2016; 11: e0164196.

58. Zhang W, Likhodii S, Zhang Y, Aref-Eshghi E, Harper PE, Randell E, et al. Classification of osteoarthritis phenotypes by metabolomics analysis. BMJ Open 2014; 4: e006286.

59. Anderson JR, Chokesuwattanaskul S, Phelan MM, Welting TJM, Lian LY, Peffers MJ, et al. (1)H NMR Metabolomics Identifies Underlying Inflammatory Pathology in Osteoarthritis and Rheumatoid Arthritis Synovial Joints. J Proteome Res 2018; 17: 3780-3790.

60. Xu Z, Chen T, Luo J, Ding S, Gao S, Zhang J. Cartilaginous Metabolomic Study Reveals Potential Mechanisms of Osteophyte Formation in Osteoarthritis. J Proteome Res 2017; 16: 1425-1435.

61. Smith MD. The normal synovium. Open Rheumatol J 2011; 5: 100-106.

62. Decker B, Mc KB, Mc GW, Slocumb CH. Comparative distribution of proteins and glycoproteins of serum and synovial fluid. Arthritis Rheum 1959; 2: 162-177.

63. Swann DA, Radin EL, Nazimiec M, Weisser PA, Curran N, Lewinnek G. Role of hyaluronic acid in joint lubrication. Ann Rheum Dis 1974; 33: 318-326.

64. Fernandes JC, Martel-Pelletier J, Pelletier JP. The role of cytokines in osteoarthritis pathophysiology. Biorheology 2002; 39: 237-246.

65. Mathiessen A, Conaghan PG. Synovitis in osteoarthritis: current understanding with therapeutic implications. Arthritis Res Ther 2017; 19: 18.

66. Ayral X, Pickering EH, Woodworth TG, Mackillop N, Dougados M. Synovitis: a potential predictive factor of structural progression of medial tibiofemoral knee osteoarthritis -- results of a 1 year longitudinal arthroscopic study in 422 patients. Osteoarthritis Cartilage 2005; 13: 361-367.

67. Ahn JK, Kim S, Hwang J, Kim J, Kim KH, Cha HS. GC/TOF-MS-based metabolomic profiling in cultured fibroblast-like synoviocytes from rheumatoid arthritis. Joint Bone Spine 2016; 83: 707-713.

68. Cillero-Pastor B, Eijkel G, Kiss A, Blanco FJ, Heeren RM. Time-of-flight secondary ion mass spectrometry-based molecular distribution distinguishing healthy and osteoarthritic human cartilage. Anal Chem 2012; 84: 8909-8916.

69. Lawrence T, Willoughby DA, Gilroy DW. Anti-inflammatory lipid mediators and insights into the resolution of inflammation. Nat Rev Immunol 2002; 2: 787-795.

70. Rocha B, Cillero-Pastor B, Ruiz-Romero C, Paine MRL, Canete JD, Heeren RMA, et al. Identification of a distinct lipidomic profile in the osteoarthritic synovial membrane by mass spectrometry imaging. Osteoarthritis Cartilage 2021; 29: 750-761.

71. Sluzalska KD, Liebisch G, Lochnit G, Ishaque B, Hackstein H, Schmitz G, et al. Interleukin-1beta affects the phospholipid biosynthesis of fibroblast-like synoviocytes from human osteoarthritic knee joints. Osteoarthritis Cartilage 2017; 25: 1890-1899.

72. Richardson DW, Dodge GR. Effects of interleukin-1beta and tumor necrosis factor-alpha on expression of matrix-related genes by cultured equine articular chondrocytes. Am J Vet Res 2000; 61: 624-630.

73. Goldring MB, Birkhead J, Sandell LJ, Kimura T, Krane SM. Interleukin 1 suppresses expression of cartilage-specific types II and IX collagens and increases types I and III collagens in human chondrocytes. J Clin Invest 1988; 82: 2026-2037.

74. Mengshol JA, Vincenti MP, Coon CI, Barchowsky A, Brinckerhoff CE. Interleukin-1 induction of collagenase 3 (matrix metalloproteinase 13) gene expression in chondrocytes requires p38, c-Jun N-terminal kinase, and nuclear factor kappaB: differential regulation of collagenase 1 and collagenase 3. Arthritis Rheum 2000; 43: 801-811.

75. Tortorella MD, Burn TC, Pratta MA, Abbaszade I, Hollis JM, Liu R, et al. Purification and cloning of aggrecanase-1: a member of the ADAMTS family of proteins. Science 1999; 284: 1664-1666.

76. Zhang W, Likhodii S, Aref-Eshghi E, Zhang Y, Harper PE, Randell E, et al. Relationship between blood plasma and synovial fluid metabolite concentrations in patients with osteoarthritis. J Rheumatol 2015; 42: 859-865.

77. Wu CL, Kimmerling KA, Little D, Guilak F. Serum and synovial fluid lipidomic profiles predict obesity-associated osteoarthritis, synovitis, and wound repair. Sci Rep 2017; 7: 44315.

78. Ohnishi A, Osaki T, Matahira Y, Tsuka T, Imagawa T, Okamoto Y, et al. Correlation of plasma amino acid concentrations and chondroprotective effects of glucosamine and fish collagen peptide on the development of osteoarthritis. J Vet Med Sci 2013; 75: 497-502.

79. Tootsi K, Vilba K, Martson A, Kals J, Paapstel K, Zilmer M. Metabolomic Signature of Amino Acids, Biogenic Amines and Lipids in Blood Serum of Patients with Severe Osteoarthritis. Metabolites 2020; 10.

80. Morris SM, Jr. Arginine: beyond protein. Am J Clin Nutr 2006; 83: 508S-512S.

81. Castro-Perez JM, Kamphorst J, DeGroot J, Lafeber F, Goshawk J, Yu K, et al. Comprehensive LC-MS E lipidomic analysis using a shotgun approach and its application to biomarker detection and identification in osteoarthritis patients. J Proteome Res 2010; 9: 2377-2389.

82. King LK, March L, Anandacoomarasamy A. Obesity & osteoarthritis. Indian J Med Res 2013; 138: 185-193.

83. Anandacoomarasamy A, Fransen M, March L. Obesity and the musculoskeletal system. Curr Opin Rheumatol 2009; 21: 71-77.

84. Oliveria SA, Felson DT, Cirillo PA, Reed JI, Walker AM. Body weight, body mass index, and incident symptomatic osteoarthritis of the hand, hip, and knee. Epidemiology 1999; 10: 161-166.

85. Srikanth VK, Fryer JL, Zhai G, Winzenberg TM, Hosmer D, Jones G. A meta-analysis of sex differences prevalence, incidence and severity of osteoarthritis. Osteoarthritis Cartilage 2005; 13: 769-781.

CHAPTER THREE

METABOLOMIC PROFILES OF CARTIALGE AND BONE REFLECT TISSUE TYPE, RADIOGRAPHY-CONFIRMED OSTEOARTHRITS, AND SPATIAL LOCATION WITHIN THE JOINT

Contribution of Authors and Co-Authors

Manuscript in Chapter 3

Author: Hope D. Welhaven

Contributions: Conceptualization, Data Curation, Formal Analysis, Investigation, Methodology, Resources, Visualization, Writing – original draft, review, and editing.

Co-Author: Ethan Viles

Contributions: Conceptualization, Methodology, Investigation, Data Curation Writing – review and editing.

Co-Author: Jenna Starke

Contributions: Conceptualization, Methodology, Investigation, Writing – review and editing.

Co-Author: Cameron Wallace

Contributions: Methodology, Investigation, Resources, Writing – review and editing.

Co-Author: Brian Bothner

Contributions: Methodology, Resources, Visualization, Validation, Writing – review and editing.

Co-Author: Ronald K. June

Contributions: Conceptualization, Methodology, Resources, Visualization, Validation, Writing – review and editing, Supervision, Project Administration, Funding Acquisition.

Co-Author: Alyssa K. Hahn

Contributions: Conceptualization, Methodology, Resources, Visualization, Validation, Writing – review and editing, Supervision, Project Administration, Funding Acquisition.

Manuscript Information

Hope D. Welhaven, Ethan Viles, Jenna Starke, Cameron Wallace, Brian Bothner, Ronald K. June, Alyssa K. Hahn

Biochemical and Biophysical Research Communications

Status of Manuscript:
☐ Prepared for submission to a peer-reviewed journal
☐ Officially submitted to a peer-reviewed journal
☐ Accepted by a peer-reviewed journal
X Published in a peer-reviewed journal

Elsevier

Vol 703, April 2024

https://doi.org/10.1016/j.bbrc.2024.149683

Highlights

- Grades III and IV cartilage and bone exhibit distinct metabolic perturbations
- Metabolic alterations across the joint during late-stage disease are not uniform
- GAG homeostasis in each tissue is negatively influenced during late-stage OA
- Metabolic perturbations in tissue and space reveal OA crosstalk

Abstract

Osteoarthritis is the most common chronic joint disease, characterized by the abnormal remodeling of joint tissues including articular cartilage and subchondral bone. However, there are currently no therapeutic drug targets to slow the progression of disease because disease pathogenesis is largely unknown. Thus, the goals of this study were to identify metabolic differences between articular cartilage and subchondral bone, compare the metabolic shifts in osteoarthritic grade III and IV tissues, and spatially map metabolic shifts across regions of osteoarthritic hip joints. Articular cartilage and subchondral bone from 9 human femoral heads were obtained after total joint arthroplasty, homogenized and metabolites were extracted for liquid chromatography-mass spectrometry analysis. Metabolomic profiling revealed that distinct metabolic endotypes exist between osteoarthritic tissues, late-stage grades, and regions of the diseased joint. The pathways that contributed the most to these differences between tissues were associated with lipid and amino acid metabolism. Differences between grades were associated with nucleotide, lipid, and sugar metabolism. Specific metabolic pathways such as glycosaminoglycan degradation and amino acid metabolism, were spatially constrained to more superior regions of the femoral head. These results suggest that radiography-confirmed grades III and IV osteoarthritis are associated with distinct global metabolic and that metabolic shifts are not uniform across the

joint. The results of this study enhance our understanding of osteoarthritis pathogenesis and may lead to potential drug targets to slow, halt, or reverse tissue damage in late stages of osteoarthritis.

Introduction

Osteoarthritis (OA) is the most prevalent joint disease affecting over 32.5 million US adults, costs the US $185 billion per year, and is the leading cause of disability worldwide [1-4]. The current paradigm of OA pathogenesis suggests that disease results from metabolic imbalances at the tissue level where catabolic pathways outweigh anabolic pathways, resulting in abnormal remodeling and eventual breakdown of the articular cartilage (AC), subchondral bone (SB), and other surrounding tissues (e.g., synovitis) [5-7]. Although it is well established that metabolic dysfunction is associated with OA, global metabolomic profiling is advantageous because it detects thousands of small-molecule intermediates called metabolites to generate a global biochemical endotype that is representative of the overall physiological status of the tissue [8]. Applying this method to study AC and SB, additional insight into the role of metabolism in OA pathogenesis can be gained. A single study has utilized metabolomic profiling to analyze osteophyte cartilage tissue compared to cartilage from the lateral posterior femoral condyle, which exhibits similarities to healthy cartilage, and found that metabolic pathways altered were suggestive of cartilage degradation (phenylalanine, arginine, and proline metabolism) and endochondral ossification (taurine and hypotaurine metabolism)[9]. Similarly, only one previous study has employed metabolomic profiling of OA sclerotic SB compared to non-sclerotic SB and found that metabolic pathways altered were suggestive of a high rate of bone turnover and matrix deposition (taurine and hypotaurine metabolism, amino acid metabolism, pyrimidine and purine metabolism) and regulation of inflammation and repair in damaged joints (sphingolipid

metabolism). Despite these recent advances, more data are needed to clarify the metabolic derangement in joint tissues[10].

It is well-known that OA is a whole-joint disease, with established interdependence and crosstalk between AC and SB. Despite this, no study to date has investigated metabolic shifts in diseased AC and SB in a single study. This tissue-centric approach is limiting because it fails to investigate the potential crosstalk between AC and SB in disease progression. Therefore, the primary goal of this pilot study was to investigate the altered metabolism in OA tissues (AC and SB) that compose the osteochondral unit (OU) to gain a greater understanding of aberrant metabolism in disease progression. To accomplish this, metabolites were extracted from grades III and IV OA tissues (AC and SB) and analyzed by liquid chromatography-mass spectrometry-based global metabolomic profiling to gain insight into tissue-specific metabolic differences, the OU, and metabolic differences associated with grade in late-stage OA.

A secondary goal of this study was to spatially map metabolic shifts across the OA joint tissues to determine if metabolic dysfunction is uniform across the joint or locally constrained. Multiple studies have employed finite element models to spatially mapped the femoral head and found that load distribution is not uniform across the joint, showing that superior regions of the femoral head experience the greatest stress and cartilage contact pressure[11-14]. Furthermore, microscopic and macroscopic indicators of OA (e.g., chondrocyte clustering, AC lesions) are not uniformly distributed across diseased joint tissues[15, 16]. Therefore, we hypothesized that metabolic alterations would not be uniform across the diseased joint and that regions that experience the greatest mechanical stress may exhibit greater evidence of OA metabolic perturbations. The identification of disease-associated metabolic shifts that localize to specific regions of the joint

will provide insight into late-stage disease progression and may reveal new therapeutic targets for more spatially targeted treatments in the joint.

Methods

Patients and Femoral Head Samples

Under Institutional Review Board (IRB) approval, femoral heads from end-stage OA (grade III or IV) joints were obtained with consent following total joint arthroplasty. OA grade was assigned based on the widely accepted Kellgren-Lawrence grading scheme which scores radiographic characteristics on a scale of 0-4 with scores increasing with progression of OA. Radiographic characteristics that are considered evidence of OA include: osteophyte formation, sclerosis of SB, presence or absence of bony formations, and joint space narrowing which is a surrogate for AC thickness and meniscal integrity[17, 18].

To investigate the relationship between spatial distribution of OU components and metabolism, femoral heads were separated into four quadrants for tissue collection. Quadrants were determined based on previous studies that have spatially mapped stress distributions across the femoral head (Fig. 3.1A-C)[11-14]. Femoral heads from end-stage OA joints exhibit substantial degradation, in particular in load-bearing regions. Therefore, it was not possible to obtain sufficient tissue from every quadrant for each femoral head. Femoral heads that did not have sufficient tissue collected from 6 out of the 8 quadrants (for both AC and SB) were excluded from this study. Therefore, while 18 femoral heads were initially obtained following total joint arthroplasty, 9 femoral heads had sufficient tissue in the required number of quadrants to be included in this pilot study (n=3 grade III, n=6 grade IV, n=9 excluded). Partial participant information was provided with each donated femoral head including age, sex, height, and weight (Table 3.1).

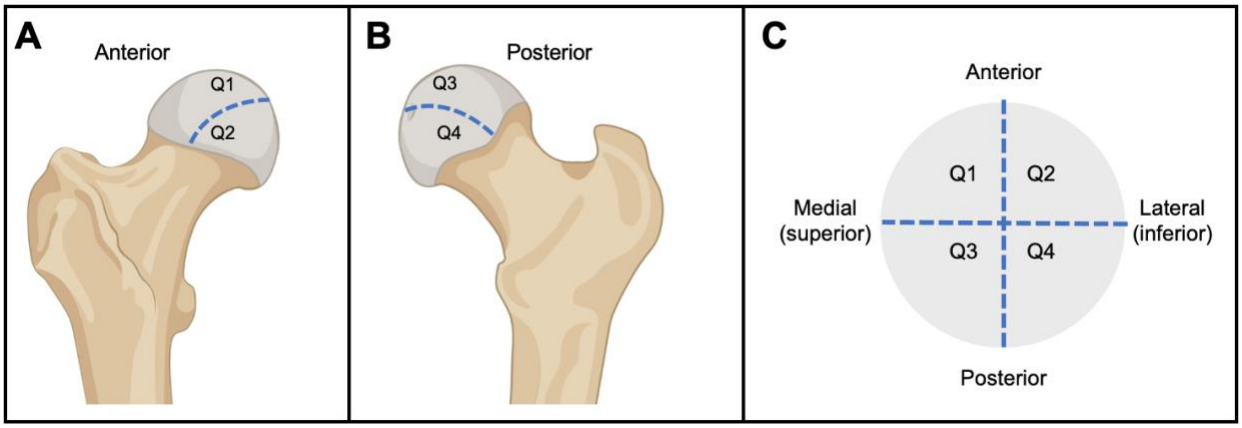

Figure 3.1. Separation of femoral head into four quadrants based on anatomical position. (A) Anterior and (B) posterior viewing of a right-side femoral head. (C) Quadrants 1 and 2 (Q1-Q2) are anterior superior and inferior quadrants respectively and quadrants 3 and 4 (Q3-Q4) are posterior superior and inferior quadrants, respectively. Both AC and SB were obtained from all four quadrants, therefore, eight possible samples could be obtained per participant.

Table 3.1. Partial patient information from total joint arthroplasty donors. Age = years. Height = inches (in). Weight = kilograms (kg). Side = right (R) or left (L) *Indicates missing patient information.

Patient	Age (years)	Sex	Height (inches)	Weight (kg)	Grade	Side
Patient 1	59	M	68	99.8	IV	R
Patient 2	41	M	73	82	IV	R
Patient 3	*	F	64	98	IV	R
Patient 4	44	M	*	*	IV	L
Patient 5	67	M	79	118	IV	R
Patient 6	79	M	69	78	IV	R
Patient 7	70	M	71	73.8	III	L
Patient 8	70	M	70	*	III	L
Patient 9	69	F	71	*	III	L

Metabolite Extraction and Global Metabolomic Profiling via LC-MS

100 mg of AC (n=31) and 100 mg of underlying SB (n=34) were shaved from each quadrant using the established quadrant system (Fig. 3.1 A-C). All AC shavings and SB punches

were submerged in 1 mL of 3:1 methanol:water (Sigma Aldrich, St. Louis, MO) because methanol is miscible with water allowing efficient extraction of lipophilic and hydrophilic metabolites. Moreover, it can be easily removed via vacuum concentration as it is highly volatile. Next, all samples were and homogenized using a tissue grinder (SPEX SamplePrep, Metuchen, NJ) for 15 second increments until fully homogenized. Samples were centrifuged at 500 *x g* for 10 minutes to remove cells and debris. The supernatant was collected and 100 μL of 4:1 methanol:water was added to extract metabolites for 30 minutes at -20°C prior to centrifugation at 16100 *x g* for 5 minutes. A vacuum concentrator (Savant AES 1010, ThermoFisher Scientific, Waltham, MA) was used to evaporate solvent from the supernatant, and the dried pellet was resuspended with 500 μL of 1:1 acetonitrile:water (Sigma Aldrich, St. Louis, MO) for 30 minutes at -20°C prior to centrifugation at 16100 *x g* for 5 minutes. Solvent was evaporated from supernatant by vacuum concentration and the dried pellet was resuspended with 1:1 water:acetonitrile for liquid chromatography-mass spectrometry (LC-MS) analysis.

Following metabolite extraction, all samples were analyzed by liquid chromatography-mass spectrometry (LC-MS) analysis. Specifically, extracts containing lipid- and water-soluble metabolites were analyzed in positive mode using an Agilent 1290 UPLC system coupled to an Agilent 6538 Q-TOF mass spectrometer (Agilent, Santa Clara, CA). Separation of metabolites was achieved using a Cogent Diamond Hydride HILIC column (150 x 2.1 mm) (MicroSolv, Eatontown, NJ) and optimized gradient elution method to separate and elute polar metabolites including polar lipids. Spectra were consequently processed and analyzed as previously described[19-21].

Statistical and Pathway Analyses

Obtained MS1 data consisting of mass-to-charge ratios (m/z), metabolite abundances, and retention times were processed using Agilent Masshunter Qualitative Analysis software and MS Convert. All data were then exported and converted using XCMS. Next, data were log transformed to correct for non-normal distribution and autoscaled (mean centered and divided by standard deviation of each variable). All statistical analyses were conducted in MetaboAnalyst [22]. To visualize and analyze differences between groups, statistical analyses employed included unsupervised multivariate hierarchical cluster analysis (HCA) and principal component analysis (PCA), supervised partial least-squares discriminant analysis (PLS-DA), and univariate fold change analysis. Volcano plot analysis, which combines both fold change and statistical significance, was also performed. Here, false discovery rate (FDR) corrections using the Benjamini-Hochberg method were applied to correct for multiple comparisons and a metabolite features significance threshold of 0.05 was used. HCA was visualized as a heatmap to identify populations of co-regulated metabolites. Populations of differentially expressed metabolite features were mapped to metabolic pathways using pathway enrichment analyses using the Functional Analysis module in MetaboAnalyst. Pathway library Kyoto Encyclopedia of Genes and Genomes (KEGG) was used to match metabolite features to putative metabolite identifications (mass tolerance: 5 ppm, positive mode). Pathway significance was determined using an FDR-corrected *a prior* threshold of $p < 0.05$.

Results

Osteochondral Unit Components are Metabolically Distinct

In total, 1,570 metabolite features were detected by LC-MS in both diseased AC (n=31) and SB (n=34) collected from grade III and IV OA patients. To investigate if the metabolome of OU components were metabolically distinct, unsupervised (HCA, PCA) and supervised (PLS-DA) multivariate statistical analyses were performed (Fig. 3.2 A-C). HCA displayed nearly perfect clustering between AC and SB samples (Fig. 3.2 A) and PCA showed minimal overlap between the profiles of each tissue. (Fig. 3.2 B). Similarly, PLS-DA showed distinct separation between AC and SB (Fig. 3.2 C). To further visualize OU metabolic endotypes and identify unique populations of statistically significant metabolite features, fold change and volcano plot analyses were performed. Fold change analysis identified 360 metabolite features that had higher concentrations in AC compared to SB, whereas 384 metabolite features had higher concentrations in SB compared to AC (Fig. 3.2 D, Supplemental Table 3.1). Furthermore, volcano plot analysis considers significance (FDR-corrected p-value < 0.05) and revealed that 318 metabolite features were significant and expressed in higher concentrations in AC compared to SB, and 372 metabolite features were significant and expressed in higher concentrations in SB compared to AC (Fig. 3.2 E).

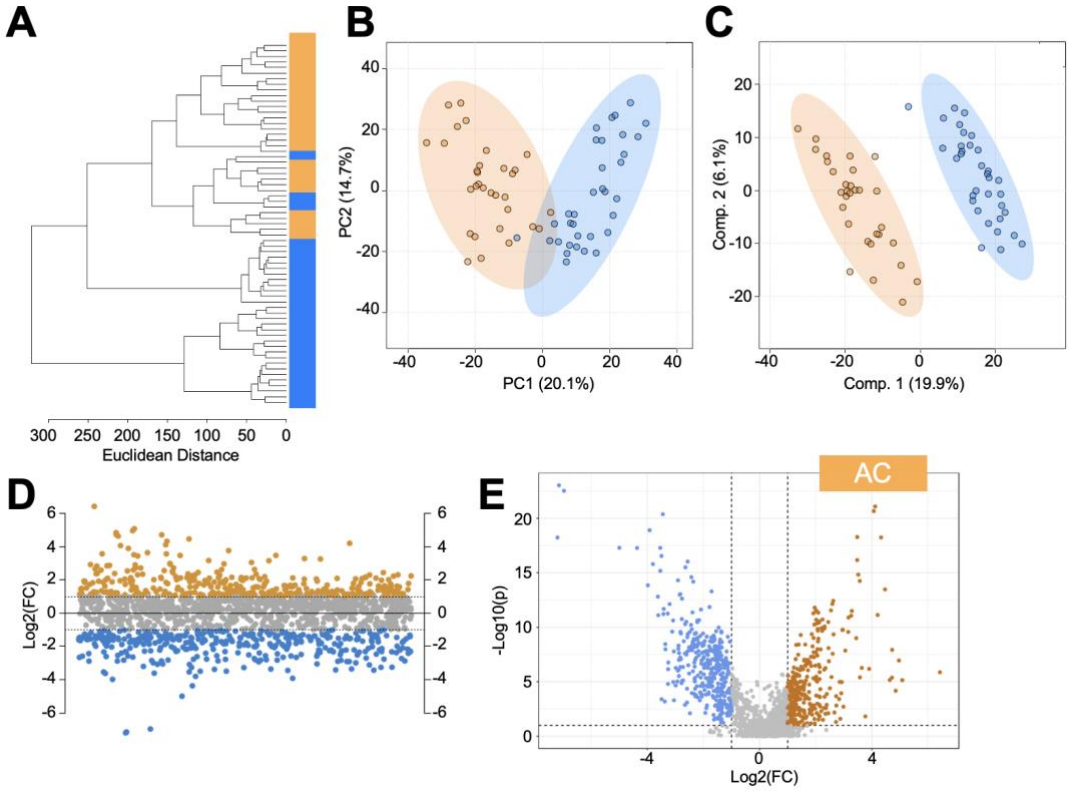

Figure 3.2. Osteochondral unit components, articular cartilage and subchondral bone, have distinct metabolic endotypes. In total, 1,517 metabolite features were detected across all AC and SB samples (n=31 AC, n=34 SB, n=65 total) and were assessed using multivariate statistical analyses. (A) HCA revealed the metabolomes of each tissue, AC and SB cluster together. (B) PCA visualized overall variation within the dataset and revealed minimal overlap between AC and SB cohorts. Principal components 1 and 2 accounted for 34.8% of the variation of data. (C) PLS-DA showed perfect clustering with no overlap of OU components, with components 1 and 2 accounting for 26% of the variation within the dataset. (D) Fold change analysis identified 360 metabolite features with a FC > 2 that were higher in AC samples compared to SB, whereas 384 metabolite features with a FC < -2 were higher in SB compared to AC. Fold change ratio: AC/SB. (E) Volcano plot analysis identified 318 metabolite features that were higher in AC compared to SB with a FC > 2 and a p-value < 0.05. Conversely, 372 metabolite features that were higher in SB compared to AC had a FC < -2 and a p-value < 0.05. The colors in A-F correspond to osteochondral unit components: orange – articular cartilage (AC), blue – subchondral bone (SB).

Next, statistically significant metabolite features identified by fold change and volcano plot analyses underwent pathway enrichment analysis. Metabolite features that had the highest concentration in AC, compared to SB, were involved in ubiquinone biosynthesis, porphyrin

metabolism, and lipid metabolism (arachidonic acid metabolism, glycosphingolipid metabolism) (Table 3.2, Supplemental Table 3.2). Conversely, metabolite features involved in amino acid metabolism (alanine, aspartate, glutamate, valine, leucine, isoleucine), nucleotide metabolism (pyrimidine metabolism, aminoacyl-tRNA biosynthesis), and energy metabolism (TCA cycle) were highest in concentration in SB compared to AC (Table 3.2, Supplemental Table 3.2).

Table 3.2. Metabolic pathways associated with articular cartilage and subchondral bone identified by fold change and volcano plot analyses. All pathways listed have a FDR-corrected significance level < 0.05. Articular cartilage = AC. Subchondral bone = SB.

Tissue	Pathway
AC	Porphyrin metabolism
	Arachidonic acid metabolism
	Glycosphingolipid biosynthesis
	Ubiquinone biosynthesis
SB	Alanine, aspartate and glutamate metabolism
	Valine, leucine and isoleucine degradation
	Pyrimidine metabolism
	Aminoacyl-tRNA biosynthesis
	Citrate cycle (TCA cycle)

Changes in Metabolic Profiles Correspond to Radiography-Confirmed Grade of OA

To examine if metabolic differences exist between grade III and IV OA OU tissues, a four-group comparison (grade III AC, grade IV AC, grade III SB, grade IV SB) was performed. HCA showed clustering of tissues within their respective cohorts (Fig. 3.3 A). Specifically, both grades of AC cluster together as well as both grades of SB with near perfect separation within grade (Fig. 3.3 A). PCA was then used to analyze the variation amongst the four groups and visualize their metabolomes. Clear separation was observed between tissues and tissue grade, with minimal overlap observed between cohorts (Fig. 3.3 B). PLS-DA was used to further examine the four groups, with some overlap observed between cohorts (Fig. 3.3 C).

Finally, a median intensity heatmap analysis was performed to visualize overall global metabolomic profiles to reveal patterns of co-regulated and differentially expressed metabolite features. Using ward clustering, clusters of metabolite features were identified and then subjected to pathway enrichment analyses where metabolites features were mapped to metabolic pathways (Fig. 3.3 D). Metabolite features that had higher concentration in grade III AC mapped to the pentose phosphate pathway and lysine degradation (Fig. 3.3 D, Cluster 2, Table 3.3, Supplemental Table 3.3). Conversely, metabolite features higher in grade IV AC mapped to glycosaminoglycan (GAG) degradation, biosynthesis of unsaturated fatty acids, and ubiquinone biosynthesis (Fig. 3.3 D, Cluster 1, Table 3.3, Supplemental Table 3.3). Metabolite features that were higher in concentration in grade III SB mapped to amino acid metabolism (valine, leucine, isoleucine, alanine, aspartate, glutamate), the TCA cycle, and pantothenate and CoA biosynthesis (Fig. 3.3 D, Cluster 3, Table 3.3, Supplemental Table 3.3). Finally, metabolite features that were higher in grade IV SB mapped to porphyrin metabolism, primary bile acid biosynthesis, and GAG degradation (Fig. 3.3 D, Cluster 4, Table 3.3, Supplemental Table 3.3). Therefore, a shared pathway between grade IV tissues, both AC and SB, was GAG degradation.

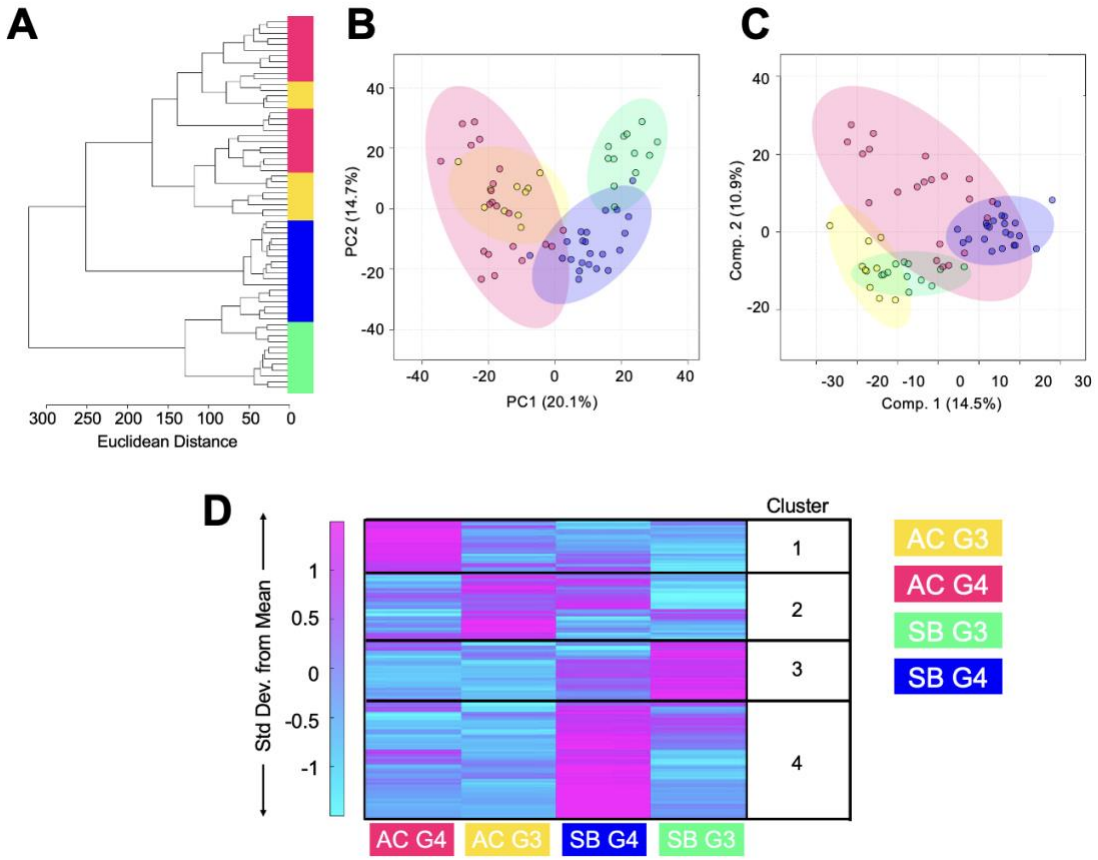

Figure 3.3. Osteochondral unit component metabolism reflects osteoarthritis grade. (A) HCA displayed that osteochondral unit components (i.e., AC and SB) cluster together, and samples that differ by OA grade (i.e., III, IV) also mostly cluster together. (B) PCA visualized overall variation within the dataset and revealed that the metabolomes of grade III and IV AC and SB are metabolically distinct from each other, with greater metabolic differences exhibited between grade III and grade IV SB as shown my minimal overlap. Principal components 1 and 2 accounted for 34.8% of the variation within the dataset. (C) PLS-DA revealed partial separation between grade III and IV AC and SB where components 1 and 2 accounted for 25.4% of the variation within the dataset. (D) Median metabolite intensity heatmap analysis revealed distinct metabolic endotypes across all groups and clusters of co-regulated metabolites. Clusters of co-regulated metabolites (1-4) outlined in black were selected and mapped to metabolic pathways. The colors in A-D correspond to: articular cartilage grade III – yellow, articular cartilage grade IV – pink, subchondral bone grade III – green, subchondral bone grade IV – blue. Articular cartilage = AC. Subchondral bone = SB.

Pairwise comparisons were also performed to investigate the metabolomes of samples that differ by tissue (grade III AC vs. grade III SB; grade IV AC vs. grade IV SB) and OA grade (AC grade III vs grade IV; SB grade III vs. grade IV). Pairwise comparisons revealed distinct metabolomes between tissues and OA grade (Fig. 3.4, 3.5; Supplemental Fig. 3.1, 3.2; Table 3.3, Supplemental Tables 3.4-3.7). The results of pairwise comparisons are further discussed in the Supplemental Results. Overall, the results of pathway enrichment analyses of fold change, volcano plot, and median metabolite intensity heatmaps from pairwise and multigroup comparisons strongly suggest that the metabolic endotypes of OU components reflect OA grade (Table 3.3).

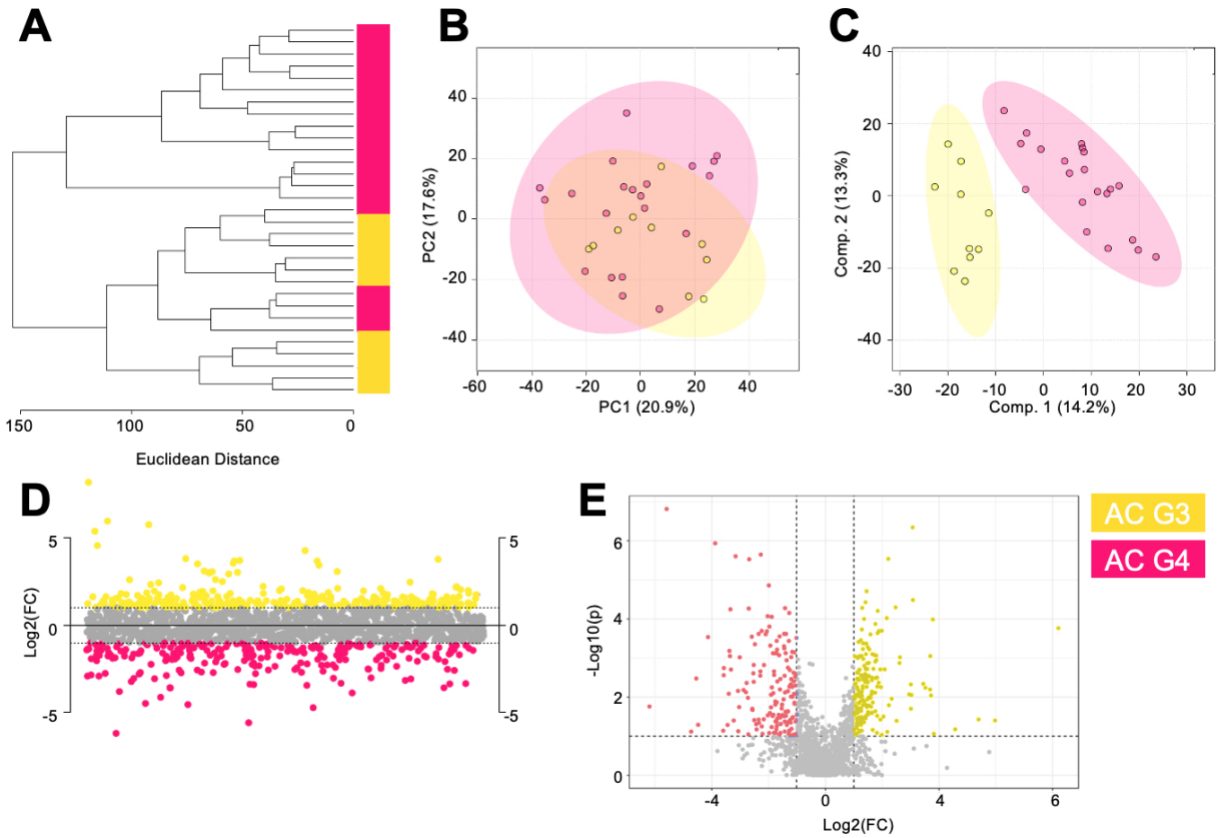

Figure 3.4. Grade of osteoarthritis influences the metabolome of articular cartilage. (A) HCA showcased that the metabolomes of grade III and IV AC are distinct from one another, as shown by clustering of most samples within their respective cohorts. (B) PCA visualized overall variation within the datasets and found some overlap between AC grades. PC1 and PC2 accounted for 38% of the variation within the dataset. (C) PLS-DA showed clear separation of AC grades. Components 1 and 2 accounted for 27.5% of the variation. (D) Fold change analysis identified 266 metabolite features that were higher in concentration in grade III AC compared to grade IV with a FC > 2, and 259 metabolite features that were higher in concentration in grade IV AC compared to grade III with a FC < -2. Fold change ratio: AC grade III/AC grade IV (E) Volcano plot analysis identified 192 metabolite features higher in grade III AC compared to grade IV that had a FC > 2 and a p-value less than 0.05, whereas 160 metabolite features were higher in grade IV AC compared to grade III that had a FC < -2 and a p-value less than 0.05. The colors in A-F correspond to: grade III articular cartilage - yellow, grade IV articular cartilage – pink. Articular cartilage = AC.

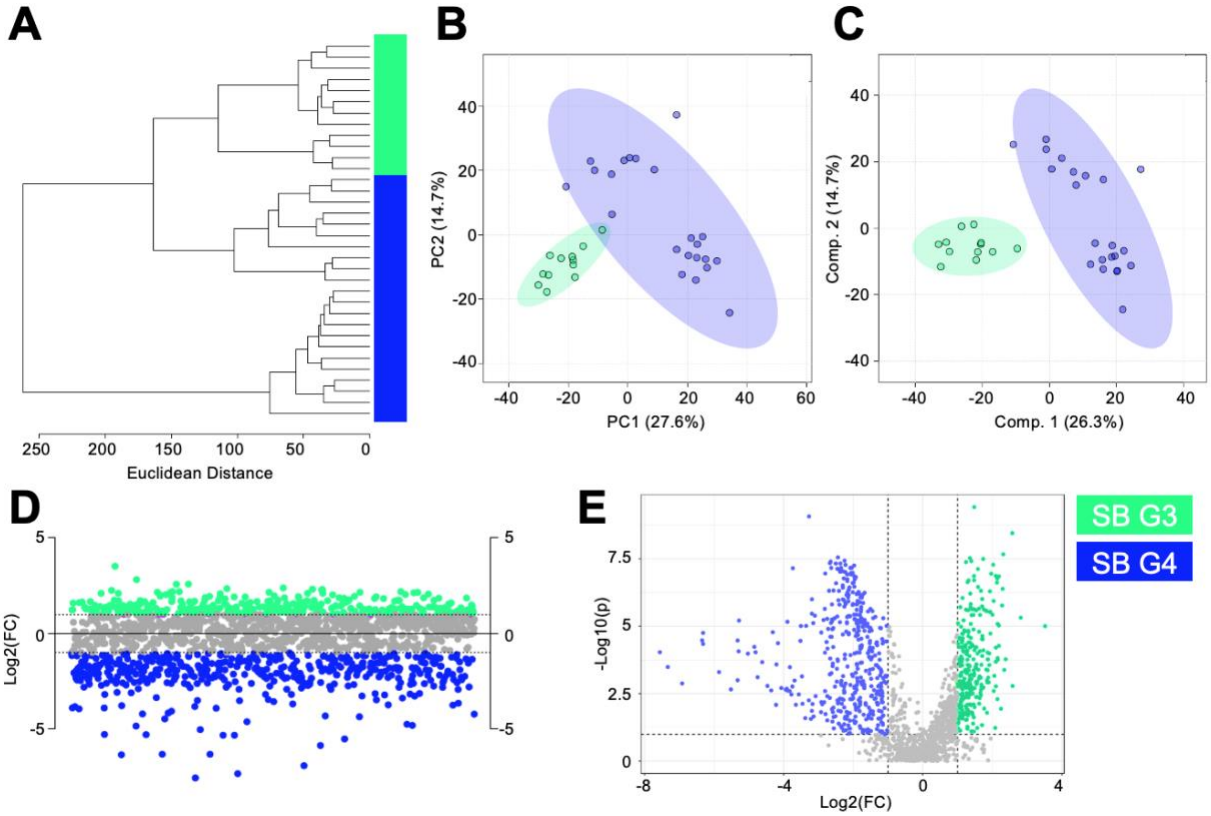

Figure 3.5. Subchondral bone metabolome reflects osteoarthritis grade. (A) HCA showcased that the metabolomes of grade III and IV SB are distinct from one another, as shown by correct clustering of all samples within their respective cohorts. (B) PCA found minimal overlap between SB grades where PC1 and PC2 accounted for 42.3% of the variation within the dataset. (C) PLS-DA showed clear separation of SB grades, with components 1 and 2 accounting for 41% of the variation within the dataset. (D) Fold change analysis identified 310 metabolite features that were higher in concentration in grade III SB compared to grade IV with a FC > 2 and identified 471 metabolite features that were higher in concentration in grade IV SB compared to grade III with a FC < -2. Fold change ratio: SB grade III/SB grade IV. (E) Volcano plot analysis identified 288 metabolite features higher in grade III SB compared to grade IV that had a FC > 2 and a p-value less than 0.05, whereas 427 metabolite features were higher in grade IV SB compared to grade III that had a FC < -2 and a p-value less than 0.05. The colors in A-F correspond to: grade III subchondral bone – green, grade IV subchondral bone – blue. Subchondral bone = SB.

Table 3.3. A) Unique metabolic pathways associated with individual groups including grade III and IV articular cartilage, and grade III and IV subchondral bone. B) Metabolic pathways detected in more than 1 group. Pathways were identified from fold change, volcano plot, and median metabolite intensity heatmap analyses. All pathways listed have a FDR-corrected significance level < 0.05. Articular cartilage = AC. Subchondral bone = SB. G3 = grade III. G4 = grade IV.

A) Pathways detected in 1 group	
Group	Pathway
AC G3	N-Glycan biosynthesis
	Tryptophan metabolism
	Pentose phosphate pathway
	Galactose metabolism
AC G4	Biosynthesis of unsaturated fatty acids
	Arachidonic acid metabolism
	Glycosphingolipid biosynthesis
	Phosphatidylinositol signaling system
SB G3	Pantothenate and CoA biosynthesis
	Aminoacyl-tRNA biosynthesis
	Purine metabolism
	Primary bile acid biosynthesis
SB G4	Pyrimidine metabolism
	Histidine metabolism
B) Pathways detected in more than 1 group	
AC G3, AC G4, SB G3, SB G4	Glycosaminoglycan degradation
AC G3, AC G4, SB G4	Ubiquinone biosynthesis
	Porphyrin metabolism
AC G3, AC G4	Lysine degradation
SB G3, SB G4	Citrate cycle (TCA cycle)
	Alanine, aspartate and glutamate metabolism
	Valine, leucine and isoleucine degradation

Metabolic Endotypes Differ Based on Spatial Location

Lastly, AC and SB from late-stage OA participants that differ by spatial location were examined using a four-quadrant system (Fig. 3.1 A-C). Specifically, quadrants 1 and 2 corresponded to anterior superior and inferior regions, whereas quadrants 3 and 4 corresponded to posterior superior and inferior regions, respectively. To investigate the metabolome of AC and SB quadrants, HCA and PLS-DA were used to visualize data. Both statistical tests displayed overlap between AC (Fig. 3.6 A-B) and SB (Fig. 3.6 D-E) quadrants which can be attributed to quadrants clustering by patient.

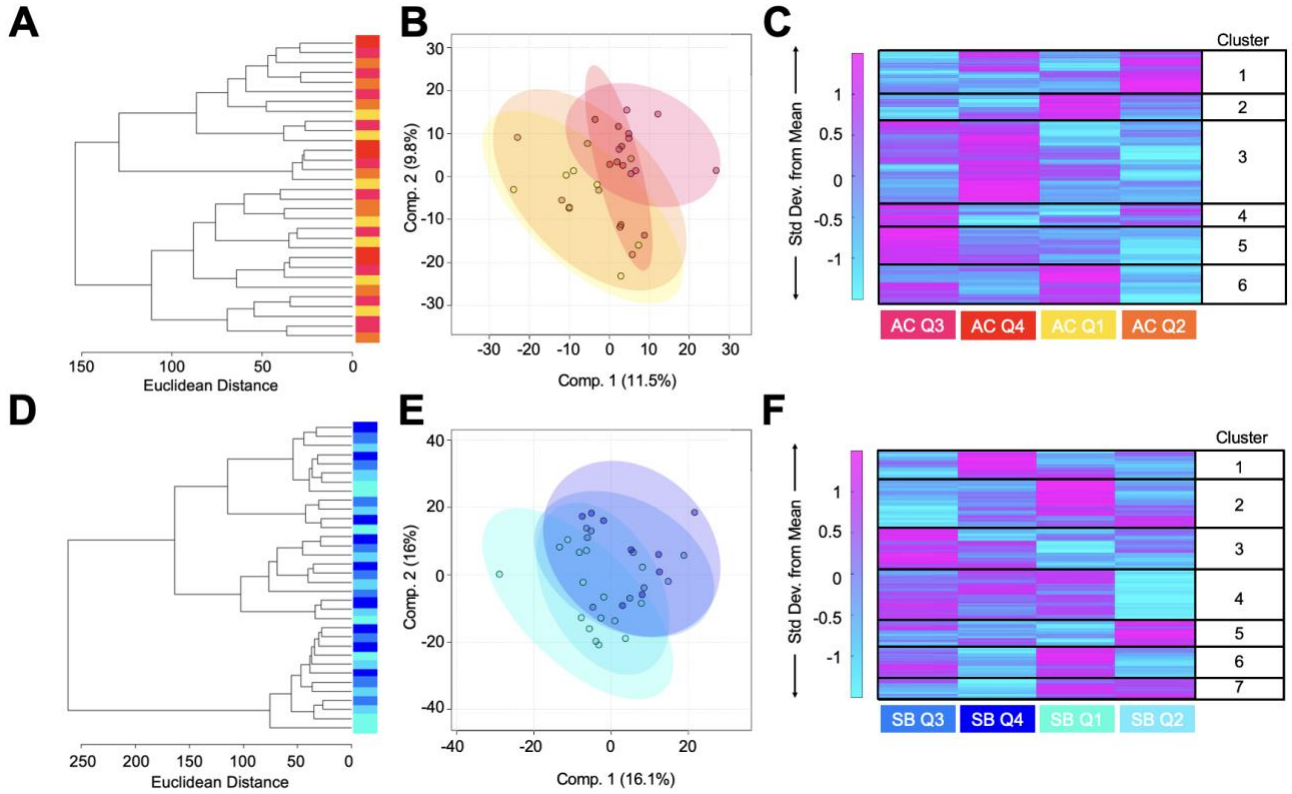

Figure 3.6. Spatial location of osteochondral unit tissues is reflected in metabolic endotypes. (A) HCA showed minimal separation between AC quadrants. (B) PLS-DA revealed that the metabolome of AC quadrants 1-4 are somewhat metabolically distinct from each other as shown by clustering of samples within respective cohorts although overlap is still evident. (C) Median metabolite intensity heatmap showcased metabolic endotypes by spatial location and identified clusters of co-regulated metabolites. Clusters of co-regulated metabolites (1-6) outlined in black were selected and mapped to metabolic pathways. (D) HCA showcased minimal separation between SB quadrants. (E) PLS-DA revealed clustering of samples within their respective cohorts although overlap is still evident. (F) Median metabolite intensity heatmap showcased metabolic endotypes by spatial location and identified clusters of co-regulated metabolites. Clusters of co-regulated metabolites (1-7) outlined in black were selected and mapped to metabolic pathways. The colors in A-F correspond to: articular cartilage quadrant 1 = yellow, articular cartilage quadrant 2 = orange, articular cartilage quadrant 3 = pink, articular cartilage quadrant 4 = red, subchondral bone quadrant 1 = seafoam green, subchondral bone quadrant 2 = teal, subchondral bone quadrant 3 = light blue, subchondral bone quadrant 4 = dark blue. Articular cartilage = AC. Subchondral bone = SB.

To identify clusters of co-regulated and differentially expressed metabolite features in AC quadrants, a median intensity heatmap analysis was performed. Clusters then underwent pathway enrichment analyses to identify biological pathways detected within and across quadrants (Fig. 3.6 C, F, Table 3.4, Supplemental Table 3.8). Metabolite features that had higher concentration in quadrant 1 mapped to tryptophan metabolism, lysine degradation, ubiquinone biosynthesis, and porphyrin metabolism (Fig. 3.6 C, Clusters 2, 6, Table 3.4, Supplemental Table 3.8). Metabolite features that were higher in concentration in quadrant 2 were contained in cluster 1, but no statistically significant pathways were detected. Metabolite features with higher concentrations in quadrant 3 corresponded to mannose type O-glycan biosynthesis and N-glycan biosynthesis (Fig. 3.6 C, Cluster 5, Table 3.4, Supplemental Table 3.8). Metabolite features that had higher concentrations in quadrant 4 mapped to linoleic acid metabolism and primary bile acid biosynthesis (Fig. 3.6 C, Cluster 3, Table 3.4, Supplemental Table 3.8). GAG degradation was detected in quadrants 1 and 3. Alanine, aspartate, and glutamate metabolism was detected in both quadrants 3 and 4 (Table 3.4, Supplemental Table 3.8). Taken together, data suggest spatial location influences, and somewhat reflects, AC metabolism during times of late-stage OA.

Table 3.4. A) Unique metabolic pathways associated with specific quadrants including grade III and IV articular cartilage quadrants 1-4. B) Metabolic pathways that were detected in multiple articular cartilage quadrants. Pathways were identified from clusters of co-regulated metabolites in a median metabolite intensity heatmap analysis and those listed have a FDR-corrected significance level of 0.05. Articular cartilage = AC. Q1-Q4 = Quadrants 1-4.

A) Pathways detected in 1 quadrant

Quadrant	Pathway
AC Q1	Tryptophan metabolism
	Lysine degradation
	Ubiquinone biosynthesis
	Porphyrin metabolism
AC Q3	Mannose type O-glycan biosynthesis
	N-Glycan biosynthesis
AC Q4	alpha-Linolenic acid metabolism
	Primary bile acid biosynthesis
B) Pathways detected in more than 1 quadrant	
AC Q1, AC Q3	Glycosaminoglycan degradation
AC Q3 AC Q4	Alanine, aspartate and glutamate metabolism

Similarly, a median intensity heatmap analysis was performed to identify co-regulated and differentially expressed metabolite features in SB quadrants (Fig. 3.6F, Table 3.5, Supplemental Table 3.9). Metabolite features that were higher in concentration in quadrant 1 mapped to amino acid metabolism (tyrosine, histidine, phenylalanine, tryptophan, alanine, aspartate, glutamate, valine, leucine, and isoleucine), porphyrin metabolism, glutathione metabolism, retinol metabolism, folate biosynthesis, pyrimidine metabolism, ubiquinone biosynthesis, and GAG biosynthesis (Fig. 3.6 F, Clusters 2, 6, Table 3.5, Supplemental Table 3.9). Metabolite features that were higher in concentration in quadrant 2 mapped to lysine degradation (Fig. 3.6 F, Cluster 5, Table 3.5, Supplemental Table 3.9). Metabolite features higher in concentration in quadrant 3 mapped to fatty acid degradation and phosphatidylinositol signaling (Fig. 3.6 F, Cluster 3, Table 3.5, Supplemental Table 3.9). Metabolite features higher in concentration in quadrant 4 were contained in cluster 1, but no statistically significant pathways were detected. Pathways detected

in both quadrants 1 and 3 included purine, arginine, and proline metabolism (Table 3.5, Supplemental Table 3.9). Pathways detected in quadrants 1, 3, and 4 included aminoacyl-tRNA biosynthesis, pantothenate and CoA biosynthesis, and lipid metabolism (glycosphingolipid biosynthesis, GAG degradation, glycerophospholipid metabolism) (Table 3.5, Supplemental Table 3.9). A pathway that was detected across all quadrants was primary bile acid biosynthesis (Table 3.5, Supplemental Table 3.9). Like AC quadrants, SB samples that differ by spatial location exhibit distinct metabolic profiles.

Table 3.5. A) Unique metabolic pathways associated with only one specific quadrant including grade III and IV subchondral bone quadrants 1-4. B) Metabolic pathways that were detected in more than 1 quadrant. Pathways were identified from clusters of co-regulated metabolites in a median metabolite intensity heatmap analysis and those listed have a FDR-corrected significance level of 0.05. Subchondral bone = SB. Q1-Q4 = Quadrants 1-4.

A) Pathways detected in 1 quadrant

Quadrant	Pathway
SB Q1	Glycosaminoglycan biosynthesis
	Tyrosine metabolism
	Folate biosynthesis
	Phenylalanine metabolism
	Retinol metabolism
	Pyrimidine metabolism
	Histidine metabolism
	Glutathione metabolism
	Porphyrin metabolism
	Phenylalanine, tyrosine and tryptophan biosynthesis
	Valine, leucine, and isoleucine metabolism
	Alanine, aspartate and glutamate metabolism
SB Q2	Lysine degradation
SB Q3	Phosphatidylinositol signaling system
	Fatty acid degradation
B) Pathways detected in more than 1 quadrant	
SB Q1, SB Q2, SB Q3, SB Q4	Primary bile acid biosynthesis
SB Q1, SB Q3, SB Q4	Aminoacyl-tRNA biosynthesis
	Pantothenate and CoA biosynthesis
	Glycosphingolipid biosynthesis
	Glycerophospholipid metabolism
	Glycosaminoglycan degradation
	Ubiquinone biosynthesis
SB Q1, SB Q3	Purine metabolism
	Arginine and proline metabolism

Discussion

To the best of our knowledge, this pilot study is the first study to perform global metabolomic profiling to study the OU components AC and SB and their spatial location in late-stage OA samples. The goals of this study were to identify metabolic differences between OU tissues, examine metabolic endotypes associated with grade III and IV OU tissues, and spatially map metabolic differences across regions of AC and SB from OA hip joints. In brief, differences in metabolism between OU components were detected and suggest the osteoarthritic OU components may have different cellular energy requirements. Additionally, different metabolic themes were associated with each OA grade, and pathways like GAG degradation were detected in both OU components and in both grade III and IV samples. Finally, regions of the femoral head that experience peak stress had distinct metabolic endotypes from others. Taken together, this study provides evidence that LC-MS-based global metabolomic profiling can be used to study OA as a whole joint disease, revealing disease-associated metabolic shifts in OU tissues and spatially constrained metabolic shifts associated with disease progression.

Global Metabolomic Profiling Detects Differences Between Articular Cartilage and Subchondral Bone

Global metabolomic profiling detected differences between OU components. Metabolite features higher in AC were associated with lipid metabolism (glycosphingolipid and arachidonic acid metabolism) and oxidative phosphorylation (ubiquinone biosynthesis). A previous study conducted by Seito *et al.*, demonstrated the importance of glycosphingolipids in OA development: alterations to chondrocyte-derived glycosphingolipids caused an imbalance in chondrocyte-homeostasis which contributed to the development of OA in transgenic mice[23]. Therefore, the

detection of imbalanced glycosphingolipid biosynthesis in AC supports the idea that glycosphingolipids are key regulatory components for AC that negatively influenced tissue health when imbalanced. Arachidonic acid is an unsaturated fatty acid, is associated with prostaglandin synthesis, and has been linked to OA pro-inflammatory responses, suggesting that disease associated metabolic shifts in AC are associated with prostaglandin generation for regulation of inflammation[24-26]. However, previous studies have primarily focused on this metabolic pathway in knee synovial fluid (SF) and its influence on joint lubrication and inflammation[26-28]. Thus, additional research is required to underpin the relationship between arachidonic acid metabolism at the hip joint and in other joints effected by OA.

Ubiquinones are electron carriers involved in oxidative phosphorylation; therefore, the detection of this pathway may suggest late-stage osteoarthritic AC requires higher ATP demand to support, or rebuild, degrading tissues but further investigation is required to underpin ATP demand during late-stage OA. Lastly, porphyrin metabolism is related to the production of heme, which is paramount to many biological processes. In a previous study, porphyrin was detected in high abundances in SF obtained from end-stage OA patients[29]. The detection of this pathway in diseased SF and AC in the present study, it is possible that this pathway is more dysregulated as OA progresses and metabolites in this pathway are secreted into the SF. However, further investigation is required to better understand the relationship between porphyrin metabolism, AC, and OA disease progression.

Metabolite features higher in SB were associated with amino acid metabolism (alanine, aspartate, glutamate, valine, leucine, and isoleucine metabolism), nucleotide-related pathways (pyrimidine metabolism and aminoacyl-tRNA biosynthesis), and energy pathways (TCA cycle).

Nucleotide-related pathways are important for DNA and amino acid synthesis[30]. Amino acids are the building blocks of proteins which are necessary structural elements of the bone extracellular matrix. Because osteophytes often form during late-stage OA, the detection of increased levels of amino acids and nucleotide-related pathways may reflect increased protein synthesis to support bone remodeling and subsequent osteophyte formation. An additional function of amino acids is to enter the TCA cycle to generate ATP. This may suggest that SB utilizes amino acids to generate ATP to help combat the breakdown and wear and tear of late-stage OA. A single study previously study also detected amino acid, energy, and nucleotide-related pathways in mouse bone, validating our findings in SB[31]. These findings suggest that osteoarthritic SB may have a higher cellular demand for nucleotides and amino acids for energy generation, protein synthesis, and bone deposition compared to AC. Taken together, detected pathway differences between AC and SB in the present study align with and support previous studies utilizing OA models and tissues. However, while the observed metabolic differences provide insight into OA in AC and SB, these differences cannot solely be attributed to OA disease progression as healthy controls were absent. Thus, observed differences may also reflect differences in physiology between AC and SB. Future work including healthy controls will confirm detected differences and attribute these differences to either physiology or OA disease progression.

Distinct Metabolic Endotypes Correspond to Radiography-Confirmed OA Grade

Global metabolomic profiling of osteoarthritic grade III and IV AC and SB confirmed that metabolic changes occur during late-stage OA. Metabolite features that had the highest concentration in grade IV AC, compared to grade III AC, mapped to biosynthesis of unsaturated fatty acids, primary bile acid biosynthesis, pyrimidine metabolism, and histidine metabolism.

Conversely, metabolite features highest in grade III AC, compared to grade IV AC, mapped to pantothenate CoA biosynthesis and purine metabolism. Those highest in grade III SB compared to grade IV SB mapped to arachidonic acid metabolism, galactose metabolism, and glycosphingolipid biosynthesis. Conversely, metabolite features associated with arachidonic acid metabolism, galactose metabolism, and glycosphingolipid biosynthesis were highest in grade IV SB compared to grade III SB. GAG degradation was a statistically significant pathway that was detected across all groups.

Galactose metabolism was a metabolic pathway that was detected at statistically significant levels in only one group, grade III AC. Galactose is involved in many cellular processes including intracellular recognition, glycosylation, GAG synthesis, and can be used to derive cellular energy[32, 33]. Previous studies have investigated the role of galactose and its potential role in regulating chondrocyte activity and found that ATDC5 chondrogenic cells and chondrocytes cultured with different concentrations of galactose exhibited increased expression of cartilage matrix type II collagen, aggrecan, and extracellular matrix[32]. This may suggest that galactose promotes chondrogenesis, cartilage repair, and potentially regeneration. Thus, perturbations in galactose metabolism in OA AC may be attempting to combat degradation in the cartilage matrix and generate energy for matrix component synthesis due to the limited bioavailability of other energy sources during late-stage OA. A noteworthy pathway detected in grade IV AC samples was unsaturated fatty acid biosynthesis. Mono and polyunsaturated fats have been associated with reduced joint space width (JSW) in humans[34] and increased cartilage degradation in mice[35]. Radiographic confirmation of grade III and IV OA is associated with a measurable reduction in JSW, with these results supporting supports previous findings that fatty acids influence the

pathophysiology of OA[17, 36-38]. Taken together, it is evident that acute metabolic differences exist between grade III and IV AC, however, further research is required to understand changes in metabolism as disease progresses from early-stage (grade I and II) to late-stage OA.

There is a large gap in knowledge surrounding OA metabolic alterations in SB. In this study, metabolite features involved in pantothenate CoA biosynthesis and purine metabolism exhibited the greatest alterations in grade III SB. Pantothenate CoA biosynthesis is related to vitamin B5 metabolism, functions as an essential cofactor for lipid synthesis, and can aid in controlling inflammation[39, 40]. The detection of this pathway may suggest SB is inflamed and/or is aiding in the synthesis of lipids. Metabolite features associated with purine metabolism were higher in grade III SB. Like pyrimidine metabolism, purine metabolism is important for DNA and amino acid synthesis, which may play a role in osteophyte formation in late-stage OA[41, 42]. Alternatively, products of purine metabolism (i.e., purine nucleotide adenosine) are key mediators in the purigenic signaling system, which plays an established role in mediating cell proliferation, differentiation, function, and death in chondrocytes and bone cells and has been previously linked to OA[43-48].

Amongst grade IV SB metabolite features, statistically significant pathways detected included pyrimidine and histidine metabolism. Histidine has been previously linked to different types of arthritis (i.e., OA and rheumatoid arthritis). Sitton *et al.*, examined free histidine levels in synovial fluid (SF) and serum in both OA and rheumatoid arthritis patients and found that that free histidine decreases in rheumatoid arthritis patients and increases in OA patients[49]. Although SF nor serum was obtained for histidine concentration analysis in our current study, the detection of dysregulated histidine metabolism in osteoarthritic SB in the present study supports previous

findings and suggests an involvement of histidine metabolism in late-stage OA SB. Like grade III and IV AC findings, end-stage OA displays different metabolic perturbations between grade III and IV SB. Future work can generate, compare, and pinpoint metabolic perturbations that change overtime as disease progresses.

A statistically significant metabolic pathway detected in all four groups was GAG degradation. A known hallmark of OA is a loss of GAG chains of proteoglycans, leading to cartilage degradation[50, 51]. Measuring levels of GAGs helps gauge chondrocyte and overall cartilage health. Previous studies have studied GAG loss during OA progression by measuring GAG concentration in SF. Kulkarni *et al*., obtained grade I-IV SF from OA patients and measured GAG concentration using spectrophotometric dye binding assays and found that GAG concentration increased as OA grade increased, reflecting greater cartilage degradation[52]. These previous findings and the detection of altered GAG degradation in osteoarthritic AC in the study herein support the paradigm that GAGs are a key component of cartilage, reflect chondrocyte health, and are negatively influenced during disease.

GAGs are also a key component of bone where they monitor the activity of osteoclastic and osteogenic factors, regulate the bioavailability of these factors, are a key structural component of the extracellular matrix, and influence bone remodeling[53]. Mansouri *et al.,* investigated GAGs and their role in bone remodeling by studying a specific proteoglycan, syndecan-2, and associated GAGs using a transgenic mouse model. Overexpression of syndecan-2 increased bone surface and mass because resorption was inhibited, increased bone marrow cell apoptosis, and decreased osteoblast and osteoclast precursor populations. These data suggest that GAGs may act as novel facilitators of crosstalk between bone remodeling cells. Considering the work of Mansouri *et al.,*

and the detection of GAG degradation in this study, it is likely that underlying SB remodeling is impacted during late-stage OA. To our knowledge no study to date has assessed changes in metabolism across all grades of OA, therefore, generating metabolic profiles of all grades, as well as healthy tissues, could improve current understanding of GAG degradation and general metabolic changes relating to disease progression over time.

Metabolism Reflects Spatial Location of Osteochondral Unit Components

It is well established that moderate mechanical loading is necessary for joint tissue homeostasis[54-56] and that superior regions of the femoral head experience the greatest stress[11-14]. However, it remains unknown if crosstalk between OA OU components and metabolic disturbances across the joint are influenced by spatial location. To determine it metabolic shifts were spatially constrained to specific regions of the joint, AC and SB samples were taken from four quadrant locations (Fig. 3.1 A-C). We found that metabolic shifts were not uniform across the joint, with variations in metabolic pathway perturbations in each quadrant. Previous evidence has identified superior regions of the femoral head to experience peak stress during physiological loading, which corresponds to quadrants 1 and 3 (Fig. 3.1 A-C). In this study, metabolite features from quadrants that correspond to superior regions experiencing higher mechanical loads mapped to amino acid metabolism (alanine, aspartate, glutamate, lysine), porphyrin metabolism, and GAG degradation. The detection of amino acid metabolism in quadrants that experience peak stress may suggest that amino acids are utilized for energy-generation purposes and protein synthesis to maintain the structural integrity of the extracellular matrix. Given that GAG degradation is an established hallmark of OA, superior quadrants that experience the greatest stress also had the greatest evidence of metabolic alterations consistent with OA. Overall, the detection of metabolic

metabolite features and pathways associated with end-stage OA, such as GAG degradation, in regions that experience peak stress may lead to drug targets and improved treatments that are localized to specific regions of the joint to slow, or prevent, disease progression.

Limitations

This study is not without limitations. Firstly, the number of participants (n=9), and samples (n=65), used for this study is small. Secondly, incomplete participant information was provided (i.e., weight, age, sex) and radiographic scans were unable to be accessed to support OA grade assignment. Thirdly, there were uneven ratios of male to female participants and grade III to grade IV samples. Finally, the lack of healthy, grade I, and II OU tissues limit analyses and therefore limits conclusions.

Conclusions

To our knowledge, this is the first study to examine OU component metabolism in late-stage osteoarthritis AC and SB. Our data demonstrate that differences in metabolism exist when comparing tissue components, metabolic endotypes reflect OA grade, and that metabolic perturbations experienced by the joint during late-stage disease are not uniform across the joint. Numerous statistically significant pathways were detected including energy and nucleotide-related pathways and those related to OU tissue homeostasis. It was evident that GAG homeostasis in OU components is negatively influenced during late-stage OA, as well as other metabolic pathways. Furthermore, these data support the notion that OA is a whole-joint disease, and that OU components, and their spatial location, should be examined to best address cartilage-bone crosstalk during disease and late-stage OA. By doing so, potential targets to slow, halt, or reverse disease

progression in localized regions of the joint may be identified to overall reduce the physical and economic burdens of OA. Expansion of this study may identify the role of the OU during each stage of disease progression to improve the current understanding of OA pathogenesis.

Acknowledgements

We thank the Mass Spectrometry Facility at Montana State University including Dr. Donald Smith and Jesse Thomas for assisting in LC-MS analysis. Funding for the Mass Spectrometry Facility used in this publication was made possible by the M.J. Murdock Charitable Trust, the National Institute of General Medical Sciences of the National Institutes of Health (P20GM103474 and S10OD28650), and the MSU Office of Research and Economic Development. This study was funded by the M.J. Murdock Charitable Trust under Award Numbers FSU-2017207 and NS-202016444 (AKH), the National Aeronautics and Space Administration under Award Number 80NSSC20M0042 (AKH), the National Science Foundation under Award Number CMMI 1554708 (RKJ), and the National Institutes of Health under Award Numbers R01AR073964 (RKJ).

Abbreviation List

OA = osteoarthritis; OU = osteochondral unit; AC = articular cartilage; SB = subchondral bone; LC-MS = liquid chromatography-mass spectrometry, HCA = hierarchical clustering analysis; PCA = principal component analysis; PLS-DA = partial least squares-discriminant analysis; FDR = false discovery rate; GAG = glycosaminoglycan

References

1. Cross M, Smith E, Hoy D, Nolte S, Ackerman I, Fransen M, et al. The global burden of hip and knee osteoarthritis: estimates from the global burden of disease 2010 study. Ann Rheum Dis 2014; 73: 1323-1330.

2. Felson DT, Lawrence RC, Dieppe PA, Hirsch R, Helmick CG, Jordan JM, et al. Osteoarthritis: new insights. Part 1: the disease and its risk factors. Ann Intern Med 2000; 133: 635-646.

3. Heidari B. Knee osteoarthritis prevalence, risk factors, pathogenesis and features: Part I. Caspian J Intern Med 2011; 2: 205-212.

4. Vina ER, Kwoh CK. Epidemiology of osteoarthritis: literature update. Curr Opin Rheumatol 2018; 30: 160-167.

5. Blain EJ. Involvement of the cytoskeletal elements in articular cartilage homeostasis and pathology. Int J Exp Pathol 2009; 90: 1-15.

6. Peters AE, Akhtar R, Comerford EJ, Bates KT. The effect of ageing and osteoarthritis on the mechanical properties of cartilage and bone in the human knee joint. Sci Rep 2018; 8: 5931.

7. Loeser RF, Goldring SR, Scanzello CR, Goldring MB. Osteoarthritis: a disease of the joint as an organ. Arthritis Rheum 2012; 64: 1697-1707.

8. Jewett MC, Hofmann G, Nielsen J. Fungal metabolite analysis in genomics and phenomics. Curr Opin Biotechnol 2006; 17: 191-197.

9. Xu Z, Chen T, Luo J, Ding S, Gao S, Zhang J. Cartilaginous Metabolomic Study Reveals Potential Mechanisms of Osteophyte Formation in Osteoarthritis. J Proteome Res 2017; 16: 1425-1435.

10. Yang G, Zhang H, Chen T, Zhu W, Ding S, Xu K, et al. Metabolic analysis of osteoarthritis subchondral bone based on UPLC/Q-TOF-MS. Anal Bioanal Chem 2016; 408: 4275-4286.

11. Harris MD, Anderson AE, Henak CR, Ellis BJ, Peters CL, Weiss JA. Finite element prediction of cartilage contact stresses in normal human hips. J Orthop Res 2012; 30: 1133-1139.

12. Henak CR, Ateshian GA, Weiss JA. Finite element prediction of transchondral stress and strain in the human hip. J Biomech Eng 2014; 136: 021021.

13. Xiong B, Yang P, Lin T, Xu J, Xie Y, Guo Y, et al. Changes in hip joint contact stress during a gait cycle based on the individualized modeling method of "gait-musculoskeletal system-finite element". J Orthop Surg Res 2022; 17: 267.

14. Zhang Z, Sui D, Qin H, Li H, Zhang Z. Contact pressure distribution of the hip joint during closed reduction of developmental dysplasia of the hip: a patient-specific finite element analysis. BMC Musculoskelet Disord 2020; 21: 600.

15. Bae WC, Payanal MM, Chen AC, Hsieh-Bonassera ND, Ballard BL, Lotz MK, et al. Topographic Patterns of Cartilage Lesions in Knee Osteoarthritis. Cartilage 2010; 1: 10-19.

16. Bentley BS, Hill RV. Assessing macroscopic and microscopic indicators of osteoarthritis in the distal interphalangeal joints: a cadaveric study. Clin Anat 2007; 20: 799-807.

17. Kellgren JH, Lawrence JS. Radiological assessment of osteo-arthrosis. Ann Rheum Dis 1957; 16: 494-502.

18. Hayashi D, Roemer FW, Guermazi A. Imaging for osteoarthritis. Ann Phys Rehabil Med 2016; 59: 161-169.

19. Carlson AK, Rawle RA, Adams E, Greenwood MC, Bothner B, June RK. Application of global metabolomic profiling of synovial fluid for osteoarthritis biomarkers. Biochem Biophys Res Commun 2018; 499: 182-188.

20. Jutila AA, Zignego DL, Hwang BK, Hilmer JK, Hamerly T, Minor CA, et al. Candidate mediators of chondrocyte mechanotransduction via targeted and untargeted metabolomic measurements. Arch Biochem Biophys 2014; 545: 116-123.

21. Welhaven HD, McCutchen CN, June RK. Effects of mechanical stimulation on metabolomic profiles of SW1353 chondrocytes: shear and compression. Biol Open 2022; 11.

22. Xia J, Wishart DS. Using MetaboAnalyst 3.0 for Comprehensive Metabolomics Data Analysis. Curr Protoc Bioinformatics 2016; 55: 14 10 11-14 10 91.

23. Seito N, Yamashita T, Tsukuda Y, Matsui Y, Urita A, Onodera T, et al. Interruption of glycosphingolipid synthesis enhances osteoarthritis development in mice. Arthritis Rheum 2012; 64: 2579-2588.

24. Bar-Or D, Rael LT, Thomas GW, Brody EN. Inflammatory Pathways in Knee Osteoarthritis: Potential Targets for Treatment. Curr Rheumatol Rev 2015; 11: 50-58.

25. Gilroy DW, Newson J, Sawmynaden P, Willoughby DA, Croxtall JD. A novel role for phospholipase A2 isoforms in the checkpoint control of acute inflammation. FASEB J 2004; 18: 489-498.

26. Van de Vyver A, Clockaerts S, van de Lest CHA, Wei W, Verhaar J, Van Osch G, et al. Synovial Fluid Fatty Acid Profiles Differ between Osteoarthritis and Healthy Patients. Cartilage 2020; 11: 473-478.

27. Mustonen AM, Nieminen P. Fatty Acids and Oxylipins in Osteoarthritis and Rheumatoid Arthritis-a Complex Field with Significant Potential for Future Treatments. Curr Rheumatol Rep 2021; 23: 41.

28. Nieminen P, Hamalainen W, Savinainen J, Lehtonen M, Lehtiniemi S, Rinta-Paavola J, et al. Metabolomics of Synovial Fluid and Infrapatellar Fat Pad in Patients with Osteoarthritis or Rheumatoid Arthritis. Inflammation 2022; 45: 1101-1117.

29. Carlson AK, Rawle RA, Wallace CW, Brooks EG, Adams E, Greenwood MC, et al. Characterization of synovial fluid metabolomic phenotypes of cartilage morphological changes associated with osteoarthritis. Osteoarthritis Cartilage 2019; 27: 1174-1184.

30. Siddiqui A, Ceppi P. A non-proliferative role of pyrimidine metabolism in cancer. Mol Metab 2020; 35: 100962.

31. Welhaven HD, Vahidi G et al. The Cortical Bone Metabolome of C57BL/6J Mice Is Sexually Dimorphic. JBMR Plus 2022; 6.

32. Yuan Z, Liu S, Song W, Liu Y, Bi G, Xie R, et al. Galactose Enhances Chondrogenic Differentiation of ATDC5 and Cartilage Matrix Formation by Chondrocytes. Front Mol Biosci 2022; 9: 850778.

33. June RK, Liu-Bryan R, Long F, Griffin TM. Emerging role of metabolic signaling in synovial joint remodeling and osteoarthritis. J Orthop Res 2016; 34: 2048-2058.

34. Lu B, Driban JB, Xu C, Lapane KL, McAlindon TE, Eaton CB. Dietary Fat Intake and Radiographic Progression of Knee Osteoarthritis: Data From the Osteoarthritis Initiative. Arthritis Care Res (Hoboken) 2017; 69: 368-375.

35. Wu CL, Jain D, McNeill JN, Little D, Anderson JA, Huebner JL, et al. Dietary fatty acid content regulates wound repair and the pathogenesis of osteoarthritis following joint injury. Ann Rheum Dis 2015; 74: 2076-2083.

36. Gold GE, Cicuttini F, Crema MD, Eckstein F, Guermazi A, Kijowski R, et al. OARSI Clinical Trials Recommendations: Hip imaging in clinical trials in osteoarthritis. Osteoarthritis Cartilage 2015; 23: 716-731.

37. Katz JN, Arant KR, Loeser RF. Diagnosis and Treatment of Hip and Knee Osteoarthritis: A Review. JAMA 2021; 325: 568-578.

38. Kohn MD, Sassoon AA, Fernando ND. Classifications in Brief: Kellgren-Lawrence Classification of Osteoarthritis. Clin Orthop Relat Res 2016; 474: 1886-1893.

39. Gheita AA, Gheita TA, Kenawy SA. The potential role of B5: A stitch in time and switch in cytokine. Phytother Res 2020; 34: 306-314.

40. Leonardi R, Jackowski S. Biosynthesis of Pantothenic Acid and Coenzyme A. EcoSal Plus 2007; 2.

41. Di Virgilio F, Adinolfi E. Extracellular purines, purinergic receptors and tumor growth. Oncogene 2017; 36: 293-303.

42. Yin J, Ren W, Huang X, Deng J, Li T, Yin Y. Potential Mechanisms Connecting Purine Metabolism and Cancer Therapy. Front Immunol 2018; 9: 1697.

43. Gratal P, Lamuedra A, Medina JP, Bermejo-Alvarez I, Largo R, Herrero-Beaumont G, et al. Purinergic System Signaling in Metainflammation-Associated Osteoarthritis. Front Med (Lausanne) 2020; 7: 506.

44. Koolpe M, Pearson D, Benton HP. Expression of both P1 and P2 purine receptor genes by human articular chondrocytes and profile of ligand-mediated prostaglandin E2 release. Arthritis Rheum 1999; 42: 258-267.

45. Kumagai H, Sacktor B, Filburn CR. Purinergic regulation of cytosolic calcium and phosphoinositide metabolism in rat osteoblast-like osteosarcoma cells. J Bone Miner Res 1991; 6: 697-708.

46. Rumney RM, Wang N, Agrawal A, Gartland A. Purinergic signalling in bone. Front Endocrinol (Lausanne) 2012; 3: 116.

47. Schofl C, Cuthbertson KS, Walsh CA, Mayne C, Cobbold P, von zur Muhlen A, et al. Evidence for P2-purinoceptors on human osteoblast-like cells. J Bone Miner Res 1992; 7: 485-491.

48. Varani K, De Mattei M, Vincenzi F, Gessi S, Merighi S, Pellati A, et al. Characterization of adenosine receptors in bovine chondrocytes and fibroblast-like synoviocytes exposed to low frequency low energy pulsed electromagnetic fields. Osteoarthritis Cartilage 2008; 16: 292-304.

49. Sitton NG, Dixon JS, Bird HA, Wright V. Serum and synovial fluid histidine: a comparison in rheumatoid arthritis and osteoarthritis. Rheumatol Int 1986; 6: 251-254.

50. Mankin HJ, Lippiello L. Biochemical and metabolic abnormalities in articular cartilage from osteo-arthritic human hips. J Bone Joint Surg Am 1970; 52: 424-434.

51. Pratta MA, Yao W, Decicco C, Tortorella MD, Liu RQ, Copeland RA, et al. Aggrecan protects cartilage collagen from proteolytic cleavage. J Biol Chem 2003; 278: 45539-45545.

52. Kulkarni P, Deshpande S, Koppikar S, Patil S, Ingale D, Harsulkar A. Glycosaminoglycan measured from synovial fluid serves as a useful indicator for progression of Osteoarthritis and complements Kellgren-Lawrence Score. BBA Clin 2016; 6: 1-4.

53. Mansouri R, Jouan Y, Hay E, Blin-Wakkach C, Frain M, Ostertag A, et al. Osteoblastic heparan sulfate glycosaminoglycans control bone remodeling by regulating Wnt signaling and the crosstalk between bone surface and marrow cells. Cell Death Dis 2017; 8: e2902.

54. Guilak F, Fermor B, Keefe FJ, Kraus VB, Olson SA, Pisetsky DS, et al. The role of biomechanics and inflammation in cartilage injury and repair. Clin Orthop Relat Res 2004: 17-26.

55. Murphy NJ, Eyles JP, Hunter DJ. Hip Osteoarthritis: Etiopathogenesis and Implications for Management. Adv Ther 2016; 33: 1921-1946.

56. Setton LA, Mow VC, Muller FJ, Pita JC, Howell DS. Mechanical behavior and biochemical composition of canine knee cartilage following periods of joint disuse and disuse with remobilization. Osteoarthritis Cartilage 1997; 5: 1-16.

CHAPTER FOUR

METABOLOMIC PROFILES AND PATHWAYS IN OSTEOARTHRITIC HUMAN CARTILAGE: A COMPARATIVE ANALYSIS WITH HEALTHY CARTILAGE

Contribution of Authors and Co-Authors

Manuscript in Chapter 4

Author: Hope D. Welhaven

Contributions: Designed experiments, harvested samples, performed metabolite extractions, ran LC-MS samples, analyzed data, interpreted results, and drafted manuscript.

Co-Author: Avery H. Welfley

Contributions: Performed metabolite extractions, analyzed data, interpreted results, and drafted manuscript.

Co-Author: Priyanka Brahmachary

Contributions: Harvested samples.

Co-Author: Annika R. Bergstrom

Contributions: Performed metabolite extractions.

Co-Author: Eden Houske

Contributions: Performed metabolite extractions.

Co-Author: Matthew Glimm

Contributions: Performed metabolite extractions.

Co-Author: Brian Bothner

Contributions: Analyzed data and interpreted results.

Co-Author: Alyssa K. Hahn

Contributions: Designed experiments, interpreted results, and drafted manuscript.

Co-Author: Ronald K. June

Contributions: Designed experiments, interpreted results, and drafted manuscript.

Manuscript Information

Hope D. Welhaven, Avery H. Welfley, Priyanka Brahmachary, Annika R. Bergstrom, Eden Houske, Matthew Glimm, Brian Bothner, Alyssa K. Hahn, Ronald K. June

Metabolites

Status of Manuscript:
☐ Prepared for submission to a peer-reviewed journal
☐ Officially submitted to a peer-reviewed journal
☐ Accepted by a peer-reviewed journal
X Published in a peer-reviewed journal

MDPI

Vol 14, Issue 4, March 2024

https://doi.org/10.3390/metabo14040183

Abstract

Osteoarthritis (OA) is a chronic joint disease with heterogenous metabolic pathology. To gain insight into OA-related metabolism, metabolite extracts from healthy (n=11) and end-stage osteoarthritic cartilage (n=35) were analyzed using liquid chromatography-mass spectrometry metabolomic profiling. Specific metabolites and metabolic pathways, including lipid- and amino acid pathways, were differentially regulated between osteoarthritis-derived and healthy cartilage. The detected alterations of amino acids and lipids highlight key differences in bioenergetic resources, matrix homeostasis, and mitochondrial alterations in OA-derived cartilage compared to healthy. Moreover, metabolomic profiles of osteoarthritic cartilage separated into four distinct endotypes highlighting the heterogenous nature of OA metabolism and diverse landscape within the joint between patients. The results of this study demonstrate that human cartilage has distinct metabolomic profiles between healthy and end-stage OA patients. By taking a comprehensive approach to assess metabolic differences between healthy and osteoarthritic cartilage, and within osteoarthritic cartilage alone, several metabolic pathways with distinct regulation patterns were detected. Additional investigation may lead to the identification of metabolites that may serve as valuable indicators of disease status or potential therapeutic targets.

Introduction

Osteoarthritis (OA) is the leading cause of disability worldwide. Since 1999, the number of global cases has increased by an astonishing 113%, equating to ~528 million individuals affected in 2019[1, 2]. In the United States alone, 32.5 million adults have OA, costing $185 billion annually[3-6]. At the heart of OA's insidious progression lies the gradual breakdown of articular

cartilage (AC) and other joint tissues. The imbalanced activity between matrix anabolism and catabolism contributes to the observed changes in AC, other tissues, and fluids affected by OA (*i.e.*, underlying bone, synovium, synovial fluid). Previous studies have examined altered metabolism in various OA-associated tissues and their cell types, such as chondrocytes, to investigate disease-associated metabolic activity[7-9]. However, significant limitations of many studies are that they are performed *in vitro* and/or lack healthy human controls, thereby hindering a complete understanding of the role metabolism plays in OA development.

Moreover, the complex nature of OA can manifest differently between individuals. Specifically, symptom severity, rate of progression, response to treatment, pain perception as well as other factors can vary from person to person[10-12]. Therefore, a "one-size-fits-all" approach to the treatment and prevention of OA is limited. More recent studies describe OA as a group of symptoms encompassing multiple distinct phenotypes and endotypes rather than a single disease[13]. Previously, phenotype was defined as a single or collection of disease characteristics that explain differences between patients and their outcomes, such as symptom severity[11-13]. Conversely, endotype is defined functionally and pathologically by a molecular mechanism noting that different mechanisms can lead to the same manifestation, such as end-stage OA[14]. Examining OA phenotypes and endotypes may shed light on the epidemiological origins and development of OA, unveil biomarkers, and lead to targeted interventions for sub-populations of OA individuals, all of which have potential to improve patient outcomes.

Metabolomics, the study of small molecule intermediates called metabolites[15], is advantageous for generating and investigating OA metabolic endotypes because it detects thousands of metabolites. This enables the generation of biochemical signatures that represent the

overall physiological state of the tissue. To our knowledge, two prior studies used a similar approach to examine synovial fluid metabolism from OA individuals. Here, researchers characterized different regulation patterns, or endotypes, based on detected differences in biochemical signatures between healthy and OA individuals[16, 17]. However, this same approach has yet to be applied to osteoarthritic cartilage. To begin filling these gaps in knowledge, we compared the metabolome of radiography-confirmed end-stage OA cartilage (Kellgran-Lawrence grades III and IV) with healthy cartilage using liquid chromatography-mass spectrometry (LC-MS) metabolomics.

Thus, the primary objective of this study was to identify disease-associated OA metabolomic profiles to shed light on the pathological mechanisms underlying OA. The secondary objective was to examine and classify endotypes of OA. Furthermore, we used tandem LC-MS (LC-MS/MS) for biochemical identification of key metabolites. This has the potential to identify novel biomarkers and drug targets to slow, halt, or reverse OA progression. With this approach, we aimed to uncover specific metabolic endotypes and metabolite identities to serve as potential indicators of disease status or therapeutic intervention across sub-populations of OA individuals.

Methods

Articular Cartilage Sample Obtainment

Under IRB approval, 35 femoral heads from end-stage OA patients were obtained following total joint arthroplasty from local musculoskeletal clinics. Partial patient information including age, sex, and BMI was provided (Supplemental Table 4.1). However, radiographic scans were not obtained due to IRB approval only permitting partial patient information to be shared.

Post-mortem cartilage samples were obtained from donors without joint disease (Articular Engineering) to serve as healthy controls for comparison.

Metabolite Extraction and Mass Spectrometry Analysis

Cartilage samples were shaved from the femoral head prior to metabolite extraction. All cartilage samples (n=35 OA, n=11 healthy) were extracted using a previously established protocol[18]. All cartilage samples were weighed prior to extraction to normalize metabolite intensity off cartilage weight. Notably, the weights of healthy cartilage consistently measured (100 mg), while the weights of OA cartilage were variable as they were obtained from end-stage OA patients who each had different amounts of intact cartilage (minimum = 16.8 mg, maximum = 223.3 mg, average = 73.0 mg). Next, cartilage shavings were submerged in 3:1 methanol:water and homogenized using a tissue homogenizer (SPEX Sample Prep 1200 GenoLyte, Fisher Scientific). Homogenization included 15 cycles of homogenizing for 20 seconds and resting for 2 minutes. Next, samples were briefly vortexed and stored at -20°C overnight to promote protein precipitation. The following day, samples were vortexed again, centrifuged for 10 minutes at 16,100 *g* at 4°C, and supernatants were collected and dried via vacuum concentration.

Dried supernatants were then resuspended with 1:1 acetonitrile:water, stored at -20°C for 30 minutes, then centrifuged again for 10 minutes at 16,100 *g* at 4°C. Similarly, supernatants were dried via vacuum concentration and then prepared for liquid chromatography-mass spectrometry (LC-MS) by resuspending with 1:1 acetonitrile:water. Additionally, 4 pooled samples (n=1 healthy, n=3 OA) were generated for identification purposes. For the healthy pool, 5 µL from each healthy extract were combined. For OA pools, 3 pooled samples were generated in the same way where 5 µL from 10 randomly selected OA extracts were combined per individual pool.

Extracted cartilage, both healthy and OA, underwent mass spectrometry analysis as previously described[19]. In brief, an Aquity UPLC Plus interfaced through an electrospray ionization source to a Waters Synapt XS was used. A Cogent Diamond Hydride HILIC column (150 x 2.1 mm) at a flow rate of 0.400 µL/min was used to separate metabolites over a 19-minute elution gradient (A = 95/5% water/acetonitrile, B = 95/5% acetonitrile:water). Every 10 injections, blank samples containing mass spectrometry-grade water were injected to minimize spectral drift and assess LC-MS performance. Cartilage extracts and blank samples underwent standard LC-MS, whereas pooled samples underwent liquid chromatography tandem mass spectrometry (LC-MS/MS) at a constant high energy ramp of 30-50V for secondary ionization to derive metabolite identifications. All samples – including cartilage extracts, pooled, and blanks – were all ran at the same time consecutively.

Statistical and Metabolomic Profiling

LC-MS data, consisting of mass-to-charge ratios (m/z), relative metabolite abundance, and retention time, were processed using MSConvert[20] and XCMS[21]. Prior to data analysis, metabolites associated with each cartilage sample were normalized by the pre-extraction recorded cartilage shaving weight. Previously established analysis pipelines were used[19, 22], and executed in MetaboAnalyst[23] where data underwent an integrity check to remove noise and avoid overfitting, interquartile range normalization, log-transformation, and autoscaling (mean-centered/standard deviation of each metabolite feature). In brief, hierarchical clustering analysis (HCA), principal component analysis (PCA), and partial least squares-discriminant analysis (PLS-DA) were used to visualize dissimilarities in metabolomic profiles between healthy and OA cartilage, as well as examine OA endotypes. T-test, fold change, and volcano plots were used to assess significance

and magnitude of change. Moreover, these populations of metabolite features were differentially regulated between groups and those identified by these tests underwent pathway enrichment analysis using MetaboAnalyst's Functional Analysis feature, which utilizes the *mummichog* algorithm to predict networks of functional activity from metabolite features of interest. The pathway library, Human MFN, was used as the primary reference library to match metabolite features to putatively identified metabolites (mass tolerance: 5 parts per million (ppm), positive mode, version 1). Significance for pathway analyses, and all other statistical tests, were determined using a false discovery rate (FDR)-corrected significance level of $p < 0.05$.

Metabolite Identification

A major hurdle in LC-MS-based metabolomics is metabolite identification[24]. To address this challenge, pooled samples were subjected to LC-MS/MS involving fragmentation allowing analysis of parent and daughter fragment ions. These data were manually analyzed to confirm metabolite identifications as follows. Firstly, all LC-MS/MS data from pooled samples were imported, peak picked, and aligned using Progenesis QI (Nonlinear Dynamics, Newcastle UK, version 3.0). Utilization of Progenesis improves efficiency of identifications and uses a computational framework that allows for the exploration of thousands of putative metabolite identifications across various databases. Here, the Human Metabolome Database (HMDB)[25] was utilized to compare theoretical fragmentation patterns to the acquired fragmentation patterns of parent and daughter ions. For a metabolite identity to be deemed valid and subsequently investigated manually, we required identities to receive a fragmentation score and overall progenesis score greater than 12 and 60 out of 100, respectively. These score criteria are based on mass error, isotope distribution, and retention time. Once identified metabolites were narrowed

based on these set scores and parameters, they were matched against populations of LC-MS-based metabolite features distinguished by statistical analyses comparing OA and healthy cartilage, as well as OA endotypes. To minimize false identifications, a threshold of 10 ppm error between observed and Progenesis-identified metabolites was enforced.

Results

Global Metabolomic Profiles of Osteoarthritis and Healthy Cartilage Unveil Altered Cellular Mechanisms Associated with Disease

In total, 10,853 metabolite features were detected by LC-MS across all cartilage samples. To visualize and assess metabolomic differences between healthy and OA cartilage, we used unsupervised (HCA, PCA) and supervised (PLS-DA) multivariate tests. HCA, visualized by a dendrogram and measured using Euclidean distance, displayed clear separation of healthy and OA cartilage (Fig. 4.1 A). A similar trend was observed when using PCA and PLS-DA where near perfect separation of groups was displayed demonstrating metabolomic profiles reflective of the disease status of cartilage (Fig. 4.1 B-C).

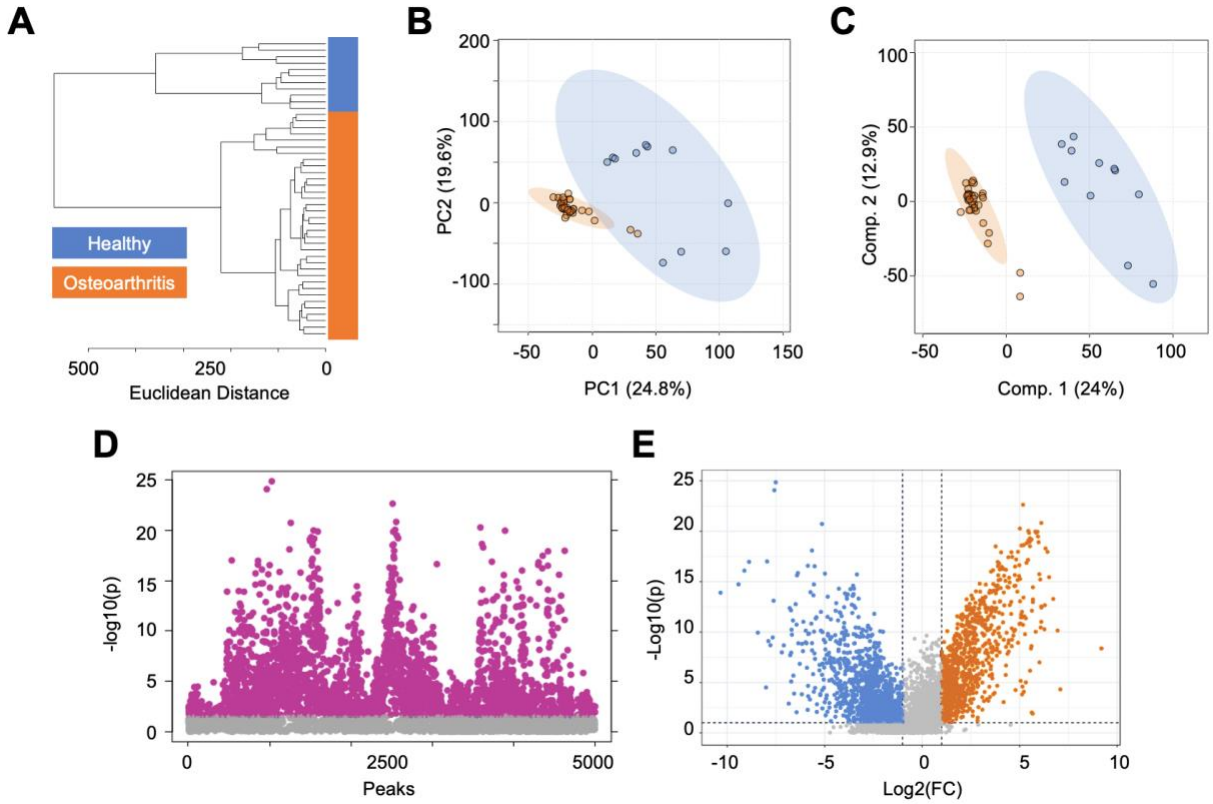

Figure 4.1. Metabolomic profiles of human cartilage from healthy and osteoarthritis patients are metabolically distinct. (A) Hierarchical clustering analysis finds that healthy and osteoarthritic cartilage samples cluster separate from each other. (B) Principal component analysis, an unsupervised test, finds minimal overlap with principal components 1 and 2 accounting for 44.4% of the variability in the dataset. (C) Partial least squares-discriminant analysis, a supervised test, shows complete separation of healthy and diseased cartilage samples with components 1 and 2 accounting for 36.9% of the variability in the dataset. (D) T-test analysis detected 2,842 metabolite features with a false discovery rate adjusted p-value less than 0.05. Orange = osteoarthritis. Blue = healthy. (E) Volcano plot analysis, using fold change and statistical significance, distinguished differentially regulated metabolites between healthy and diseased cartilage. Specifically, 1,010 metabolite features were higher in abundance in diseased cartilage compared to healthy cartilage ($\log2(FC) > 2$, $p < 0.05$) , whereas 1,399 were higher in abundance in healthy cartilage compared to diseased cartilage ($\log2(FC) < -2$, $p < 0.05$).

Next, t-test and volcano plot analyses were performed to distinguish dysregulated populations of metabolite features between healthy and OA cartilage. Populations distinguished by both analyses were then analyzed using MetaboAnalyst's Functional Analysis feature to find

biological pathways that differ in regulation across groups. Volcano plot analysis found 1,010 metabolite features that were higher in abundance in OA cartilage compared to healthy (Fig. 4.1 D). These metabolite features mapped to numerous lipid-related pathways (omega-3 & 6 fatty acid metabolism, fatty acid activation & oxidation, polyunsaturated and saturated fatty acid beta-oxidation, glycosphingolipid metabolism), the carnitine shuttle, leukotriene metabolism, and others (Table 4.1, Supplemental Table 4.2). Conversely, volcano plot also found 1,399 metabolite features that were higher in abundance in healthy cartilage compared to OA cartilage (Fig. 4.1 D). These features mapped to the urea cycle, purine metabolism, glycerophospholipid metabolism, vitamin metabolism (K, E), squalene and cholesterol biosynthesis, aminosugar metabolism, and various amino acid metabolic pathways (methionine, cysteine, histidine, glycine, serine, alanine, threonine, tryptophan) (Table 4.1, Supplemental Table 4.2). T-test distinguished 2,842 metabolite features that were significantly dysregulated between groups (FDR $p < 0.05$) (Fig. 4.1 E).

Table 4.1. Metabolic pathways associated with healthy and diseased cartilage identified by volcano plot analyses. All reported pathways have a FDR-corrected significance level < 0.05.

Group	Regulation	Pathway
Osteoarthritis	FC > 2, p < 0.05	Carnitine shuttle
		De novo fatty acid biosynthesis
		Fatty acid activation
		Fatty Acid Metabolism
		Fatty acid oxidation
		Fatty acid oxidation, peroxisome
		Glycosphingolipid biosynthesis - ganglioseries
		Glycosphingolipid biosynthesis - globoseries
		Leukotriene metabolism
		N-Glycan Degradation
		Omega-3 fatty acid metabolism
		Omega-6 fatty acid metabolism
		Phosphatidylinositol phosphate metabolism
		Phytanic acid peroxisomal oxidation
		Polyunsaturated fatty acid biosynthesis
		R Group Synthesis
		Saturated fatty acids beta-oxidation
Healthy	FC < -2, p < 0.05	Aspartate and asparagine metabolism
		Glycerophospholipid metabolism
		Glycine, serine, alanine and threonine metabolism
		Histidine metabolism
		Methionine and cysteine metabolism
		Purine metabolism
		Squalene and cholesterol biosynthesis
		Tryptophan metabolism
		Urea cycle/amino group metabolism
		Vitamin E metabolism
		Vitamin K metabolism

Additionally, features distinguished by volcano plot (Supplemental Table 4.3) and t-test (Supplemental Table 4.4) were matched to putative identifications made using LC-MS/MS to unveil metabolic indicators of disease. Putatively identified metabolites that were statistically significant in both t-test and volcano plot analyses and were higher in healthy cartilage compared to OA cartilage included N-acetyl-leukotriene E4, demethylphylloquinone, 7C-aglycone, androsterone sulfate, and others (Supplemental Fig. 4.1 A). The majority of identified metabolites distinguished by these analyses were higher in abundance in healthy cartilage, with the exception of guanidinoethyl methyl phosphate, cervonyl carnitine, erythromycin propionate, and glycocholic acid (Supplemental Fig. 4.1 B). Collectively, these findings unveil specific metabolites and metabolic pathways that show altered cellular mechanisms of OA and reflect disease status of cartilage.

Endotype Characterization Supports Heterogenous Nature of Osteoarthritis

To examine the heterogenous nature of OA metabolism and better understand differences in the diverse metabolic landscape within OA, we examined metabolomic endotypes. Clustering techniques – HCA (Fig. 4.2 A) and ensemble clustering (Supplemental Fig. 4.2) – were utilized to identify OA endotypes across all cartilage samples. The application of both methods aimed to minimize subjectivity in delineating OA cartilage endotypes and determine OA participants that consistently cluster together. These analyses unveiled four distinct endotypes of OA participants. Considering patient-specific factors like age, the ratio of males to females, and overall number of participants within each endotypes, we found no clear pattern related to participant demographics that correlated with these four endotypes (Supplemental Table 4.1).

Once endotypes were distinguished and patient-specific factors were examined, we used PCA and PLS-DA to gain additional insight into these endotypes. This revealed limited overlap between endotype groups (Fig. 4.2 B-C). Notably, endotype 4 exhibited considerable variability portrayed by a substantial ellipse. In contrast, endotypes 1-3 showed a closer metabolomic resemblance where the proximity of smaller and tighter clustered ellipses were observed. Subsequent ANOVA analysis identified 2,506 metabolite features that were significantly different between endotypes with FDR-corrected $p < 0.05$ (Fig. 4.2 D). This subset of features was then matched to putative identifications made using LC-MS/MS data. Identifications consisted of lipid and lipid-like metabolites including cervonyl carnitine, lucidenic acid A, 6-Epi-7-isocucurbic acid glucoside, various phosphatidylcholine species, and others (Supplemental Fig. 4.3 A, Supplemental Table 4.5). Additionally, metabolites related to arachidonic acid and leukotriene metabolism were identified including arachidonic acid, panaxydol linoleate, leukotriene F4, and N-acetyl-leukotriene E4 (Supplemental Fig. 4.3 B, Supplemental Table 4.5).

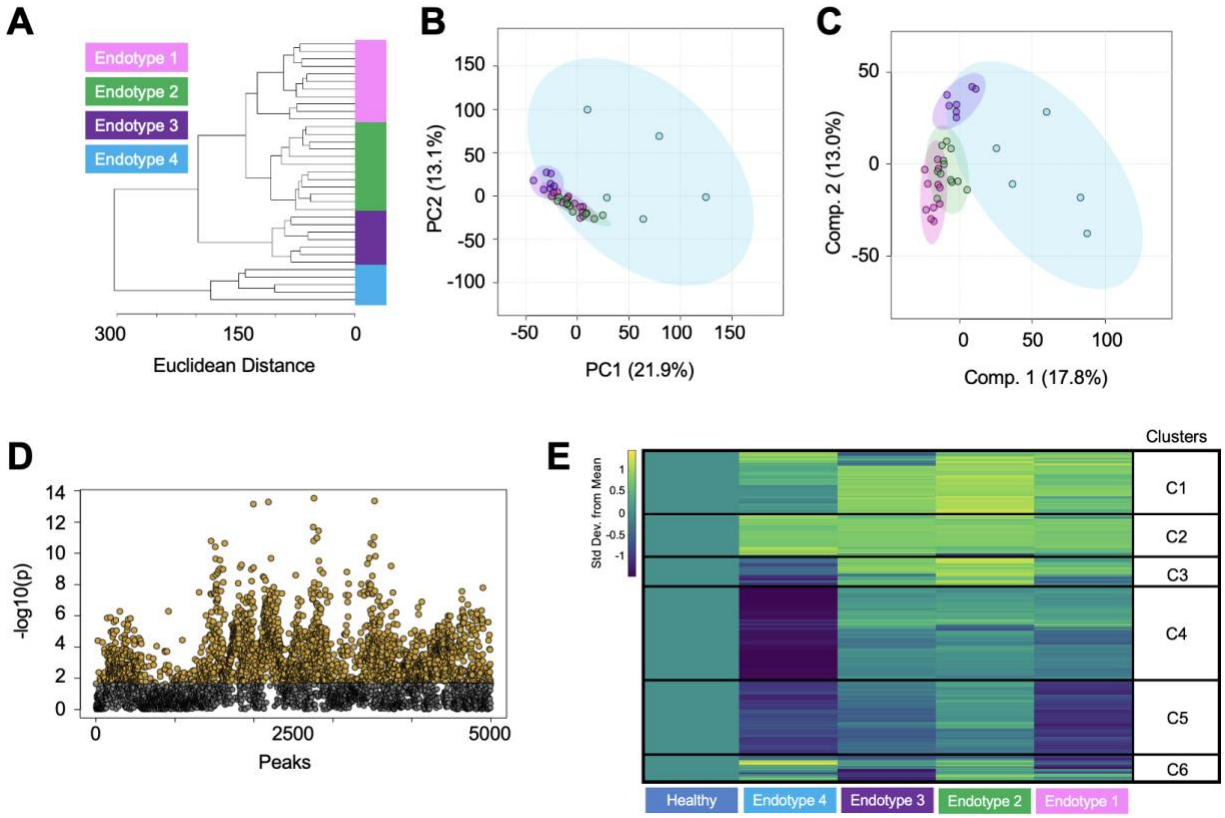

Figure 4.2. Metabolomic assessment of osteoarthritic cartilage classifies unique patient endotypes. (A) Hierarchical clustering of cartilage from patients with osteoarthritis cluster into 4 distinct endotypes. (B) Endotypes were further examined and visualized by principal component analysis. Principal components 1 and 2 account for 35% of the variability in the dataset and showed moderate overlap of osteoarthritis endotypes. (C) Partial least squares-discriminant analysis slightly refines separation of groups with components 1 and 2 accounting for 30.8% of the variability in the dataset. (D) ANOVA analysis detected 2,508 metabolite features with a false discovery rate adjusted p-value less than 0.05. (E) Metabolite features distinguished by ANOVA were visualized using a median metabolite intensity heatmap analysis where osteoarthritis endotypes were normalized to healthy cartilage. Clusters of co-regulated metabolite features (C1-C6) were then subjected to pathway analyses to pinpoint distinct metabolomic endotypes across osteoarthritic cartilage. Columns represent endotype and rows indicate metabolite features. Warmer colors (yellow) indicate higher metabolite abundance, whereas cooler colors (blue) indicate lower metabolite abundance. Endotype colors correspond to: pink – Endotype 1; green – Endotype 2; purple – Endotype 3; blue – Endotype 4.

Additionally, this subset of statistically significant metabolite features were further examined using a median metabolite intensity heatmap analysis normalized to healthy cartilage to find

dissimilarities in metabolomic regulation across the four OA endotype groups compared to healthy cartilage (Fig. 4.2 E). For this analysis, the median intensity for each metabolite feature is calculated and this same calculation is then extended to each endotype group to observe and compare major differences in metabolomic regulation between endotypes. Metabolite features within heatmap clusters 1 and 2, which exhibited higher abundances across endotypes compared to healthy cartilage, mapped to 16 statistically significant pathways including leukotriene metabolism, selenoamino acid metabolism, the carnitine shuttle, and numerous lipid-related pathways (Table 4.2, Supplemental Table 4.6). Heatmap clusters 3 and 4, comprised of metabolites that were lowest in endotype 4 but highest in other endotypes, mapped to 16 statistically significant pathways including vitamin A metabolism, phytanic acid peroxisomal oxidation, lysine and tyrosine metabolism, keratan sulfate degradation, N-glycan degradation, lineolate metabolism, butanoate metabolism, and various lipid-related pathways. Metabolites composing heatmap cluster 5 were relatively lower across endotypes compared to healthy samples which mapped to 7 statistically significant pathways including purine metabolism, leukotriene metabolism, urea cycle, aminosugar metabolism, and various amino acid pathways (methionine, cysteine, tryptophan, aspartate, asparagine). Lastly, heatmap cluster 6 consisted of metabolites with mixed regulation patterns across endotypes; however, no statistically significant pathways were detected. All pathways reported had an FDR-corrected $p < 0.05$. Collectively, these findings underscore the heterogenous nature of OA metabolism among those with OA and provide compelling evidence to support the diverse landscape of metabolic regulation associated with this disease.

Table 4.2. Metabolic pathways associated with osteoarthritis endotypes classified by median intensity heatmap analysis. All pathways reported have a FDR-corrected significance level < 0.05. Clusters defined in Figure 4.2E.

Cluster	Pathway	Cluster	Pathway
1	Fatty acid activation	4	Glycosphingolipid biosynthesis - globoseries
1	Saturated fatty acids beta-oxidation	4	Lysine metabolism
1	De novo fatty acid biosynthesis	4	Tyrosine metabolism
1	Fatty Acid Metabolism	4	Polyunsaturated fatty acid biosynthesis
1	Omega-6 fatty acid metabolism	4	Glycosphingolipid biosynthesis - ganglioseries
1	Carnitine shuttle	4	Keratan sulfate degradation
1	R Group Synthesis	4	N-Glycan Degradation
1	Fatty acid oxidation	4	Linoleate metabolism
1	Fatty acid oxidation, peroxisome	4	Vitamin A (retinol) metabolism
1	Leukotriene metabolism	4	Butanoate metabolism
2	Fatty acid oxidation	4	Trihydroxycoprostanoyl-CoA beta-oxidation
2	Polyunsaturated fatty acid biosynthesis	4	Glycerophospholipid metabolism
2	De novo fatty acid biosynthesis	4	Omega-3 fatty acid metabolism
2	Phytanic acid peroxisomal oxidation	4	Starch and Sucrose Metabolism
2	R Group Synthesis	5	Purine metabolism
2	Selenoamino acid metabolism	5	Leukotriene metabolism
3	Phytanic acid peroxisomal oxidation	5	Urea cycle/amino group metabolism
3	Omega-6 fatty acid metabolism	5	Methionine and cysteine metabolism
		5	Tryptophan metabolism
		5	Aminosugars metabolism
		5	Aspartate and asparagine metabolism

Discussion

While altered metabolism is increasingly recognized as a crucial factor in the development of OA, further data are needed to understand the role of aberrant metabolism in OA pathophysiology. This study found distinct human cartilage-derived metabolomic profiles between healthy and end-stage OA patients. Through a comprehensive analysis aimed at discerning

differences in the metabolome of healthy and OA cartilage, several metabolites and pathways associated with matrix metabolism, lipid metabolism, mitochondrial function, vitamin metabolism, and amino acid metabolism were differentially regulated between healthy and OA cartilage. Moreover, investigation of metabolic diversity within the metabolome of OA cartilage alone mapped to distinct metabolomic endotypes displaying the heterogeneous nature of OA. Considering these metabolomic findings, a greater understanding of altered cartilage metabolism in OA may lead to the identification of candidate biomarkers and drug targets to slow, halt, or reverse cartilage damage in end-stage OA.

Matrix Metabolism

OA cartilage exhibited greater evidence of altered matrix metabolism compared to healthy cartilage. Specifically, keratan sulfate degradation and N-Glycan degradation were upregulated in OA cartilage compared to healthy cartilage. Keratan sulfate, a type of glycosaminoglycan (GAG), plays a vital role in cartilage matrix homeostasis and maintenance. Homeostatic GAG content in both synovial fluid (SF) and cartilage are indicative of joint health, whereas, an increase in GAGs within SF suggests increased cartilage turnover. This is subsequently reflected by a decrease in GAG content within the cartilage itself[26-28]. Furthermore, alterations in N-glycan degradation likely reflect changes in joint lubrication as N-glycans are an important component of lubricin, a glycoprotein that lines cartilage surfaces and serves as a key joint lubricant with chondroprotective properties[29].

Lipid and Mitochondria-Related Metabolism

Several lipid-related pathways were upregulated in OA cartilage compared to healthy cartilage and were differentially regulated across OA endotypes. Notably, the present study

identified several significant lipid-related pathways that have been previously linked to OA, including the carnitine shuttle, arachidonic acid metabolism, omega-3 and -6 metabolism, glycosphingolipid metabolism, and glycerophospholipid metabolism. Cartilage relies on bone and SF for lipid transport, underscoring the critical role of lipid metabolism in maintaining cartilage homeostasis. Arachidonic acid (AA), leukotriene F4, N-acetyl-leukotriene E4, and panaxydol linoleate were identified using LC-MS/MS data and were at higher concentrations in OA cartilage compared to healthy and differed in abundance across OA endotypes (Supplemental Figures 4.1 and 4.3). AA, a type of omega-6 polyunsaturated fatty acid known to be associated with inflammation, is typically found in lower levels in healthy cartilage and increases as OA progresses[30]. Additionally, elevated AA have been detected in OA SF[16, 31], synovium[32], and more broadly, the severity of synovitis and histological changes in OA have been correlated with serum levels of omega-3 and -6[33, 34].

The detection of perturbed lipid pathways and a handful of identified lipid species in OA cartilage may reflect adaptive responses in mitochondrial function and biofuel utilization in response to OA. While healthy cartilage relies on both glucose and lipids as energy sources, OA cartilage exhibits a greater dependence on lipids[35, 36]. This metabolic switch to lipid utilization can lead to the accumulation of lipids, increased production of reactive oxygen species and nitric oxide, and decreased ATP production, leading to eventual tissue breakdown and death[37-40].

Central to this metabolic switch is the carnitine shuttle, which plays a key role in regulating oxidative status by transporting lipids across the mitochondrial membrane to generate ATP. The upregulation of the carnitine shuttle in OA cartilage compared to healthy cartilage, and across OA endotypes, is supported by previous studies which not only detected the carnitine shuttle but also

elevated levels of acylcarnitine and other carnitine species[17] in SF of OA patients. Moreover, cervonyl carnitine, a type of acylcarnitine, was identified using LC-MS/MS data and was significantly higher in all OA cartilage samples compared to healthy cartilage and differed in abundance across OA endotypes (Supplemental Figures 1 and 3). Cervonyl carnitine is often produced as a result of a disorder or disease (*i.e.*, cancer, diabetes, cardiovascular disease) and disrupts energy production[41]. It has been well documented that OA perturbs energy production in cartilage, therefore, the detection of this species in the present study could be a result of receiving cartilage from donors with radiography-confirmed OA.

We have previously detected cervonyl carnitine in SF from patients who sustained a traumatic knee injury[19]. Here, we hypothesized that a metabolic switch toward lipid utilization and the involvement of mechanisms like the carnitine shuttle were necessary to meet heightened energy demands post-injury and that ongoing analysis of these species may help manage post-traumatic OA. Thus, the detection of cervonyl carnitine in OA cartilage and in SF post-injury further highlights its potential as a marker that can be monitored over time to assess β-oxidation, joint health, while also potentially predicting the onset and progression of OA. Furthermore, cervonyl carnitine warrants further investigation as a potential biomarker and druggable target for the purpose of slowing, halting, or reversing OA.

Vitamin Metabolism

Vitamin E metabolism was notably upregulated in OA cartilage compared to healthy. Vitamin E has antioxidant properties, which could prove beneficial in counteracting the heightened oxidative stress experienced by the joint during OA[42]. Additionally, vitamin A was dysregulated across OA endotypes. The relationship between OA and vitamin A, including the Vitamin A

derivative all-trans-retinoic acid, have garnered attention due to its key role in skeletal development and cartilage maintenance[43, 44]. Specifically, all-trans retinoic acid can regulate type X collagen and matrix metalloproteinase-13 driving a hypertrophic phenotype[44, 45]. Moreover, elevated vitamin A metabolite levels have been detected in SF, serum, and cartilage from OA individuals suggesting its potential role in OA within cartilage[43].

In contrast, vitamin K metabolism was downregulated in OA cartilage compared to healthy cartilage. These findings align with prior research that explored the relationship between OA and vitamin K, which is important for its role as a cofactor for the carboxylation of vitamin K-dependent proteins, including matrix Gla proteins, osteocalcin, and Gas-6[46]. These proteins are present in the joint and play a key role in the maintenance of cartilage and bone. Their absence or deficiency can lead to an increased incidence and progression of knee OA[46-48]. Specifically, alterations in vitamin K levels parallel the abnormalities observed in OA disease progression, encompassing aspects such as hypertrophic and apoptotic chondrocytes, cartilage mineralization, and endochondral ossification[49, 50].

Amino Acid Metabolism

Amino acid metabolism was significantly downregulated in OA cartilage compared to healthy cartilage. While histidine metabolism was not differently regulated across endotypes, the pronounced downregulation compared to healthy cartilage aligns with a previous study that identified declining trends in serum histidine levels as OA advances[51]. Additionally, the ratio of branched-chain amino acids to histidine has emerged as a potential indicator of disease progression[52]. In contrast, various amino acids including tryptophan, methionine, cysteine,

aspartate, and asparagine were upregulated in healthy cartilage compared to OA cartilage as confirmed by pairwise and endotype comparisons.

This pattern mirrors similar observations made in our prior work comparing SF metabolism from healthy, early, and late-stage OA patients, where these amino acid pathways were upregulated in healthy SF[16]. Focusing solely on OA cartilage, these same amino acid pathways displayed different regulation patterns across OA endotypes. This aligns with previous literature, indicating that these amino acids tend to decrease as OA progresses, with levels being highest in healthy cartilage, moderately high in early-stage OA, and diminishing with end-stage OA[53, 54]. Furthermore, specific amino acids like glycine and alanine, both of which are abundant in collagen, have been putatively identified as potential markers to distinguish osteoarthritic cartilage from healthy[7]. This observed dysregulation of amino acids may indicate their potential role in responding to disease and could reflect the degree of joint damage. Nevertheless, further research is required to underpin the relationship between amino acid metabolism and OA.

Limitations

This study included healthy cartilage samples to examine disease-associated metabolic changes, however, it is not without limitations. Firstly, the sample size for this study was not uniform, as 11 healthy cartilage and 35 OA cartilage samples were obtained. Secondly, relevant clinical covariates (*e.g.*, age, BMI, sex, prior medical history) and the time of death (to calculate the time between death and sample extraction) were not available for the obtained healthy cartilage samples. Furthermore, patient sex and age, with the exception of three patients, were provided for OA donors, yet BMI was not provided. Considering partial information provided for both healthy

and OA cartilage samples, age-, BMI-, and sex-matching analyses were not performed, nor can this information be used to shed light on driving factors that differentiate OA endotypes.

Conclusions

The results of this study provide clear evidence of OA-induced metabolic perturbations in human articular cartilage. Considering the heterogenous nature of OA, the detection of metabolic differences between healthy and OA individuals, and within OA individuals alone, can be further examined to pinpoint the diverse landscape of OA. With this approach, we uncovered specific metabolomic patterns and identified metabolites that may serve as valuable indicators of disease status or therapeutic targets. Expansion of this study will delineate joint-level metabolic activity in cartilage and how that is reflected, or associated, with the metabolism of other musculoskeletal tissues and fluids.

Acknowledgements

Authors thank the Montana State University Mass Spectrometry Facility including Dr. Donald Smith and Jesse Thomas for assisting with mass spectrometry analysis, interpretation, and metabolite identification. Funding for the Mass Spectrometry Facility used in this publication was made possible by the M.J. Murdock Charitable Trust, the National Institute of General Medical Sciences of the National Institutes of Health (P20GM103474 and S10OD28650). Additionally, we thank Brady Hislop for his assistance in analyzing data and building data analysis pipelines. This study was funded by the National Institutes of Health under Award Numbers R01AR073964 and R01AR081489 (RKJ), the National Science Foundation under Award Number CMMI 1554708 (RKJ), the M.J. Murdock Charitable Trust under Award Numbers FSU-2017207 and NS-

202016444 (AKH), and the National Aeronautics and Space Administration under Award Number 80NSSC20M0042 (AKH).

Abbreviations List

OA = osteoarthritis; LC-MS = liquid chromatography-mass spectrometry; LC-MS/MS = liquid chromatography tandem mass spectrometry; HCA = hierarchical clustering analysis; PCA = principal component analysis ; PLS-DA = partial least squares-discriminant analysis

FDR = false discovery rate; GAG = glycosaminoglycan; SF = synovial fluid; AA = arachidonic acid

References

1. Long H, Liu Q, Yin H, Wang K, Diao N, Zhang Y, et al. Prevalence trends of site-specific osteoarthritis from 1990 to 2019: findings from the Global Burden of Disease Study 2019. Arthritis Rheumatol 2022.

2. Vina ER, Kwoh CK. Epidemiology of osteoarthritis: literature update. Curr Opin Rheumatol 2018; 30: 160-167.

3. Barbour KE, Helmick CG, Boring M, Brady TJ. Vital Signs: Prevalence of Doctor-Diagnosed Arthritis and Arthritis-Attributable Activity Limitation - United States, 2013-2015. MMWR Morb Mortal Wkly Rep 2017; 66: 246-253.

4. Bitton R. The economic burden of osteoarthritis. Am J Manag Care 2009; 15: S230-235.

5. Hootman JM, Helmick CG, Barbour KE, Theis KA, Boring MA. Updated Projected Prevalence of Self-Reported Doctor-Diagnosed Arthritis and Arthritis-Attributable Activity Limitation Among US Adults, 2015-2040. Arthritis Rheumatol 2016; 68: 1582-1587.

6. Neogi T. The epidemiology and impact of pain in osteoarthritis. Osteoarthritis Cartilage 2013; 21: 1145-1153.

7. Shet K, Siddiqui SM, Yoshihara H, Kurhanewicz J, Ries M, Li X. High-resolution magic angle spinning NMR spectroscopy of human osteoarthritic cartilage. NMR Biomed 2012; 25: 538-544.

8. Xue M, Huang N, Luo Y, Yang X, Wang Y, Fang M. Combined Transcriptomics and Metabolomics Identify Regulatory Mechanisms of Porcine Vertebral Chondrocyte Development In Vitro. Int J Mol Sci 2024; 25.

9. Zignego DL, Hilmer JK, June RK. Mechanotransduction in primary human osteoarthritic chondrocytes is mediated by metabolism of energy, lipids, and amino acids. J Biomech 2015; 48: 4253-4261.

10. Bartlett SJ, Ling SM, Mayo NE, Scott SC, Bingham CO, 3rd. Identifying common trajectories of joint space narrowing over two years in knee osteoarthritis. Arthritis Care Res (Hoboken) 2011; 63: 1722-1728.

11. Collins JE, Katz JN, Dervan EE, Losina E. Trajectories and risk profiles of pain in persons with radiographic, symptomatic knee osteoarthritis: data from the osteoarthritis initiative. Osteoarthritis Cartilage 2014; 22: 622-630.

12. Karsdal MA, Bihlet A, Byrjalsen I, Alexandersen P, Ladel C, Michaels M, et al. OA phenotypes, rather than disease stage, drive structural progression--identification of structural progressors from 2 phase III randomized clinical studies with symptomatic knee OA. Osteoarthritis Cartilage 2015; 23: 550-558.

13. Bruyere O, Cooper C, Arden N, Branco J, Brandi ML, Herrero-Beaumont G, et al. Can we identify patients with high risk of osteoarthritis progression who will respond to treatment? A focus on epidemiology and phenotype of osteoarthritis. Drugs Aging 2015; 32: 179-187.

14. Deveza LA, Nelson AE, Loeser RF. Phenotypes of osteoarthritis: current state and future implications. Clin Exp Rheumatol 2019; 37 Suppl 120: 64-72.

15. Patti GJ, Yanes O, Siuzdak G. Innovation: Metabolomics: the apogee of the omics trilogy. Nat Rev Mol Cell Biol 2012; 13: 263-269.

16. Carlson AK, Rawle RA, Wallace CW, Brooks EG, Adams E, Greenwood MC, et al. Characterization of synovial fluid metabolomic phenotypes of cartilage morphological changes associated with osteoarthritis. Osteoarthritis Cartilage 2019; 27: 1174-1184.

17. Zhang W, Likhodii S, Zhang Y, Aref-Eshghi E, Harper PE, Randell E, et al. Classification of osteoarthritis phenotypes by metabolomics analysis. BMJ Open 2014; 4: e006286.

18. Welhaven HD, Viles E, Starke J, Wallace C, Bothner B, June RK, et al. Metabolomic profiles of cartilage and bone reflect tissue type, radiography-confirmed osteoarthritis, and spatial location within the joint. Biochem Biophys Res Commun 2024; 703: 149683.

19. Welhaven HD, Welfley AH, Pershad P, Satalich J, O'Connell R, Bothner B, et al. Metabolic phenotypes reflect patient sex and injury status: A cross-sectional analysis of human synovial fluid. Osteoarthritis Cartilage 2023.

20. Kessner D, Chambers M, Burke R, Agus D, Mallick P. ProteoWizard: open source software for rapid proteomics tools development. Bioinformatics 2008; 24: 2534-2536.

21. Smith CA, Want EJ, O'Maille G, Abagyan R, Siuzdak G. XCMS: processing mass spectrometry data for metabolite profiling using nonlinear peak alignment, matching, and identification. Anal Chem 2006; 78: 779-787.

22. Welhaven HD, Vahidi G et al. The Cortical Bone Metabolome of C57BL/6J Mice Is Sexually Dimorphic. JBMR Plus 2022; 6.

23. Pang Z, Zhou G, Ewald J, Chang L, Hacariz O, Basu N, et al. Using MetaboAnalyst 5.0 for LC-HRMS spectra processing, multi-omics integration and covariate adjustment of global metabolomics data. Nat Protoc 2022; 17: 1735-1761.

24. Xiao JF, Zhou B, Ressom HW. Metabolite identification and quantitation in LC-MS/MS-based metabolomics. Trends Analyt Chem 2012; 32: 1-14.

25. Wishart DS, Guo A, Oler E, Wang F, Anjum A, Peters H, et al. HMDB 5.0: the Human Metabolome Database for 2022. Nucleic Acids Res 2022; 50: D622-D631.

26. Elliott RJ, Gardner DL. Changes with age in the glycosaminoglycans of human articular cartilage. Ann Rheum Dis 1979; 38: 371-377.

27. Hjertquist SO, Lemperg R. Identification and concentration of the glycosaminoglycans of human articular cartilage in relation to age and osteoarthritis. Calcif Tissue Res 1972; 10: 223-237.

28. Thonar EJ, Masuda K, Hauselmann HJ, Uebelhart D, Lenz ME, Manicourt DH. Keratan sulfate in body fluids in joint disease. Acta Orthop Scand Suppl 1995; 266: 103-106.

29. Jay GD, Torres JR, Warman ML, Laderer MC, Breuer KS. The role of lubricin in the mechanical behavior of synovial fluid. Proc Natl Acad Sci U S A 2007; 104: 6194-6199.

30. Ioan-Facsinay A, Kloppenburg M. Bioactive lipids in osteoarthritis: risk or benefit? Curr Opin Rheumatol 2018; 30: 108-113.

31. Van de Vyver A, Clockaerts S, van de Lest CHA, Wei W, Verhaar J, Van Osch G, et al. Synovial Fluid Fatty Acid Profiles Differ between Osteoarthritis and Healthy Patients. Cartilage 2020; 11: 473-478.

32. Cillero-Pastor B, Eijkel G, Kiss A, Blanco FJ, Heeren RM. Time-of-flight secondary ion mass spectrometry-based molecular distribution distinguishing healthy and osteoarthritic human cartilage. Anal Chem 2012; 84: 8909-8916.

33. Baker KR, Matthan NR, Lichtenstein AH, Niu J, Guermazi A, Roemer F, et al. Association of plasma n-6 and n-3 polyunsaturated fatty acids with synovitis in the knee: the MOST study. Osteoarthritis Cartilage 2012; 20: 382-387.

34. Lippiello L, Walsh T, Fienhold M. The association of lipid abnormalities with tissue pathology in human osteoarthritic articular cartilage. Metabolism 1991; 40: 571-576.

35. Dalmao-Fernandez A, Lund J, Hermida-Gomez T, Vazquez-Mosquera ME, Rego-Perez I, Blanco FJ, et al. Impaired Metabolic Flexibility in the Osteoarthritis Process: A Study on Transmitochondrial Cybrids. Cells 2020; 9.

36. Smith RL, Soeters MR, Wust RCI, Houtkooper RH. Metabolic Flexibility as an Adaptation to Energy Resources and Requirements in Health and Disease. Endocr Rev 2018; 39: 489-517.

37. Blanco FJ, Lopez-Armada MJ, Maneiro E. Mitochondrial dysfunction in osteoarthritis. Mitochondrion 2004; 4: 715-728.

38. Blanco FJ, Rego I, Ruiz-Romero C. The role of mitochondria in osteoarthritis. Nat Rev Rheumatol 2011; 7: 161-169.

39. Lane RS, Fu Y, Matsuzaki S, Kinter M, Humphries KM, Griffin TM. Mitochondrial respiration and redox coupling in articular chondrocytes. Arthritis Res Ther 2015; 17: 54.

40. Wu L, Liu H, Li L, Liu H, Cheng Q, Li H, et al. Mitochondrial pathology in osteoarthritic chondrocytes. Curr Drug Targets 2014; 15: 710-719.

41. Dambrova M, Makrecka-Kuka M, Kuka J, Vilskersts R, Nordberg D, Attwood MM, et al. Acylcarnitines: Nomenclature, Biomarkers, Therapeutic Potential, Drug Targets, and Clinical Trials. Pharmacol Rev 2022; 74: 506-551.

42. Collins JA, Wood ST, Nelson KJ, Rowe MA, Carlson CS, Chubinskaya S, et al. Oxidative Stress Promotes Peroxiredoxin Hyperoxidation and Attenuates Pro-survival Signaling in Aging Chondrocytes. J Biol Chem 2016; 291: 6641-6654.

43. Davies MR, Ribeiro LR, Downey-Jones M, Needham MR, Oakley C, Wardale J. Ligands for retinoic acid receptors are elevated in osteoarthritis and may contribute to pathologic processes in the osteoarthritic joint. Arthritis Rheum 2009; 60: 1722-1732.

44. Underhill TM, Weston AD. Retinoids and their receptors in skeletal development. Microsc Res Tech 1998; 43: 137-155.

45. Flannery CR, Little CB, Caterson B, Hughes CE. Effects of culture conditions and exposure to catabolic stimulators (IL-1 and retinoic acid) on the expression of matrix metalloproteinases (MMPs) and disintegrin metalloproteinases (ADAMs) by articular cartilage chondrocytes. Matrix Biol 1999; 18: 225-237.

46. Misra D, Booth SL, Tolstykh I, Felson DT, Nevitt MC, Lewis CE, et al. Vitamin K deficiency is associated with incident knee osteoarthritis. Am J Med 2013; 126: 243-248.

47. Shea MK, Kritchevsky SB, Hsu FC, Nevitt M, Booth SL, Kwoh CK, et al. The association between vitamin K status and knee osteoarthritis features in older adults: the Health, Aging and Body Composition Study. Osteoarthritis Cartilage 2015; 23: 370-378.

48. Wallin R, Schurgers LJ, Loeser RF. Biosynthesis of the vitamin K-dependent matrix Gla protein (MGP) in chondrocytes: a fetuin-MGP protein complex is assembled in vesicles shed from normal but not from osteoarthritic chondrocytes. Osteoarthritis Cartilage 2010; 18: 1096-1103.

49. Luo G, Ducy P, McKee MD, Pinero GJ, Loyer E, Behringer RR, et al. Spontaneous calcification of arteries and cartilage in mice lacking matrix GLA protein. Nature 1997; 386: 78-81.

50. Price PA, Williamson MK, Haba T, Dell RB, Jee WS. Excessive mineralization with growth plate closure in rats on chronic warfarin treatment. Proc Natl Acad Sci U S A 1982; 79: 7734-7738.

51. Zhang Q, Li H, Zhang Z, Yang F, Chen J. Serum metabolites as potential biomarkers for diagnosis of knee osteoarthritis. Dis Markers 2015; 2015: 684794.

52. Zhai G, Wang-Sattler R, Hart DJ, Arden NK, Hakim AJ, Illig T, et al. Serum branched-chain amino acid to histidine ratio: a novel metabolomic biomarker of knee osteoarthritis. Ann Rheum Dis 2010; 69: 1227-1231.

53. Abdelrazig S, Ortori CA, Doherty M, Valdes AM, Chapman V, Barrett DA. Metabolic signatures of osteoarthritis in urine using liquid chromatography-high resolution tandem mass spectrometry. Metabolomics 2021; 17: 29.

54. Igari T, Tsuchizawa M, Shimamura T. Alteration of tryptophan metabolism in the synovial fluid of patients with rheumatoid arthritis and osteoarthritis. Tohoku J Exp Med 1987; 153: 79-86.

CHAPTER FIVE

METABOLIC PHENOTYPES REFLECT PATIENT SEX AND INJURY STATUS: A CROSS-SECTIONAL ANALYSIS OF HUMAN SYNOVIAL FLUID

Contribution of Authors and Co-Authors

Manuscript in Chapter 5

Author: Hope D. Welhaven

Contributions: Designed experiments, performed metabolite extractions, ran LC-MS samples, analyzed and interpreted data, and drafted manuscript.

Co-Author: Avery H. Welfley

Contributions: Performed metabolite extractions and analyzed and interpreted data.

Co-Author: Prayag Pershad

Contributions: Obtained samples and provided clinical input.

Co-Author: James Satalich

Contributions: Obtained samples and provided clinical input.

Co-Author: Robert O'Connell

Contributions: Performed repairs and assisted in conception and design of experiments.

Co-Author: Alexander R. Vap

Contributions: Performed repairs and assisted in conception and design of experiments.

Co-Author: Brian Bothner

Contributions: Designed experiments, analyzed data, drafted and edited the manuscript.

Co-Author: Ronald K. June

Contributions: Corresponding author, designed experiments, analyzed data, drafted and edited the manuscript.

Manuscript Information

Hope D. Welhaven, Avery H. Welfley, Prayag Pershad, James Satalich, Robert O'Connell, Brian Bothner, Alexander R. Vap, Ronald K. June

Osteoarthritis and Cartilage

Status of Manuscript:

☐ Prepared for submission to a peer-reviewed journal
☐ Officially submitted to a peer-reviewed journal
☐ Accepted by a peer-reviewed journal
X Published in a peer-reviewed journal

Elsevier

Vol. 31, Supplement 1, S1-S434, March 2023

https://doi.org/10.1016/j.joca.2023.01.382

Abstract

Objective: Osteoarthritis is a heterogeneous disease. The objective was to compare differences in underlying cellular mechanisms and endogenous repair pathways between synovial fluid from male and female participants with different injuries to improve current understanding of the pathophysiology of downstream post-traumatic osteoarthritis.

Design: Synovial fluid from n=33 knee arthroscopy patients between 18 and 70 years with no prior knee injuries was obtained pre-procedure and injury pathology assigned post-procedure. Synovial fluid was extracted and analyzed via liquid chromatography-mass spectrometry metabolomic profiling to examine differences in metabolism between injury pathologies (ligament, meniscal, and combined ligament and meniscal) and patient sex. Samples were pooled and underwent secondary fragmentation to identify metabolites.

Results: Different knee injuries uniquely altered synovial fluid metabolites and downstream pathways including amino acid, lipid, and inflammatory-associated metabolic pathways. Notably, sexual dimorphic metabolic phenotypes were examined between males and females and within injury pathology. Cervonyl carnitine and other identified metabolites differed in concentrations between sexes.

Conclusions: These results suggest that different injuries and patient sex are associated with distinct metabolic phenotypes. Considering these phenotypic associations, a greater understanding of metabolic mechanisms associated with specific injuries, sex, and post-traumatic osteoarthritis development may yield data regarding how endogenous repair pathways differ between male and female injury types. Ongoing metabolomic analysis of synovial fluid in injured male and female patients can be performed to monitor post-traumatic osteoarthritis development and progression.

Introduction

Post-traumatic osteoarthritis (PTOA) accounts for approximately 12% of osteoarthritis (OA) cases equating to 5.6 million cases annually[1, 2]. One of the most prevalent risk factors that contributes to PTOA is joint injury. Within the United States, nearly 250,000 anterior cruciate ligament (ACL) injuries occur annually where approximately 70% of injured patients undergo ACL reconstruction[3, 4]. ACL injuries are frequently accompanied by damage to other tissues and structures within the knee such as the meniscus[5]. PTOA prevalence is influenced by the type of injury, where ACL injury alone has a prevalence range between 13-39%, whereas this range is significantly higher amongst those with combined ligament and meniscal injuries (21-48%)[2, 6, 7].

Other patient-specific risk factors that contribute to PTOA include age, body mass index (BMI), and sex. Annually, 15% of knee injuries were attributed to high-school athletes with young female athletes being twice as likely to sustain knee injuries requiring surgical repair compared to male athletes[8]. Furthermore, females are more likely to develop and experience more severe OA compared to males[9, 10]. These sex-differences can likely be attributed to hormonal and anatomical differences where females have wider pelvises, small femurs, thinner articular cartilage at the distal femur, a smaller ACL, and a narrower intercondylar notch[11, 12].

Although it is established that PTOA is associated with injury as well as other patient-specific risk factors like sex, underlying mechanisms and metabolic alterations following injury at the joint level remain unknown. Examining acute differences in response to various injury types amongst males and females has the potential to positively influence patient treatment, outcomes, and reduce the burden of both PTOA and OA. The application of metabolomic profiling may

identify biochemical phenotypes that represent and capture the physiological and metabolic status of the tissue of interest.

A handful of studies have used metabolomic profiling of various samples including blood, urine, and synovial fluid (SF) to understand the pathology of OA[13-16]. SF is an optimal sample type as it is in direct contact with joint tissue where joint cells (i.e., chondrocytes, bone cells) are secreted into the joint cavity[13, 14, 17]. Thus, SF content is reflective of joint status during times of health and disease and provides a better representation of joint metabolism compared to blood and urine samples which are diluted in the circulatory compartment. While metabolomics has been applied to SF to underpin OA pathogenesis, the authors are not aware of any study using this method to quantitatively investigate acute metabolic perturbations induced by different knee injuries among males and females. By doing so, the local and systemic response to joint injury can be further examined and has the potential to influence treatment and intervention to benefit overall patient health post-injury in the future.

The primary goal of this study was to compare differences in underlying cellular mechanisms and endogenous repair pathways between synovial fluid from male and female participants with different injuries to improve current understanding of the pathophysiology of downstream post-traumatic osteoarthritis. The secondary goal of this study was to identify differences in pathway regulation and metabolite concentration between male and female participants. To accomplish both goals, metabolites were extracted from injured participants' SF and analyzed via liquid chromatography-mass spectrometry (LC-MS). Global metabolomic profiling was applied to find specific metabolic perturbations associated with types of injury and patient sex. The identification of dysregulated metabolic pathways and metabolites may underpin

mechanisms that differ between injured male and females and may shed light on how PTOA manifest later in life. Moreover, ongoing metabolomic analysis of SF post-repair can be performed in conjunction with measurement of patient outcomes to oversee PTOA development and progression.

Methods

Participant Information and Inclusion Criteria

In this cross-sectional study, 58 participants were screened for eligibility between July 2021 and February 2022 at Virginia Commonwealth University. Inclusion criteria to participate in this cross-sectional study were (1) age between the age of 18-70 and (2) no history of prior knee injuries, chronic pain, or autoimmune disease(s). Under IRB approval, participant SF was obtained from 45 knee arthroscopy patients prior to repair (Fig. 5.1, Table 5.1, Supplemental Table 5.1). Of the 45 participants, 12 were excluded because the reason for surgery was not related to a traumatic injury (n=11) and inadequate volume of SF (n=1). The time between injury and joint repair was not uniform across all participants, however, varying windows of time (days) between injury and repair did not influence metabolic results. De-identified patient information provided included patient sex, age, BMI, and injury pathology. To limit potential bias, patient information including pathology, BMI, age, and sex were blinded throughout data analysis.

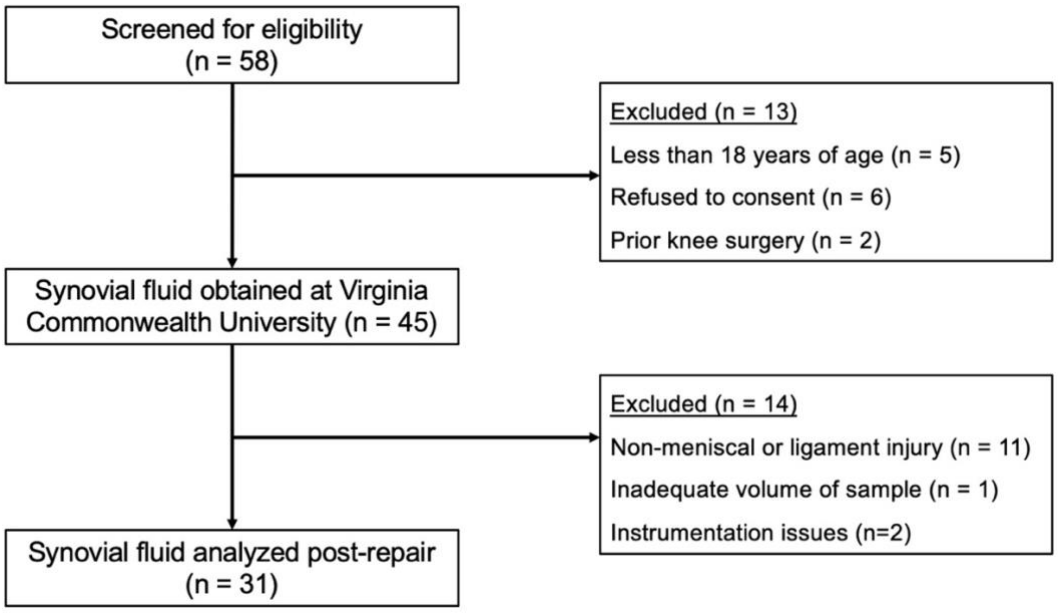

Figure 5.1. Participant eligibility and screening.

Table 5.1. Participant information. Values indicate number of participants in each group.

Sex		BMI		Age		Ligament	Meniscus	Ligament & Meniscus
Female	17	18-24.9	13	18-29	12	5	11	1
Male	14	25-31.9	12	31-44	9	5	6	3
Total	31	32-50	6	45-70	10	10	17	4

Synovial Fluid Sampling, Extraction, and Metabolic Profiling

For all participants, SF was acquired in the operating room pre-procedure by one of two surgeons, and pathology assignment (i.e., right medial meniscus tear) was assigned post-procedure based on observations made in the operating room and the postoperative pathology report. Participant injury pathologies were categorized into one of three pathology groups: ligament (L), meniscal (M), and combined ligament and meniscal (LM) injuries. A concise overview of the

metabolite extraction and MS methods used in this study are discussed in detail in the supplementary material. In brief, all SF samples (n=33) were extracted with methanol and acetonitrile, centrifuged, dried down via vacuum concentration, and prepped for LC-MS analysis. To derive metabolite identifications, two pooled samples containing extracted SF from samples selected at random were prepped for liquid chromatography tandem mass spectrometry (LC-MS/MS) analysis which entails fragmentation of parent ions. All sample data, including chromatograms and spectra, were manually inspected to determine if any issues arose during the mass spectrometry run. In doing so, two samples (n=2) were removed from the analysis as they resembled quality control blanks and high levels of background noise.

All data (n=31) were processed using MSConvert[18] and XCMS[19]. MetaboAnalyst[20] was utilized to statistically analyze samples, visualize dissimilarities, and pinpoint pathway dysregulation between males and females with different injuries. To identify metabolite features data from LC-MS/MS data of pooled samples were analyzed with Progenesis QI (Nonlinear Dynamics, Newcastle, UK). Full details on metabolomic profiling, including statistical and pathway analyses, and metabolite identification can be found in the supplementary material.

Results

The Synovial Fluid Metabolome Differs by Injury Pathology

In total, 7,794 metabolite features were detected by LC-MS in the 33 SF samples. To assess global differences between injury pathologies, all metabolite features were analyzed using Principal Component Analysis (PCA) and Partial Least Squares-Discriminant Analysis (PLS-DA) (Fig. 5.2 A-B). PCA displayed overlap of groups with PC1 and PC2 accounting for 40.1% of the

variability in the dataset, whereas PLS-DA showed less overlap with Components 1 and 2 accounting for 31.6% of the variability in the dataset.

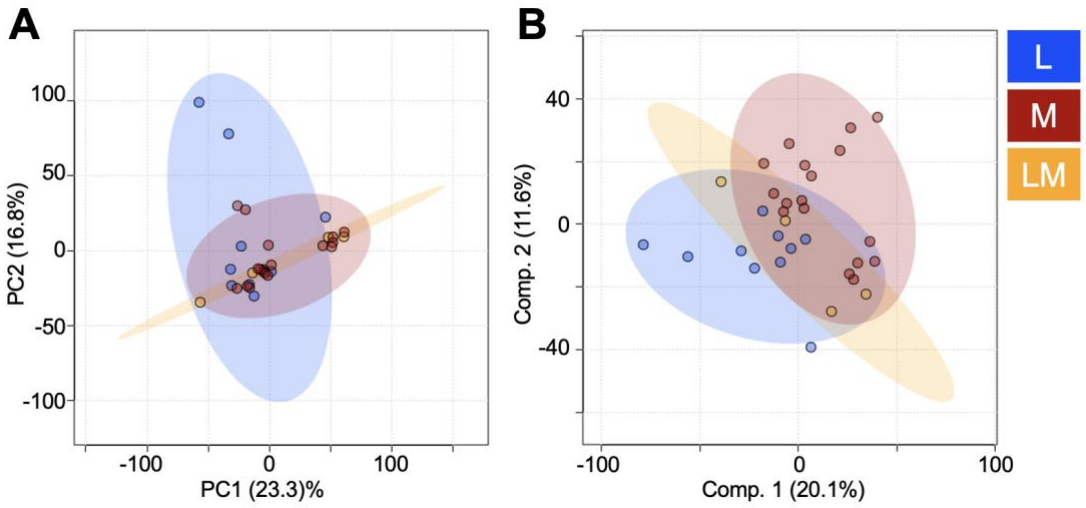

Figure 5.2. Global profiles considering all detected metabolite features show moderate differences between injury pathologies. (A) Principal component analysis, an unsupervised test, shows some overlap when considering all 7,794 features and accounts for 40.1% of the variability in the dataset. (B) Partial least squares-discriminant analysis, a supervised test, similarly shows some overlap of groups and accounts for 31.7% of the variability in the dataset. These two tests combined suggest that global profiles generated by all metabolite features detected somewhat differ and that additional analyses are required to pinpoint specific phenotypic changes. The colors in A and B correspond to: Ligament injuries - light blue; Meniscal injuries - red; Ligament and Meniscal injuries - yellow. L = ligament injuries. M = meniscal injuries. LM = ligament and meniscal injuries.

Although distinct metabolic patterns at the global level showed overlapping groups, the top 25 highest PLS-DA Variable Importance in Projection (VIP) scoring metabolites had scores > 2.2 and were selected for further analysis to examine and pinpoint phenotypic differences in regulation between pathology groups. VIP scores reflect how much a variable contributes to the model and are calculated by summing the squared correlations between the PLS-DA components and the original value with appropriate weighting. Of the 25 metabolite features, 8 were the most abundant in M injuries, the least abundant in L injuries, and intermediary abundance levels in LM injuries

(Fig. 5.3 A Cluster 1). Conversely, 8 of the 25 metabolite features were the most abundant in L injuries, the least abundant in M injuries, and intermediary abundance levels in LM injuries (Fig. 5.3 A Cluster 2). Lastly, 9 metabolite features were similar in abundance in L and LM injuries, and lowest in M injuries (Fig. 5.3 A Cluster 3). Additionally, PLS-DA VIP metabolites features with a score < 2 were then matched to identifications made using LC-MS/MS. In total, 7 metabolites were identified where tryptophanoland gandoeric acid were highest in abundance among LM participants, whereas isoleucyl-proline, alpha linoleic acid, linoleic acid, lansiumamide C, and eriojaposide B were highest in abundance among M injuries (Supplemental Table 5.2).

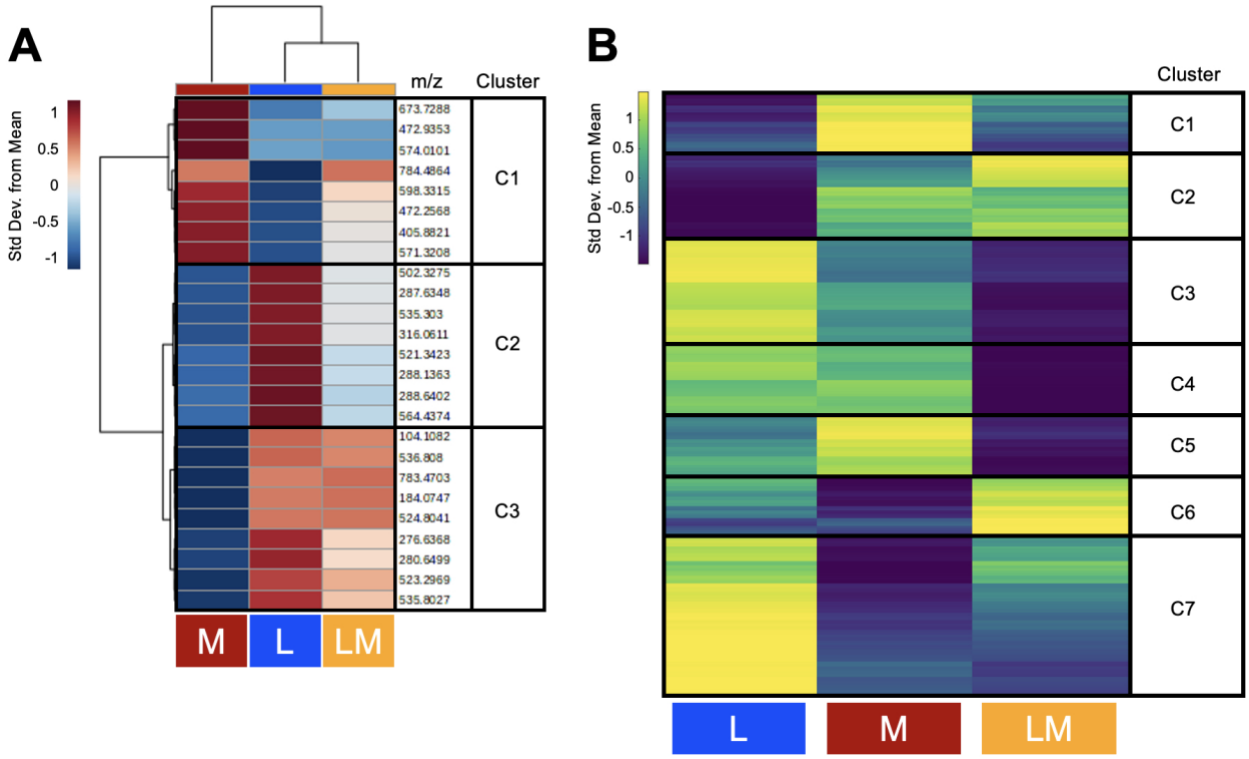

Figure 5.3. Heatmap analyses of participants reveal metabolite features and metabolic pathways that are differently regulated between injury pathologies. (A) Hierarchical clustering analysis visualized by a group median heatmap of the 25 PLS-DA Variable in Importance Projection Scores shows that different injury pathologies trigger distinct metabolic regulation patterns post-injury. Clusters 1-3 (C1-C3) highlight different regulation patterns between injuries. (B) Clusters of coregulated metabolite features within synovial fluid from participants with different knee injuries indicate that distinct metabolic phenotypes across injury pathologies. Clusters (1-3) were subjected to pathway enrichment analyses to identify pathways that differed in regulation between injury pathologies. Warmer colors (yellow) and cooler colors (blue) indicate higher and lower metabolite intensities, respectively. The colors in A-C correspond to: Ligament injuries - light blue; Meniscal injuries - red; Ligament and Meniscal injuries - yellow. L = ligament injuries. M = meniscal injuries. LM = ligament and meniscal injuries.

Functional pathway enrichment analyses were conducted to underpin endogenous repair pathways that differ between injury pathologies. To do so, a median metabolite intensity heatmap analysis was performed to visualize global changes across the metabolome to distinguish patterns, or clusters, of co-regulated and differentially expressed metabolite features (Fig. 5.3 B). Clusters of metabolites identified underwent pathway enrichment analyses using MetaboAnalyst's

functional analysis feature. Conversely, features that had the highest concentration in M injuries, and lowest in L injuries, mapped to lipid-related pathways (fatty acid oxidation and activation, glycosphingolipid metabolism, omega-6 fatty acid metabolism), histidine metabolism, TCA cycle, and glycolysis (Fig. 5.3 B Cluster 1). Arginine and proline metabolism was detected in both L and M injuries and was lowest in LM injuries (Fig. 5.3 B Clusters 1&2). Additionally, those highest in M injuries but lowest in LM injuries mapped to other lipid-related pathways (mono-unsaturated fatty acid beta-oxidation, omega-3 fatty acid metabolism, fatty acid biosynthesis, saturated fatty acids beta-oxidation, dimethyl-branched-chain fatty acid mitochondrial beta-oxidation) (Fig. 5.3 B Cluster 5). Metabolite features that had the highest concentration in LM injuries, and the lowest in L injuries, mapped to amino acid metabolism (lysine, glycine, serine, alanine, threonine), trihydroxycoprostanoyl-CoA beta-oxidation, proteoglycan biosynthesis, and vitamin B3 metabolism (Fig. 5.3 B Cluster 2). Additionally, features highest in LM injuries, but lowest in M injuries, mapped to phosphatidylinositol phosphate metabolism, the carnitine shuttle, and linoleate metabolism (Fig. 5.3 B Cluster 6). Metabolite features that had the highest concentration in L injuries, and lowest in M injuries, mapped to sialic acid metabolism, aspartate and asparagine metabolism, and glycerophospholipid metabolism (Fig. 5.3 B Cluster 7). Additionally, biopterin metabolism was highest in L injuries but lowest in LM injuries (Fig. 5.3 B Cluster 3) (Table 5.2, Supplemental Table 5.3). All pathways reported had an FDR-corrected p-value < 0.05. Taken together, the regulation of each pathology group is distinct further supporting the notion that the SF metabolome differ by injury pathology. However, we are unable to speculate as to why key metabolites from each of the L and M groups is not necessarily as prominent in the LM group.

Table 5.2. Metabolic pathways associated with ligament, meniscal, and ligament and meniscal injuries identified by median metabolite intensity heatmap analysis. All reported pathways have a FDR-corrected significance level < 0.05. L = ligament injuries. M = meniscal injuries. LM = ligament and meniscal injuries. Clusters defined in Figure 5.3 B.

Cluster	Pathway	Highest	Lowest
1, 2	Arginine and Proline Metabolism	L, M	LM
1	Fatty acid oxidation	M	L
1	Histidine metabolism	M	L
1	Glycolysis and Gluconeogenesis	M	L
1	Squalene and cholesterol biosynthesis	M	L
1	TCA cycle	M	L
1	Glycosphingolipid metabolism	M	L
1	Fatty acid activation	M	L
1	Leukotriene metabolism	M	L
1	Omega-6 fatty acid metabolism	M	L
2	Trihydroxycoprostanoyl-CoA beta-oxidation	LM	L
2	Proteoglycan biosynthesis	LM	L
2	Vitamin B3 metabolism	LM	L
2	Lysine metabolism	LM	L
2	Glycine, serine, alanine and threonine metabolism	LM	L
2	Valine, leucine and isoleucine degradation	LM	L
3	Biopterin metabolism	L	LM
5	Mono-unsaturated fatty acid beta-oxidation	M	LM
5	Porphyrin metabolism	M	LM
5	Omega-3 fatty acid metabolism	M	LM
5	De novo fatty acid biosynthesis	M	LM
5	Fatty Acid Metabolism	M	LM
5	Saturated fatty acids beta-oxidation	M	LM
5	Dimethyl-branched-chain fatty acid mitochondrial beta-oxidation	M	LM
6	Phosphatidylinositol phosphate metabolism	LM	M
6	Linoleate metabolism	LM	M
6	Carnitine shuttle	LM	M
7	Sialic acid metabolism	L	M
7	Aspartate and asparagine metabolism	L	M
7	Glycerophospholipid metabolism	L	M

Participant Sex Influences Metabolomic Profiles Across Injury Pathologies

To determine if participant sex influences the SF metabolome, PCA, PLS-DA, and volcano plot analyses were conducted. PCA displayed overlap (Fig. 5.4 A) whereas PLS-DA revealed some overlap of male and female participants suggesting the SF metabolome reflects participant sex (Fig. 5.4 B). While overlap was observed in both PCA and PLS-DA, this can possibly be attributed to analyzing all participant SF considering only the factor of sex. To further investigate potential sexual dimorphism, volcano plot assessed male and female participant SF-derived metabolites using significance and fold change. This analysis identified 6 metabolites features that were significant and had higher concentrations in males compared to females, and 35 metabolite features that were significant and in higher concentration in females compared to males ($FC > 2$, $p < 0.05$) (Fig. 5.4 C).

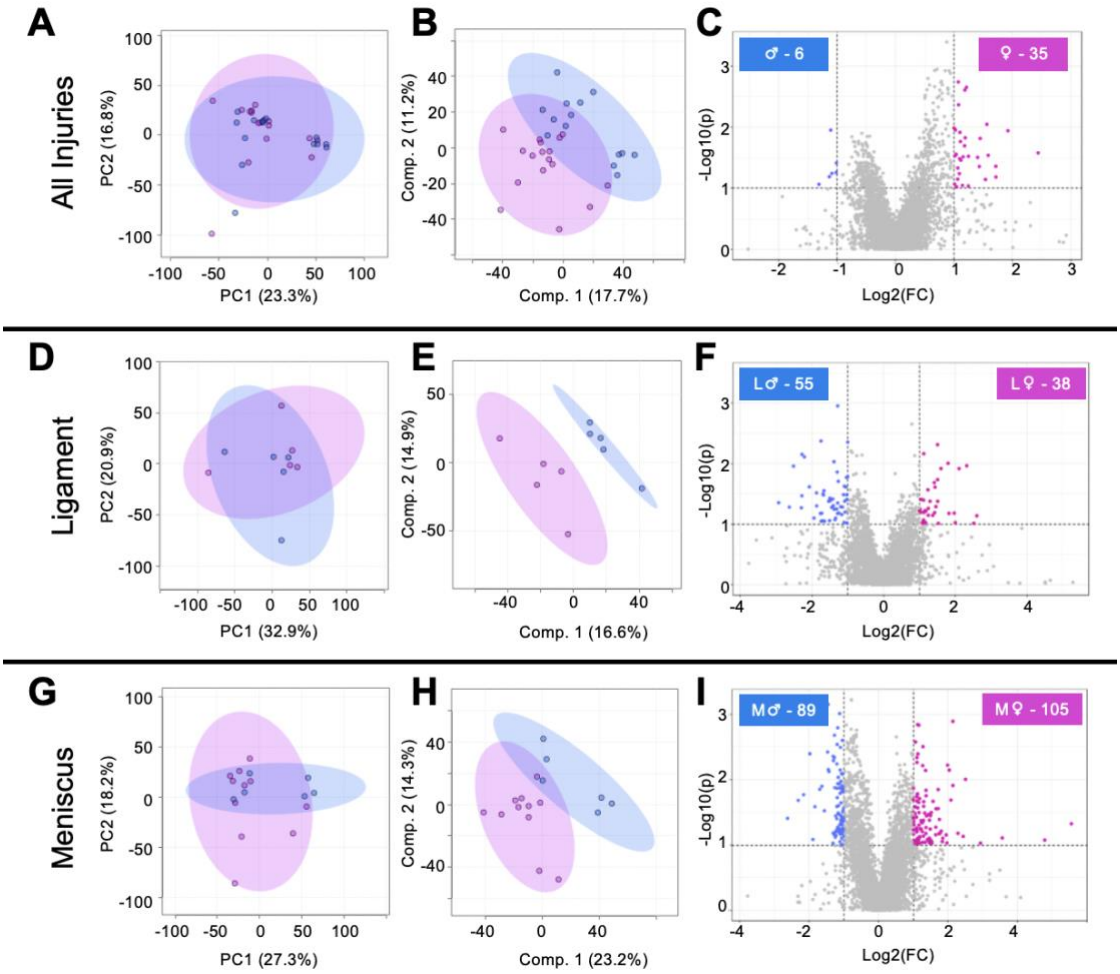

Figure 5.4. Metabolomic profiles of synovial fluid-derived metabolite features are associated with participant sex and injury pathology. (A) PCA and (B) PLS-DA display some overlap when comparing all male and female participant suggesting that the SF metabolome is potentially influenced by participant sex. (C) Volcano plot analysis identified 35 etabolite features in females that had a FC > 2 and p-value < 0.05. Conversely, 6 had a FC < -2 and a p-value < 0.05 in males. Similarly, (D) PCA, (E) PLS-DA, and (F) volcano plot analysis was applied to examine metabolic differences between male and female participants with ligament injuries and the same suite of analyses were applied to identify differences between male and female participants with meniscal injuries (G-I). Considering the identification of subpopulations of metabolite features that differ in regulation between male and female participants (A-C), male and female participants with ligament injuries (D-F), and male and female participants with meniscal injuries (G-I), it is evident that the metabolome is influenced by participant sex and injury pathology. The colors in A-I correspond to male and female participants: pink – females, blue – males. L = ligament injuries. M = meniscal injuries.

In a similar way, pairwise comparisons were performed to examine participant sex differences within injury pathology for L and M injuries. LM injuries were not examined due to insufficient sample size (LM Male n = 4, LM Female n = 1). Considering L injuries, PCA displayed some overlap (Fig. 5.4 D) while PLS-DA displayed clear separation of participants that differ by sex (Fig. 5.4 E). Volcano plot analysis identified 55 metabolite features that were significant and had higher concentrations in L males, whereas 38 were significant and in higher concentrations in L females (FC > 2, $p < 0.05$) (Fig. 5.4 F).

These same analyses were performed to analyze metabolic phenotypes associated with male and female M injuries. PCA displayed some overlap (Fig. 5.4 G), whereas PLS-DA showed near complete separation of male and female participants with M injuries, further supporting the notion that differences at the metabolic differences are associated with participant sex (Fig. 5.4 H). Volcano plot analysis identified 89 metabolite features that were significant and had higher concentration in M males, and 105 features that were significant and had higher concentrations in M females (FC > 2, $p < 0.05$) (Fig. 5.4 I).

Populations of metabolite features from volcano plot analyses were then matched to identifications made using LC-MS/MS data. As expected with LC-MS/MS, not all metabolite features were able to be identified (Supplemental Table 5.4). Of the 18 identified metabolites, a noteworthy metabolite that was statistically significant across all volcano plot analyses was cervonyl carnitine. Specifically, cervonyl carnitine was detected in higher abundances in all females compared to males and when considering injury pathology) (Fig. 5.5 A-C). Although an identified metabolite was not higher in abundance in all males compared to males and when considering injury pathology, identified metabolites that were higher in abundance in males

compared to females included alpha-Chaconine (M males), Lucidenic acid A (M males), lysine (L males), arginine (M males), as well as others (Supplemental Table 5.4). Overall, the detection of distinct global phenotypes and differences in regulation of identified metabolites between male and female participants strongly suggests that participant sex influences SF metabolism across injury pathologies.

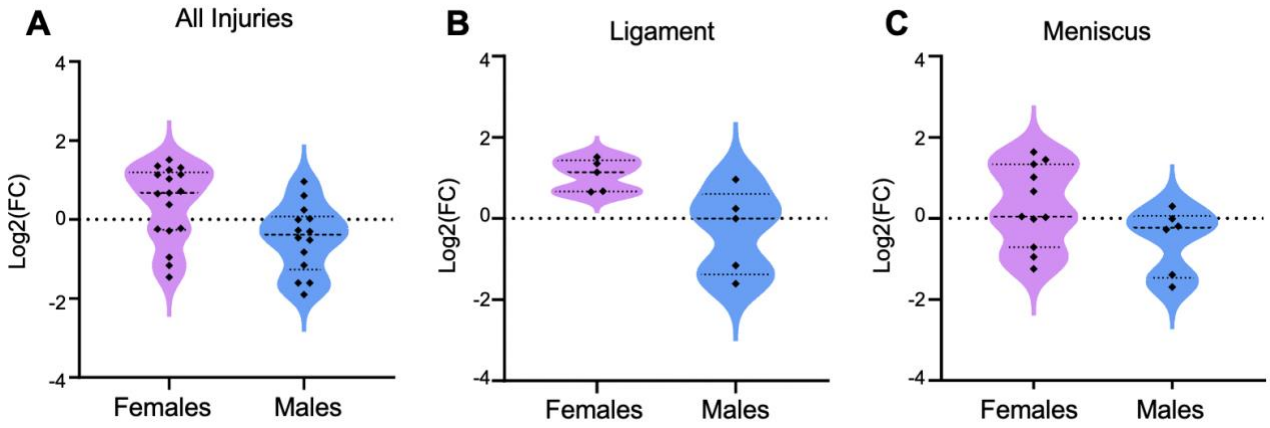

Figure 5.5. Cervonyl Carnitine differs in concentration between male and female participants. The identified metabolite, Cervonyl carnitine, was higher in concentration in (A) all female participants compared to males, (B) in females with ligament injuries and (C) meniscal injuries compared to males within the same injury pathology group. Mass-to-charge intensities of interest were normalized and used to generate plots. To correct for multiple comparisons, FDR p-value corrections were performed and were less than < 0.05. The colors correspond to male and female participants: pink – females, blue – males.

Discussion

To our knowledge, this is the first study to examine acute metabolic responses following different injury types in male and female human SF using mass-spectrometry. The goals of this study were to (1) identify metabolic perturbations that differ across injury pathologies including L, M, and combined LM injuries and (2) examine metabolic differences associated with sex. By applying mass spectrometry-based metabolomics, metabolic phenotypes between injury

pathologies vary suggesting different types of injury trigger specific acute metabolic responses. Additionally, SF-derived metabolites reflected participant sex, and male and female participants with similar injuries were metabolically distinct from each other. The detection of metabolites and generation of metabolomic phenotypes based on sex and injury pathology can be used to improve patient treatment and allow for more precise treatment to benefit joint and patient health post-injury.

Acute Metabolic Responses Post-Injury Varies Based on Injury Pathology

Previous studies used metabolomics to examine post-injury metabolic shifts in animal models[17, 21, 22], and only one study to date has examined metabolic shifts in human SF induced by different injuries using nuclear magnetic resonance spectroscopy (NMR)[23]. This study detected significant changes in glucose, amino acids, lipids, and lactate indicating increased demand for these compounds within the joint post-injury. The results of this cross-sectional study closely align with previously generated metabolic phenotypes, showing similar pathway regulation differences between injuries. Specifically, differences in lipid- and oxidative-related metabolism (M injuries), amino acid metabolism (all injuries), and inflammatory-associated pathways (LM injuries) differed in regulation between injury pathologies (Fig. 5.6).

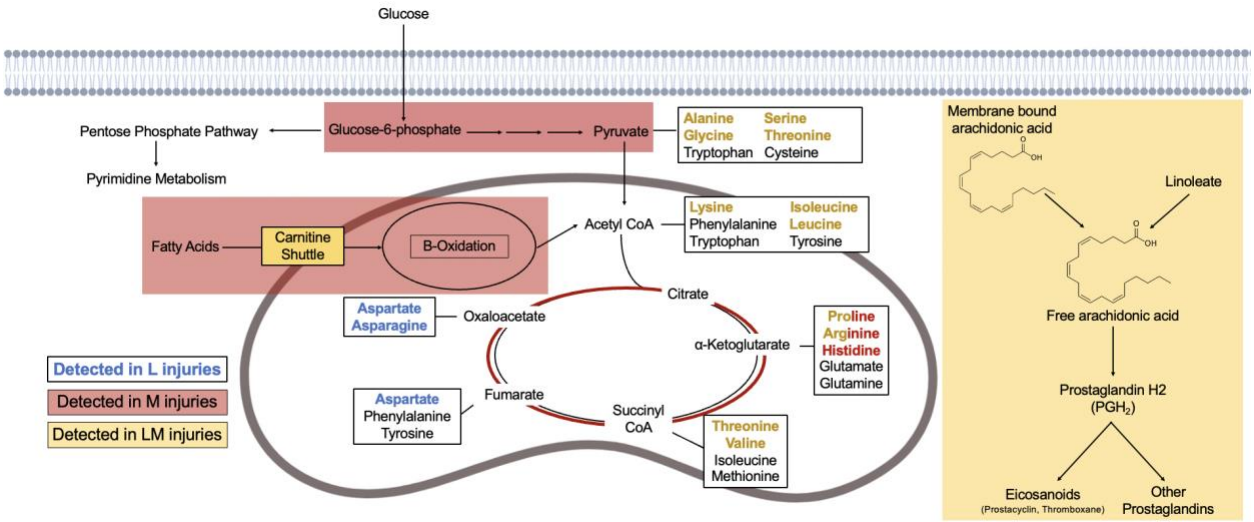

Figure 5.6. Alterations in synovial fluid metabolism post-injury are associated with different injury types. Metabolites that differ in abundance across ligament, meniscal, and ligament and meniscal injuries are associated with amino acid, lipid, and inflammation-related pathways. Multiple amino acids were detected within each injury pathology. Amino acids bolded in blue, red, and yellow were detected in synovial fluid from participants with ligament, meniscus, and ligament and meniscus injuries, respectively. Metabolite features detected among participants with meniscal injuries mapped to lipid-related pathways including fatty acid activation, oxidation, and biosynthesis, beta-oxidation related pathways, and others (red). Ligament and meniscal injuries were associated with linoleate metabolism, which is related to arachidonic acid metabolism and the generation of prostaglandins and eicosanoids (yellow). Additionally, the metabolite features involved in the carnitine shuttle was detected in high abundances in participants with ligament and meniscal injuries. L = ligament injuries. M = meniscal injuries. LM = ligament and meniscal injuries.

Participants with L injuries showed the greatest dysregulation of sialic acid metabolism compared to other injuries. Sialic acid plays a vital role in cell differentiation, proliferation, and inflammation. Previous studies have linked elevated plasma sialic acid concentration to inflammation[24, 25] and OA[26]. Enriched sialic acid metabolism in SF from L participants may reflect joint inflammation post-injury and could be monitored long-term. However, additional investigation is needed to understand the relationship between sialic acid and joint inflammation following injury and downstream PTOA development.

Aspartate and asparagine metabolism was the most dysregulated in participants with L injuries compared to other injuries. Both amino acids have anti-inflammatory effects and are found in low concentrations in OA patient serum[27, 28]. Sheep SF analysis post-ACL injury also showed increased levels of these amino acids compared to non-injured controls[17]. Proline and arginine metabolism was detected in both L and M injuries and was the lowest in LM injuries. Proline, a downstream product of arginine, contributes to collagen synthesis[29] and has been associated with OA[28]. A prior study detected higher concentrations of these amino acids in SF immediately following injury that then decreased overtime in a non-invasive mouse ACL tear model[22] leading authors to hypothesize that these amnio acids could be markers of injury but further investigation is needed.

Amongst M participants, lipid-related oxidative metabolic pathways were the most dysregulated compared to L and LM participants. During normal conditions, SF relies on lipid species to provide lubrication and reduce joint friction, therefore, this dysregulation likely reflects the lubrication and inflammatory statuses of the joint tissue post-M injury. Moreover, the dysregulation of fatty acid biosynthesis, oxidation, and degradation as well as glycolysis and the TCA cycle across participants with M injuries may reflect mitochondrial health and dysfunction in other joint tissues post-injury. Functioning mitochondria rely on glucose and fatty acids to yield energy, but dysfunctional mitochondria switch to relying on fatty acids more than glucose[30, 31]. This can lead to the accumulation of fatty acids[32, 33] resulting in lower ATP production, impaired stress response, an increase in reactive oxygen species, apoptosis, and combined can lead to systemic irreparable damage[34]. Previous studies have also found dysregulated lipid metabolism in

SF from OA patients[13] and altered fatty acid metabolism in injured mice[21], suggesting its significance in joint health.

Previous metabolomics studies on SF and the results of this cross-sectional study suggest that M injuries may trigger mitochondrial dysfunction leading to an influx of fatty acids into the mitochondria where they become the primary energy source. This could cause accumulation and potential development of PTOA, or early-stage OA develop. The response appears to be more pronounced in M injuries, indicating distinct metabolic mechanisms are associated with specific injuries, Further investigation into metabolic regulation following injury could provide insights into the contribution of endogenous repair pathways to PTOA development.

Linoleate metabolism was the most dysregulated pathway among LM participants compared to L and M participants. Linoleic acid, a prominent fatty acid in SF, may be related to the degree of joint disease based on previous studies[35, 36]. This pathway is upstream of arachidonic acid metabolism which generates fast-acting and short-lived signaling molecules such as the pro-inflammatory prostaglandin, PGH2, by cleaving and converting arachidonic acid[37, 38]. Arachidonic acid has been detected in OA SF, with higher levels in early stages and lower levels in late-stage OA[38, 39]. Furthermore, arachidonic acid metabolism was upregulated in SF from both naïve and germ-free mice following non-invasive ACL injury compared to healthy non-injured mice[21]. Therefore, the detection of linoleic acid and metabolites in this study may be associated with signaling, prostaglandin generation, and inflammation post-LM injury. Larger studies with SF samples from healthy and PTOA individuals are needed to confirm if metabolites related to linoleate metabolism could serve as markers to monitor PTOA development.

Combined, the magnified dysregulation of amino acid-related pathways in LM participants, and fewer in M and L participants, suggest that traumatic joint injuries in general require a higher cellular demand for amino acids for various reasons (i.e., energy generation, collagen synthesis, inflammation). Few studies have determined the cellular density in healthy and injured menisci and ligaments[40-42], making it valuable to combine cellular density data with metabolomics for better insights into amino acid metabolism post-injury. Additional studies comparing the SF metabolome from healthy non-injured, recently injured, and PTOA patients are needed to fully comprehend the metabolic mechanisms driving PTOA progression.

The Synovial Fluid Metabolome Differs in Association with Participant Sex and Injury Pathology

Females have a higher risk of knee injury and PTOA development compared to males[8-10]. Despite empirical sex differences, diagnosis and treatment do not differ[43]. Therefore, the detection of sex differences at the metabolic level in the present study support sex as a prevalent PTOA risk factor. SF-derived metabolite features were associated with participant sex, and metabolically distinct profiles were observed between males and females with similar injuries. This is the first study, to our knowledge, to assess sex differences considering different injury pathologies in human SF.

Cervonyl carnitine was higher in all female participants compared to all male participants. Carnitines regulate oxidative and metabolic statuses, maintain membrane stability, and contribute to β-oxidation by transporting fatty acids into mitochondria[44, 45]. Circulating estrogen levels are much higher in females than males, resulting in an increased expression of fatty acid oxidation proteins and pathways such as adenosine monophosphate-activated protein kinase (AMPK)[46, 47]. AMPK is a key energy sensor that promotes ATP production[48, 49]. The proposed mechanism for

estrogen activation of AMPK entails estrogen binding to estrogen-receptor β (ERβ), causing an increase in Ca^{2+} stimulating Ca^{2+}/Calmodulin-dependent protein kinase kinase β (CaMKKβ) to phosphorylate the AMPKα subunit where anabolism is inhibited and catabolism is activated resulting in the transport of fatty acids into the mitochondria to perform β-oxidation and generate ATP[50] (Supplemental Fig. 4.1).

Atypical AMPK activity has been implicated in OA where impaired mitochondrial function increases reactive oxygen species and decreases ATP production causing cartilage degeneration, inflammation, and abnormal subchondral bone remodeling[49]. Therefore, elevated carnitine species in females compared to males may demonstrate that females rely on different metabolic pools and mechanisms, like AMPK activation via estrogen, to meet energy demands post-injury. Monitoring carnitine-related species overtime could gauge β-oxidation rates, AMPK activity and function, joint health, and predict PTOA onset and development. Additional research is needed to explore the sexual dimorphic nature of traumatic knee injury in both human and animal injury models and enhance current understanding of the relationship between injury and sex. These findings underscore patient sex as a significant risk factor for injury and PTOA, warranting further investigation to positively influence patient treatment strategies.

Limitations

While this study finds that metabolic phenotypes reflect patient sex and injury pathology, it is not without limitations. Firstly, a major limitation is the lack of healthy non-injured participants as well as participates with PTOA which limits analyses and study conclusions. Secondly, sample size in general was small and was not uniform across injury pathology groups.

Thirdly, a common limitation of LC-MS/MS is that not all metabolite features detected are able to be identified. Therefore, metabolite features that best reflect injury pathology may not have been identified in the current study but have noteworthy metabolic regulation patterns that can be further pursued in additional studies.

Conclusions

The results of this cross-sectional study demonstrate that injured males and females have distinct metabolic phenotypes. Considering sex differences associated with injury rates and PTOA development, the detection of dysregulated metabolites between male and females can be used to positively influence patient treatment and intervention. Future studies aim to investigate the interaction between PTOA, sex, and other PTOA risk factors (i.e., BMI, age). This mass spectrometry-based global approach differentiated participants with L, M, and LM injuries highlighting differences in lipid- and oxidative-related metabolism, amino acid metabolism, and inflammatory-associated pathways. Additional comparison of these metabolic phenotypes to healthy non-injured and PTOA phenotypes is needed to pinpoint joint-level metabolic activity post-injury over time. Completion of this work has the potential to improve patient treatment and identify biomarkers and druggable targets to slow, stop or reverse PTOA progression.

Acknowledgements

We thank the Mass Spectrometry Facility at Montana State University including Dr. Donald Smith and Jesse Thomas for assisting in LC-MS analysis, interpretation, and metabolite identification. Funding for the Mass Spectrometry Facility used in this publication was made

possible by the M.J. Murdock Charitable Trust, the National Institute of General Medical Sciences of the National Institutes of Health (P20GM103474 and S10OD28650). This study was funded by the National Science Foundation under Award Number CMMI 1554708 (RKJ), and the National Institutes of Health under Award Numbers R01AR073964 (RKJ).

Abbreviations List

PTOA = post-traumatic osteoarthritis; OA = osteoarthritis; ACL = anterior cruciate ligament; BMI = body mass index; SF = synovial fluid; LC-MS = liquid chromatography-mass spectrometry; LC-MS/MS = liquid chromatography tandem mass spectrometry; PCA = principal component analysis; PLS-DA = partial least squares-discriminant analysis; VIP = variable importance in projection; NMR = nuclear magnetic resonance; AMPK = adenosine monophosphate-activated protein kinase

References

1. Brown TD, Johnston RC, Saltzman CL, Marsh JL, Buckwalter JA. Posttraumatic osteoarthritis: a first estimate of incidence, prevalence, and burden of disease. J Orthop Trauma 2006; 20: 739-744.

2. Thomas AC, Hubbard-Turner T, Wikstrom EA, Palmieri-Smith RM. Epidemiology of Posttraumatic Osteoarthritis. J Athl Train 2017; 52: 491-496.

3. Gottlob CA, Baker CL, Jr., Pellissier JM, Colvin L. Cost effectiveness of anterior cruciate ligament reconstruction in young adults. Clin Orthop Relat Res 1999: 272-282.

4. Griffin LY, Albohm MJ, Arendt EA, Bahr R, Beynnon BD, Demaio M, et al. Understanding and preventing noncontact anterior cruciate ligament injuries: a review of the Hunt Valley II meeting, January 2005. Am J Sports Med 2006; 34: 1512-1532.

5. Slauterbeck JR, Kousa P, Clifton BC, Naud S, Tourville TW, Johnson RJ, et al. Geographic mapping of meniscus and cartilage lesions associated with anterior cruciate ligament injuries. J Bone Joint Surg Am 2009; 91: 2094-2103.

6. Oiestad BE, Engebretsen L, Storheim K, Risberg MA. Knee osteoarthritis after anterior cruciate ligament injury: a systematic review. Am J Sports Med 2009; 37: 1434-1443.

7. Wu WH, Hackett T, Richmond JC. Effects of meniscal and articular surface status on knee stability, function, and symptoms after anterior cruciate ligament reconstruction: a long-term prospective study. Am J Sports Med 2002; 30: 845-850.

8. Ingram JG, Fields SK, Yard EE, Comstock RD. Epidemiology of knee injuries among boys and girls in US high school athletics. Am J Sports Med 2008; 36: 1116-1122.

9. Blaker CL, Ashton DM, Doran N, Little CB, Clarke EC. Sex- and injury-based differences in knee biomechanics in mouse models of post-traumatic osteoarthritis. J Biomech 2021; 114: 110152.

10. Srikanth VK, Fryer JL, Zhai G, Winzenberg TM, Hosmer D, Jones G. A meta-analysis of sex differences prevalence, incidence and severity of osteoarthritis. Osteoarthritis Cartilage 2005; 13: 769-781.

11. Faber SC, Eckstein F, Lukasz S, Muhlbauer R, Hohe J, Englmeier KH, et al. Gender differences in knee joint cartilage thickness, volume and articular surface areas: assessment with quantitative three-dimensional MR imaging. Skeletal Radiol 2001; 30: 144-150.

12. Hitt K, Shurman JR, 2nd, Greene K, McCarthy J, Moskal J, Hoeman T, et al. Anthropometric measurements of the human knee: correlation to the sizing of current knee arthroplasty systems. J Bone Joint Surg Am 2003; 85-A Suppl 4: 115-122.

13. Carlson AK, Rawle RA, Adams E, Greenwood MC, Bothner B, June RK. Application of global metabolomic profiling of synovial fluid for osteoarthritis biomarkers. Biochem Biophys Res Commun 2018; 499: 182-188.

14. Carlson AK, Rawle RA, Wallace CW, Brooks EG, Adams E, Greenwood MC, et al. Characterization of synovial fluid metabolomic phenotypes of cartilage morphological changes associated with osteoarthritis. Osteoarthritis Cartilage 2019; 27: 1174-1184.

15. Kim S, Hwang J, Kim J, Ahn JK, Cha HS, Kim KH. Metabolite profiles of synovial fluid change with the radiographic severity of knee osteoarthritis. Joint Bone Spine 2017; 84: 605-610.

16. Sitton NG, Dixon JS, Bird HA, Wright V. Serum and synovial fluid histidine: a comparison in rheumatoid arthritis and osteoarthritis. Rheumatol Int 1986; 6: 251-254.

17. Mickiewicz B, Heard BJ, Chau JK, Chung M, Hart DA, Shrive NG, et al. Metabolic profiling of synovial fluid in a unilateral ovine model of anterior cruciate ligament

reconstruction of the knee suggests biomarkers for early osteoarthritis. J Orthop Res 2015; 33: 71-77.

18. Kessner D, Chambers M, Burke R, Agus D, Mallick P. ProteoWizard: open source software for rapid proteomics tools development. Bioinformatics 2008; 24: 2534-2536.

19. Smith CA, Want EJ, O'Maille G, Abagyan R, Siuzdak G. XCMS: processing mass spectrometry data for metabolite profiling using nonlinear peak alignment, matching, and identification. Anal Chem 2006; 78: 779-787.

20. Pang Z, Zhou G, Ewald J, Chang L, Hacariz O, Basu N, et al. Using MetaboAnalyst 5.0 for LC-HRMS spectra processing, multi-omics integration and covariate adjustment of global metabolomics data. Nat Protoc 2022; 17: 1735-1761.

21. Hahn AK, Wallace CW, Welhaven HD, Brooks E, McAlpine M, Christiansen BA, et al. The microbiome mediates epiphyseal bone loss and metabolomic changes after acute joint trauma in mice. Osteoarthritis Cartilage 2021; 29: 882-893.

22. Wallace CW, Hislop B, Hahn AK, Erdogan AE, Brahmachary PP, June RK. Correlations between metabolites in the synovial fluid and serum: A mouse injury study. J Orthop Res 2022.

23. Damyanovich AZ, Avery L, Staples JR, Marshall KW. (1)H NMR metabolic profiling of synovial fluid from patients with anterior cruciate ligament tears and hemarthrosis. Osteoarthritis Cartilage 2023; 31: 1066-1077.

24. Alturfan AA, Uslu E, Alturfan EE, Hatemi G, Fresko I, Kokoglu E. Increased serum sialic acid levels in primary osteoarthritis and inactive rheumatoid arthritis. Tohoku J Exp Med 2007; 213: 241-248.

25. Browning LM, Krebs JD, Jebb SA. Discrimination ratio analysis of inflammatory markers: implications for the study of inflammation in chronic disease. Metabolism 2004; 53: 899-903.

26. Cui Z, Liu K, Wang A, Liu S, Wang F, Li J. Correlation between sialic acid levels in the synovial fluid and the radiographic severity of knee osteoarthritis. Exp Ther Med 2014; 8: 255-259.

27. Ohnishi A, Osaki T, Matahira Y, Tsuka T, Imagawa T, Okamoto Y, et al. Correlation of plasma amino acid concentrations and chondroprotective effects of glucosamine and fish collagen peptide on the development of osteoarthritis. J Vet Med Sci 2013; 75: 497-502.

28. Tootsi K, Vilba K, Martson A, Kals J, Paapstel K, Zilmer M. Metabolomic Signature of Amino Acids, Biogenic Amines and Lipids in Blood Serum of Patients with Severe Osteoarthritis. Metabolites 2020; 10.

29. Rockel JS, Kapoor M. The Metabolome and Osteoarthritis: Possible Contributions to Symptoms and Pathology. Metabolites 2018; 8.

30. Dalmao-Fernandez A, Lund J, Hermida-Gomez T, Vazquez-Mosquera ME, Rego-Perez I, Blanco FJ, et al. Impaired Metabolic Flexibility in the Osteoarthritis Process: A Study on Transmitochondrial Cybrids. Cells 2020; 9.

31. Smith RL, Soeters MR, Wust RCI, Houtkooper RH. Metabolic Flexibility as an Adaptation to Energy Resources and Requirements in Health and Disease. Endocr Rev 2018; 39: 489-517.

32. Castro-Perez JM, Kamphorst J, DeGroot J, Lafeber F, Goshawk J, Yu K, et al. Comprehensive LC-MS E lipidomic analysis using a shotgun approach and its application to biomarker detection and identification in osteoarthritis patients. J Proteome Res 2010; 9: 2377-2389.

33. Cillero-Pastor B, Eijkel G, Kiss A, Blanco FJ, Heeren RM. Time-of-flight secondary ion mass spectrometry-based molecular distribution distinguishing healthy and osteoarthritic human cartilage. Anal Chem 2012; 84: 8909-8916.

34. Blanco FJ, Rego I, Ruiz-Romero C. The role of mitochondria in osteoarthritis. Nat Rev Rheumatol 2011; 7: 161-169.

35. Bastiaansen-Jenniskens YM, Siawash M, van de Lest CH, Verhaar JA, Kloppenburg M, Zuurmond AM, et al. Monounsaturated and Saturated, but Not n-6 Polyunsaturated Fatty Acids Decrease Cartilage Destruction under Inflammatory Conditions: A Preliminary Study. Cartilage 2013; 4: 321-328.

36. Oliviero F, Lo Nigro A, Bernardi D, Giunco S, Baldo G, Scanu A, et al. A comparative study of serum and synovial fluid lipoprotein levels in patients with various arthritides. Clin Chim Acta 2012; 413: 303-307.

37. Bar-Or D, Rael LT, Thomas GW, Brody EN. Inflammatory Pathways in Knee Osteoarthritis: Potential Targets for Treatment. Curr Rheumatol Rev 2015; 11: 50-58.

38. Van de Vyver A, Clockaerts S, van de Lest CHA, Wei W, Verhaar J, Van Osch G, et al. Synovial Fluid Fatty Acid Profiles Differ between Osteoarthritis and Healthy Patients. Cartilage 2020; 11: 473-478.

39. Hu Y, Wu Q, Qiao Y, Zhang P, Dai W, Tao H, et al. Disturbances in Metabolic Pathways and the Identification of a Potential Biomarker Panel for Early Cartilage Degeneration in a Rabbit Anterior Cruciate Ligament Transection Model. Cartilage 2021; 13: 1376S-1387S.

40. Mesiha M, Zurakowski D, Soriano J, Nielson JH, Zarins B, Murray MM. Pathologic characteristics of the torn human meniscus. Am J Sports Med 2007; 35: 103-112.

41. Pereira H, Caridade SG, Frias AM, Silva-Correia J, Pereira DR, Cengiz IF, et al. Biomechanical and cellular segmental characterization of human meniscus: building the basis for Tissue Engineering therapies. Osteoarthritis Cartilage 2014; 22: 1271-1281.

42. Sonnery-Cottet B, Bazille C, Hulet C, Colombet P, Cucurulo T, Panisset JC, et al. Histological features of the ACL remnant in partial tears. Knee 2014; 21: 1009-1013.

43. O'Connor MI. Sex differences in osteoarthritis of the hip and knee. J Am Acad Orthop Surg 2007; 15 Suppl 1: S22-25.

44. Adeva-Andany MM, Calvo-Castro I, Fernandez-Fernandez C, Donapetry-Garcia C, Pedre-Pineiro AM. Significance of l-carnitine for human health. IUBMB Life 2017; 69: 578-594.

45. Mingorance C, Rodriguez-Rodriguez R, Justo ML, Herrera MD, de Sotomayor MA. Pharmacological effects and clinical applications of propionyl-L-carnitine. Nutr Rev 2011; 69: 279-290.

46. Purdom T, Kravitz L, Dokladny K, Mermier C. Understanding the factors that effect maximal fat oxidation. J Int Soc Sports Nutr 2018; 15: 3.

47. Oosthuyse T, Bosch AN. The effect of the menstrual cycle on exercise metabolism: implications for exercise performance in eumenorrhoeic women. Sports Med 2010; 40: 207-227.

48. Steinberg GR, Macaulay SL, Febbraio MA, Kemp BE. AMP-activated protein kinase--the fat controller of the energy railroad. Can J Physiol Pharmacol 2006; 84: 655-665.

49. Wang J, Li J, Song D, Ni J, Ding M, Huang J, et al. AMPK: implications in osteoarthritis and therapeutic targets. Am J Transl Res 2020; 12: 7670-7681.

50. Yang S, Wang J. Estrogen Activates AMP-Activated Protein Kinase in Human Endothelial Cells via ERbeta/Ca(2+)/Calmodulin-Dependent Protein Kinase Kinase beta Pathway. Cell Biochem Biophys 2015; 72: 701-707.

CHAPTER SIX

TISSUE-SPECIFIC AND SPATIALLY DEPENDENT METABOLIC SIGNATURES PERTURBED BY INJURY IN SKELETALLY MATURE MALE AND FEMALE C57BL/6 MICE

Contribution of Authors and Co-Authors

Manuscript in Chapter 6

Author: Hope D. Welhaven

Contributions: Designed experiments, performed injuries and metabolite extractions, ran LC-MS samples, sectioned whole joints, performed MALDI imaging, analyzed and interpreted data, and drafted manuscript.

Co-Author: Avery H. Welfley

Contributions: Performed injuries and metabolite extractions, analyzed and interpreted data.

Co-Author: Donald F. Smith

Contributions: Assisted in MALDI sample preparation and imaging.

Co-Author: Priyanka Brahmachary

Contributions: Performed injuries and metabolite extractions.

Co-Author: Brian Bothner

Contributions: Designed experiments, analyzed data, drafted and edited the manuscript.

Co-Author: Ronald K. June

Contributions: Corresponding author, designed experiments, analyzed data, drafted and edited the manuscript.

Manuscript Information

Hope D. Welhaven, Avery H. Welfley, Priyanka Brahmachary, Don Smith, Brian Bothner,

Ronald K. June

Status of Manuscript:

X Prepared for submission to a peer-reviewed journal
☐ Officially submitted to a peer-reviewed journal
☐ Accepted by a peer-reviewed journal
☐ Published in a peer-reviewed journal

Abstract

Objective: Although it is widely acknowledged that injury is a common risk factor for post-traumatic osteoarthritis (PTOA), little is known about alterations in metabolism and microarchitecture that occur throughout the joint post-injury. Thus, the objective was to identify tissue-specific and spatially dependent metabolic signatures perturbed by injury between male and female mice.

Design: Male and female C57Bl/6J mice, aged 21 weeks, were subjected to non-invasive ACL injury. Serum, synovial fluid, and whole joints were harvested at 8 days post-injury for liquid chromatography-mass spectrometry-based metabolomics to investigate differences between tissues and between injured, contralateral, and naïve limbs and shed light on local and systemic responses post-injury. Additionally, matrix-assisted laser desorption ionization-mass spectrometry imaging (MALDI-MSI) was performed on whole joints to spatially locate and identify differences in populations of metabolites between injured, contralateral, and naïve joints.

Results: Metabolomic analyses revealed distinct metabolic profiles associated with both sex and injury status. Specifically, differences in metabolism between male and female injured and naïve mice mapped to various amino acid pathways as well as purine and pyrimidine metabolism. Moreover, the application of MALDI-MSI characterized molecular differences between cartilage and bone and across injured, contralateral, and naïve joints.

Conclusions: These findings indicate significant metabolic and pathological shifts following joint injury, with notable sex-specific associations. By integrating metabolomics and MALDI-MSI approaches, this study provides insights into the comprehensive effects of injury and sex on the joint, advancing our understanding of PTOA development.

Introduction

Post-traumatic osteoarthritis (PTOA) accounts for 12% of all osteoarthritis (OA) cases, equating to 5.6 million cases annually[1, 2]. The most prevalent risk factor for PTOA is joint injury. The annual incidence rate of anterior cruciate ligament (ACL) injuries is 250,000, commonly occurring in individuals between the ages of 16 and 24. Unfortunately, upwards of 50% of patients will develop PTOA within 10-20 years of injury[3-6]. Behind injury, a noteworthy PTOA risk factor is sex. Young female athletes are two to eight times more likely to sustain a traumatic knee injury requiring surgical repair compared to their male counterparts[7, 8]. Following repair, female athletes experience greater joint instability and physiological stress and have a 25% less chance of returning to their sport within 5 years compared to male athletes[8-10]. Later in life, females are more likely to develop OA and often experience greater symptom severity[11, 12]. This sexual dimorphism can be boiled down to anatomical and hormonal differences where females have wider pelves, smaller femurs, different muscle angles, and physically smaller ACLs[13, 14]. Despite these empirical sex differences, many studies fail to include both female and male subjects and, specific to sports, male-dominated sports are typically focused on.

Preclinical mouse models have improved the field's understanding of PTOA where PTOA can be induced through ACL destabilization of the medial meniscus (DMM), intraarticular injection to induce degradation, or ACL transection[15]. Each is met with challenging procedures and often fails to fully replicate in vivo pathophysiology. A non-invasive PTOA model, involving tibial compression overload, has been shown to simulate clinical ACL tears where natural joint processes occurring at the early time points after injury are observed[15-18]. A handful of studies have employed this non-invasive PTOA model and have observed changes in musculoskeletal tissues

post-injury at different time scales. Specifically, changes in trabecular bone have been detected within 7 days post-injury using microCT[16] and synovial fluid (SF) and serum metabolism has been shown to rapidly shift after injury (days 1 and 7 post-injury)[19].

While it is well known that injury and sex are prevalent PTOA risk factors, underlying mechanisms and changes in metabolism and microarchitecture following injury remain incompletely understood. Thus, preclinical models can be leveraged to examine acute differences in response to injury at different time scales and across various tissues using mass spectrometry-based approaches. Metabolomics – the study of small molecule intermediates called metabolites – captures the physiological and metabolic status of the joint. While SF and serum have been assessed post-injury in human and mouse models[19-23], metabolomics can also be applied to whole joint tissue to characterize metabolic changes occurring in bone and cartilage post-injury. We hypothesize that a metabolomic assessment of all three tissues in injured and naïve male and female mice will reveal metabolic shifts that are both unique and conserved across tissues. Once characterized, these markers could be measured through SF needle biopsy or simple bloodwork in the clinical setting to improve post-injury care. Moreover, investigating all three tissues post-injury will shed light on whether shifts in metabolism parallel pathological changes in bone.

A second mass spectrometry-based approach is matrix-assisted laser desorption ionization-mass spectrometry imaging (MALDI-MSI). This technique produces a two-dimensional chemical map that can spatially locate and detect differences in osteochondral metabolites that compose the mouse knee joint. MALDI-MSI is a powerful tool that can complement traditional measurements used to examine cartilage and bone, as it spatially resolves and characterizes molecular species in a single molecular imaging experiment in a label-free way[24]. By capturing spatial and temporal

information with high resolution, the molecular aspects of injury on the joint can be examined[25, 26]. A small handful of studies have applied MALDI-MSI to study musculoskeletal tissues such as cartilage[27, 28] and synovium[29], however, no study to date has utilized MALDI-MSI to characterize molecular changes between male and female injured and naïve mice.

The first objective of this study was to characterize metabolomic differences within and across whole joints, SF, and serum from injured and naïve male and female mice using liquid chromatography-mass spectrometry (LC-MS). Investigating differences in metabolism in different tissues and between injured, contralateral, and naïve limbs is important as it will shed light on both local and systemic metabolic responses following injury. The second objective of this study was to spatially locate and identify osteochondral metabolites using MALDI-MSI. By combining untargeted metabolomic profiling and MALDI-MSI, we can pinpoint the origin of metabolic and pathological shifts and gain a better understanding of the effects of injury and sex on the joint as a whole.

Methods

Animals

C57Bl/6J male and female mice (N=20, n = 10 female, n = 10 male) were utilized to compare the spatial and metabolic effects of injury and sex on the whole joints, SF, and serum. Mice were purchased from Jackson Labs at 18 weeks of age and acclimated to the Montana State University Animal Research Center for 3 weeks. All mice were housed in cages of 3-5 mice and fed a standard chow-fed diet *ad libitum* (PicoLab Rodent Diet 20, 20% protein). All animal procedures were approved by the Institutional Animal Care and Use Committee at Montana State University.

Joint Injury Model and Experimental Design

Once acclimated, mice were randomly assigned to experimental groups: injured or non-injured. Those assigned to the injury group were subjected to a non-invasive injury model where the ACL is ruptured in a way that closely mimics ACL rupture in humans, an injury associated with degeneration of bone and cartilage[15, 30]. Historically, this model begins to display changes in subchondral trabecular bone at 7 days[16]. Thus, experimental groups are as follows with five mice in each group: male injured mice, male naïve mice, female injured mice, and female naïve mice.

On the day of injury, mice were anesthetized using isoflurane inhalation. Mice were then placed in the custom-built tibial compression system where a single compressive overload to the lower leg was applied (target force = 12N, loading rate = 130 mm/s)[20]. The injured side was also randomized for mice assigned to injury groups. After 8 days, all mice were euthanized via cervical dislocation followed by a thoracotomy. Samples collected included both whole joints, SF, and serum from every mouse. Whole joints were harvested, all soft tissue was removed and were stored intact. SF was recovered and then extracted using established protocols[31], with some modifications. To access the SF, skin was removed from the leg, and using a scalpel, the tibial plateau was palpated to identify the joint line. Next, an anterior incision was made through the patellar tendon then retracted to access the joint capsule where a second incision was made to access the SF via Whatman paper (Sigma, WHA1441042). Once saturated, Whatman paper with adsorbed SF was placed in a 1.5 mL microcentrifuge tube where 150 uL of 80:20 methanol:H2O was added. Blood samples were obtained by cardiac puncture, collected in a standard red top serum tube microtainer (BD Microtainer Red Tubes No Additive, 365963), inverted six times, then incubated at room temperature for 60 minutes to activate clotting factors. Serum samples were centrifuged at 2000 x g for 10 minutes at 4°C to remove cells and remaining clotting factors.

Resulting supernatant designated as serum were transferred to a clean 1.5 mL microcentrifuge tube. All samples were stored at -80°C until metabolite extraction.

Metabolite Extraction and Mass Spectrometry Instrumentation

Whole joints selected for metabolomic analysis were removed from -80°C, allowed to thaw over ice, and disarticulated to separate the tibia and femur. The distal end of the tibia and proximal end of the femur were trimmed and centrifuged for 5 minutes at 16,100 x g at 4°C to remove bone marrow. Next, bones were combined in one homogenization tube, precipitated with 1 mL of 80:20 methanol:H2O, and homogenized using a tissue homogenizer (1200 GenoLyte, Fischer Scientific). Following homogenization, whole joint samples were placed at -20°C overnight.

The next day, SF and serum were centrifuged for 5 minutes at 500 x g at 4°C to remove cells and debris. Supernatant was transferred and three times the volume 80:20 methanol:H2O was added. Upon vortexing for 3 minutes, samples were chilled at -20°C for 30 minutes. At this point, all samples including whole joint, SF, and serum samples were extracted the same and together. Thus, all samples were removed from -20°C, centrifuged for 5 minutes at 16,100 x g at 4°C, and supernatant was dried via vacuum concentration. To remove any remaining proteins, as well as lipids and waxes, dried extracts were then resuspended with 250 uL of 1:1 acetonitrile:H2O, vortexed, chilled at -20°C for 30 minutes, and centrifuged again for 5 minutes at 16,100 x g at 4°C. Supernatant was dried once more and once dried, extracts were prepped for LC-MS using 100 uL of 1:1 acetonitrile:water. Additionally, pooled samples were generated by randomly pooling a total of 50 uL for each tissue type (n=4/tissue), then pooled samples from each tissue type were also

pooled for identification purposes. All solvents used were mass spectrometry HPLC grade (Fischer Scientific).

All samples, including extracted tissues and pools, were analyzed via LC-MS as previously described[22]. In brief, a Waters Acquity UPLC Plus interfaced via an electrospray ionization source (positive mode) to a Waters Synapt XS was used. For chromatography, an Acquity Waters HILIC column (150 x 2.1mm) at a flow rate of 0.400 uL/min was utilized to separate metabolites over a 12-minute gradient (A=95/5% water/acetonitrile, B = 95/5% acetonitrile/water). Every 10 injections, a quality control blank, an internal standard, and a matrix blank were injected to minimize spectra drift, assess LC-MS performance, and monitor overtime. All extracted tissues underwent LC-MS, whereas pooled samples were analyzed via liquid chromatography-tandem mass spectrometry (LC-MS/MS) at a constant energy ramp of 30-50V for secondary ionization to derive metabolite identifications.

Statistical and Metabolomic Profiling

All LC-MS data – mass-to-charge ratios (m/z), relative metabolite abundance, and retention time – were processed using MSConvert and Progenesis QI. Using previously established pipelines for analysis[22, 32, 33], data underwent interquartile range normalization, log-transformation, and autoscaling in MetaboAnalyst (version 6.0)[34]. Analyses performed in MetaboAnalyst to visualize metabolomic differences between injured and naïve male and female mice across tissue types included principal component analysis (PCA), and partial least squares-discriminant analysis (PLS-DA). To distinguish populations of differentially regulated metabolite features across experimental groups, fold change, volcano plot analysis, and PLS-DA VIP Score analyses were

performed. Heatmap analysis was conducted to pinpoint clusters of metabolite features that are co-regulated and differentially regulated across experimental groups.

Populations of metabolite features distinguished by these tests were then subjected to pathway enrichment analyses using MetaboAnalyst's Functional Analysis feature where the *mummichog* algorithm is used to project metabolite features onto pathways to derive biological relevance. To do this, Kyoto Encyclopedia of Genes and Genomes (KEGG) *Mus muscis* pathway library was used as the primary reference library to reference metabolites and metabolic pathways (positive mode, mass tolerance = 5 parts per million, version 1). Significance for statistical and pathway analyses was determined using a false discovery rate (FDR)-corrected significance level of $p < 0.05$.

Metabolite Identification

Pooled samples were subjected to LC-MS/MS where ions are fragmented. This acquired fragmentation pattern can then be matched against theoretical fragmentation patterns to identify metabolites. All fragmentation data were imported, peak picked, and aligned using Progenesis QI (Nonlinear Dynamics, Newcastle UK, version 3.0). Here, Progenesis QI efficiently identifies metabolites using a computational framework that compares fragmentation patterns across various databases. For the present study, databases searched included the Human Metabolome Database (HMDB), METLIN, and ChemSpider. Once patterns are searched across databases, metabolite identities are assigned a fragmentation and overall Progenesis score. In This score is determined based on retention time, isotope distribution, and mass error. For a metabolite identification to be deemed legitimate, fragmentation and overall Progenesis scores were required to be greater than 30 and 65 (out of 100), respectively. Once identified and filtered by score, they were matched

against populations of LC-MS-based features distinguished by statistical analyses to unveil potential metabolic indicators of disease as well as sexually dimorphic identities. To minimize false identifications when comparing LC-MS and LC-MS/MS metabolite features and identifications, a tolerance level of 10 parts per million was enforced.

MALDI-MSI Sample Preparation

Whole joints selected for MALDI-MSI were removed from -80°C and prepped according to the novel protocol developed for whole joint sectioning and imaging (Fig. 6.1). Firstly, whole joints were thawed over ice, and the distal end of the tibia and proximal end of the femur were trimmed. Next, whole joints were embedded in warm 5% carboxymethylcellulose sodium salt (ThermoFischer, A18105-36) and 10% gelatin (Thermo Scientifiic, AC611995000)[35, 36] . This medium as selected over optimal cutting temperature (OCT) as it is incompatible with mass spectrometry analysis due to the presence of polyethylene glycol, a major ion suppressor. Embedded whole joints were mounted to the chuck and sagittal 8 um sections were cryosectioned using a Tissue-Tek Accu-Edge 4689 blade in a cryostat set to -30°C (OTF5000 Cryostat, Bright Instrument Co Ltd). Specifically, the medial and lateral aspects of the joint were sectioned as these are the primary sites of degeneration for this injury model[16, 37]. Because whole joints did not undergo formalin fixation or paraffin embedding, Cryofilm 3C 16 UF (SECTION-LAB, Hiroshima, Japan) was applied and adhered to the tissue block to assist in transferring sections to indium tin oxide (ITO) slides (Delta Technologies, CB-401N, 4-10 Ω/sq, 25 x 50 mm)[38]. Sections were adhered to ITO slides using double-stick tape and then directly stored at -80°C until matrix application.

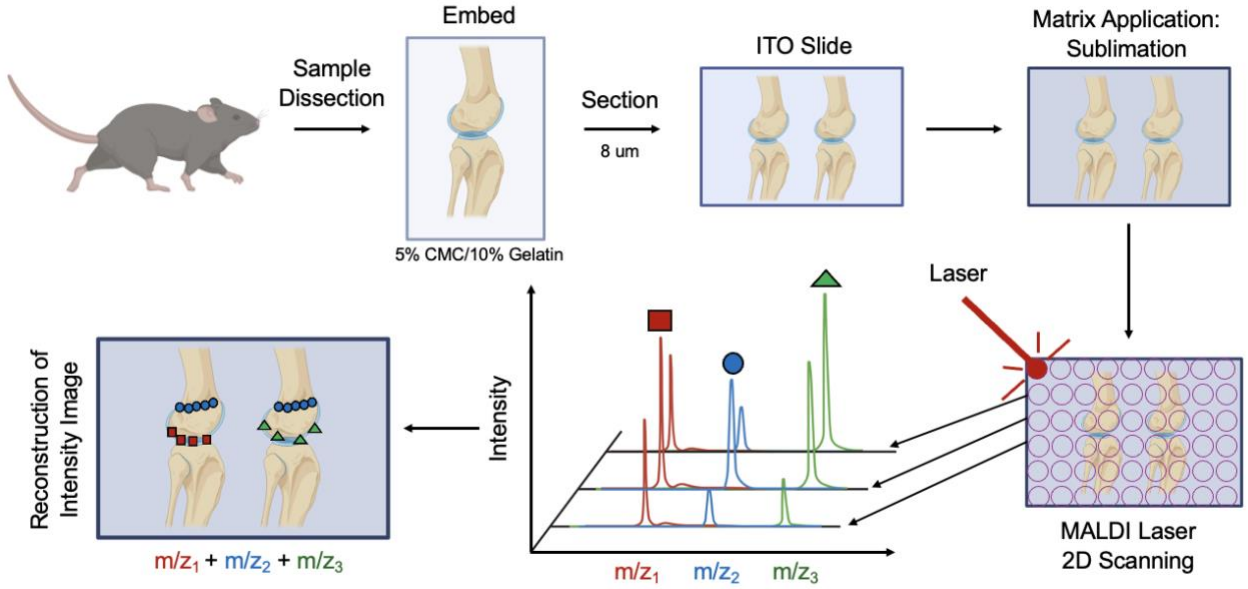

Figure 6.1. MALDI-MSI experimental workflow to spatially image osteochondral metabolites. Whole joints were obtained from C57Bl6/J male and female injured and naïve mice, embedded in 5% carboxylmethylcellulose (CMC)/10% gelatin, sectioned (8 um), transferred to indium tin oxide (ITO) slides, and sublimed with 2,5-dihydroxybenzoic acid matrix. Data were then acquired using 2D laser scanning followed by reconstruction of intensity images representing m/z values and intensity.

Matrix Application

An in-house sublimation apparatus (Chemglass Life Sciences, CG-3038) was used for matrix application (Supplemental Fig. 6.1). Application using sublimation was chosen over matrix spraying because it forms smaller more homogenous matrix crystals, lacks liquid reducing the risk of molecule migration, and is more reproducible[39]. Moreover, solvent exposure from matrix spraying can cause microcracks in bone marrow and bone[36]. Four whole joint sections were present on each ITO slide, and slides were weighed before sublimation. 300 mg of 2,5-dihydroxybenzoic acid (DHB) (Alfa Aesar, 490-79-9) was uniformly dispersed in the base of the sublimation apparatus, ITO slides were affixed to the flat bottom condenser using conductive adhesive which was then filled with tap water (22°C). The two glass compartments of the sublimator were

assembled using an O-ring seal and connected to a vacuum pump. Tissue sections on ITO slides were sublimated at 50°C for 3 minutes under 68 mTorr vacuum, resulting in a uniform matrix layer (0.05 mg/cm^2). Optimization of matrix deposition through sublimation was determined by adjusting temperature of the hot plate, amount of matrix, and time of sublimation. Following sublimation, matrix was recrystallized using a hydration chamber with 300 uL of 5% methanol 0.1% formic acid spotted onto Whatman paper. The chamber was heated in a 37°C oven for 1 minute, then ITO slides were sealed in the chamber and heated at 37°C for 1 minute.

MALDI Image Acquisition

A Bruker AutoFlex III MALDI Time-of-Flight (TOF) mass spectrometer (Bruker Daltonics) equipped with a MTP Slide Adapater II Imaging Plate (Bruker Daltonics) was used for image acquisition. Due to the size of the sublimator and ITO slides (25 x 50 mm), two small aluminum slide trays were milled to properly fit ITO slides into the imaging plate. Using a Smartbeam Nd:YAG laser (355 nm) and Bruker FlexImaging, images were collected in positive ionization and TOF modes in the 50-1000 m/z mass range averaging 200 laser shots per pixel with a 100-um lateral resolution (range = 90%, offset = 10%, laser power = 30%). Imaging data collected were analyzed using FlexImaging and MSiReader. Following MALDI-MSI, ITO slides with sections will be washed with ethanol to remove DHB, then stained with Safranin O and Fast Green. Digital images will be obtained to define and correlate obtained MALDI-MSI images with histological information. Additionally, serial sections not subjected to MALDI-MSI will be stained and digitally imaged to properly align features seen in the histology with molecular information.

Results

Injury Perturbs the Metabolome Across Whole Joints, Synovial Fluid, and Serum

In total, 2,770 metabolite features were detected by LC-MS across all samples (n=92). First, whole joints, SF, and serum were assessed to determine if metabolomic profiles were distinct between tissues. Using PLS-DA, the metabolomes of whole joints, SF, and serum are substantially distinct when assessing all samples (Supplemental Fig. 6.2 A) and only injured samples (Supplemental Fig. 6.2 B). ANOVA analysis revealed 2,264 and 1,891 metabolite features that were significantly dysregulated across all samples and only injured samples, respectively (Supplemental Fig. 6.2 C-D).

To visualize, assess, and distinguish metabolic differences associated with injury within each sample type, PLS-DA, fold change, and volcano plot analyses were conducted. First, using PLS-DA, differences associated with injury were assessed in whole joint, SF, and serum (Fig. 6.2 A-C). When comparing injured and naïve whole joints and SF, some overlap is observed (Fig. 6.2 A-B), whereas distinct separation with no overlap is observed when comparing serum from injured and naïve mice (Fig. 6.2 C). To distinguish populations of metabolite features driving these differences, fold change analysis was performed (Fig. 6.2 D-F).

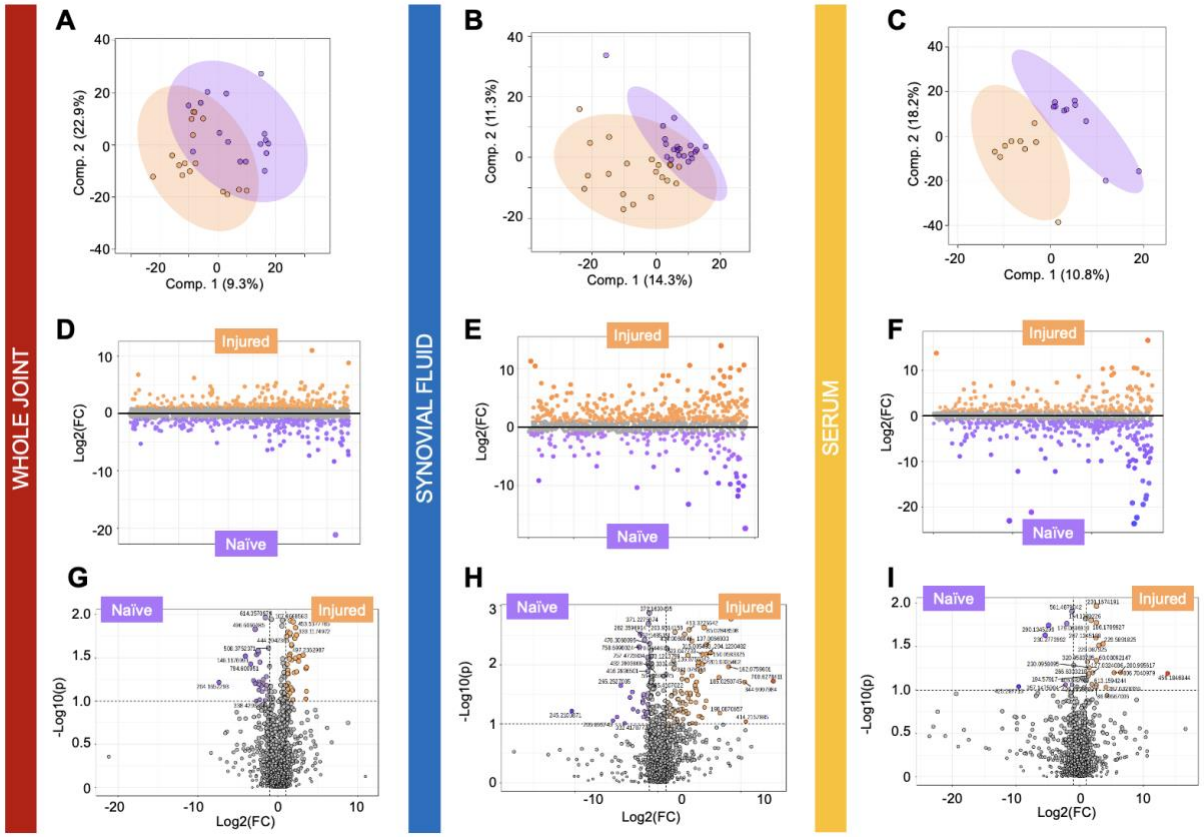

Figure 6.2. Global metabolomic profiles of whole joints, synovial fluid, and serum are driven by injury status. (A-C) Partial Least Squares-Discriminant Analysis (PLS-DA) finds some overlap between injured and naïve whole joint and synovial fluid and near-perfect separation of injured and naïve serum. (D-F) Fold change analysis distinguished populations of metabolite features driving separation of metabolomic profiles. (D) Specifically, 250 and 291 metabolite features were highest in injured and naïve whole joints, respectively. (E) 373 and 155 metabolite features were highest in injured and naïve synovial fluid, respectively. (F) 386 and 195 features were highest in injured and naïve serum, respectively. (G-I) To further examine metabolic differences associated with injury status across tissue types, volcano plot analysis was performed and identified numerous metabolite features that had a fold change > 2, a p-value < 0.05, and were differentially regulated between injured and naïve whole joints (G, n = 70), synovial fluid (H, n = 131), and serum (I, n = 26). The colors in A-I correspond to: purple = naïve, orange = injured, red = whole joint, blue = synovial fluid, yellow = serum.

Populations of features distinguished by fold change analysis were subjected to pathway analysis where 2 pathways – pantothenate and CoA biosynthesis and histidine metabolism – were highest in injured whole joints, whereas 5 pathways including various amino acid pathways and

terpenoid backbone synthesis were highest in naïve whole joints (Table 6.1 A). Features highest in injured SF compared to naïve mapped to 8 significant pathways including various amino acid pathways, glutathione metabolism, and pyrimidine metabolism. Conversely, features highest in naïve SF compared to injured mapped to 4 significant pathways including biosynthesis of unsaturated fatty acids, purine metabolism, terpenoid backbone biosynthesis, and valine, leucine, and isoleucine biosynthesis (Table 6.1 B). Features highest in injured serum, compared to naïve serum, mapped to 5 significant pathways including 4 amino acid pathways and nicotinate and nicotinamide metabolism. Conversely, those highest in naïve serum, compared to injured serum, mapped to 11 significant pathways including purine and pyrimidine metabolism, vitamin B6 metabolism, glutathione metabolism, amino acid pathways, and various others (Table 6.1 C). Volcano plot analysis, which combines both fold change and significance, identified numerous features that were highest in injured and naïve whole joints, SF, and serum (Fig. 6.2 G-I). Features distinguished by volcano plot analysis were matched to metabolite identifications made using LC-MS/MS data to unveil potential metabolic indicators of injury (Supplemental Table 6.1). Of these, 3,4-Dimethyl-5-pentyl-2-furanundecanoic acid was differentially regulated between naïve and injured whole joints, whereas numerous amino acid putative identified metabolites, such as D/L-glutamine, was highest in injured SF compared to naïve (Supplemental Table 6.1).

Table 6.1. Metabolic pathways detected in naïve and injured (A) whole joints, (B) synovial fluid, and (C) serum. All pathways listed were false discovery rate (FDR)-corrected using the Benjamini-Hochberg method.

A) Pathways detected in whole joints		
Group	Pathway	FDR p-value
Injure	Pantothenate and CoA biosynthesis	0.024163
Injure	Histidine metabolism	0.040172
Naïve	Lysine degradation	0.015987
Naïve	Drug metabolism - cytochrome P450	0.015987
Naïve	Arginine and proline metabolism	0.017842
Naïve	Terpenoid backbone biosynthesis	0.020499
Naïve	Valine, leucine and isoleucine degradation	0.045619
B) Pathways detected in synovial fluid		
Injured	Alanine, aspartate and glutamate metabolism	0.022076
Injured	Arginine and proline metabolism	0.022076
Injured	Pyrimidine metabolism	0.037936
Injured	Lysine degradation	0.037936
Injured	Glutathione metabolism	0.037936
Injured	Arginine biosynthesis	0.044408
Injured	D-Amino acid metabolism	0.044408
Injured	Glycine, serine and threonine metabolism	0.045814
Naïve	Biosynthesis of unsaturated fatty acids	0.017571
Naïve	Purine metabolism	0.022971
Naïve	Valine, leucine and isoleucine biosynthesis	0.03946
Naïve	Terpenoid backbone biosynthesis	0.040529
C) Pathways detected in serum		
Injured	Arginine and proline metabolism	0.033874
Injured	Drug metabolism - cytochrome P450	0.032385
Injured	Glutathione metabolism	0.041471
Injured	Glycerophospholipid metabolism	0.029415
Injured	One carbon pool by folate	0.045182
Injured	Purine metabolism	0.011805
Injured	Pyrimidine metabolism	0.041047
Injured	Terpenoid backbone biosynthesis	0.019908
Injured	Valine, leucine and isoleucine biosynthesis	0.0086968
Injured	Valine, leucine and isoleucine degradation	0.0064471
Injured	Vitamin B6 metabolism	0.019908
Naïve	Arginine biosynthesis	0.01868
Naïve	beta-Alanine metabolism	0.025558
Naïve	D-Amino acid metabolism	0.03923
Naïve	Histidine metabolism	0.014393
Naïve	Nicotinate and nicotinamide metabolism	0.037164

Systemic Response Following Joint Injury Across Limbs in Whole Joints and Synovial Fluid

To further examine metabolic differences associated with injury - injured, contralateral, and naive whole joints and SF were examined. PLS-DA analysis of all three joint types revealed overlap, where the metabolome of injured whole joints and SF resides between contralateral and naïve whole joints and SF (Fig. 6.3 A, C), suggesting metabolic differences associated with injury at the whole joint and SF levels are observed in the contralateral limb.

Next, a median intensity heatmap analysis normalized to naïve samples was performed to visualize and pinpoint clusters of metabolite features that are co-regulated and differentially expressed across limbs. Clusters of metabolite features were then subjected to pathway analyses. Comparing injured, contralateral, and naïve whole joints, 22 significant pathways were detected across 8 clusters (Fig. 6.3 B, Table 6.2). Noteworthy pathways that were highest in injured joints, and similar in regulation in contralateral and naïve joints, mapped to glycerophospholipid metabolism (Cluster 3). Glutathione and purine metabolism were highest in injured whole joints, but lowest in contralateral joints (Cluster 4). Conversely, lysine degradation was highest in contralateral whole joints, and lower in injured and naïve whole joints (Cluster 5). Metabolite features that were higher in both injured and contralateral joints mapped to a handful of pathways including amino acid pathways, biosynthesis of unsaturated fatty acids, porphyrin metabolism, and selenocompound metabolism (Clusters 6-8). Metabolite features lowest in both injured and contralateral whole joints compared to naïve joints mapped to nitrogen metabolism (Clusters 1, 2).

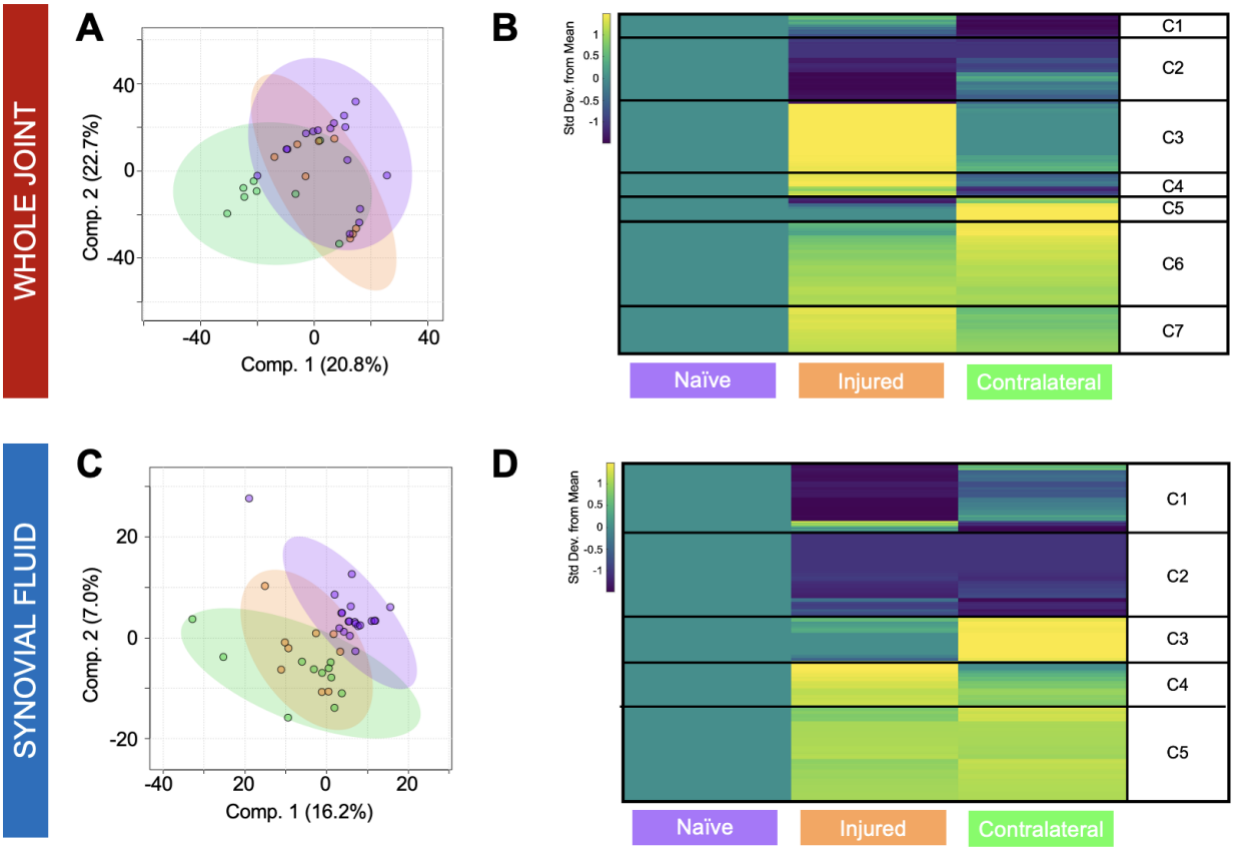

Figure 6.3. Distinct metabolomic profiles exist between injured, contralateral, and naïve limbs. Partial Least Squares-Discriminant Analysis (PLS-DA) reveals overlap between injured, contralateral, and naïve (A) whole joints and (C) synovial fluid with injured samples clustering together between contralateral and naïve samples. To pinpoint pathways driving metabolomic differences between limbs with different injury statuses, median intensity heatmap analyses where injured and contralateral limbs were normalized to naïve limbs were performed. Clusters of co-regulated metabolite features within (B) whole joint and (D) synovial fluid samples were subjected to pathway analyses to identify biological pathways that differ in regulation across limbs in both whole joint and synovial fluid samples. Combined, data provide strong evidence of distinct metabolomic regulation associated with injury status. Columns represent limbs (naïve, injured, contralateral) and rows represent metabolite features. Cooler and warmer colors indicate lower and higher metabolite abundance relative to the mean, respectively. Colors in A-D correspond to: naïve = purple, orange = injured, green = contralateral.

Table 6.2. Metabolic pathways associated with injured, contralateral, and naïve whole joints identified by median metabolite intensity heatmap analysis. Clusters defined in Figure 6.3B. All pathways listed were false discovery rate (FDR)-corrected using the Benjamini-Hochberg method.

Cluster	Pathway	FDR p-value
1	Nitrogen metabolism	0.038724
3	Glycerophospholipid metabolism	0.026682
4	Glutathione metabolism	0.037509
4	Purine metabolism	0.039218
5	Lysine degradation	0.029907
6	Tyrosine metabolism	0.020728
6	Phenylalanine, tyrosine and tryptophan biosynthesis	0.021793
6	Drug metabolism - cytochrome P450	0.024627
6	Ubiquinone and other terpenoid-quinone biosynthesis	0.032414
7	Biosynthesis of unsaturated fatty acids	0.040583
8	Glycine, serine and threonine metabolism	0.026954
8	Porphyrin metabolism	0.042532
8	Selenocompound metabolism	0.046842
1,3	Alanine, aspartate and glutamate metabolism	0.029542
1,4	Pyrimidine metabolism	0.02755
1,4	Arginine biosynthesis	0.032888
1,4,8	Arginine and proline metabolism	0.04208
1,8	D-Amino acid metabolism	0.04524
2,6	Phenylalanine metabolism	0.029633
2,7,8	Valine, leucine and isoleucine biosynthesis	0.0262
3,4	Histidine metabolism	0.024963
7,8	Valine, leucine and isoleucine degradation	0.033736

Similarly, SF metabolic shifts in SF following injury across limbs were assessed using a median heatmap analysis (Fig. 6.3 D, Table 6.3). Metabolite features lowest in injury, but similar in regulation in contralateral and naïve SF, mapped to fructose and mannose metabolism, cysteine and methionine metabolism, taurine and hypotaurine metabolism, and pyruvate metabolism (Cluster 1). Metabolite features lowest in both injured and contralateral SF, compared to naïve SF, mapped to 5 pathways including amino acid pathways and purine metabolism (Cluster 2). Interestingly, metabolite features highest in contralateral SF, but similar in regulation in injured

and naïve SF, mapped to sphingolipid metabolism and biosynthesis of unsaturated fatty acids (Cluster 3). Those highest in injured SF, but lower in contralateral and naïve SF, mapped to beta-alanine metabolism and glutathione metabolism (Cluster 5). Lastly, metabolite features relatively higher in both injured and contralateral SF, compared to naïve SF, mapped to pyrimidine metabolism and terpenoid backbone biosynthesis (Cluster 6). All pathways reported had an FDR-corrected $p < 0.05$.

Table 6.3. Metabolic pathways associated with injured, contralateral, and naïve synovial fluid identified by median metabolite intensity heatmap analysis. Clusters defined in Figure 6.3D. All pathways listed were false discovery rate (FDR)-corrected using the Benjamini-Hochberg method.

Cluster	Pathway	FDR p-value
1	Fructose and mannose metabolism	0.045507
1	Cysteine and methionine metabolism	0.045507
1	Taurine and hypotaurine metabolism	0.048399
1	Pyruvate metabolism	0.048399
2	Tryptophan metabolism	0.015813
2	Purine metabolism	0.015952
2	Alanine, aspartate and glutamate metabolism	0.015952
2	D-Amino acid metabolism	0.018787
2	Arginine biosynthesis	0.043755
3	Sphingolipid metabolism	0.019835
3	Biosynthesis of unsaturated fatty acids	0.028159
5	beta-Alanine metabolism	0.042318
5	Glutathione metabolism	0.045005
6	Pyrimidine metabolism	0.015242
6	Terpenoid backbone biosynthesis	0.021309
1,2	Phenylalanine metabolism	0.014108
1,2	Lysine degradation	0.014873
1,2	Arginine and proline metabolism	0.017409
1,2	Drug metabolism - cytochrome P450	0.01907
1,2	Phenylalanine, tyrosine and tryptophan biosynthesis	0.019654
1,2	Tyrosine metabolism	0.03806
1,4,6	Valine, leucine and isoleucine degradation	0.03037
2,5	Histidine metabolism	0.040028
4,5	Valine, leucine and isoleucine biosynthesis	0.048673

Additionally, pairwise comparisons of injured, contralateral, and naïve whole joints and SF were performed to further examine the effects of injury across different joints (Supplemental Figures 6.3, 6.4, Supplemental Tables 6.2, 6.3). The results of pairwise comparisons are further discussed in the Supplemental results. Collectively, the results of PLS-DA, fold change, volcano plot, and heatmap analysis strongly suggest that injury influences the whole joint and SF metabolome and produces a systemic response that influences both the injured and contralateral joints.

Collectively, it is evident that injury perturbs metabolism spanning the whole joint, SF, and serum. Moreover, the metabolome of injured, contralateral, and naïve limbs are metabolically distinct suggesting that injury has a systemic response that stretches beyond the injured joint itself.

Sex Influences Metabolomic Profiles Across Tissues of Injured and Naive Mice

To examine the effects of sex and its interactions with injury on the whole joint, SF, and serum metabolomes, a series of pairwise comparisons were performed. First, general sex differences were examined in male and female whole joints (Supplemental Fig. 6.5 A-C) revealing distinct metabolomic profiles between sexes. Next, whole joints from injured males and females were assessed using PLS-DA which revealed clear separation of mice within their respective cohorts (Fig. 6.4 A). Similarly, injury differences are evident when comparing whole joints from injured and naïve females (Fig. 6.4 B) and from injured and naïve males as seen by minimal PLS-DA overlap (Fig. 6.4 C). Fold change analysis distinguished populations of metabolite features that are differentially regulated among injured male and female whole joints (Fig. 6.4 D), injured and naïve females (Fig. 6.4 E), and injured and naïve males (Fig. 6.4 F). Populations of metabolite features distinguished by fold change analyses underwent pathway analyses. Pathways that were

highest in whole joints from injured males mapped to purine metabolism and alanine, aspartate, and glutamate metabolism. Conversely, pathways highest in whole joints from injured females mapped to cysteine and methionine metabolism, pyruvate metabolism, tyrosine metabolism, and vitamin B6 metabolism. Pathways that were consistent across whole joints from males regardless of injury status included arginine biosynthesis, beta-alanine metabolism, glycerophospholipid metabolism, primary bile acid biosynthesis, and sphingolipid metabolism. Lastly, pathways that were consistent across whole joints from females included lysine degradation, terpenoid backbone biosynthesis, and valine, leucine, and isoleucine degradation (Supplemental Table 6.4). To unveil metabolic indicators reflective of both injury and sex, volcano plot analysis was performed comparing whole joints from injured males and females (Fig. 6.4 G), as well as injured and naïve females (Fig. 6.4 H) and males (Fig. 6.4 I). Putative metabolite identifications related to terpenoid backbone biosynthesis were identified including (6R)-6-(L-Erythro-1,2-Dihydroxypropyl)-5,6,7,8-tetrahydro-4a-hydroxypterin which was associated with whole joints from females. Notably, Sterebin E which is also associated with terpenoid backbone biosynthesis was associated with whole joints from males (Supplemental Table 6.1).

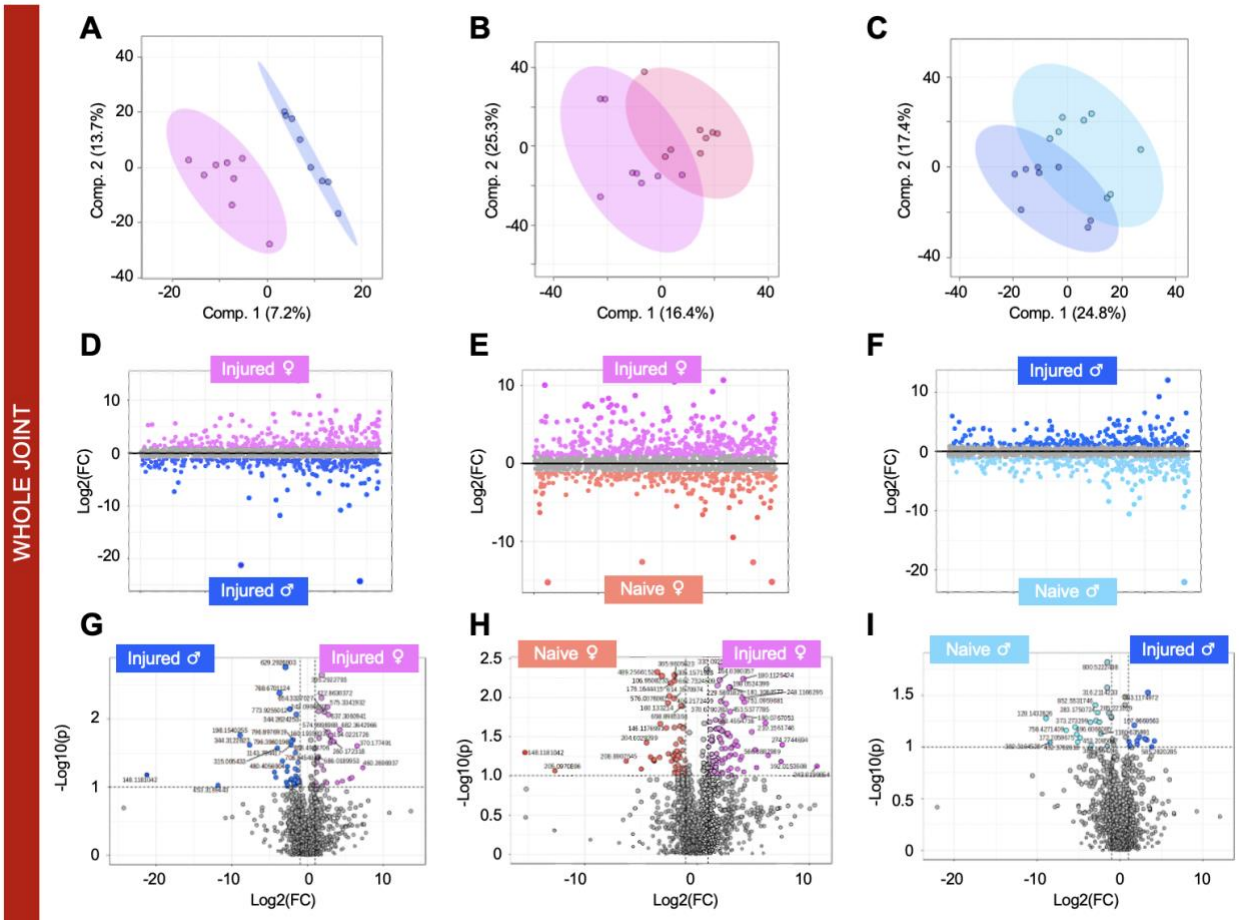

Figure 6.4. Whole joint metabolome differs by sex and injury. (A-C) Partial Least Squares-Discriminant Analysis (PLS-DA) finds (A) perfect separation of injured whole joints from males and females and minimal overlap when comparing (B) female and (C) male injured and naïve mice. (D-F) Fold change analysis distinguished populations of metabolite features driving separation of metabolomic profiles. (D) Specifically, 315 and 314 metabolite features were highest in injured females and males, respectively. (E) 509 and 319 metabolite features were highest in injured females and naïve females, respectively. (F) 242 and 288 features were highest in injured males and naïve males, respectively. (G-I) To further examine metabolic differences associated with injury and sex, volcano plot analysis was performed and identified numerous metabolite features that had a fold change > 2, a p-value < 0.05, and were differentially regulated between injured males and females (G, n = 110), injured and naïve females (H, n = 158), and injured and naïve males (I, n = 32). The colors in A-I correspond to: pink = injured females, peach = naïve females, royal blue = injured males, light blue = naïve males.

The same series of analyses were performed to assess metabolic differences between injured and naïve male and female mice within SF and serum samples. Within SF, general sex differences were evident (Supplemental Figure 6.5 D-F). By employing PLS-DA, it is evident that the metabolome is influenced by both injury and sex where minimal overlap is observed between SF from injured males and females (Fig. 6.5 A), naïve and injured females (Fig. 6.5 B), and males (Fig. 6.5 C). Fold change analysis distinguished populations of metabolite features that are differentially regulated among SF from injured males and females (Fig. 6.5 D), injured and naïve females (Figure 5E), and injured and naïve males (Fig. 6.5 F). These populations underwent pathway analyses revealing overlapping and distinctly regulated pathways across SF groups (Supplemental Table 6.5). Specifically, phenylalanine metabolism was consistently higher in females compared to males, regardless of injury status. Pathways unique to SF from injured males mapped to alpha-linolenic acid metabolism, butanoate metabolism, TCA cycle, propanoate metabolism, and tryptophan metabolism. Conversely, those unique to SF from injured females mapped to arginine biosynthesis, glycerophospholipid metabolism, and pyrimidine metabolism. Unique to naïve females and males included beta-alanine metabolism and biosynthesis of unsaturated fatty acids. On the other hand, pathways unique to injured males and females included D-amino acid metabolism, glycine, serine and threonine metabolism, and lysine degradation. Lastly, a pathway that was differentially regulated between injured females and naïve males was histidine metabolism. To pinpoint metabolite features contributing to the observed sexual dimorphism, volcano plot analysis was performed comparing SF from injured males and females (Fig. 6.5 G), as well as injured and naïve females (Fig. 6.5 H) and males (Fig. 6.5 I). Among those

identified, 3-Methylhistamine was associated with females and was highest in injured SF, whereas D/L-Valine was associated with males and was highest in injured males (Supplemental Table 6.1).

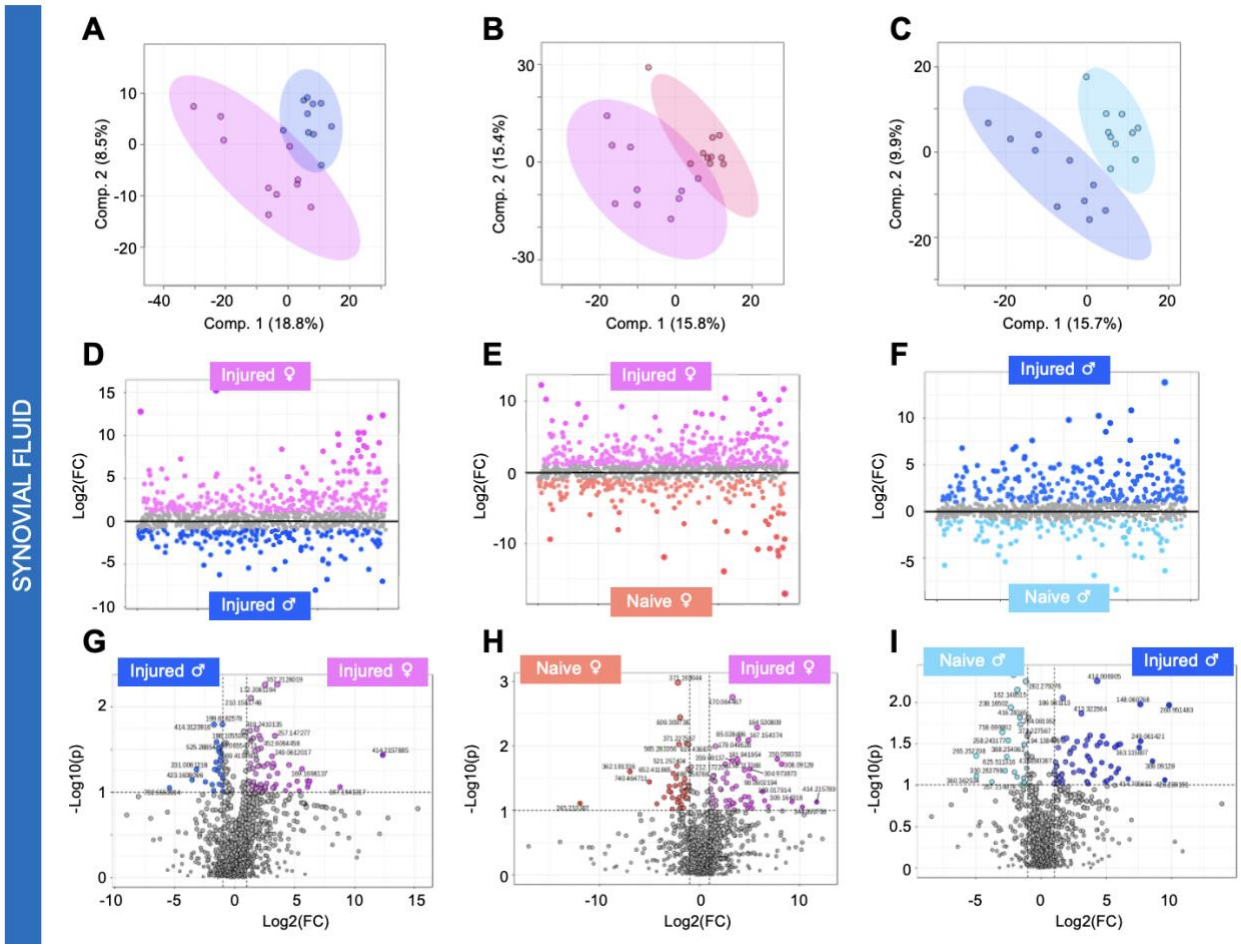

Figure 6.5. Metabolomic profiles of synovial fluid show sexual dimorphism across injured and naïve mice. (A-C) Partial Least Squares-Discriminant Analysis (PLS-DA) finds minimal overlap when comparing (A) injured SF from males and females, (B) female and (C) male injured and naïve mice. (D-F) Fold change analysis identified populations of metabolite features driving separation of metabolomic profiles. (D) Specifically, 335 and 175 metabolite features were highest in injured females and males, respectively. (E) 386 and 195 metabolite features were highest in injured females and naïve females, respectively. (F) 253 and 115 features were highest in injured males and naïve males, respectively. (G-I) To further examine metabolic differences associated with injury and sex among SF samples, volcano plot analysis was performed and identified numerous metabolite features that had a fold change > 2, a p-value < 0.05, and were differentially regulated between injured males and females (G, n = 95), injured and naïve females (H, n = 101), and injured and naïve males (I, n = 99). The colors in A-I correspond to: pink = injured females, peach = naïve females, royal blue = injured males, light blue = naïve males.

Lastly, serum was assessed in a similar way to determine if metabolomic differences were evident considering sex and injury. Like whole joint and SF analyses, comparing males and females, regardless of injury status, reveals evident sex differences (Supplemental Figure 6.5 G-I). To delve deeper into the interactions of sex and injury at the level of serum, PLS-DA was performed and showcased extremely distinct separation of injured males and females (Fig. 6.6 A). When controlling for sex, some overlap is present when comparing injured and naïve females (Fig. 6.6 B) and males (Fig. 6.6 C). Fold change distinguished populations of metabolite features that are differentially regulated between injured males and females (Fig. 6.6 D), injured and naïve females (Fig. 6.6 E), and males only (Fig. 6.6 F). These metabolite features were then subjected to pathway analyses, revealing numerous statistically significant pathways (Supplemental Table 6.6). Those detected in females, regardless of injury status, included arginine and proline metabolism and pantothenate and CoA biosynthesis. Conversely, pathways detected in males, regardless of injury status, included cysteine and methionine metabolism, glycerophospholipid metabolism, nicotinate and nicotinamide metabolism, nitrogen metabolism, phenylalanine metabolism, and tyrosine metabolism. Porphyrin metabolism was unique to injured males, whereas primary bile acid biosynthesis and pyrimidine metabolism were unique to injured females. Lastly, pathways that were repeatedly detected in injured mice, regardless of sex, mapped to alanine, aspartate, and glutamate metabolism, lysine degradation, and purine metabolism. To examine metabolic differences beyond pathways, volcano plot analysis was performed comparing serum from injured males and females (Fig. 6.6 G) as well as injured and naive females (Fig. 6.6 H) and males only (Fig. 6.6 I). Similar to SF, D/L-Valine was associated with males. Notably, 1/3-methyhistidine was

associated with injury regardless of sex and was detected in the SF from injured females (Supplemental Table 6.1).

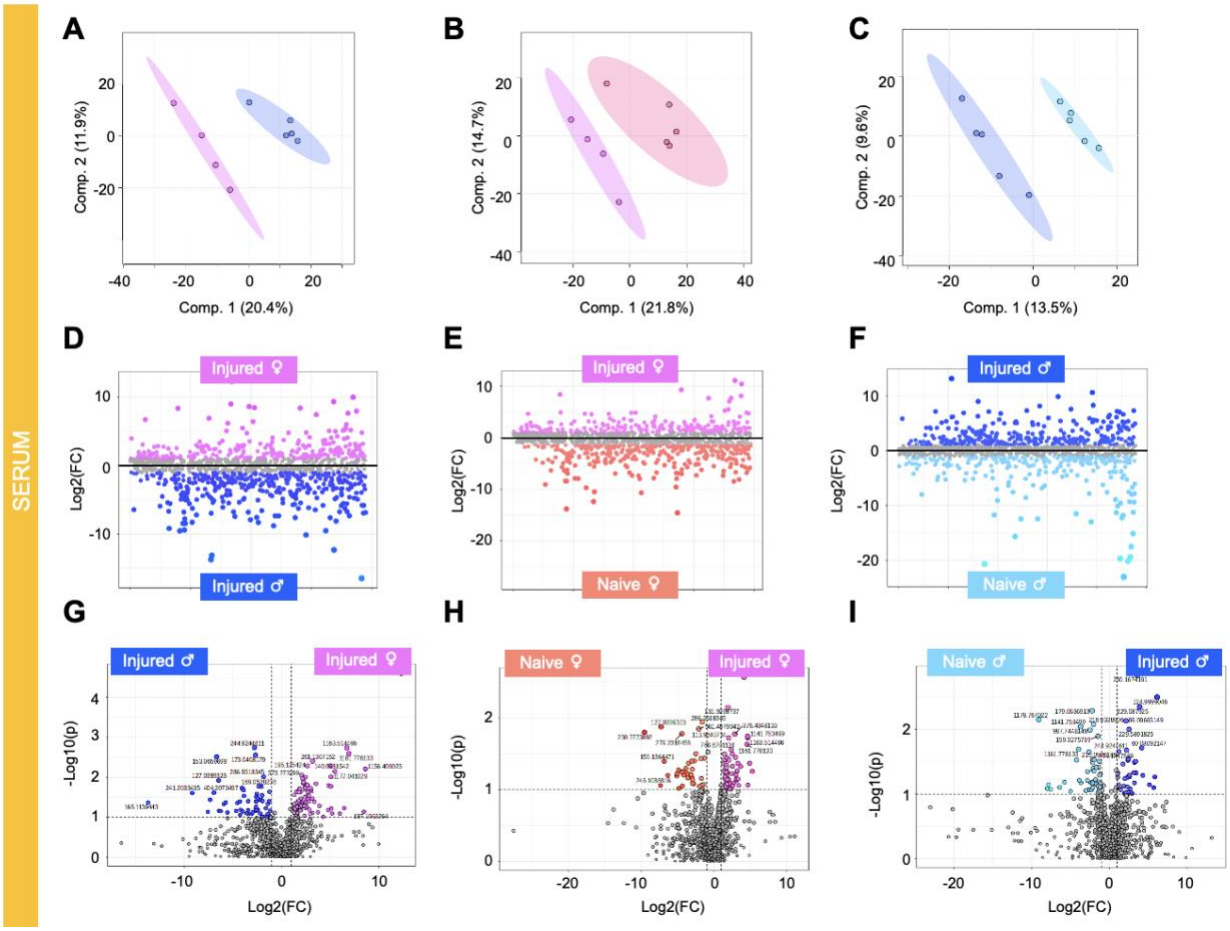

Figure 6.6. Serum metabolism reflects both injury status and sex. (A-C) Partial Least Squares-Discriminant Analysis (PLS-DA) finds clear separation with no overlap when comparing (A) injured SF from males and females, (B) female and (C) male injured and naïve mice. (D-F) Fold change analysis identified populations of metabolite features driving separation of serum metabolomic profiles. (D) Specifically, 267 and 407 metabolite features were highest in injured females and males, respectively. (E) 319 and 260 metabolite features were highest in injured females and naïve females, respectively. (F) 304 and 267 features were highest in injured males and naïve males, respectively. (G-I) To further examine metabolic differences associated with injury and sex across serum samples, volcano plot analysis was performed and identified numerous metabolite features that had a fold change > 2, a p-value < 0.05, and were differentially regulated between injured males and females (G, n = 82), injured and naïve females (H, n = 92), and injured and naïve males (I, n = 87). The colors in A-I correspond to: pink = injured females, peach = naïve females, royal blue = injured males, light blue = naïve males.

Considering metabolic differences associated with sex and injury across all tissues – whole joints, SF, and serum – a handful of pathways are conserved. Alanine, aspartate, and glutamate metabolism were detected in whole joints of injured males and SF and serum of injured males and females. Arginine biosynthesis was detected among whole joints from males; however, it was detected in serum from injured females and SF from injured males and females. Beta-alanine, glyoxylate, and dicarboxylate metabolism were detected across all male naïve tissues. Cysteine and methionine metabolism was detected in both whole joint and SF from injured females. Interestingly, lysine degradation and pyrimidine metabolism were detected across all three tissues in injured females. Moreover, it was associated with injured males in SF and serum.

MALDI-MSI Spatially Locates and Detects Differences in Osteochondral Metabolites

To characterize and examine metabolites that are tissue specific and compose the whole joint, MALDI-MSI was performed. A novel protocol encompassing sample preparation, matrix application, and instrumentation was developed to avoid losing metabolites (50-1500 m/z) that are typically removed during formalin fixation and paraffin embedding of bone. In doing so, this allows for the visualization of the spatial distribution of metabolites, particularly focused on lipids. Considering preliminary data, different populations of metabolites were observed considering spatial areas of the joint – including cartilage, bone, and the growth plate – suggesting unique metabolite signatures. Ions 369 and 563 m/z displays a distribution among cortical bone and in some areas of cartilage and the growth plate, whereas 617 and 853 m/z is distributed within the marrow cavity and in bone underlying cartilage (Fig. 6.7). With this approach, it is evident that MALDI-MSI spatially locates and detects differences in osteochondral metabolites that compose the joint, and unique patterns among male and female injured and naïve whole joints will be further

examined following complete data analysis. Moreover, LC-MS/MS data will be leveraged to identify lipids of interest from MALDI-MSI data.

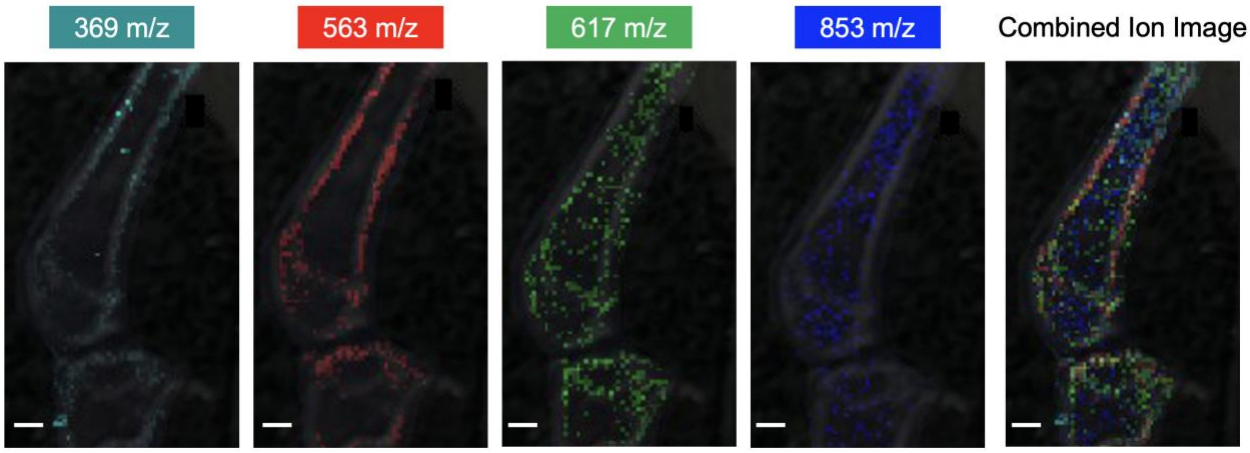

Figure 6.7. MALDI-MSI analysis of whole joint. Heatmap images for individual ions - m/z 369 (teal), 563 (red), 617 (green), and 853 (blue) – and a combined ion image from sagittal whole joint section after of 2,5-dihydroxybenzoic acid (DHB) matrix application. Scale bars = 1 mm.

Discussion

To our knowledge, this is the first study to examine structural and metabolic responses following injury in different tissues – whole joints, SF, and serum – using LC-MS metabolomic profiling and MALDI-MSI. The goals of this study were to (1) identify tissue-specific and spatially dependent metabolic signatures perturbed by injury and (2) pinpoint metabolic differences associated with sex. Metabolomic profiling has been used to profile SF following injury in mouse models as it reflects cartilage morphological changes, however, changes in bone are traditional investigated using microCT leaving key questions unanswered about the whole joint response.

Effects of Injury Across Whole Joints, Synovial Fluid, and Serum

Distinct metabolomic profiles of whole joints, SF, and serum reveal acute changes occur in response to injury. Various amino acid pathways exhibit differential regulation across tissues with many overlapping between tissues. Lysine degradation displayed differential regulation across injured, contralateral, and naive whole joints (Table 6.1 A, Table 6.2) while being downregulated in SF contralateral and injured limbs compared to naïve (Table 6.3). Detection of this pathway may be associated with collagen, where lysine residues are crucial for collagen's structural integrity through hydroxylation and cross-link formation[40]. Specific to bone, collagen is a major component of the structural organic matrix and when lysyl hydroxylase levels are altered in osteoblasts, defective cross-linking patterns, fibrillogenesis, and matrix mineralization are observed[40-42] underscoring the importance of lysine hydroxylation in bone quality. In SF, lysine metabolism tends to decrease as OA progresses[32], suggesting this pathway could represent acute joint changes following injury that could be monitored to oversee joint health and disease.

Arginine and proline metabolism was upregulated in naïve whole joints and in injured SF (Table 6.1 A, B). Like lysine, proline is associated with collagen, where it contributes to collagen synthesis. Arginine has anti-inflammatory effects and has been shown to decrease in concentration as OA develops[43, 44]. Arginine and proline metabolism has been detected in rabbit SF post-ACL injury[45], in human SF from patients who sustained traumatic knee injuries[22], and in mouse serum 1-day post-ACL injury and decreased by day 7[19]. Combined, this may indicate a short-term protective mechanism, or cascade of pathways, to enhance ATP production post-injury. The detection of this pathway in SF from injured mice aligns with previous work, however, additional research is required to understand pathway regulation in bone post-injury.

Phenylalanine, tyrosine, and tryptophan biosynthesis exhibited differential regulation when comparing injured, contralateral, and naive limbs at the whole joint (Fig. 6.2 B, Cluster 6) and SF levels (Fig. 6.2 D, Cluster 2). While higher in injured and contralateral whole joints compared to naïve ones, these pathways showed the opposite trend in SF. These aromatic amino acids can bind to the calcium-sensing receptor, in turn raising intracellular calcium and modulating bone turnover[46]. Moreover, phenylalanine and tyrosine metabolism have been associated with the sclerosis of subchondral bone in OA[47]. In a noninvasive mouse injury model, tryptophan metabolism was higher in mouse SF 7 days post-injury compared to naïve controls. Tryptophan has been noted as a promising biomarker of OA where its concentration decreases as disease progresses[48, 49]. The detection of this pathway in both injured and contralateral whole joints is novel suggesting at systemic response is produced in both injured and contralateral whole joints. Moreover, these results hold promise as amino acids in general have been shown to play a role in the response to acute injury[50], been detected post-injury across mammalian models[19, 22, 45], and noted as molecules that change in concentration as disease progresses.

Purine and pyrimidine metabolism were detected across tissues from injured mice. Pyrimidine metabolism was highest in injured whole joints and injured and contralateral SF, while purine metabolism was highest in SF from naïve mice, but highest in serum from injured mice. Both pathways, derived from the pentose phosphate pathways, synthesize nucleotides and amino acids. Purigenic signaling, mediated by purine nucleotides like adenosine and ATP, contributes to OA pathophysiology, influencing processes such as cell proliferation, tissue regeneration, and inflammation[51-54]. Detection of these pathways provides insight into energy generation, inflammation, and signaling at the site of injury in both whole joints and SF.

Sexual Dimorphism of Injury Among the Metabolome of Whole Joints, Synovial Fluid, and Serum

Considering both injury and sex, purine and pyrimidine metabolism showed dysregulated. Purine metabolism was consistently detected across all tissues from injured males, particularity in serum, could be explained considering that circulating uric acid—an end product of purine metabolism— is much higher in males compared to females[55] where female hormones decrease uric acid levels[56]. Conversely, pyrimidine metabolism was dominate in tissues from injured females, necessitating further research to understand its sexual dimorphic regulation.

Glycine, serine, and threonine metabolism was detected in serum and SF in injured males and females. In a previous study on female sheep post-ACL injury, this pathway was notably perturbed among injured animals with serine identified as a potential biomarker for early degenerative changes[21]. Serine, a glucogeneic amino acid, influences adenosine monophosphate kinase (AMPK), which acts as a key "energy sensor" that maintains energy homeostasis and promotes ATP synthesis, via serine/threonine phosphorylation[57-59]. Mechanisms like AMPK are differentially influenced by circulating sex hormones like estrogen which can bind to estrogen receptor beta, triggering downstream metabolic cascades to generate ATP[60, 61]. The influence of circulating sex hormones, like estrogen, on mechanisms like AMPK may affect energy metabolism post-injury, warranting further investigation into sexual dimorphic patterns.

Cysteine and methionine metabolism was highest in whole joints and SF from injured females but in serum from injured males. Histidine metabolism was higher in injured males in serum and whole joints, but in injured females at the SF level. These three amino acids are related to matrix metalloproteinases (MMPs) regulate tissue remodeling and degradation of extracellular matrix proteins, cell proliferation, and immune responses[62]. MMP activation is modulated by a

cysteine switch and the catalytic domain of MMPs is regulated by these amino acids because zinc binds to histidines with assistance from conserved methionine sequences[62, 63]. MMP activity has been shown to be influenced by hormones[64], like estrogen and progesterone, particularity in chondrocytes. In a previous study, chondrocytes from 25 postmenopausal OA patients were cultured with different concentrations of 17B-estradiol and found that physiological levels of estrogen suppressed the expression of MMP-1 and that hormone replacements could benefit female OA patients in the early stages of disease[65]. Thus, differential regulation of AMPK and MMP-associated amino acids between males and females' post-injury suggest reliance on different metabolic pools, mechanisms, and biofuels to meet energy demands and maintain matrix properties following joint injury. Further investigation into amino acid concentrations at different tissue levels is needed to understand metabolic differences associated with injury site versus circulating serum.

MALDI-MSI Provides New Insight into Composition of Osteochondral Tissue at the Metabolite Level

To our knowledge, this is the first study to examine the spatial distribution of osteochondral metabolites, with an emphasis on lipids, following joint injury. Here, we developed an innovative protocol to localize and spatially locate osteochondral metabolites that compose whole joints from injured and naïve mice using MALDI-MSI. Only a handful of studies have employed MALDI-MSI to musculoskeletal tissues, with many being in human samples, to visualize the spatial distribution of proteins and peptides[26, 29]. While many of these studies have provided the field with a new tool to study these tissues, findings are narrowed to these larger molecules. Traditionally, histological sectioning and imaging of whole joints – and bone samples in general – first require formalin fixation and paraffin-embedding to preserve and demineralize the bone. However, this

can result in removal, cross-linking, or delocalization of molecules species, especially lipid species[36].

Lipid metabolism has gained attention and has been associated with PTOA and OA development. Specifically, proteomic and metabolomic analyses have shown an important connection between OA and lipid metabolism by analyzing SF, cartilage, bone, and circulatory fluids from humans and mice[27, 32, 66-69]. Thus, specific sample preparation and application of MALDI-MSI at the level of small molecules (50-1500 m/z) provides key insight into joint composition, with an emphasis on lipids, and how it changes post-injury. Moreover, this two-pronged approach utilizing LC-MS-based metabolomics and MALDI-MSI sheds light on lipids and their role at the metabolite level both globally and spatially. The relationship between lipid-related pathways detected in whole joints using metabolomics and lipids using MALDI-MSI will be further examined upon completion of MALDI-MSI data analysis. Moreover, we aim to identify differences in populations across injured and contralateral limbs as well as spatially map patterns where subchondral bone changes are observed in this injury model[16]. MALDI-MSI at the level of proteins, peptides, and lipids can be leveraged and combined with existing techniques to better understand how the joint responds post-injury at multiple length scales.

Limitations

Our study has notable limitations. Firstly, this study focused on the early response to joint injury where mice were euthanized at 8 days post-injury. Additional timepoints within the first 7 days of injury as well as upwards of 56 days post-injury[16] may shed light on the arc of structural and metabolic changes across serum, SF, and whole joints. Secondly, while multiple samples were obtained from each mouse, sample size was small (N=20, n=5/group). Thirdly, metabolite

extraction protocols and use of HILIC column bias data towards assessing polar molecules. Moreover, DHB was used for MALDI-MSI, which is optimal for positive ionization mode. Combined, LC-MS and MALDI-MSI analysis were both conducted in positive ionization mode focusing on polar molecules, thus additional investigation into nonpolar species is warranted.

Conclusions

The findings of our study, integrating LC-MS based metabolomics and MALDI-MSI, underscore significant metabolic and pathological shifts following joint injury, with discernible sex-specific associations. The detection of novel differences associated with both injury and sex across serum, SF, and whole joints enhances our current understanding on the post-injury response within and beyond the joint. Moreover, it is evident that the whole joint is influenced by injury at multiple length scales, further supported by differences in the SF metabolome, suggesting a systemic response is produced in both injured and contralateral joints. Further investigation into molecules perturbed by injury in males and females, at the level of the metabolome and spatially, is imperative for pinpointing the effects injury comprehensively. Completion of this work has the potential to refine and improve pre-clinical PTOA models and deepen our insights into PTOA development, thereby advancing strategies for prevention and treatment.

Acknowledgements

The authors thank the Montana State University Mass Spectrometry Facility including Dr. Donald Smith and Jesse Thomas for assisting with LC-MS, LC-MS/MS, and MALDI-MSI. for the Mass Spectrometry Facility used in this publication was made possible by the M.J. Murdock Charitable Trust, the National Institute of General Medical Sciences of the National Institutes of

Health (P20GM103474 and S10OD28650). Additionally, we thank Brady Hislop for his assistance in analyzing data and building data analysis pipelines. Lastly, we thank Erik Myers for designing two adapters for MALDI-MSI purposes. This study was funded by the National Institutes of Health under Award Numbers R01AR073964 and R01AR081489 (RKJ) and the National Science Foundation under Award Number CMMI 1554708 (RKJ).

Abbreviations List

PTOA = post-traumatic osteoarthritis; OA = osteoarthritis; ACL = anterior cruciate ligament; DMM = destabilization of the medial meniscus; SF = synovial fluid; MALDI-MSI = matrix assisted laser desorption ionization-mass spectrometry imaging; LC-MS = liquid chromatography-mass spectrometry; LC-MS/MS = liquid chromatography tandem mass spectrometry; m/z = mass-to-charge ratio; PCA = principal component analysis; PLS-DA = partial least squares-discriminant analysis; VIP = variable importance in projection; KEGG = Kyoto Encyclopedia of Genes and Genomes; FDR = false discovery rate; HMBD = Human Metabolome Database; OCT = optimal cutting temperature; ITO = indium tin oxide; DHB = 2,5-dihydroxybenzoic acid; TOF = time of flight; AMPK = adenosine monophosphate-activated protein kinase; MMPs = matrix metalloproteinases

References

1. Brown TD, Johnston RC, Saltzman CL, Marsh JL, Buckwalter JA. Posttraumatic osteoarthritis: a first estimate of incidence, prevalence, and burden of disease. J Orthop Trauma 2006; 20: 739-744.

2. Thomas AC, Hubbard-Turner T, Wikstrom EA, Palmieri-Smith RM. Epidemiology of Posttraumatic Osteoarthritis. J Athl Train 2017; 52: 491-496.

3. Gottlob CA, Baker CL, Jr., Pellissier JM, Colvin L. Cost effectiveness of anterior cruciate ligament reconstruction in young adults. Clin Orthop Relat Res 1999: 272-282.

4. Griffin LY, Albohm MJ, Arendt EA, Bahr R, Beynnon BD, Demaio M, et al. Understanding and preventing noncontact anterior cruciate ligament injuries: a review of the Hunt Valley II meeting, January 2005. Am J Sports Med 2006; 34: 1512-1532.

5. Lohmander LS, Englund PM, Dahl LL, Roos EM. The long-term consequence of anterior cruciate ligament and meniscus injuries: osteoarthritis. Am J Sports Med 2007; 35: 1756-1769.

6. Cinque ME, Dornan GJ, Chahla J, Moatshe G, LaPrade RF. High Rates of Osteoarthritis Develop After Anterior Cruciate Ligament Surgery: An Analysis of 4108 Patients. Am J Sports Med 2018; 46: 2011-2019.

7. Giugliano DN, Solomon JL. ACL tears in female athletes. Phys Med Rehabil Clin N Am 2007; 18: 417-438, viii.

8. Bruder AM, Culvenor AG, King MG, Haberfield M, Roughead EA, Mastwyk J, et al. Let's talk about sex (and gender) after ACL injury: a systematic review and meta-analysis of self-reported activity and knee-related outcomes. Br J Sports Med 2023; 57: 602-610.

9. Ardern CL, Taylor NF, Feller JA, Webster KE. Fifty-five per cent return to competitive sport following anterior cruciate ligament reconstruction surgery: an updated systematic review and meta-analysis including aspects of physical functioning and contextual factors. Br J Sports Med 2014; 48: 1543-1552.

10. Tan SH, Lau BP, Khin LW, Lingaraj K. The Importance of Patient Sex in the Outcomes of Anterior Cruciate Ligament Reconstructions: A Systematic Review and Meta-analysis. Am J Sports Med 2016; 44: 242-254.

11. Blaker CL, Ashton DM, Doran N, Little CB, Clarke EC. Sex- and injury-based differences in knee biomechanics in mouse models of post-traumatic osteoarthritis. J Biomech 2021; 114: 110152.

12. Srikanth VK, Fryer JL, Zhai G, Winzenberg TM, Hosmer D, Jones G. A meta-analysis of sex differences prevalence, incidence and severity of osteoarthritis. Osteoarthritis Cartilage 2005; 13: 769-781.

13. Faber SC, Eckstein F, Lukasz S, Muhlbauer R, Hohe J, Englmeier KH, et al. Gender differences in knee joint cartilage thickness, volume and articular surface areas: assessment with quantitative three-dimensional MR imaging. Skeletal Radiol 2001; 30: 144-150.

14. Hitt K, Shurman JR, 2nd, Greene K, McCarthy J, Moskal J, Hoeman T, et al. Anthropometric measurements of the human knee: correlation to the sizing of current knee arthroplasty systems. J Bone Joint Surg Am 2003; 85-A Suppl 4: 115-122.

15. Christiansen BA, Guilak F, Lockwood KA, Olson SA, Pitsillides AA, Sandell LJ, et al. Non-invasive mouse models of post-traumatic osteoarthritis. Osteoarthritis Cartilage 2015; 23: 1627-1638.

16. Christiansen BA, Anderson MJ, Lee CA, Williams JC, Yik JH, Haudenschild DR. Musculoskeletal changes following non-invasive knee injury using a novel mouse model of post-traumatic osteoarthritis. Osteoarthritis Cartilage 2012; 20: 773-782.

17. Wu P, Holguin N, Silva MJ, Fu M, Liao W, Sandell LJ. Early response of mouse joint tissue to noninvasive knee injury suggests treatment targets. Arthritis Rheumatol 2014; 66: 1256-1265.

18. Anderson MJ, Diko S, Baehr LM, Baar K, Bodine SC, Christiansen BA. Contribution of mechanical unloading to trabecular bone loss following non-invasive knee injury in mice. J Orthop Res 2016; 34: 1680-1687.

19. Wallace CW, Hislop B, Hahn AK, Erdogan AE, Brahmachary PP, June RK. Correlations between metabolites in the synovial fluid and serum: A mouse injury study. J Orthop Res 2022.

20. Hislop BD, Devine C, June RK, Heveran CM. Subchondral bone structure and synovial fluid metabolism are altered in injured and contralateral limbs 7 days after non-invasive joint injury in skeletally-mature C57BL/6 mice. Osteoarthritis Cartilage 2022.

21. Mickiewicz B, Heard BJ, Chau JK, Chung M, Hart DA, Shrive NG, et al. Metabolic profiling of synovial fluid in a unilateral ovine model of anterior cruciate ligament reconstruction of the knee suggests biomarkers for early osteoarthritis. J Orthop Res 2015; 33: 71-77.

22. Welhaven HD, Welfley AH, Pershad P, Satalich J, O'Connell R, Bothner B, et al. Metabolic phenotypes reflect patient sex and injury status: A cross-sectional analysis of human synovial fluid. Osteoarthritis Cartilage 2023.

23. Hahn AK, Wallace CW, Welhaven HD, Brooks E, McAlpine M, Christiansen BA, et al. The microbiome mediates epiphyseal bone loss and metabolomic changes after acute joint trauma in mice. Osteoarthritis Cartilage 2021; 29: 882-893.

24. Seeley EH, Caprioli RM. Molecular imaging of proteins in tissues by mass spectrometry. Proc Natl Acad Sci U S A 2008; 105: 18126-18131.

25. Amstalden van Hove ER, Smith DF, Heeren RM. A concise review of mass spectrometry imaging. J Chromatogr A 2010; 1217: 3946-3954.

26. Cillero-Pastor B, Eijkel GB, Kiss A, Blanco FJ, Heeren RM. Matrix-assisted laser desorption ionization-imaging mass spectrometry: a new methodology to study human osteoarthritic cartilage. Arthritis Rheum 2013; 65: 710-720.

27. Cillero-Pastor B, Eijkel G, Kiss A, Blanco FJ, Heeren RM. Time-of-flight secondary ion mass spectrometry-based molecular distribution distinguishing healthy and osteoarthritic human cartilage. Anal Chem 2012; 84: 8909-8916.

28. Peffers MJ, Cillero-Pastor B, Eijkel GB, Clegg PD, Heeren RM. Matrix assisted laser desorption ionization mass spectrometry imaging identifies markers of ageing and osteoarthritic cartilage. Arthritis Res Ther 2014; 16: R110.

29. Cillero-Pastor B, Eijkel GB, Blanco FJ, Heeren RM. Protein classification and distribution in osteoarthritic human synovial tissue by matrix-assisted laser desorption ionization mass spectrometry imaging. Anal Bioanal Chem 2015; 407: 2213-2222.

30. Little CB, Hunter DJ. Post-traumatic osteoarthritis: from mouse models to clinical trials. Nat Rev Rheumatol 2013; 9: 485-497.

31. Seifer DR, Furman BD, Guilak F, Olson SA, Brooks SC, 3rd, Kraus VB. Novel synovial fluid recovery method allows for quantification of a marker of arthritis in mice. Osteoarthritis Cartilage 2008; 16: 1532-1538.

32. Carlson AK, Rawle RA, Wallace CW, Brooks EG, Adams E, Greenwood MC, et al. Characterization of synovial fluid metabolomic phenotypes of cartilage morphological changes associated with osteoarthritis. Osteoarthritis Cartilage 2019; 27: 1174-1184.

33. Welhaven HD, Vahidi G et al. The Cortical Bone Metabolome of C57BL/6J Mice Is Sexually Dimorphic. JBMR Plus 2022; 6.

34. Pang Z, Zhou G, Ewald J, Chang L, Hacariz O, Basu N, et al. Using MetaboAnalyst 5.0 for LC-HRMS spectra processing, multi-omics integration and covariate adjustment of global metabolomics data. Nat Protoc 2022; 17: 1735-1761.

35. Nelson KA, Daniels GJ, Fournie JW, Hemmer MJ. Optimization of whole-body zebrafish sectioning methods for mass spectrometry imaging. J Biomol Tech 2013; 24: 119-127.

36. Good CJ, Neumann EK, Butrico CE, Cassat JE, Caprioli RM, Spraggins JM. High Spatial Resolution MALDI Imaging Mass Spectrometry of Fresh-Frozen Bone. Anal Chem 2022; 94: 3165-3172.

37. Lockwood KA, Chu BT, Anderson MJ, Haudenschild DR, Christiansen BA. Comparison of loading rate-dependent injury modes in a murine model of post-traumatic osteoarthritis. J Orthop Res 2014; 32: 79-88.

38. Kawamoto T, Kawamoto K. Preparation of thin frozen sections from nonfixed and undecalcified hard tissues using Kawamot's film method (2012). Methods Mol Biol 2014; 1130: 149-164.

39. Shanmugaraj N, Rutten T, Svatos A, Schnurbusch T, Mock HP. Fast and Reproducible Matrix Deposition for MALDI Mass Spectrometry Imaging with Improved Glass Sublimation Setup. J Am Soc Mass Spectrom 2023; 34: 513-517.

40. Yamauchi M, Terajima M, Shiiba M. Lysine Hydroxylation and Cross-Linking of Collagen. Methods Mol Biol 2019; 1934: 309-324.

41. Pornprasertsuk S, Duarte WR, Mochida Y, Yamauchi M. Overexpression of lysyl hydroxylase-2b leads to defective collagen fibrillogenesis and matrix mineralization. J Bone Miner Res 2005; 20: 81-87.

42. Saito M, Marumo K. Collagen cross-links as a determinant of bone quality: a possible explanation for bone fragility in aging, osteoporosis, and diabetes mellitus. Osteoporos Int 2010; 21: 195-214.

43. Tootsi K, Vilba K, Martson A, Kals J, Paapstel K, Zilmer M. Metabolomic Signature of Amino Acids, Biogenic Amines and Lipids in Blood Serum of Patients with Severe Osteoarthritis. Metabolites 2020; 10.

44. Ohnishi A, Osaki T, Matahira Y, Tsuka T, Imagawa T, Okamoto Y, et al. Correlation of plasma amino acid concentrations and chondroprotective effects of glucosamine and fish collagen peptide on the development of osteoarthritis. J Vet Med Sci 2013; 75: 497-502.

45. Hu Y, Wu Q, Qiao Y, Zhang P, Dai W, Tao H, et al. Disturbances in Metabolic Pathways and the Identification of a Potential Biomarker Panel for Early Cartilage Degeneration in a Rabbit Anterior Cruciate Ligament Transection Model. Cartilage 2021; 13: 1376S-1387S.

46. Ding KH, Cain M, Davis M, Bergson C, McGee-Lawrence M, Perkins C, et al. Amino acids as signaling molecules modulating bone turnover. Bone 2018; 115: 15-24.

47. Yang G, Zhang H, Chen T, Zhu W, Ding S, Xu K, et al. Metabolic analysis of osteoarthritis subchondral bone based on UPLC/Q-TOF-MS. Anal Bioanal Chem 2016; 408: 4275-4286.

48. Igari T, Tsuchizawa M, Shimamura T. Alteration of tryptophan metabolism in the synovial fluid of patients with rheumatoid arthritis and osteoarthritis. Tohoku J Exp Med 1987; 153: 79-86.

49. Kang KY, Lee SH, Jung SM, Park SH, Jung BH, Ju JH. Downregulation of Tryptophan-related Metabolomic Profile in Rheumatoid Arthritis Synovial Fluid. J Rheumatol 2015; 42: 2003-2011.

50. Leimer EM, Tanenbaum LM, Nettles DL, Bell RD, Easley ME, Setton LA, et al. Amino Acid Profile of Synovial Fluid Following Intra-articular Ankle Fracture. Foot Ankle Int 2018; 39: 1169-1177.

51. Corciulo C, Cronstein BN. Signaling of the Purinergic System in the Joint. Front Pharmacol 2019; 10: 1591.

52. Croucher LJ, Crawford A, Hatton PV, Russell RG, Buttle DJ. Extracellular ATP and UTP stimulate cartilage proteoglycan and collagen accumulation in bovine articular chondrocyte pellet cultures. Biochim Biophys Acta 2000; 1502: 297-306.

53. Gratal P, Lamuedra A, Medina JP, Bermejo-Alvarez I, Largo R, Herrero-Beaumont G, et al. Purinergic System Signaling in Metainflammation-Associated Osteoarthritis. Front Med (Lausanne) 2020; 7: 506.

54. Pinto-Cardoso R, Pereira-Costa F, Pedro Faria J, Bandarrinha P, Bessa-Andres C, Correia-de-Sa P, et al. Adenosinergic signalling in chondrogenesis and cartilage homeostasis: Friend or foe? Biochem Pharmacol 2020; 174: 113784.

55. Akasaka H, Yoshida H, Takizawa H, Hanawa N, Tobisawa T, Tanaka M, et al. The impact of elevation of serum uric acid level on the natural history of glomerular filtration rate (GFR) and its sex difference. Nephrol Dial Transplant 2014; 29: 1932-1939.

56. Mumford SL, Dasharathy SS, Pollack AZ, Perkins NJ, Mattison DR, Cole SR, et al. Serum uric acid in relation to endogenous reproductive hormones during the menstrual cycle: findings from the BioCycle study. Hum Reprod 2013; 28: 1853-1862.

57. Steinberg GR, Macaulay SL, Febbraio MA, Kemp BE. AMP-activated protein kinase--the fat controller of the energy railroad. Can J Physiol Pharmacol 2006; 84: 655-665.

58. Wang J, Li J, Song D, Ni J, Ding M, Huang J, et al. AMPK: implications in osteoarthritis and therapeutic targets. Am J Transl Res 2020; 12: 7670-7681.

59. Yi D, Yu H, Lu K, Ruan C, Ding C, Tong L, et al. AMPK Signaling in Energy Control, Cartilage Biology, and Osteoarthritis. Front Cell Dev Biol 2021; 9: 696602.

60. Purdom T, Kravitz L, Dokladny K, Mermier C. Understanding the factors that effect maximal fat oxidation. J Int Soc Sports Nutr 2018; 15: 3.

61. Yang S, Wang J. Estrogen Activates AMP-Activated Protein Kinase in Human Endothelial Cells via ERbeta/Ca(2+)/Calmodulin-Dependent Protein Kinase Kinase beta Pathway. Cell Biochem Biophys 2015; 72: 701-707.

62. Cui N, Hu M, Khalil RA. Biochemical and Biological Attributes of Matrix Metalloproteinases. Prog Mol Biol Transl Sci 2017; 147: 1-73.

63. Visse R, Nagase H. Matrix metalloproteinases and tissue inhibitors of metalloproteinases: structure, function, and biochemistry. Circ Res 2003; 92: 827-839.

64. Verma RP, Hansch C. Matrix metalloproteinases (MMPs): chemical-biological functions and (Q)SARs. Bioorg Med Chem 2007; 15: 2223-2268.

65. Lee YJ, Lee EB, Kwon YE, Lee JJ, Cho WS, Kim HA, et al. Effect of estrogen on the expression of matrix metalloproteinase (MMP)-1, MMP-3, and MMP-13 and tissue inhibitor of metalloproternase-1 in osteoarthritis chondrocytes. Rheumatol Int 2003; 23: 282-288.

66. Eveque-Mourroux MR, Emans PJ, Boonen A, Claes BSR, Bouwman FG, Heeren RMA, et al. Heterogeneity of Lipid and Protein Cartilage Profiles Associated with Human Osteoarthritis with or without Type 2 Diabetes Mellitus. J Proteome Res 2021; 20: 2973-2982.

67. Pousinis P, Gowler PRW, Burston JJ, Ortori CA, Chapman V, Barrett DA. Lipidomic identification of plasma lipids associated with pain behaviour and pathology in a mouse model of osteoarthritis. Metabolomics 2020; 16: 32.

68. Carlson AK, Rawle RA, Wallace CW, Adams E, Greenwood MC, Bothner B, et al. Global metabolomic profiling of human synovial fluid for rheumatoid arthritis biomarkers. Clin Exp Rheumatol 2019; 37: 393-399.

69. Welhaven HD, Viles E, Starke J, Wallace C, Bothner B, June RK, et al. Metabolomic profiles of cartilage and bone reflect tissue type, radiography-confirmed osteoarthritis, and spatial location within the joint. Biochem Biophys Res Commun 2024; 703: 149683.

CHAPTER SEVEN

THE METABOLOME OF INDIVIDUALS WITH KNEE OSTEOARTHRITIS IS INFLUENCED BY 18-MONTHS OF EXERCISE AND WEIGHT LOSS INTERVENTION AND SEX: THE IDEA TRIAL

Contribution of Authors and Co-Authors

Manuscript in Chapter 7

Author: Hope D. Welhaven

Contributions: Designed experiments, performed metabolite extractions, ran LC-MS samples, analyzed and interpreted data, and drafted manuscript.

Co-Author: Avery H. Welfley

Contributions: Performed metabolite extractions, analyzed and interpreted data, and drafted manuscript.

Co-Author: Brian Bothner

Contributions: Interpreted data.

Co-Author: Stephen P. Messier

Contributions: Designed trial parameters and interpreted results.

Co-Author: Richard F. Loeser

Contributions: Designed trial parameters and interpreted results.

Co-Author: Ronald K. June

Contributions: Designed experiments, interpreted results, and drafted manuscript.

Manuscript Information

Hope D. Welhaven, Avery H. Wefley, Brian Bothner, Stephen P. Messier, Richard F. Loeser,

Ronald K. June

Status of Manuscript:

☐ Prepared for submission to a peer-reviewed journal
X Officially submitted to a peer-reviewed journal
☐ Accepted by a peer-reviewed journal
☐ Published in a peer-reviewed journal

Abstract

Objective: The Intensive Diet and Exercise for Arthritis (IDEA) trial was conducted to evaluate the effects of diet and exercise on osteoarthritis (OA), the most prevalent form of arthritis. Various risk factors, such as obesity and sex, contribute to the debilitating nature of OA. While diet and exercise are known to improve OA symptoms, cellular and molecular mechanisms underlying these interventions, as well as effects of participant sex, remain elusive.

Methods: Serum was obtained at three timepoints from IDEA participants assigned to groups of diet, exercise, or combined diet and exercise (n=10 per group). All serum metabolites were extracted and analyzed via liquid chromatography-mass spectrometry combined with metabolomic profiling. Extracted serum was pooled and fragmentation patterns were analyzed to identify metabolites that statistically differentially regulated between groups.

Results: Changes in metabolism across male and female IDEA participants after 18-months of diet, exercise, and combined diet and excise intervention mapped to lipid, amino acid, carbohydrate, vitamin, and matrix metabolism. The diverse metabolic landscape detected across IDEA participants shows that intervention type impacts the serum metabolome of individuals with OA in distinct patterns. Moreover, differences in the serum metabolome corresponded with participant sex.

Conclusions: These findings suggest that intensive weight loss among male and female subjects offers potential metabolic benefits for individuals with knee OA. This provides a deeper understanding of dysregulation occurring during OA development that may pave the way for improved interventions, treatments, and quality of life of those impacted by this disease.

Introduction

Obesity is the most modifiable risk factor and is a known accelerant of osteoarthritis (OA)[1, 2]. Weight loss via diet and exercise improves symptomatic knee OA and is recommended for overweight and obese patients with OA[3, 4]. However, the cellular and molecular mechanisms underlying weight-loss-related symptom improvement remain elusive. OA affects both males and females, but knee OA is more severe and prevalent among females[5, 6]. Known female-specific OA risk factors include genetics, anatomy, and increased likelihood to sustain a traumatic knee injury compared to male counterparts[7, 8], although sexual dimorphism at the molecular and cellular levels remains unclear.

Metabolomics, the study of small molecule intermediates called metabolites, can provide insight into OA pathogenesis, patient risk factors, and metabolic perturbations caused by diet and exercise interventions. This powerful tool has been applied in other musculoskeletal studies to analyze the metabolism of various fluids and tissues (e.g., synovial fluid) during disease progression[9-13] and after mechanical loading[14-16]. Nuclear Magnetic Resonance (NMR) metabolomics provided insight into urine signatures in the multi-faceted Intensive Diet and Exercise for Arthritis (IDEA) trial. The IDEA trial was conducted to assess the effects of weight loss, via diet and exercise, on primary and secondary outcomes in OA participants. Using NMR metabolomics, dysregulated amino acid and lipid metabolism were found in a subset of IDEA urine samples from participants with radiographic progression compared to non-progressors [17]. While this study provided insight into disease progression based on urine profiles, further investigation is required to better understand current methods of weight loss, the role of obesity and sex, and underlying molecular mechanisms driving OA.

Therefore, the objectives of this study were to (1) compare serum global metabolomic profiles to analyze changes in metabolism over the course of 18-months of an exercise and weight loss intervention, (2) illuminate metabolic pathways influenced by different types of interventions, and (3) identify signatures that are sex dependent.

Methods

Study Design, Interventions, and Participants

The participants in this study were a subset of those enrolled in the IDEA trial. In total, 30 participants were randomly selected (n=30) with 10 participants per intervention group (Diet, D: n = 10, Exercise, E: n = 10, Diet and Exercise, DE: n = 10). Participants included in this study were matched for age, sex, and BMI (Table 7.1). Race and ethnicity were not provided for this study, thus were not assessed.

Table 7.1. Participant information for each intervention type. Baseline BMI and age are detailed by group and broken down by sex. Data are presented as mean ± standard deviation from the mean.

	Exercise (E)	Diet (D)	Diet & Exercise (D+E)
BMI	33.14 ± 2.03	33.39 ± 2.20	32.93 ± 2.83
BMI Female	32.75 ± 2.52	32.75 ± 2.52	33.75 ± 3.27
BMI Male	33.53 ± 1.58	34.02 ± 1.89	32.12 ± 2.37
Age	65.99 ± 4.21	65.78 ± 4.34	65.89 ± 1.79
Age Female	65.80 ± 5.26	65.80 ± 5.26	65.65 ± 0.62
Age Male	66.19 ± 3.50	65.76 ± 3.86	66.11 ± 2.59

The IDEA trial was conducted at Wake Forest University and Wake Forest School of Medicine between July 2006 and November 2011. This trial was a single-blind, 18-month,

randomized controlled trial to determine whether a ≥10% loss in body weight induced by different intervention types would improve primary (e.g., knee joint compression forces and IL-6 levels) and secondary clinical outcomes (e.g., pain, function, mobility). Participants (n=454) were assigned to one of three interventions: diet (D), exercise (E), or diet and exercise (D+E). Additional details about intervention types, radiographic measurements, participant inclusion criteria, and study design are provided in the initial study reports[3, 4].

Diet parameters for D and D+E participants included up to 2 meal-replacement shakes per day, and a third meal selected from a weekly menu plan composed of traditional foods within 500-760 kcals each. Participants were allowed to have snacks (snack bar, fruit, or vegetables) that were 100-120 kcal each. All meal plans were developed and overseen by staff to assure macronutrient-balanced energy intake. Exercise parameters included three sixty-minute sessions per week for 18 months. For the first six months, the sixty-minute sessions were center-based and consisted of an aerobic phase (i.e., walking) for 15-minutes, a strength training phase for 20-minutes, another aerobic phase, and a cool-down phase for 10-minutes. For the remainder of the study, participants had the option of continuing to exercise at the center, transitioning to a home-based exercise routine, or using a combination of center and home-based exercise[3].

Serum Sampling, Extraction, and Metabolite Profiling

Blood samples were collected from participants following a 10-hour fast at three different time points: baseline, 6-months, and 18-months[204]. At each time point, samples were collected, and serum was stored at -80°C until extraction. To extract serum metabolites, 100 uL aliquots were centrifuged at 500xg for 5 minutes to remove cells and debris. Next, supernatant was transferred to a fresh mass-spectrometry grade microcentrifuge tube, 500 uL of cold acetone were added,

samples were vortexed vigorously, and chilled overnight at -80°C to precipitate proteins. The following day, serum samples were vortexed again, centrifuged at 16,100xg for 10 minutes, and supernatant was evaporated by vacuum concentration. Once dry, metabolites were resuspended with 1:1 acetonitrile:water.

The extracted serum samples (n=90) were analyzed using liquid chromatography-mass spectrometry (LC-MS). Samples were analyzed in positive mode using an Agilent 1290 LC coupled through an electrospray ionization source to an Agilent Quadrupole Time of Flight (Q-TOF) mass spectrometer. Ions were separated using a Cogent Diamond Hydride HILIC chromatography column (2.2 µM, 120 Å, 150 mm x 2.1 mm, MicroSolv Leland, NC, United States) at a flow rate of 0.400 uL/min. For quality control purposes, the order of sample injection was randomized, 5 uL of each sample was injected, and blank samples containing neat 1:1 acetonitrile:water were injected every 10 samples.

LC-MS data consisted of mass-to-charge ratios (m/z), metabolite abundances, and retention times which were processed using Agilent Masshunter Qualitative Analysis software and MSConvert[18]. Data were then exported and converted using XCMS[19]. Using in-house standardized procedures[20], MetaboAnalyst (version 5.0) was used to perform a suite of statistical analyses to visualize data and distinguish subsets of metabolite features. These included: hierarchical clustering analysis (HCA), principal component analysis (PCA), Partial Least Squares-Discriminant Analysis (PLS-DA), ANOVA, volcano plot analysis, fold change, and student's t-tests. Additionally, fold change, volcano plot, and median intensity heatmap analyses were used to find metabolite features that are co-regulated and dysregulated between groups. Populations of metabolites distinguished by these three analyses underwent pathway enrichment analyses using

the Mummichog algorithm within MetaboAnalyst to map clusters of key metabolites to cellular pathways. Significance was determined using FDR-corrected p-values with an *a priori* threshold of $p < 0.05$.

Metabolite Identification through Pooled Analysis

Additionally, 10 pooled samples were created by combining original extracts. For each pool, 10 uL from 5 randomly selected participant samples were combined. This process was repeated for all pools (n = 10). Pooled samples were then subjected to liquid chromatography tandem mass spectrometry (LC-MS/MS) for metabolite identification purposes. Pooled samples were injected and analyzed using an Acquity UPLC Plus coupled through an electrospray ionization source to a Waters Synapt XS. Like serum samples, ions were separated using a Cogent Diamond Hydride HILIC chromatography column (2.2 µM, 120 Å, 150 mm x 2.1 mm, MicroSolv Leland, NC, United States) at a flow rate of 0.400 uL/min.

Pooled LC-MS/MS data were analyzed using Progenesis QI (Nonlinear Dynamics, Newcastle, UK, version 3.0). Data were imported, peaks were determined, and spectra were aligned. Next, acquired parent and daughter fragments were compared against theoretical fragmentation patterns using the Human Metabolome Database[21] for metabolite identification. We defined successful metabolite identifications as those with a Progenesis score greater than 60/100 and a fragmentation score > 20. The properties that contribute to these scores include mass error, isotope distribution similarity, and retention time error. Parts per million (ppm) error was calculated between LC-MS and LC-MS/MS data, and those with a ppm error greater than 20 were not considered.

Results

Changes in BMI and Weight After 18-months of Intensive Weight Loss Interventions

Both changes in weight and BMI over 18 months were calculated for all participants selected for this analysis (n=30, n=10 per intervention). At baseline, 96.7% of participants selected for metabolomics had a BMI of 30 or greater. At 18 months, 62.5% of D+E participants, 40.0% of D participants, and 22.2% of E participants had a BMI less than 30. Considering weight loss, D+E (↓11.8%, $p = 0.012$) and D (↓9.4%, $p = 0.0075$) participants lost more weight than the E group (↓3.9%, $p = 0.2973$) (Supplemental Table 7.1)[3, 4].

Weight loss and BMI measures for participant selected for this analysis were representation of the overall IDEA population (n=454)[4]. Beyond the average weight loss per group, the amount of weight loss independent of group assignment was examined. Specifically, ranges of weight loss were categorized into 0-5%, 5-10%, 10%+ and weight gained and was determined to not influence metabolic results. However, sample size may limit conclusions and requires investigation among a larger subset of IDEA participants. Of the participants selected for this analysis, one E participant had a net weight loss of zero, and one participant from the D and D+E groups gained weight over 18 months. Weight loss data was not available for four participants in the randomly selected participants for this analysis (Supplemental Table 7.1).

Weight Loss Interventions Differentially Influence the Serum Metabolome Over 18-Months

To examine variations in metabolism over the course of the 18-month period in response to three interventions – D, E, D+E – we calculated the changes between pre-trial and 18-month metabolite feature intensities, termed delta change (e.g., for each co-detected metabolite we subtracted the pre-trial intensity from the intensity at 18 months on a per-participant basis). The calculated delta change values were used for analysis throughout this study, for both intervention- and sex-associated differences. Across all intervention groups 2,142 unique metabolite features were co-detected. PCA and PLS-DA were used to analyze global metabolic differences in the calculated delta change values across the three intervention groups: diet (D), exercise (E), and combined diet and exercise (D+E).

PCA displays some overlap between groups with principal components (PC) 1 and 2 representing 32.3% of the total variability between groups (Fig. 7.1 A). PLS-DA shows greater separation and minimal overlap of groups with components 1 and 2 accounting for 5.2% and 12% of the variability, respectively (Fig. 7.1 B), suggesting that changes in metabolism reflect intervention type. A median metabolite intensity heatmap was used to perform additional analysis on the metabolite features with the 25 highest VIP scores (Fig. 7. 1 C). VIP scores are calculated by summing the squared correlations between PLS-DA components and the original value and the metabolite feature. Of these 25 metabolites, 11 were more abundant in D participants, whereas 13 were more abundant in E participants and 1 was more abundant in D+E participants. Interestingly, the metabolite feature intensities in the D+E group overlap with those detected in the D and E group. The heatmap analysis of the top 25 VIP metabolite features demonstrated substantial metabolic differences between intervention types (Fig. 7.1 C) .

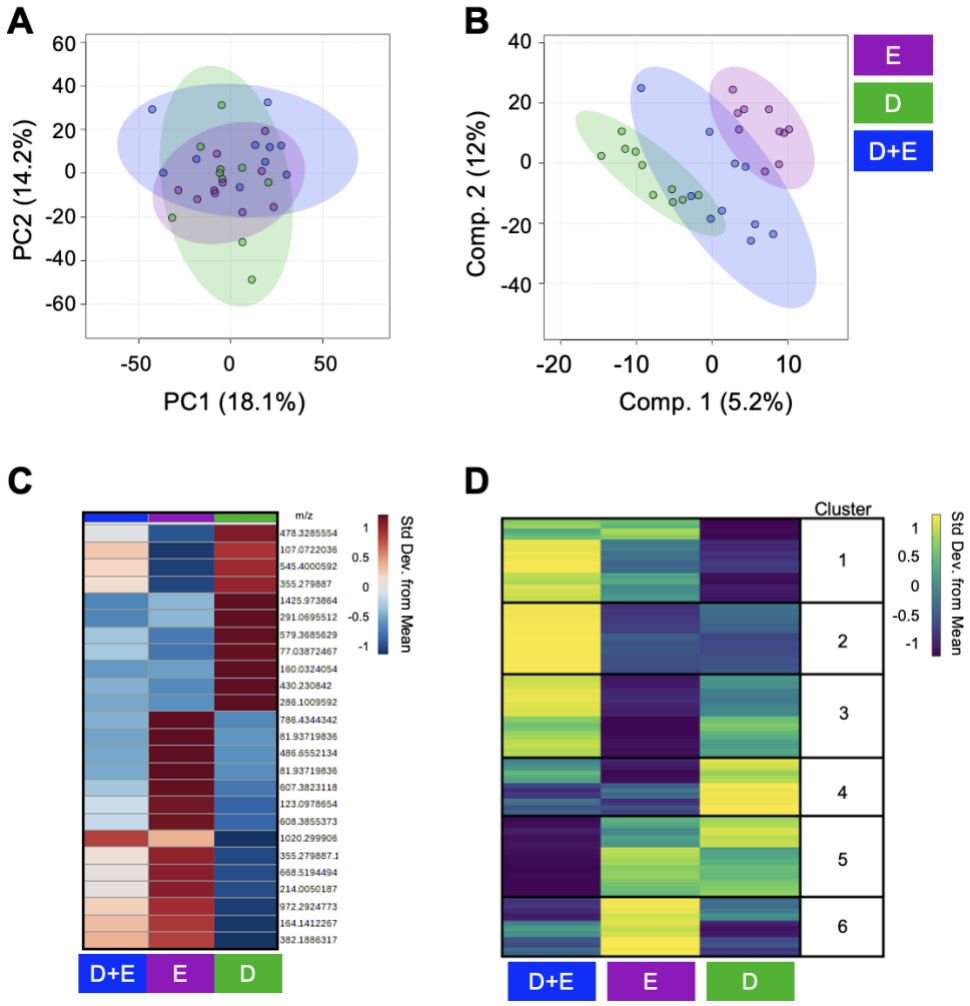

Fig. 7.1. Metabolomic profiles differ between intervention groups after 18-months. (A) Principal component analysis (PCA), an unsupervised multivariate test, displays overlap of intervention groups in 2D, whereas (B) Partial least squares-discriminant analysis (PLS-DA), a supervised multivariate test, displays less overlap of interventions suggesting that the metabolome of participants assigned to different intervention groups for 18-months are distinct from each other. (C) A group median heatmap analysis of the top 25 PLS-DA Variable in Importance Projection (VIP) Scores, visualized using hierarchical clustering, highlights that exposure to 18-months of different interventions are associated with distinct metabolic regulation patterns. (D) Clusters of coregulated metabolite features (1-6) derived from participants serum across interventions underwent pathway enrichment analysis revealing distinct metabolic patterns that are associated with intervention type. Cooler colors (blue) and warmer colors (yellow) indicate lower and higher metabolite intensities relative to the mean. Colors in A-D correspond to: green – diet (D); purple – exercise (E); blue – diet and exercise (D+E).

To assess pathways affected by these interventions, we performed functional pathway enrichment analysis. First, we created a median metabolite intensity heatmap using delta values to distinguish clusters of similarly or differentially regulated metabolites on a global scale (Fig. 7.1 D). These clusters were analyzed using MetaboAnalyst's Functional Analysis feature to underpin any significant pathways (false discovery rate adjusted p-values ≤ 0.05). Metabolite features highest in abundance among D+E participants and lowest in D participants mapped to xenobiotics metabolism, R-group synthesis, various fatty acid metabolisms, vitamin E metabolism, carnitine shuttle-related metabolism, and cytochrome P450 metabolism. Comparatively, metabolite features highest in D+E participants and lowest in both D and E groups mapped to di-unsaturated fatty acid beta-oxidation, linoleate metabolism, dynorphin metabolism, glycerophospholipid biosynthesis and metabolism, and squalene and cholesterol biosynthesis. Features highest in D+E participants and lowest in the E participants mapped to polyunsaturated fatty acid biosynthesis, glycerophospholipid metabolism, biopterin metabolism, alkaloid biosynthesis, and fatty acid activation and oxidation.

Metabolite features highest in abundance among D participants and lowest in both the D+E and E participants mapped to metabolism of vitamin metabolism (B6, C), carbohydrate and sugar metabolism (hexose, starch, sucrose, fructose, mannose), lipid-related pathways (glycerophospholipid, glycosphingolipid, omega-6), N-glycan biosynthesis and degradation, as well as pathways related to energy metabolism (pentose phosphate, glycolysis, gluconeogenesis). Metabolites features highest in abundance among E participants and lowest in D+E and D groups mapped to amino group metabolism (glutamate, histidine, methionine, cysteine, tryptophan, alanine, and aspartate), nitrogen metabolism, purine metabolism, vitamin B3 metabolism, and

metabolisms involved with the formation of putative anti-inflammatory metabolites from eicosapentaenoic acid. Finally, metabolites highest in both E and D groups and lowest in D+E participants mapped to various amino group metabolisms (glycine, serine, threonine, arginine, proline, alanine, aspartate, lysine, and asparagine), N-glycan degradation, urea cycle, butanoate metabolism, chondroitin sulfate degradation, keratan sulfate degradation, heparan sulfate degradation, and cytochrome P450 metabolism (Table 7.2).

Table 7.2. Metabolic pathways associated with diet, exercise, and diet plus exercise interventions identified by median metabolite intensity heatmap analysis. All reported pathways have a FDR-corrected significance level < 0.05. D = diet. E = exercise. DE = diet and exercise. Clusters defined in Fig. 7.1 D.

Cluster	Highest	Lowest	Pathway
1	D+E	D	Xenobiotics metabolism
1	D+E	D	R Group Synthesis
1	D+E	D	Fatty acid oxidation, peroxisome
1	D+E	D	Fatty acid oxidation
1	D+E	D	Fatty acid activation
1	D+E	D	Vitamin E metabolism
1	D+E	D	D+E novo fatty acid biosynthesis
1	D+E	D	Omega-6 fatty acid metabolism
1	D+E	D	Carnitine shuttle
1	D+E	D	Drug metabolism - cytochrome P450
2	D+E	D, E	Di-unsaturated fatty acid beta-oxidation
2	D+E	D, E	Linoleate metabolism
2	D+E	D, E	Dynorphin metabolism
2	D+E	D, E	Glycerophospholipid metabolism
2	D+E	D, E	Squalene and cholesterol biosynthesis
2	D+E	D, E	Glycosphingolipid biosynthesis - ganglioseries
3	D+E	E	Polyunsaturated fatty acid biosynthesis
3	D+E	E	Glycerophospholipid metabolism
3	D+E	E	Biopterin metabolism
3	D+E	E	Alkaloid biosynthesis II
3	D+E	E	Fatty acid oxidation
3	D+E	E	Fatty acid activation
4	D	D+E, E	Phosphatidylinositol phosphate metabolism
4	D	D+E, E	Propanoate metabolism
4	D	D+E, E	Vitamin B6 (pyridoxine) metabolism
4	D	D+E, E	Glycolysis and Gluconeogenesis
4	D	D+E, E	Tryptophan metabolism
4	D	D+E, E	N-Glycan biosynthesis
4	D	D+E, E	Starch and Sucrose Metabolism
4	D	D+E, E	Mono-unsaturated fatty acid beta-oxidation
4	D	D+E, E	Ascorbate (Vitamin C) and Aldarate Metabolism
4	D	D+E, E	Lipoate metabolism
4	D	D+E, E	Purine metabolism
4	D	D+E, E	Fructose and mannose metabolism
4	D	D+E, E	Hexose phosphorylation
4	D	D+E, E	Vitamin H (biotin) metabolism
4	D	D+E, E	Biopterin metabolism
4	D	D+E, E	Caffeine metabolism
4	D	D+E, E	Glycerophospholipid metabolism
4	D	D+E, E	Pentose phosphate pathway
4	D	D+E, E	Glycosphingolipid metabolism
4	D	D+E, E	Pyrimidine metabolism
4	D	D+E, E	Galactose metabolism
4	D	D+E, E	Glycosphingolipid biosynthesis - globoseries
4	D	D+E, E	Porphyrin metabolism
4	D	D+E, E	N-Glycan D+Egradation
4	D	D+E, E	Omega-6 fatty acid metabolism
5	E, D	D+E	Urea cycle/amino group metabolism
5	E, D	D+E	Glycine, serine, alanine and threonine metabolism
5	E, D	D+E	Drug metabolism - cytochrome P450
5	E, D	D+E	Arginine and Proline Metabolism
5	E, D	D+E	Butanoate metabolism
5	E, D	D+E	Lysine metabolism
5	E, D	D+E	Drug metabolism - other enzymes
5	E, D	D+E	N-Glycan D+Egradation
5	E, D	D+E	Chondroitin sulfate D+Egradation
5	E, D	D+E	Keratan sulfate D+Egradation
5	E, D	D+E	Heparan sulfate D+Egradation
5	E, D	D+E	Beta-Alanine metabolism
5	E, D	D+E	Alanine and Aspartate Metabolism
5	E, D	D+E	Aspartate and asparagine metabolism
6	E	D+E, D	Glutamate metabolism
6	E	D+E, D	Glutathione Metabolism
6	E	D+E, D	Putative anti-Inflammatory metabolites formation from EPA
6	E	D+E, D	Nitrogen metabolism
6	E	D+E, D	Histidine metabolism
6	E	D+E, D	Biopterin metabolism
6	E	D+E, D	Pyrimidine metabolism
6	E	D+E, D	Methionine and cysteine metabolism
6	E	D+E, D	Tryptophan metabolism
6	E	D+E, D	Purine metabolism
6	E	D+E, D	Vitamin B3 (nicotinate and nicotinamiD+E) metabolism
6	E	D+E, D	Alanine and Aspartate Metabolism

Additionally, pairwise comparisons using delta change values between the three intervention groups were performed to further investigate how weight loss interventions differentially influence OA metabolism (Supplemental Fig. 7.2, Supplemental Table 7.2). Specifically, PCA and PLS-DA were used to visualize the metabolomes of participants and is detailed in Supplemental results. Populations of metabolite features distinguished by fold change when comparing intervention groups underwent pathway analyses. Pathways associated with both D+E and E groups included N-glycan biosynthesis and ubiquinone and other terpenoid-quinone biosynthesis. All other overlapping pathways were associated with both D and E participants which included aminoacyl-tRNA biosynthesis, cytochrome P450 metabolism, purine metabolism, and glutathione metabolism. No significant pathways were associated exclusively with either the D or E participants (Supplemental Table 7.3). Additionally, populations of metabolite features distinguished by fold change when comparing intervention groups were matched against metabolite identifications made using LC-MS/MS data. Many of these were detected across comparisons and displayed diverse regulation patterns (Supplemental Table 7.4). Altogether, the results show that different weight loss interventions influence OA metabolism in distinct ways.

Serum Metabolome is Affected by Sex After 18-Months of Intervention

To examine potential sexual dimorphism within the serum metabolome, PCA, PLS-DA, fold change, and volcano plot analyses were used to compare male and female participants, both in general and within intervention groups. PCA comparison of all male and female participants finds overlap with principal components 1 and 2 accounting for more than 30% of the variability in the dataset. PLS-DA reveals distinct endotypes based on sex, with components 1 and 2 accounting for 19.6% of the variability (Fig. 7. 2 A-B). Fold change revealed that 283 metabolites

had a greater change (FC>2) in abundance during the 18-month period in female participants than in male participants, mapping to glycolysis/gluconeogenesis, ubiquinone and other terpenoid-quinone biosynthesis, various amino acid metabolisms, and metabolism of starch and sucrose. Comparatively, 345 features had a greater change in abundance during the 18-month period in male participants than female participants, and these metabolites mapped to purine metabolism (Fig. 7.2 C, Supplemental Table 7.5).

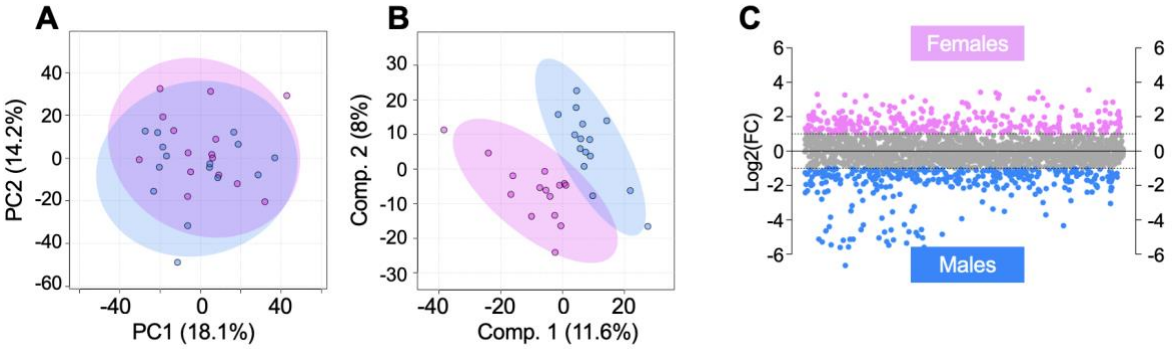

Fig. 7.2. Serum metabolome of all IDEA participants, excluding the factor of intervention, is influenced by participant sex. (A) While PCA displays overlapping of male and female IDEA participants, (B) PLS-DA improves clustering of participants within their respective sex group suggesting the serum metabolome is sexually dimorphic. (C) Fold change analysis was conducted to pinpoint populations of metabolite features that are differentially regulated between males and females. This revealed 283 metabolite features that had a FC > 2 and were higher in abundance in female participants, whereas 345 had a FC < -2 and were higher in abundance in male participants. The colors in A-C correspond to: pink – females; blue – males.

Likewise, a pairwise comparison was conducted between male and female D+E participants. PCA finds some overlap of male and female participants, with PCs 1 and 2 accounting for 47.3% of the total variability (Fig. 7.3 A). PLS-DA, however, finds complete separation of participants based on sex with components 1 and 2 representing 26% of the variability (Fig. 7. 3 B). Among female participants, 586 metabolites had at least a 2-fold greater change in abundance during the 18-month period than they did in male participants. These metabolites mapped to

tryptophan metabolism, glycosaminoglycan degradation, biosynthesis of unsaturated fatty acids, and caffeine metabolism. 532 features had at least a 2-fold increase in male participants. These mapped to aminoacyl-tRNA biosynthesis, lysine degradation, various amino acid metabolisms, and glutathione metabolism (Fig. 7.3 C, Supplemental Table 7.5).

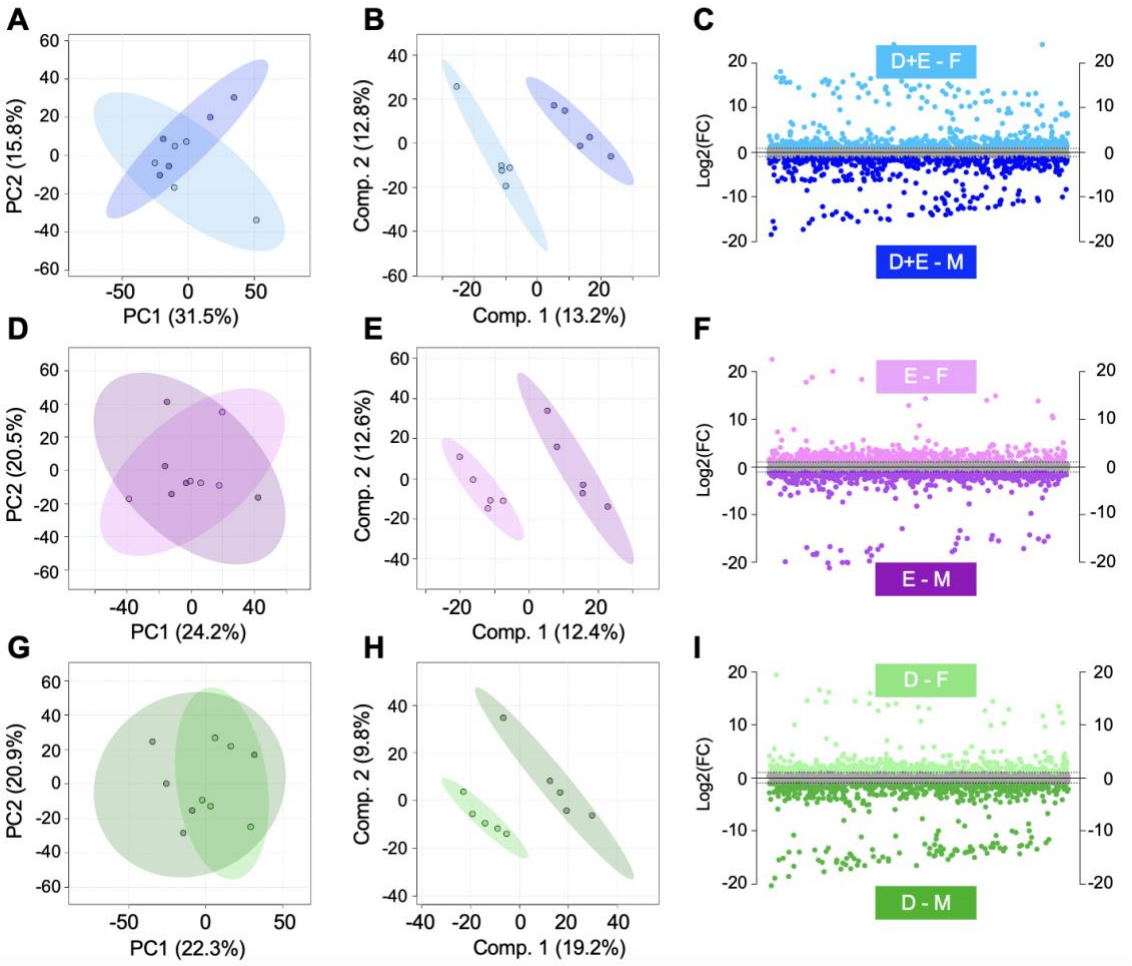

Fig. 7.3. Global analysis of intervention groups after 18-months reveals that the serum metabolome is influenced by sex. (A) PCA displayed some overlap of D+E males and females whereas (B) PLS-DA perfectly separated D+E males and females suggesting that the serum metabolome is potentially influenced by participant sex. (C) Fold change analysis identified 568 metabolite features that had a FC > 2 and were higher in abundance in D+E females. Conversely, 532 had a FC < -2 and were higher in abundance in D+E males. Similarly (D) PCA, (E) PLS-DA, and (F) fold change was applied and revealed a similar sexual dimorphic pattern when comparing male and female E participants. This same suite of analyses was applied to examine sex-associated metabolic patterns between male and female D participants (G-I). Populations of metabolite features distinguished by fold change analyses were then subjected to functional pathway enrichment analyses to pinpoint biological pathways. Considering differences in metabolic regulation associated with sex across D+E (A-C), E (D-F) and E (G-I) participants, it is evident that that serum metabolome of IDEA participants is influenced by sex. The colors in A-I correspond to: light and dark blue – female and male diet and exercise (D+E) participants; light and dark purple – female and male exercise (E) participants; light and dark green– female and male diet participants.

Among E participants, PCA shows some overlap between male and female participants, with PCs 1 and 2 accounting for 44.7% of the total variability (Fig. 7.3 D). PLS-DA shows complete separation of groups with components representing 25% of the variability (Fig. 7.3 E). Among female participants, 433 metabolites had a 2-fold or greater change in abundance than they did in male participants, mapping to caffeine metabolism. 617 metabolite features had a greater change in male participants compared to female participants, mapping valine, leucine, and isoleucine biosynthesis (Fig. 7.3 F, Supplemental Table 7.5).

Finally, in D participants, PCA shows overlap between male and female participants, with the first two PCs accounting for 43.2% of variability in the dataset (Fig. 7.3 G). PLS-DA shows complete separation of groups with components representing 29% of the variability (Fig. 7.3 H). Additionally, 524 metabolites had a 2-fold or greater change in abundance in female participants than they did in male participants. These mapped to aminoacyl-tRNA biosynthesis, and valine, leucine, and isoleucine biosynthesis. 632 features had a greater change in male participants, mapping to purine metabolism (Fig. 7.3 I, Supplemental Table 7.5).

Populations distinguished through fold change analyses assessing sexual dimorphism across intervention groups (Fig. 7.3) were matched against LC-MS/MS identified metabolites. Notably, many of these identified metabolites were statistically significant across pairwise comparisons between interventions and were sex-associated. Of these, docasanedioic acid showcased consistently higher abundance patterns in all female participants within each intervention groups. Excluding D male and female participants, stearoylcarnitine was higher in abundance in female participants when comparing metabolic patterns associated with sex within the E and D+E groups. Strikingly, N-acetyldemethylphosphoinothricin was detected when

investigating both intervention- and sex-associated differences. Specifically, it was higher in male participants when examining sex differences within intervention groups. However, when considering interventions only, it was the highest among D participants compared to E and D+E participants (Supplemental Table 7.4). In summation, the data vividly illustrates the striking divergence in serum metabolism between male and female participants subjected to different weight loss interventions.

Discussion

This metabolomics study, in conjunction with the IDEA trial, demonstrates that intensive weight loss intervention, including diet and combined diet and exercise, influences the metabolome of OA patients differently from exercise. When comparing participants after 18-months of different weight loss interventions, changes in energy, vitamin, carbohydrate, amino acid, and lipid metabolism were detected. Moreover, these data demonstrate clear metabolic differentiation between IDEA participants based on participant sex. Overall, intensive weight loss and exercise influence the serum metabolome of OA individuals, and sex may independently influence the nature of metabolic changes in OA. The integration of the present metabolomic profiles with the previously reported IDEA study outcomes[4, 17] enhances the understanding of the effects of dietary weight loss and exercise in individuals with OA and provides insights into intervention effectiveness and potential biomarker identification.

Previously, NMR metabolomics was used to assess urine from IDEA participants finding detected metabolites corresponding to energy, amino acid, and lipid metabolisms. The present study detected similar metabolic themes in serum extracts across intervention groups. D+E participants exhibited elevated lipid-related pathways such as the carnitine shuttle compared to

both D and E participants (Table 2). Notably, the carnitine shuttle's primary function is facilitating transport of fatty acids into the mitochondria for ATP generation via beta-oxidation. A prior study finds that short-term consumption of a high fat diet increases levels of circulating fatty acids and carnitines[22]. Specific to OA, higher concentrations of carnitines are observed in synovium from end-stage knee OA patients[23]. Additionally, L-carnitine supplementation is a potential treatment to mitigate OA-related inflammation and oxidative stress[24, 25].

D+E participants also displayed changes in other noteworthy lipid-related pathways such as polyunsaturated fatty acid (PUFA) biosynthesis, omega-6 fatty acid metabolism, linoleate metabolism, and glycerophospholipid metabolism after 18-months of intervention. Omega-3 and -6 fatty acids, as well as linoleic acid, a polyunsaturated omega-6, have all been implicated in the pathogenesis of OA[26, 27]. Glycosphingolipids, a key membrane component, have been previously linked to exercise, obesity, metabolic syndrome, and insulin resistance[28-30]. Dysregulation of membrane-related pathways may stem from exercise intervention (E and D+E participants), requiring further investigation. These findings suggest that the combination of diet and exercise act on pathways like the carnitine shuttle, PUFA, and glycosphingolipid metabolism to impact fat utilization for energy, oxidative, and inflammatory functions.

D participants had elevated glycolysis, pentose phosphate pathway, purine and pyrimidine metabolism, and various sugar and vitamin metabolisms compared to E and D+E participants (Table 2). Glycolysis and the pentose phosphate pathway play central roles in central energy metabolism as well as production of nucleotides and amino acid precursors, oxidative stress reduction, and ATP generation. Disruptions in these pathways can lead to insufficient ATP, NADH

accumulation, inflammation, generation of reactive oxygen species, and altered rates of gluconeogenesis.

Carbohydrate pathways like starch and sucrose metabolism are linked to central energy metabolism, possibly serving as biofuels for ATP production. Notable related pathways are hexose phosphorylation and vitamin C metabolism which were both detected among D participants. Vitamin C is a hexose derivative from glucose that has antioxidant capabilities and serves as a defense against reactive oxygen species, is critical for collagen synthesis by enhancing pro-collagen hydroxylation and has been hypothesized to have a protective role in OA[25, 31, 32]. Moreover, a study that investigated the association between vitamin C and knee OA found that low intake of vitamin C is a potential risk factor for knee OA[32]. However, neither vitamin intake nor serum concentration was measured in this study. Additionally, likely variability in participant meal and snack choices warrants further investigation to understand the relationship between vitamin and carbohydrate metabolism, diet intervention, and OA.

Exercise is a common treatment for improving symptoms of obesity and related conditions such as cardiovascular disease, type II diabetes, and OA[33, 34]. Additionally, the anti-inflammatory effects of exercise have been well documented[35-37]. This could explain the detection of increased putative anti-inflammatory and amino acid pathways including glutamate, histidine, alanine, aspartate, methionine, cysteine, and glutathione metabolism across E participants compared to D+E and D participants. Thus, the finding that these pathways were highest in E participants and detected in lower abundances in both D and D+E participants suggests that these metabolic changes are as a result of the diet. Notably, cysteine and glutamate are essential to produce glutathione, a key antioxidant that helps scavenge reactive oxygen species produced during

normal cell metabolism and has been hypothesized to play a key role in the inflammatory response in OA[38]. Oxidative status, as reflected by the ratio of cysteine, glycine, and glutamate, tends to decrease with age, thereby increasing stress and cell death in chondrocytes[39]. Therefore, detection of glutathione, cysteine, and glutamate metabolism may reflect oxidative stress resistance in the presence of exercise. Moreover, amino acids like alanine, aspartate, and glutamate have been previously associated with OA and have been detected in higher concentrations among OA patients[40]. Histidine concentration distinguishes between the synovial fluid of OA and RA patients[41] and decreases as OA progresses[42]. Taken together, these findings suggest that metabolism of these amino acids may undergo significant changes in response to exercise in OA patients, suggesting amino acids could potentially be monitored overtime to oversee OA development. Moreover, additional research is needed to better understand the relationship between amino acid metabolism, weight loss interventions, and OA.

While it is recognized that knee OA is more common and often more severe in female patients[5, 6], metabolic differences associated with knee OA that differ by sex remain uncertain. An increasing number of studies find sexual dimorphism in the context of OA and contribute mounting evidence indicating that the etiology and progression of OA may exhibit sex-specific changes as shown in these data. Divergent pathways between male and female IDEA participants mapped to glycolysis/gluconeogenesis, amino acid metabolism, and lipid-related metabolisms (Supplemental Table 5).

Sex-dependent differences in bone size and angle and pelvis and joint size are well documented[43, 44]. At the hormonal level, females have greater circulating levels of estrogen with levels fluctuating throughout the menstrual cycle and post-menopause. Thus, it is not surprising

that these varying hormone levels appear to influence the serum metabolome. Both E and D+E female participants had elevated caffeine metabolism compared to male participants. For pre- and post-menopausal women, hormonal cycles may affect amino acid metabolism where protein oxidation is impacted by estrogen levels[45]. Understanding these sex-related metabolic differences could refine current OA prevention and treatment strategies.

Limitations

This study is not without limitations. First, this study lacks serum from both healthy controls and individuals with OA who did not undergo an intervention. Second, serum-derived metabolomic data may reflect joint health and provide insight into the effects of intervention and sex. However, the relationship between serum and synovial fluid is complex with many metabolites correlated between these compartments but many more metabolites without correlations[76, 183]. As such, the relationship between joint health and the serum metabolomic requires further investigation. A third limitation is the relatively small samples size of 10 individuals per intervention group which was necessitated by the time and cost of performing an extensive metabolomics analysis.

Conclusions

The outcomes of this comprehensive metabolomics investigation, in conjunction with the overarching findings of the IDEA study, emphasize that intensive weight loss has symptomatic and potential metabolic benefits among individuals with knee OA. Metabolic perturbations associated with these interventions, as well as patient sex, likely play a role in OA development and should be considered for downstream treatment strategies. By further applying metabolomics

in parallel with these findings a greater understanding of the joint-level dysregulation during OA progression may shed light on the impacts of obesity, weight reduction, patient treatments, and interventions. Expansion with larger sample sizes will delve into the associations between other measurements obtained throughout the duration of the IDEA study and metabolomic results among all study participants. These insights hold promise for enhancing the current approach to managing and improving the quality of life of those affected by OA.

Acknowledgements

We thank the Montana State University Mass Spectrometry Facility including Dr. Donald Smith and Jesse Thomas for aiding in LC-MS analysis and interpretation. Funding for the Montana State University Mass Spectrometry Facility was made possible through the M.J. Murdock Charitable Trust, the National Institute of General Medical Sciences of the National Institutes of Health (P20GM103474 and S10OD28650). Additionally, authors thank Brady Hislop for his assistance in developing analysis pipelines and analyzing data. This study was supported by grants from the National Institutes of Health (NIAMS R01AR073964 and R01AR081489) and the National Science Foundation (CMMI 1554708).

Abbreviations List

OA = osteoarthritis; IDEA = Intensive Diet and Exercise for Arthritis; NMR = nuclear magnetic resonance; D = diet; E = exercise, D+E = diet and exercise; LC-MS = liquid chromatography-mass spectrometry; LC-MS/MS = liquid chromatography tandem mass spectrometry; m/z = mass-to-charge ratio; HCA = hierarchical clustering analysis; PCA = principal component analysis; PLS-DA = partial least squares-discriminant analysis; PUFA = polyunsaturated fatty acid

References

1. Neogi T. The epidemiology and impact of pain in osteoarthritis. Osteoarthritis Cartilage 2013; 21: 1145-1153.

2. Bitton R. The economic burden of osteoarthritis. Am J Manag Care 2009; 15: S230-235.

3. Messier SP, Legault C, Mihalko S, Miller GD, Loeser RF, DeVita P, et al. The Intensive Diet and Exercise for Arthritis (IDEA) trial: design and rationale. BMC Musculoskelet Disord 2009; 10: 93.

4. Messier SP, Mihalko SL, Legault C, Miller GD, Nicklas BJ, DeVita P, et al. Effects of intensive diet and exercise on knee joint loads, inflammation, and clinical outcomes among overweight and obese adults with knee osteoarthritis: the IDEA randomized clinical trial. JAMA 2013; 310: 1263-1273.

5. Blaker CL, Ashton DM, Doran N, Little CB, Clarke EC. Sex- and injury-based differences in knee biomechanics in mouse models of post-traumatic osteoarthritis. J Biomech 2021; 114: 110152.

6. Srikanth VK, Fryer JL, Zhai G, Winzenberg TM, Hosmer D, Jones G. A meta-analysis of sex differences prevalence, incidence and severity of osteoarthritis. Osteoarthritis Cartilage 2005; 13: 769-781.

7. Loughlin J. Familial inheritance of osteoarthritis: documented family subsets. Clin Orthop Relat Res 2004: S22-25.

8. O'Connor MI. Sex differences in osteoarthritis of the hip and knee. J Am Acad Orthop Surg 2007; 15 Suppl 1: S22-25.

9. Carlson AK, Rawle RA, Wallace CW, Adams E, Greenwood MC, Bothner B, et al. Global metabolomic profiling of human synovial fluid for rheumatoid arthritis biomarkers. Clin Exp Rheumatol 2019; 37: 393-399.

10. Carlson AK, Rawle RA, Wallace CW, Brooks EG, Adams E, Greenwood MC, et al. Characterization of synovial fluid metabolomic phenotypes of cartilage morphological changes associated with osteoarthritis. Osteoarthritis Cartilage 2019; 27: 1174-1184.

11. Hugle T, Kovacs H, Heijnen IA, Daikeler T, Baisch U, Hicks JM, et al. Synovial fluid metabolomics in different forms of arthritis assessed by nuclear magnetic resonance spectroscopy. Clin Exp Rheumatol 2012; 30: 240-245.

12. Kim S, Hwang J, Kim J, Ahn JK, Cha HS, Kim KH. Metabolite profiles of synovial fluid change with the radiographic severity of knee osteoarthritis. Joint Bone Spine 2017; 84: 605-610.

13. Zhang W, Likhodii S, Zhang Y, Aref-Eshghi E, Harper PE, Randell E, et al. Classification of osteoarthritis phenotypes by metabolomics analysis. BMJ Open 2014; 4: e006286.

14. Jutila AA, Zignego DL, Hwang BK, Hilmer JK, Hamerly T, Minor CA, et al. Candidate mediators of chondrocyte mechanotransduction via targeted and untargeted metabolomic measurements. Arch Biochem Biophys 2014; 545: 116-123.

15. Salinas D, Mumey BM, June RK. Physiological dynamic compression regulates central energy metabolism in primary human chondrocytes. Biomech Model Mechanobiol 2019; 18: 69-77.

16. Zignego DL, Hilmer JK, June RK. Mechanotransduction in primary human osteoarthritic chondrocytes is mediated by metabolism of energy, lipids, and amino acids. J Biomech 2015; 48: 4253-4261.

17. Loeser RF, Pathmasiri W, Sumner SJ, McRitchie S, Beavers D, Saxena P, et al. Association of urinary metabolites with radiographic progression of knee osteoarthritis in overweight and obese adults: an exploratory study. Osteoarthritis Cartilage 2016; 24: 1479-1486.

18. Kessner D, Chambers M, Burke R, Agus D, Mallick P. ProteoWizard: open source software for rapid proteomics tools development. Bioinformatics 2008; 24: 2534-2536.

19. Smith CA, Want EJ, O'Maille G, Abagyan R, Siuzdak G. XCMS: processing mass spectrometry data for metabolite profiling using nonlinear peak alignment, matching, and identification. Anal Chem 2006; 78: 779-787.

20. Brahmachary PP, Welhaven HD, June RK. Metabolomic Profiling to Understand Chondrocyte Metabolism. Methods Mol Biol 2023; 2598: 141-156.

21. Wishart DS, Guo A, Oler E, Wang F, Anjum A, Peters H, et al. HMDB 5.0: the Human Metabolome Database for 2022. Nucleic Acids Res 2022; 50: D622-D631.

22. Moholdt T, Parr EB, Devlin BL, Debik J, Giskeodegard G, Hawley JA. The effect of morning vs evening exercise training on glycaemic control and serum metabolites in overweight/obese men: a randomised trial. Diabetologia 2021; 64: 2061-2076.

23. Adams SB, Jr., Setton LA, Kensicki E, Bolognesi MP, Toth AP, Nettles DL. Global metabolic profiling of human osteoarthritic synovium. Osteoarthritis Cartilage 2012; 20: 64-67.

24. Baghban F, Hosseinzadeh M, Mozaffari-Khosravi H, Dehghan A, Fallahzadeh H. The effect of L-Carnitine supplementation on clinical symptoms, C-reactive protein and malondialdehyde in obese women with knee osteoarthritis: a double blind randomized controlled trial. BMC Musculoskelet Disord 2021; 22: 195.

25. Malek Mahdavi A, Mahdavi R, Kolahi S. Effects of l-Carnitine Supplementation on Serum Inflammatory Factors and Matrix Metalloproteinase Enzymes in Females with Knee Osteoarthritis: A Randomized, Double-Blind, Placebo-Controlled Pilot Study. J Am Coll Nutr 2016; 35: 597-603.

26. Bastiaansen-Jenniskens YM, Siawash M, van de Lest CH, Verhaar JA, Kloppenburg M, Zuurmond AM, et al. Monounsaturated and Saturated, but Not n-6 Polyunsaturated Fatty Acids Decrease Cartilage Destruction under Inflammatory Conditions: A Preliminary Study. Cartilage 2013; 4: 321-328.

27. Oliviero F, Lo Nigro A, Bernardi D, Giunco S, Baldo G, Scanu A, et al. A comparative study of serum and synovial fluid lipoprotein levels in patients with various arthritides. Clin Chim Acta 2012; 413: 303-307.

28. Hla T, Dannenberg AJ. Sphingolipid signaling in metabolic disorders. Cell Metab 2012; 16: 420-434.

29. Holland WL, Brozinick JT, Wang LP, Hawkins ED, Sargent KM, Liu Y, et al. Inhibition of ceramide synthesis ameliorates glucocorticoid-, saturated-fat-, and obesity-induced insulin resistance. Cell Metab 2007; 5: 167-179.

30. Merrill AH, Jr. Sphingolipid and glycosphingolipid metabolic pathways in the era of sphingolipidomics. Chem Rev 2011; 111: 6387-6422.

31. Plotnikoff R, Karunamuni N, Lytvyak E, Penfold C, Schopflocher D, Imayama I, et al. Osteoarthritis prevalence and modifiable factors: a population study. BMC Public Health 2015; 15: 1195.

32. Sanghi D, Mishra A, Sharma AC, Raj S, Mishra R, Kumari R, et al. Elucidation of dietary risk factors in osteoarthritis knee-a case-control study. J Am Coll Nutr 2015; 34: 15-20.

33. Gleeson M, Bishop NC, Stensel DJ, Lindley MR, Mastana SS, Nimmo MA. The anti-inflammatory effects of exercise: mechanisms and implications for the prevention and treatment of disease. Nat Rev Immunol 2011; 11: 607-615.

34. Pedersen BK, Saltin B. Evidence for prescribing exercise as therapy in chronic disease. Scand J Med Sci Sports 2006; 16 Suppl 1: 3-63.

35. Cerqueira E, Marinho DA, Neiva HP, Lourenco O. Inflammatory Effects of High and Moderate Intensity Exercise-A Systematic Review. Front Physiol 2019; 10: 1550.

36. Petersen AM, Pedersen BK. The anti-inflammatory effect of exercise. J Appl Physiol (1985) 2005; 98: 1154-1162.

37. Walsh NP, Gleeson M, Shephard RJ, Gleeson M, Woods JA, Bishop NC, et al. Position statement. Part one: Immune function and exercise. Exerc Immunol Rev 2011; 17: 6-63.

38. Surapaneni KM, Venkataramana G. Status of lipid peroxidation, glutathione, ascorbic acid, vitamin E and antioxidant enzymes in patients with osteoarthritis. Indian J Med Sci 2007; 61: 9-14.

39. Carlo MD, Jr., Loeser RF. Increased oxidative stress with aging reduces chondrocyte survival: correlation with intracellular glutathione levels. Arthritis Rheum 2003; 48: 3419-3430.

40. Anderson JR, Chokesuwattanaskul S, Phelan MM, Welting TJM, Lian LY, Peffers MJ, et al. (1)H NMR Metabolomics Identifies Underlying Inflammatory Pathology in Osteoarthritis and Rheumatoid Arthritis Synovial Joints. J Proteome Res 2018; 17: 3780-3790.

41. Kim S, Hwang J, Kim J, Lee SH, Cheong YE, Lee S, et al. Metabolic discrimination of synovial fluid between rheumatoid arthritis and osteoarthritis using gas chromatography/time-of-flight mass spectrometry. Metabolomics 2022; 18: 48.

42. Zhang Q, Li H, Zhang Z, Yang F, Chen J. Serum metabolites as potential biomarkers for diagnosis of knee osteoarthritis. Dis Markers 2015; 2015: 684794.

43. Barnett SC, Murray MM, Flannery SW, Team BT, Menghini D, Fleming BC, et al. ACL Size, but Not Signal Intensity, Is Influenced by Sex, Body Size, and Knee Anatomy. Orthop J Sports Med 2021; 9: 23259671211063836.

44. Leong A. Sexual dimorphism of the pelvic architecture: a struggling response to destructive and parsimonious forces by natural & mate selection. Mcgill J Med 2006; 9: 61-66.

45. Wohlgemuth KJ, Arieta LR, Brewer GJ, Hoselton AL, Gould LM, Smith-Ryan AE. Sex differences and considerations for female specific nutritional strategies: a narrative review. J Int Soc Sports Nutr 2021; 18: 27.

46. Wallace CW, Hislop B, Hahn AK, Erdogan AE, Brahmachary PP, June RK. Correlations between metabolites in the synovial fluid and serum: A mouse injury study. J Orthop Res 2022.

47. Zhang W, Likhodii S, Aref-Eshghi E, Zhang Y, Harper PE, Randell E, et al. Relationship between blood plasma and synovial fluid metabolite concentrations in patients with osteoarthritis. J Rheumatol 2015; 42: 859-865.

CHAPTER EIGHT

EFFECTS OF MECHANICAL STIMULATION ON METABOLOMIC PROFILES OF SW1353 CHONDROCYTES: SHEAR AND COMPRESSION

Contribution of Authors and Co-Authors

Manuscript in Chapter 8

Author: Hope D. Welhaven

Contributions: Designed experiments, performed metabolite extractions, ran LC-MS samples, analyzed and interpreted data, and drafted manuscript.

Co-Author: Carley N. McCutchen

Contributions: Performed cell culturing and mechanical stimulation of SW1353 cells

Co-Author: Ronald K. June

Contributions: Corresponding author, designed experiments, analyzed data, drafted and edited the manuscript.

Manuscript Information

Hope D. Welhaven, Carley N. McCutchen, Ronald K. June

Biology Open

Status of Manuscript:

☐ Prepared for submission to a peer-reviewed journal
☐ Officially submitted to a peer-reviewed journal
☐ Accepted by a peer-reviewed journal
X Published in a peer-reviewed journal

The Company of Biologists

Vol. 11, Issue 1, February 2022

https://doi.org/10.1242/bio.058895

Abstract

Mechanotransduction is a biological phenomenon where mechanical stimuli are converted to biochemical responses. A model system for studying mechanotransduction are the chondrocytes of articular cartilage. Breakdown of this tissue results in decreased mobility, increased pain, and reduced quality of life. Either disuse or overloading can disrupt cartilage homeostasis, but physiological cyclical loading promotes cartilage homeostasis. To model this, we exposed SW1353 cells to cyclical mechanical stimuli, shear and compression, for different durations of time (15 and 30 min). By utilizing liquid chromatography-mass spectroscopy (LC-MS), metabolomic profiles were generated detailing metabolite features and biological pathways that are altered in response to mechanical stimulation. In total, 1,457 metabolite features were detected. Statistical analyses identified several pathways of interest. Taken together, differences between experimental groups were associated with inflammatory pathways, lipid metabolism, beta-oxidation, central energy metabolism, and amino acid production. These findings expand our understanding of chondrocyte mechanotransduction under varying loading conditions and time periods.

Introduction

Mechanotransduction is the study of the cellular responses to applied mechanical loads and deformations [1]. In the past, mechanotransduction has been studied in sensory cells, such as hair cells showing intricate mechanisms of mechanosensing [2]. Beyond sensory cells, the musculoskeletal system, consisting of bone, cartilage, muscle, tendons, and ligaments, functions to provide support, stability, and movement for the organism. In doing so, these tissues experience

a variety of mechanical loads (compressive, tense, and shear) that, through cellular mechanotransduction, must be interpreted, dispersed, and transduced by resident cells. Physiological levels of loading are necessary for cell growth, proliferation, and survival in tissues like articular cartilage (AC) [3, 4].

AC provides near-frictionless articulation on the ends of long bones which provides a smooth surface for joint movement, resists extreme loads that are applied to the joint, and reduces the stress placed on underlying bone [5]. Chondrocytes synthesize an extracellular matrix (ECM) which is the main component of cartilage [6]. The ECM performs mechanotransduction and helps to maintain homeostasis during mechanical loads. Therefore, under load associated with joint motion, the ECM is stimulated to support cartilage homeostasis. Although sub-injurious mechanical loading is required to maintain cellular homeostasis, loads large in duration and/or magnitude can lead to biological imbalances that disrupt homeostasis and induce joint disease such as osteoarthritis (OA) [7].

OA is a chronic joint disease that is caused by many factors including inflammation and joint injury that results in the eventual breakdown of AC. Degradation of tissue ultimately leads to joint pain, limited mobility, and reduced quality of life. Therefore, investigation of mechanotransduction and metabolism of AC, chondrocytes, and the ECM may elucidate the effects of mechanical loading on the joint.

To this end, there has been substantial research in the field to expand our understanding of how chondrocytes respond to the mechanical stimuli experienced by the joint [8-13]. Building on these results, this study examined how chondrocytes respond to cyclical shear and compressive loading *in* vitro by utilizing untargeted metabolomics.

Metabolomics is an analytical profiling technique used to investigate large numbers of small molecule intermediates called metabolites. These molecules "act as a spoken language, broadcasting signals from the genetic architecture and the environment [14]." Metabolomic profiling analyzes thousands of small molecules characterizing the cellular phenotype and provides an unbiased view of metabolic shifts induced by experimental conditions [15]. This technique is applicable to the study of chondrocyte metabolism and OA because it has the ability to provide metabolic information, such as involved pathways and intermediates, in response to applied stimuli, such as shear and compression. While many studies have investigated the effects of mechanical stimuli on the joint, few have investigated if mechanical stimuli impact the metabolism of involved tissues.

Much of what is known about cartilage's biosynthetic response, ECM and proteoglycan synthesis, and overall cartilage health has been historically studied through the lens of compressive loading[16-24]. Bricca *et al* varied doses of exercise and revealed that cyclical loading serves as a protective tool for chondrocytes to withstand loads that are increasing in magnitude and frequency [24]. In contrast, extended periods of increasing load can interfere with homeostasis leading to deterioration of the ECM which can induce joint disease such as OA [22].

While numerous studies investigating compressive loading, fewer studies have examined shear stress, its effect on anabolic and catabolic genes, and its influence on chondrocytes. Smith *et al* compared the effect of shear stress and hydrostatic pressure on chondrocytes and determined that shear stress increased release of proinflammatory mediators, nitric oxide production, and induced apoptosis molecular changes but decreased protein expression (aggrecan, type II collagen)[25]. Chih-Chang *et al* aimed to investigate the mechanisms underlying chondrocyte

urokinase plasminogen activator (uPA) expression by shear stress and determined shear-stress is somewhat protective against uPA upregulation induced by OA[26]. The molecular switch, RhoA, regulates signaling cascades triggered by mechanotransduction. Wan *et al* investigated the relationship between this molecular switch and shear stress. The results of this study suggest shear stress of differing intensities is crucial to chondrocytes in light of RhoA activation, inhibition, and general function[27]. Additional studies measured mechanical strain in cartilage and the effects of shear[22] and shear and compressive loading[23] with non-invasive imaging and found localized changes in the cartilage mechanical environment that ultimately led to cartilage deformations. To study the mechanobiology of these load-bearing tissues, varying loading frequency and amplitude were applied to bone and cartilage explants *in vitro* through a dual frequency system. Both studies revealed that cyclical compression and shear force during these activities stimulates cellular signaling and chondrocyte metabolism by tracking solute transport [23].

Considering how chondrocyte and cellular mechanotransduction has been studied historically, the June lab has heavily investigated the effects of compression on chondrocyte metabolism through metabolomics[8, 10, 11, 13, 28]. The combined results of these studies suggest physiological dynamic compression in chondrocytes is primarily mediated by amino acid, lipid, and central energy metabolism[29]. These findings inspired the June lab to combine glucose modeling and cellular mechanotransduction to further investigate the role of energy metabolism in chondrocyte mechanotransduction. Like this study and previous studies conducted by the June lab, chondrocytes were exposed to compression for 30 minutes. The results of this study suggested that changes in central energy metabolism, specifically changes in protein synthesis, shift as exposure time to dynamic compression increases[28].

With this knowledge and previous studies conducted by Chan and others, additional data is needed to understand mechanotransduction and its effect on metabolism considering both shear and compressive loading. Many have investigated compressive loading and its beneficial effects on cellular mechanotransduction, few studies have examined the role of metabolism. Further, no study to data has investigated how chondrocytes respond metabolically to both shear and compressive loading. Therefore, the objective of this study is to identify mechanosensitive differences between shear and compressive stimulation after 0, 15, and 30 minutes of 5 +/- 1.9% cyclical strain at 1.1Hz for SW1353 chondrocytes, encapsulated in physiologically stiff agarose. After loading, metabolite extracts were analyzed by liquid-chromatography-mass spectrometry (LC-MS) in search of metabolites that differentiate between the type and duration of loading. These data provide insight into how SW1353 chondrocytes respond to mechanical stimuli thus expanding our knowledge of chondrocyte mechanotransduction.

Methods

SW 1353 Chondrocyte Culture and Encapsulation

SW1353 chondrocytes were cultured in DMEM with 10% fetal bovine serum and antibiotics (10,000 I.U./mL penicillin and 10,000 μg/mL streptomycin). Cells were first expanded in monolayer for one passage at 5% CO_2 at 37°C prior to gel encapsulation. For encapsulation, cells were seeded in physiologically stiff agarose (4.5% v/v, Sigma: Type VII-A A0701) at a concentration of 500,000 cells/hydrogel (diameter: 7mm, height: 12.7mm). Hydrogel constructs were individually placed in wells, submerged in DMEM with 10% fetal bovine serum, and allowed to equilibrate for 24 hours prior to mechanical stimulation.

Mechanical Stimulation

Cell encapsulated hydrogels were randomly assigned to five experimental groups (n=5 per experimental group): unloaded controls (0 minutes of mechanical stimuli), 15 or 30 minutes of cyclical shear, or 15 or 30 minutes of cyclical compression. Hydrogels were placed in DMEM with 10% fetal bovine serum without antibiotics and mechanically stimulated with cyclical shear or compression using a custom-built sinusoidal loading apparatus. Sinusoidal compressive and shear strains of 5.00±1.90% (based on initial 12.70mm ± 0.01mm gel height and 7.00mm ± 0.01mm gel diameter, respectively) were applied at 1.1 Hz to simulate the preferred stride rate of humans for 0, 15 and 30 minutes [12, 13]. All hydrogel mechanical testing was performed in physiological cell culture conditions (5% CO_2, 37°C).

Metabolite Extractions

Immediately after mechanical stimulation, hydrogels were flash frozen in liquid nitrogen, pulverized and placed in 70:30 (v/v) methanol : acetone. Samples were vortexed for 5 minutes and placed in -20°C for 5 minutes. This two-step process was repeated 4 times and samples were stored overnight (-20°C) for macromolecule precipitation. The next day proteins and other macromolecules were pelleted by centrifugation. The supernatant containing the metabolites was transferred to a separate tube and dried by vacuum concentration for 6.5 hours to remove solvents. Dried metabolites were resuspended in 100μL mass spectrometry grade 50:50 (v/v) water : acetonitrile solution immediately prior to high performance liquid chromatography-mass spectrometry (HPLC-MS) analysis.

Untargeted Metabolomic Analysis

Metabolomics is the analysis of small molecules (metabolites) in a biological system that provides a global description of cellular function at a given point in time. Extracted metabolites were analyzed using HPLC-MS (Agilient 6538 Q-TOF mass spectrometer) in positive mode (resolution: ~20ppm, accuracy: ~5ppm, possible ionization adducts: H^+, Na^+). Peak intensities for m/z values in the experimental sample set were identified and exported using Agilient MassHunter Qualitative Analysis software. All data was log transformed and autoscaled prior to analysis. All statistical analyses utilized the transformed and scaled data using MetaboAnalyst [30]. Statistical analyses performed included hierarchical cluster analysis (HCA), principal component analysis (PCA), partial least-squares discriminant analysis (PLS-DA), variable importance in projection (VIP) scores, volcano plot, fold change, and heatmap analysis. (See Supplementary Materials and Methods).

Results

A total of 1,457 distinct metabolite features were detected across all experimental groups. First, all experimental groups (control, 15 min. compression and shear, 30 min. compression and shear) were analyzed (Fig. 8.1). HCA and PCA examined overall variation between groups in the dataset. Neither shows complete separation between experimental groups (Fig. 8.1A-B), although the first two principal components are associated with more than 30% of the overall variance indicating moderate underlying structure in the dataset. To further examine this dataset, we applied PLS-DA to assess differences between experimental groups. Separation between experimental groups was observed with minimal overlap (Fig. 8.1 C) using this supervised method.

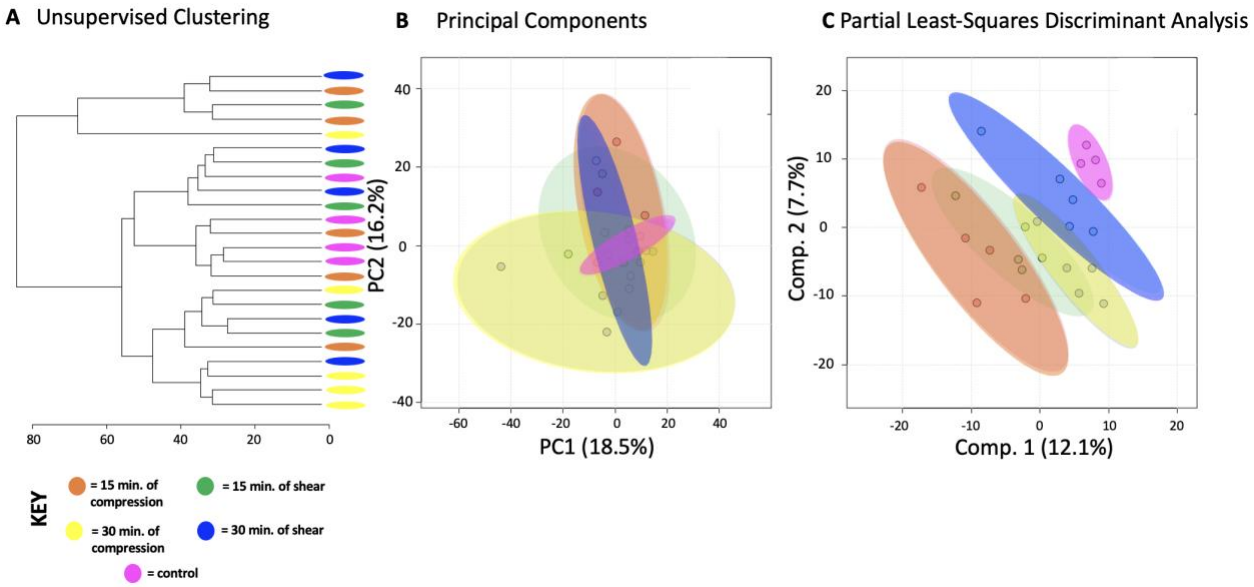

Figure 8.1. SW1353 chondrocytes have shared and distinct responses to shear and compressive forces. A total of 1,457 metabolites were analyzed by both unsupervised hierarchical clustering (HCA) and principal component analysis (PCA) and supervised partial least-squares discriminant analysis (PLS-DA). (A). Unsupervised HCA visualized by a dendrogram did not distinguish distinct clusters between the five experimental groups (control, 15. Min compression and shear, 30 min. compression and shear). HCA assigns Euclidean distances to illustrate dissimilarity between samples and reveal clusters of samples with similar metabolomic profiles. (B) PCA, like HCA, did not display distinguished clusters between the five experimental groups. PCA is shown as a scatterplot with the first two PC on the x and y axes. The x axis shows PC1, which accounts for 18.3% of the variation in the dataset. PC2 is on the y-axis and accounts for 14.2% of the variation in the dataset. (C) Supervised PLS-DA finds some separation between the five experimental groups, with similarity between different time points and different forces. PLS-DA is shown as a scatterplot of the top two components, with component 1 accounting for 14.6% and component 2 accounting for 7.6% of the variation in the dataset. The colors in A-C correspond to sample cohorts: pink – control , orange – 15 minutes compression, yellow – 30 minutes compression, green – 15 minutes shear, blue –30 minutes shear.

To compare the effects of shear and compression on metabolomic profiles, samples exposed to each loading type, shear and compression, were analyzed separately (Figs. 8.2-3). When analyzing differences between compressive samples between 0, 15, and 30 minutes of loading, HCA and PCA find clustering of samples within their respective timepoints indicating

chondrocyte mechanotransduction (Fig. 8.2 A-B). PLS-DA shows further discrimination with all samples clustering within their respective cohorts (Fig. 8.2 C).

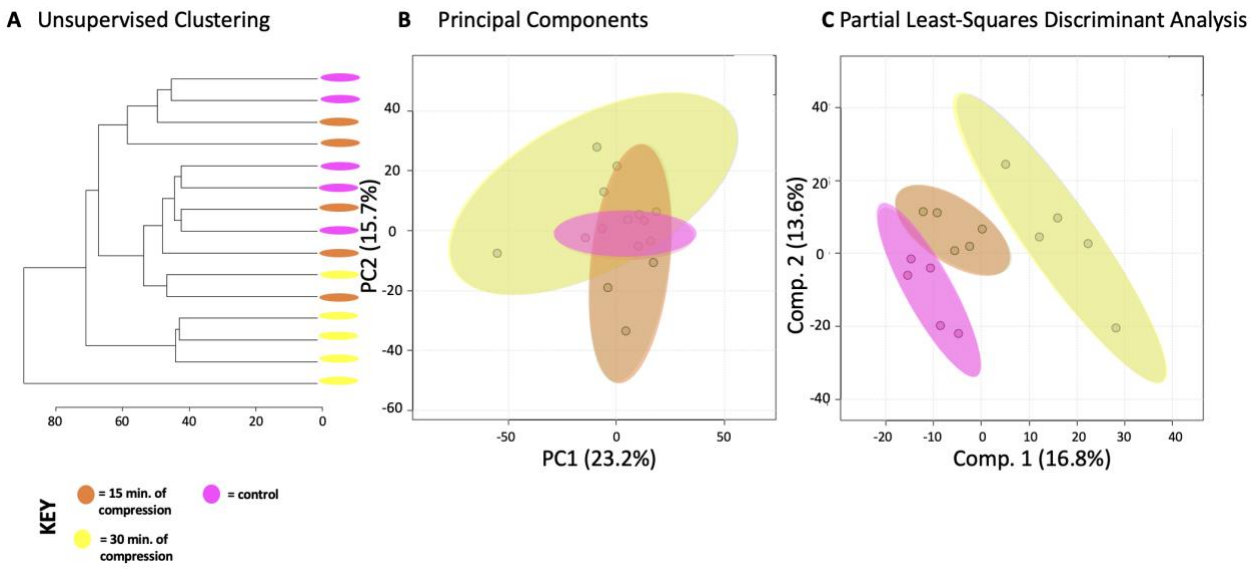

Figure 8.2. Differing amounts of exposure to compression reveal distinct metabolic profiles. Comparison of samples exposed to compression reveal metabolomic profiles of chondrocytes between 15 and 30 minutes of compression differ. (A) Samples compressed at different times separate into distinct clusters by HCA as illustrated in the dendrogram. (B) PCA displays some clustering of samples within their respective cohorts: chondrocytes exposed to compressive forces for 15 minutes (orange) and 30 minutes (yellow). Control chondrocytes that weren't exposed to mechanical stimuli is displayed for comparison purposes (pink). PCA is shown as a scatterplot of the first two PCs (PC1 and PC2), which account for 23.2% and 15.7% of the overall variation in the dataset, respectively. (C) PLS-DA finds clear separation between samples. PLS-DA is visualized as a scatterplot of the top two components, which account for 16.8% and 13.6% of the overall variation in the dataset.

We found similar results for shear stimulation. HCA and PCA revealed clustering of samples within each time point (Fig. 8.3 A-B). PLS-DA shows further separation between samples from different shear groups (Fig. 8.3 C). These data show that SW1353 chondrocytes respond to both shear and compression with alterations in their metabolomic profiles.

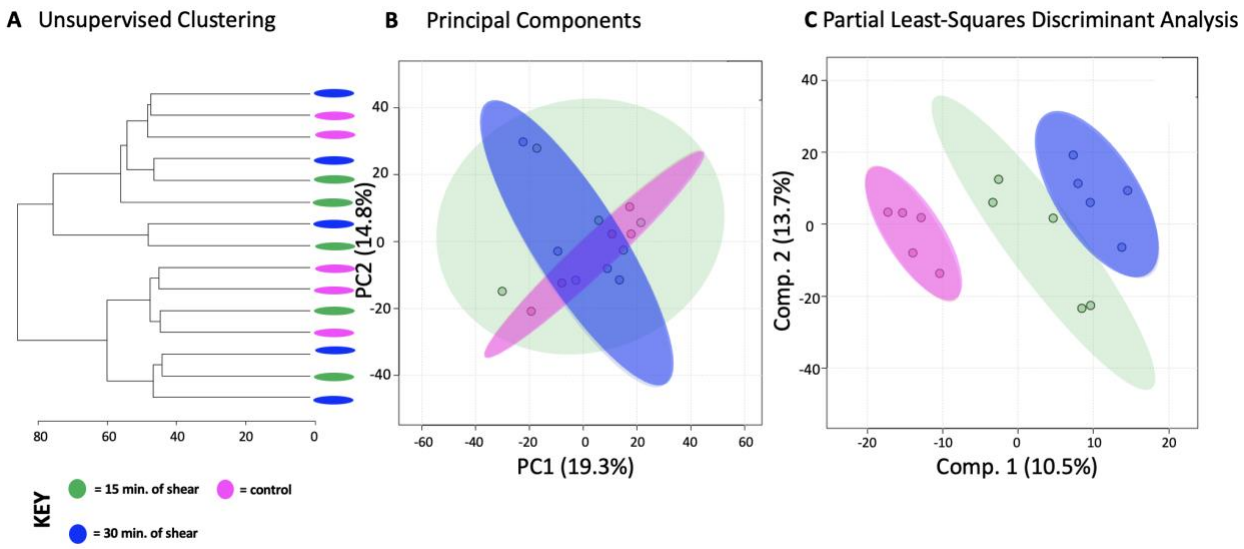

Figure 8.3. Differing amounts of shear force reveal distinct metabolic profiles. Metabolomic profiles of chondrocytes exposed to 15 and 30 minutes of shear force differ. (A) Samples compressed at different times separate into weakly distinct clusters by HCA as illustrated in the dendrogram. (B) PCA displays some clustering of samples within their respective cohorts: chondrocytes exposed to shear force for 15 minutes (green) and 30 minutes (blue). Control chondrocytes that weren't exposed to mechanical stimuli is displayed for comparison purposes (pink). PCA is shown as a scatterplot of the first two PCs (PC1 and PC2), which account for 19.3% and 14.8% of the overall variation in the dataset, respectively. (C) PLS-DA finds clear separation between samples. PLS-DA is visualized as a scatterplot of the top two components, which account for 10.5% and 13.7% of the overall variation in the dataset.

Chondrocytes exposed to shear and compression for the same amount of time showed interesting similarities and differences between types of mechanical stimulation. When comparing compression and shear at 15 minutes, HCA and PCA showed limited separation and clustering (Fig. 8.4 A-B). But PLS-DA clearly distinguishes samples between shear and compression at the 15-minute timepoint (Fig. 8.4 C). Similarly, compression and shear samples that were both exposed to 30 minutes of stimulation were compared.

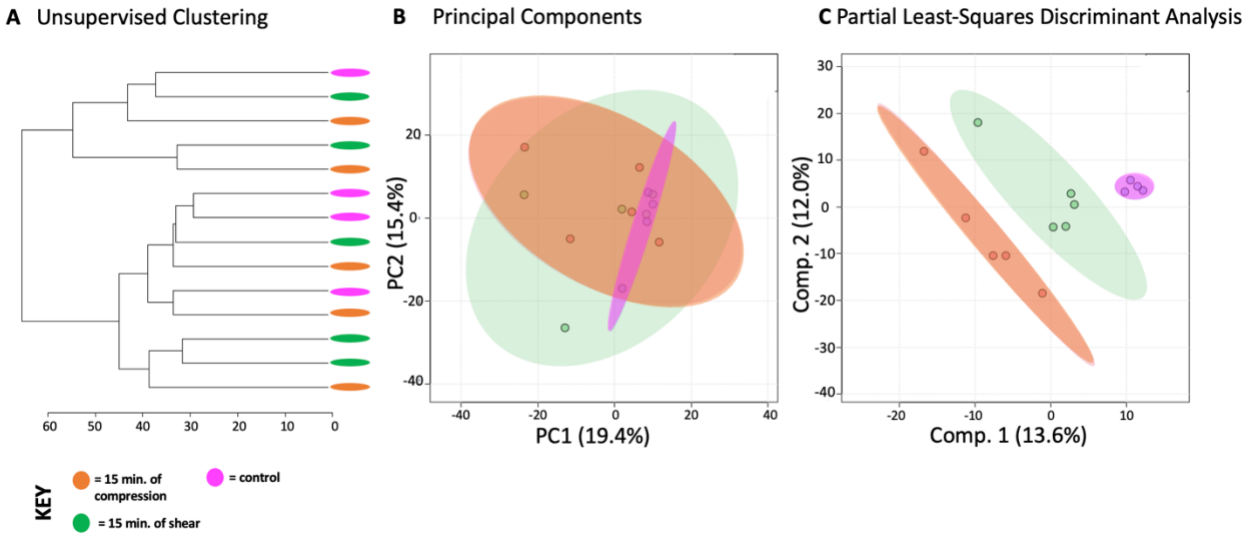

Figure 8.4. Metabolic profiles of differing forces with an equal exposure time of 15 minutes vary. Metabolomic profiles of chondrocytes exposed to compression and shear forces for 15 minutes differ metabolically(A). Samples exposed to different forces for the same amount of time somewhat separate into clusters by HCA as illustrated in the dendrogram. (B) PCA displays some clustering of samples within their respective cohorts: chondrocytes exposed to compression for 15 minutes (orange) and chondrocytes exposed to shear forces for 15 minutes (green). Control chondrocytes that weren't exposed to mechanical stimuli is displayed for comparison purposes (pink). PCA is shown as a scatterplot of the first two PCs (PC1 and PC2), which account for 19.4% and 15.4% of the overall variation in the dataset respectively. (C) PLS-DA finds clear separation between samples. PLS-DA is visualized as a scatterplot of the top two components, which account for 13.6% and 12.0% of the overall variation in the dataset.

Both HCA and PCA found clear separation and clustering of samples at 30 minutes (Fig. 8.5 A-B) that was confirmed by PLS-DA (Fig. 8.5 C). With this knowledge, we used VIP scores from PLS-DA and volcano plot analysis to identify specific metabolites that contributed to the differences between experimental groups. Specific metabolite features of interest were then matched to metabolite identities and pathways using MetaboAnalyst. Significant pathways consist of sialic acid metabolism (all experimental groups); prostaglandin formation from arachidonate, fatty acid metabolism, tyrosine metabolism (15 min. of compression vs 30 min. of compression);

porphyrin metabolism (15 min. of shear vs 30 min. of shear); carnitine shuttle (15C vs. 15S); squalene and cholesterol biosynthesis (30C vs. 30S).

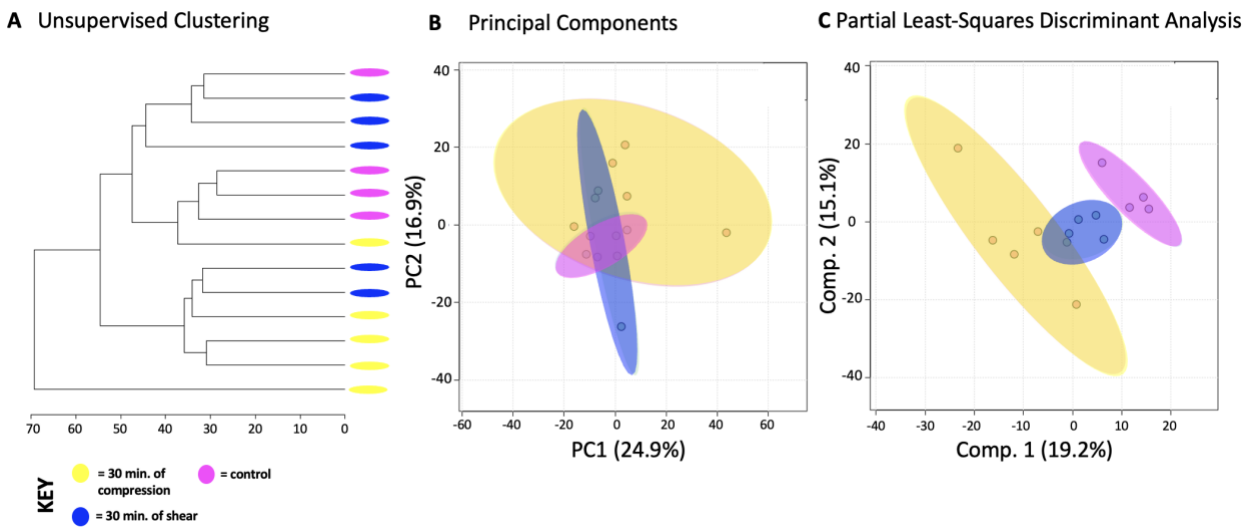

Figure 8.5. Metabolic profiles of differing forces with an equal exposure time of 30 minutes vary. Metabolomic profiles of chondrocytes exposed to compression and shear forces for 30 minutes display distinct metabolomic profiles (A). Samples exposed to different forces for the same amount of time somewhat separate into clusters by HCA as illustrated in the dendrogram. (B) PCA displays clear clustering of samples within their respective cohorts: chondrocytes exposed to compression for 30 minutes (yellow) and chondrocytes exposed to shear forces for 30 minutes (blue). Control chondrocytes that weren't exposed to mechanical stimuli is displayed for comparison purposes (pink). PCA is shown as a scatterplot of the first two PCs (PC1 and PC2), which account for 24.9% and 16.9% of the overall variation in the dataset respectively. (C) PLS-DA finds clear separation between samples. PLS-DA is visualized as a scatterplot of the top two components, which account for 19.2% and 15.1% of the overall variation in the dataset.

Co-regulated metabolite features and associated pathways between shear and compressive stimulation were identified using heatmap analysis. Using the median metabolite intensities and HCA, 7 clusters were identified based on Euclidian distance. Metabolites from these clusters were then used to determine associated pathways (Fig. 8.6). In total, 372 pathways were detected, and 80 of the 372 are statistically significant ($p < 0.05$).

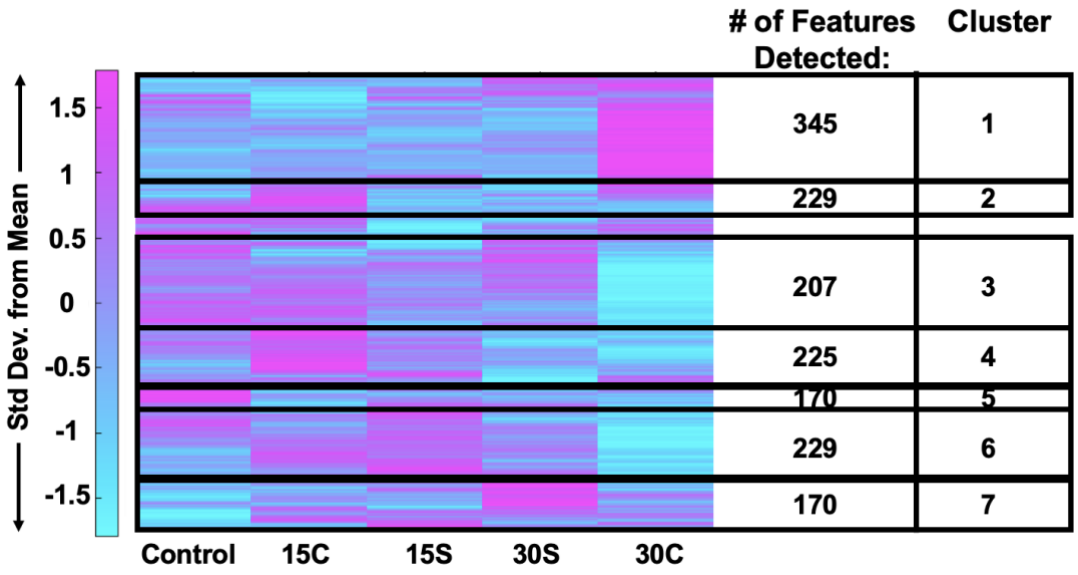

Figure 8.6. Heatmap analysis reveals that metabolic phenotypes differ when exposure time and mechanical force differ. Median intensities were clustered into 5 groups: control samples (n=4), 15 minutes of compression (n=5), 30 minutes of compression (n=5), 15 minutes of shear (n=5) and 30 minutes of shear force (n=5). 1,457 metabolite intensities were detected in SW1353 cells. To determine associated pathways and metabolites, *MS Peaks to Pathways* was employed.

Cluster 1 contained 354 metabolite features that were upregulated in samples exposed to 30 minutes of compression. These mapped to 25 statistically significant enriched pathways including primary bile acid biosynthesis, histidine metabolism, fructose and mannose metabolism, pyrimidine and purine metabolism, and alanine, aspartate, and glutamine metabolism. Cluster 2 and 4 contained 229 and 225 metabolite features, respectively, that were upregulated in samples exposed to 15 minutes of compression. These features corresponded to 23 statistically significant enriched pathways including various amino acid metabolic pathways.

Cluster 3 contained 207 metabolite features that were downregulated in samples exposed to 30 minutes of compression. These mapped to 7 statistically significant enriched pathways including alanine, aspartate, and glutamate metabolism, N-glycan biosynthesis, mannose type O-

glycan biosynthesis, arginine biosynthesis, steroid hormone biosynthesis, and pyrimidine metabolism.

Cluster 5 containing 170 metabolite features that were upregulated in control samples. These features corresponded to 8 statistically significant enriched pathways including butanoate metabolism, sphingolipid metabolism, propanoate metabolism, the citrate cycle (TCA cycle), histidine metabolism, and various amino acid metabolic pathways.

Clusters 6 and 7 contained 229 and 170 metabolites that corresponded to samples exposed to shear for both 15 and 30 minutes. The features of the two combined clusters corresponded to 17 statistically significant enriched pathways including various amino acid metabolic pathways, the pentose phosphate pathway, glycolysis and gluconeogenesis.

Amino acid metabolic pathways unique to compressed SW1353 cells include alanine, asparagine, aspartate, glutamate, glutamine, histidine, isoleucine, leucine, and valine metabolism. Metabolic pathways shared by both SW1353 cells exposed to compression and shear included arginine, cysteine, glycine, lysine, methionine, proline, serine and threonine. Amino acids that weren't detected within this dataset include phenylalanine, tryptophan, and tyrosine. All significant ($p < 0.05$) detected pathways were investigated and compared to findings in the literature. Those that were detected in this study but have yet been detected nor discussed by others were not examined further.

Discussion

Cartilage provides a smooth surface for movement, reduces stress placed on underlying bone, and requires a strong and smooth ECM to resist high loads created in the joint. To further investigate the role of cartilage and mechanotransduction in chondrocytes, we investigated the

effects of mechanical stimuli on the ECM and how differing types of load (shear and compression) and exposure times affect the metabolism of SW1353 chondrocytes. In total, 1,457 metabolites were detected, and metabolic profiles were generated for each experimental condition (time pt. 0, 15, 30 min., mechanical stimulus - shear or compression).

In every pairwise comparison, metabolomic profiles from different experimental groups differed from each other. When comparing all experimental groups, sialic acid metabolism was the most notable pathway determined from the top 100 VIP metabolites when comparing all groups. This finding corresponds to sialic acid being an inflammatory biomarker for OA and rheumatoid arthritis (RA), while also contributing to the lubrication of the joint [31]. Additionally, lipid metabolism (fatty acid metabolism, cholesterol biosynthesis, prostaglandin formation from arachidonate) was upregulated in compressed samples. Based on potential crosstalk between joint tissues, the permeability of AC, and the ability of fats like phospholipids to act as lubricants, overexpression of fat associated pathways may lead to cartilage lesions, joint space narrowing, joint immobilization, and ultimately contributing to the development of OA [32-37]. Central energy metabolism and beta-oxidation were present across experimental groups and strongly upregulated amongst compressed samples (TCA cycle, carnitine shuttle). We interpret this as exposure to mechanical stimuli driving a high chondrocyte ATP demand: the TCA cycle and the carnitine shuttle may have been upregulated to meet this need. Amino acid metabolism differed between samples exposed to shear and compression while several specific amino acids were unique to compression. Taken together, compression may induce mechanosensitive pathways that are needed to produce a broader set of products than shear such as amino acids, both non-essential and essential.

Many studies have shown the diverse effects of mechanical stimulation on the musculoskeletal system, chondrocytes, ECM, cell metabolism, and its relation to OA [12, 13, 28, 29]. Bushmann *et al* investigated the effects of static and dynamic mechanical compression on matrix biosynthesis, chondrocyte proliferation, and quantified proteoglycan and glycosaminoglycan content. Using cell culture and radiolabeling, *in vitro* chondrocytes form a mechanically functional matrix that preserves certain physiological features of chondrocyte behavior and response to physical stimuli [20, 38]. O'Connor *et al* examined the effects of mechanical stimulation on chondrocyte metabolism and transient receptor potential vanilloid 4 (TRPV4). The results of this study suggest that dynamic loading has a profound effect on cell physiology, ion channel function, and TRPV4 mediated mechanotransduction [39].

Jutila *et al* report the effects of compressive loading at early time points (0, 15 and 30 minutes). Through the utilization of targeted and untargeted metabolomics, 54 metabolites were found to mediate chondrocyte mechanotransduction [12, 13]. Other studies identified the effects of physiological compression on energy metabolism and maintenance of the pericellular and extracellular matrices [28, 29]. In addition, many pathways related to the metabolism of energy, lipids, and amino acids were identified through targeted and untargeted metabolomics. The results of our study are consistent with these prior studies and together indicate that extended exposure to mechanical stimuli affects chondrocytes, ECM components, and alters cellular metabolism.

Inflammation

Exposure to shear and compression lead to metabolic shifts associated with inflammation and deterioration in SW1353 cells. The 100 most significant metabolites across all sample groups were involved in sialic acid metabolism (Fig. 1). Sialic acid (SA) is an acylated derivative of

neuraminic acid attached to glycoproteins and glycolipids. Serum SA levels are a known marker of inflammation and has been reported as a useful biomarker of inflammation in patients with OA and RA [40]. Additionally, studies find that differing levels of SA are linked to OA severity and could be used as a diagnostic tool in the future [31, 40-44]. Our study provides further evidence that sialic acid production could be a potential marker for OA due to its metabolic presence when mechanically stimulated with shear and compressive forces. Sialic acid is also a key component of the superficial zone protein lubricin that decreases cartilage-on-cartilage friction [12, 13, 45, 46]. Therefore, these findings may suggest different loading types and exposure times may promote changes in metabolism that correspond to changes in cartilage structure and function. Taken together, this is the first study to find sialic acid metabolism to be upregulated after mechanical stimuli and further research may identify its effects on the ECM, cartilage health, and OA.

Further analysis showed that prostaglandin formation from arachidonate was a significant pathway associated with compression. Prostaglandin metabolites were upregulated after 30 minutes of compression. Studies show that prostaglandin formation from arachidonate can be triggered by obesity, age, and mechanical stress [47]. Individually or combined, these stimuli result in cartilage deterioration which can be attributed to the innate immune system, by pathogen-associated molecular patterns (PAMPs), damage-associated molecular patterns (DAMPs), and alarmins [48]. Alarmins are triggered by signals from cellular damage, abnormal proteins, leaky vasculature, and fragments of cartilage matrix [47, 48]. Prostaglandins such as PGD2, PGE2, and others are anti-inflammatory molecules that initiate a decrease in inflammation and trigger recovery to normal cellular function [49-51]. Upon the application of low fluid shear stress anti-inflammatory molecules are activated, inflammation is halted, and recovery is initiated [47, 50, 51].

The results of this study suggest that increased compressive loading leads to an increased presence of inflammatory pathways such as prostaglandin formation from arachidonate in SW1353 cells. Therefore, if confirmed in primary cells, increased compressive stimulation may result in increased inflammation, which in excess could lead to OA if not balanced by other physiological processes.

Lipid Metabolism

In this study, a common metabolic theme of SW1353 cells stimulated by compression was upregulation of metabolite features corresponding to lipid metabolism. The pathways detected include fatty acid biosynthesis, cholesterol biosynthesis, and prostaglandin formation from arachidonate which were significantly upregulated after 30 minutes of compression. Further, butanoate and sphingolipid metabolism were significantly upregulated in control samples, implying downregulation upon mechanical stimulation.

When joint homeostasis is altered, increased protease activity can result in cartilage lesions, joint space narrowing, and ultimately, breakdown of the tissues [32-37]. Hence cartilage health and metabolism greatly rely on the chondrocyte microenvironment. On the metabolic level, both fatty acid metabolism and cholesterol biosynthesis are required to maintain healthy ECM and cartilage [52-55]. Cartilage contains stores of lipid deposits, especially in chondrocytes, during times of health and disease. Expected lipid content in both healthy and pathological cartilage include palmitic, linolic, and oleic acid, but fatty acids and arachidonate acid are elevated in OA samples and associated with increased histological severity [56]. Beyond prostaglandin synthesis from arachidonate, in this study both fatty acid metabolism and cholesterol biosynthesis were upregulated in loaded samples indicating that chondrocyte metabolism was altered as a result of

shear and compression stimulation. Future studies may determine the role of mechanical stimuli in regulating the cartilage ECM through these pathways.

Central Metabolism

Injurious mechanical stimuli, traumatic injury, and others factors such as obesity, age, and gender initiate the breakdown of cartilage leading to OA. In contrast, lower levels of mechanical stimuli result in matrix synthesis to support cartilage homeostasis. Both repair and maintenance require additional energy production to produce ATP. Pathways that generate ATP are pathways related to central metabolism including glycolysis, the TCA cycle, beta-oxidation, and the carnitine shuttle. In this study, pathways related to the glycolysis, TCA cycle, and the carnitine shuttle were significantly upregulated consistent with prior results [10, 28, 29].

The carnitine shuttle was upregulated in all mechanically stimulated samples after 15 minutes of either compression or shear. Beta-oxidation breaks down fatty acids to produce energy and is regulated by the carnitine shuttle. Carnitines stimulate cell proliferation, induce ATP synthesis, and serum carnitines were associated with OA grade [57, 58].

Metabolites and corresponding pathways involved in glycolysis and the TCA cycle were upregulated in SW1353 cells exposed to 15 minutes of shear. These pathways were the only two detected pathways unique to shear force. In chondrocytes, anaerobic glycolysis is restricted as oxygen and nutrients are limited in avascular cartilage. But previous studies have found that both aerobic and anaerobic glycolysis occur in chondrocytes [59]. Specific to OA, the rate of anerobic glycolysis in diseased cartilage is higher compared to healthy cartilage [60]. Other intermediates that can be incorporated into glycolysis to yield energy are fructose, mannose, and galactose. In this

study, fructose, mannose, and galactose metabolism were upregulated in SW1353 cells exposed to compression.

The TCA cycle produces ATP from pyruvate and other sources such as sugar, fat, and proteins. Intermediate TCA metabolites include citrate, malate, succinate, fumarate, and various others. Studies find that patients with OA have higher levels of synovium metabolites associated with the TCA cycle compared to healthy controls [57, 61, 62]. The results of this study provide evidence that mechanical stimulation by compression specifically generates additional ATP. This ATP may be used to maintain and produce matrix thus requiring upregulation of the TCA cycle and the carnitine shuttle.

Beyond glycolysis and the TCA cycle, the pentose phosphate pathway (PPP) was upregulated in SW1353 cells exposed to compression. The PPP pathway utilizes glucose-6-phosphate which is a product of glycolysis. The PPP gives rise to NADH and ribose-5-phosphate which is used to make subunits for DNA, RNA, and amino acids such as histidine from phosphoribosyl pyrophosphate (PRPP). Here, histidine and beta-alanine metabolism were upregulated only in SW1353 cells exposed to compression. Histamine is the decarboxylated amine form of histidine, and previous studies have found that histamines stimulate chondrocytes proliferation in humans [63, 64]. Therefore, the upregulation of histidine metabolism in this study suggests that SW1353 cells exposed to compression may proliferate in response mechanical stimuli.

Finally, two pathways detected in SW1353 cells stimulated by 30 minutes of compression were pyrimidine and purine metabolism (p-value < 0.05). Pyrimidine and purine metabolism stem from the pentose phosphate pathway. These two pathways function to recycle nucleosides and

participate in *de novo* nucleotide synthesis. Upregulation of these pathways may relate to an increase in cellular demand of complex molecules such as RNA upon mechanical stimulation (e.g. to support transcription). Beyond nucleotide and nucleoside production, pyrimidine and purine metabolism give rise to various amino acids. In particular, pyrimidine interconversions can lead to beta-alanine metabolism. Previous studies have found increased levels of beta-alanine in urine, synovium, synovial fluid, and in subchondral bone in OA animal models [65-68].

Amino Acid Metabolism

Metabolomic profiles for SW1353 cells stimulated by either shear or compression show that amino acid metabolism is commonly upregulated by these types of loading with certain responses specific to the type and/or duration of loading. Amino acid pathways unique to compressive stimulation include metabolism of alanine, asparagine, aspartate, glutamate, glutamine, histidine, isoleucine, leucine, and valine metabolism. In contrast, arginine, cysteine, glycine, lysine, methionine, proline, serine, and threonine were induced by both shear and stimuli compression (Fig. 8.7).

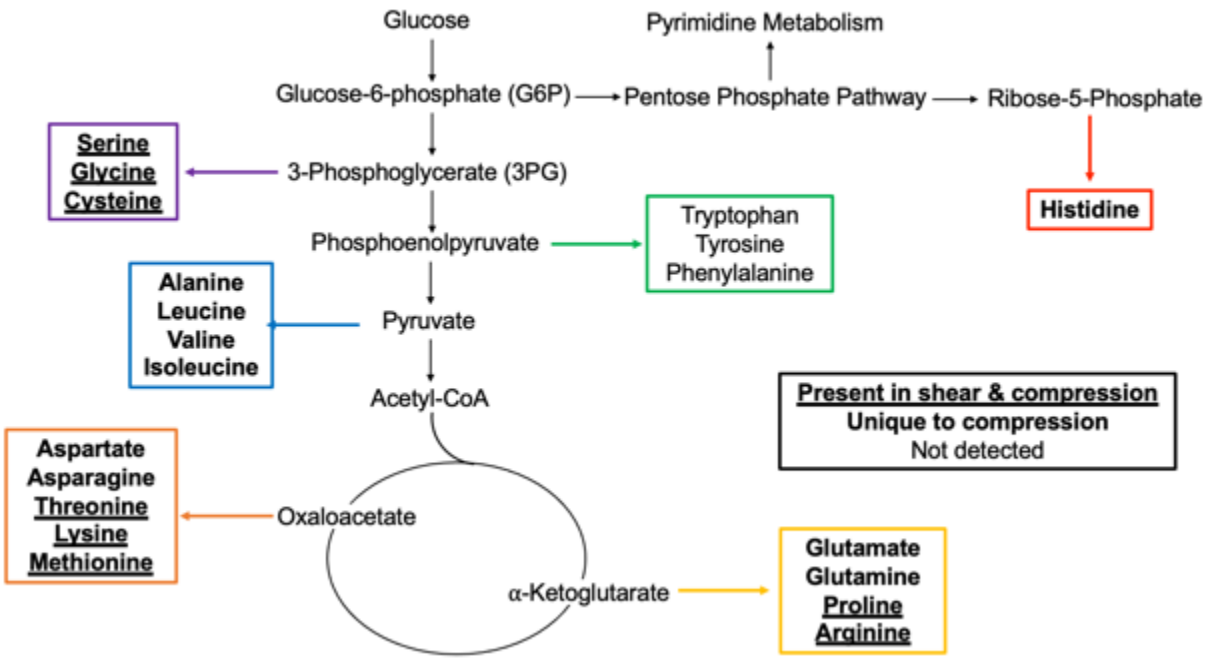

Figure 8.7. Mapping of mechanically stimulated amino acids in metabolic pathways. Amino acids that are bolded and underlined were upregulated in SW1353 cells that were exposed to compression and shear force. Those bolded only were upregulated in cells exposed to compression. Amino acids that aren't bolded nor underlined weren't detected (tryptophan, tyrosine, phenylalanine). Intermediates of interest include ribose-5-phosphate, 3-phosphoglycerate, pyruvate, α-ketoglutarate and oxaloacetate. Additionally, pyrimidine metabolism was upregulated in samples exposed to 30 minutes of compression which stems from the pentose phosphate pathway.

Amino acids are the building blocks of proteins and determine structure and function. Depending on cellular demand, amino acids can be converted into intermediates, or produced from glucose, through central energy metabolism. The results of this study suggest that major precursors of interest when analyzing the relationship between mechanical stimuli and metabolism include ribose-5-phosphate (histidine), 3-phosphoglycerate (serine, glycine, cysteine), pyruvate (alanine, leucine, valine, isoleucine), α-ketoglutarate (glutamate, glutamine, proline, arginine) and oxaloacetate (aspartate, asparagine, threonine, lysine, methionine) (Fig. 7). The results of this study suggest that the upregulation of metabolic pathways may correspond to the synthesis of

essential and non-essential amino acids that are needed to synthesize musculoskeletal associated proteins in response to mechanical stimuli. Furthermore, the application of different stimuli, such as compression and shear, results in different metabolic profiles that impact synthesis of various proteins.

These data display that shear force does not elicit the same metabolic response as compression. The differences in response may correlate to the differences in mechanics. Compressive forces are colinear, meaning, forces align with each other. Conversely, shear force is unaligned, meaning forces are mechanically exerted in opposite directions. Because shear and compressive mechanics differ, fluid flow may be affected. We hypothesize that compression can drive fluid flow while shear does not necessarily do the same. Therefore, different loading may induce or trigger different protein synthesis cascades in response to flow independent or dependent mechanotransduction.

Limitations

This study has important limitations and opportunities for future studies. First, the behavior of the chondrocyte cell line SW1353 cells may differ from primary human chondrocytes. Second, although our *in vitro* approach is required to apply well-defined mechanical loads, this approach may yield different results from an *in vivo* model or one where the pericellular matrix is present. Third, exposure to mechanical stimuli for both periods shorter than 15 minutes and beyond 30 minutes could expand our knowledge on the varying metabolic phenotypes beyond the those in this study. Finally, this was an untargeted metabolomic study. By performing a more targeted metabolomic analysis utilizing MS/MS, uncertainty of predicted identities of key metabolite features and their associated pathways can be reduced.

Conclusion

To our knowledge, this is the first study to generate global metabolomic profiles of SW1353 cells exposed to both shear and compression at early time points. Pathways were identified within experimental groups which provide insight into the role of the extracellular matrix, articular cartilage homeostasis, and the potential outcomes of metabolic alterations that ultimately lead to osteoarthritis. Furthermore, these metabolomic profiles support the link between mechanical stimuli and cartilage remodeling. Expansion of this study may identify cartilage loading protocols to bolster matrix synthesis that may be relevant to drug development.

Acknowledgements

The authors gratefully acknowledge funding from NSF (CMMI 1554708) and NIH (R01AR073964). Funding for the Proteomics, Metabolomics and Mass Spectrometry Facility was made possible in part by the MJ Murdock Charitable Trust and the National Institute of General Medical Sciences of the National Institutes of Health under Award Number P20GM103474. The content is solely the responsibility of the authors and does not necessarily represent the official views of the National Institutes of Health.

Abbreviations List

ECM = extracellular matrix; OA = osteoarthritis; LC-MS = liquid chromatography-mass spectrometry; HPLC-MS = high precision liquid chromatography and mass spectrometry; HCA = hierarchical cluster analysis; PCA = principal component analysis; PC = principal components

PLS-DA = partial least-squares discriminant analysis; VIP = variable important in projection

FDR = false discovery rate; m/z = mass-to-charge ratio

References

1. Paluch EK, Nelson CM, Biais N, Fabry B, Moeller J, Pruitt BL, et al. Mechanotransduction: use the force(s). BMC Biol 2015; 13: 47.

2. Gillespie PG, Muller U. Mechanotransduction by hair cells: models, molecules, and mechanisms. Cell 2009; 139: 33-44.

3. Jaalouk DE, Lammerding J. Mechanotransduction gone awry. Nat Rev Mol Cell Biol 2009; 10: 63-73.

4. Orr AW, Helmke BP, Blackman BR, Schwartz MA. Mechanisms of mechanotransduction. Dev Cell 2006; 10: 11-20.

5. Sophia Fox AJ, Bedi A, Rodeo SA. The basic science of articular cartilage: structure, composition, and function. Sports Health 2009; 1: 461-468.

6. Sanchez-Adams J, Leddy HA, McNulty AL, O'Conor CJ, Guilak F. The mechanobiology of articular cartilage: bearing the burden of osteoarthritis. Curr Rheumatol Rep 2014; 16: 451.

7. Racunica TL, Teichtahl AJ, Wang Y, Wluka AE, English DR, Giles GG, et al. Effect of physical activity on articular knee joint structures in community-based adults. Arthritis Rheum 2007; 57: 1261-1268.

8. Zignego DL, Jutila AA, Gelbke MK, Gannon DM, June RK. The mechanical microenvironment of high concentration agarose for applying deformation to primary chondrocytes. J Biomech 2014; 47: 2143-2148.

9. Zignego DL, Hilmer JK, Bothner B, Schell WJ, June RK. Primary human chondrocytes respond to compression with phosphoproteomic signatures that include microtubule activation. J Biomech 2019; 97: 109367.

10. Salinas D, Mumey BM, June RK. Physiological dynamic compression regulates central energy metabolism in primary human chondrocytes. Biomech Model Mechanobiol 2019; 18: 69-77.

11. McCutchen CN, Zignego DL, June RK. Metabolic responses induced by compression of chondrocytes in variable-stiffness microenvironments. J Biomech 2017; 64: 49-58.

12. Jutila AA, Zignego DL, Schell WJ, June RK. Encapsulation of chondrocytes in high-stiffness agarose microenvironments for in vitro modeling of osteoarthritis mechanotransduction. Ann Biomed Eng 2015; 43: 1132-1144.

13. Jutila AA, Zignego DL, Hwang BK, Hilmer JK, Hamerly T, Minor CA, et al. Candidate mediators of chondrocyte mechanotransduction via targeted and untargeted metabolomic measurements. Arch Biochem Biophys 2014; 545: 116-123.

14. Jewett MC, Hofmann G, Nielsen J. Fungal metabolite analysis in genomics and phenomics. Curr Opin Biotechnol 2006; 17: 191-197.

15. Carlson AK, Rawle RA, Adams E, Greenwood MC, Bothner B, June RK. Application of global metabolomic profiling of synovial fluid for osteoarthritis biomarkers. Biochem Biophys Res Commun 2018; 499: 182-188.

16. Sah RL, Grodzinsky AJ, Plaas AH, Sandy JD. Effects of tissue compression on the hyaluronate-binding properties of newly synthesized proteoglycans in cartilage explants. Biochem J 1990; 267: 803-808.

17. Sah RL, Doong JY, Grodzinsky AJ, Plaas AH, Sandy JD. Effects of compression on the loss of newly synthesized proteoglycans and proteins from cartilage explants. Arch Biochem Biophys 1991; 286: 20-29.

18. Gray ML, Pizzanelli AM, Lee RC, Grodzinsky AJ, Swann DA. Kinetics of the chondrocyte biosynthetic response to compressive load and release. Biochim Biophys Acta 1989; 991: 415-425.

19. Gray ML, Pizzanelli AM, Grodzinsky AJ, Lee RC. Mechanical and physiochemical determinants of the chondrocyte biosynthetic response. J Orthop Res 1988; 6: 777-792.

20. Buschmann MD, Gluzband YA, Grodzinsky AJ, Kimura JH, Hunziker EB. Chondrocytes in agarose culture synthesize a mechanically functional extracellular matrix. J Orthop Res 1992; 10: 745-758.

21. Bricca A, Struglics A, Larsson S, Steultjens M, Juhl CB, Roos EM. Impact of Exercise Therapy on Molecular Biomarkers Related to Cartilage and Inflammation in Individuals at Risk of, or With Established, Knee Osteoarthritis: A Systematic Review and Meta-Analysis of Randomized Controlled Trials. Arthritis Care Res (Hoboken) 2019; 71: 1504-1515.

22. Chan DD, Cai L, Butz KD, Nauman EA, Dickerson DA, Jonkers I, et al. Functional MRI can detect changes in intratissue strains in a full thickness and critical sized ovine cartilage defect model. J Biomech 2018; 66: 18-25.

23. Chan DD, Cai L, Butz KD, Trippel SB, Nauman EA, Neu CP. In vivo articular cartilage deformation: noninvasive quantification of intratissue strain during joint contact in the human knee. Sci Rep 2016; 6: 19220.

24. Bricca A, Juhl CB, Grodzinsky AJ, Roos EM. Impact of a daily exercise dose on knee joint cartilage - a systematic review and meta-analysis of randomized controlled trials in healthy animals. Osteoarthritis Cartilage 2017; 25: 1223-1237.
25. Smith RL, Carter DR, Schurman DJ. Pressure and shear differentially alter human articular chondrocyte metabolism: a review. Clin Orthop Relat Res 2004: S89-95.

26. Yeh CC, Chang SF, Huang TY, Chang HI, Kuo HC, Wu YC, et al. Shear stress modulates macrophage-induced urokinase plasminogen activator expression in human chondrocytes. Arthritis Res Ther 2013; 15: R53.

27. Wan Q, Kim SJ, Yokota H, Na S. Differential activation and inhibition of RhoA by fluid flow induced shear stress in chondrocytes. Cell Biol Int 2013; 37: 568-576.

28. Salinas D, Minor CA, Carlson RP, McCutchen CN, Mumey BM, June RK. Combining Targeted Metabolomic Data with a Model of Glucose Metabolism: Toward Progress in Chondrocyte Mechanotransduction. PLoS One 2017; 12: e0168326.

29. Zignego DL, Hilmer JK, June RK. Mechanotransduction in primary human osteoarthritic chondrocytes is mediated by metabolism of energy, lipids, and amino acids. J Biomech 2015; 48: 4253-4261.

30. Xia J, Wishart DS. Using MetaboAnalyst 3.0 for Comprehensive Metabolomics Data Analysis. Curr Protoc Bioinformatics 2016; 55: 14 10 11-14 10 91.

31. Alturfan AA, Uslu E, Alturfan EE, Hatemi G, Fresko I, Kokoglu E. Increased serum sialic acid levels in primary osteoarthritis and inactive rheumatoid arthritis. Tohoku J Exp Med 2007; 213: 241-248.

32. Villalvilla A, Gomez R, Largo R, Herrero-Beaumont G. Lipid transport and metabolism in healthy and osteoarthritic cartilage. Int J Mol Sci 2013; 14: 20793-20808.

33. Sohn DH, Sokolove J, Sharpe O, Erhart JC, Chandra PE, Lahey LJ, et al. Plasma proteins present in osteoarthritic synovial fluid can stimulate cytokine production via Toll-like receptor 4. Arthritis Res Ther 2012; 14: R7.

34. Pan J, Wang B, Li W, Zhou X, Scherr T, Yang Y, et al. Elevated cross-talk between subchondral bone and cartilage in osteoarthritic joints. Bone 2012; 51: 212-217.

35. Maroudas A, Bullough P, Swanson SA, Freeman MA. The permeability of articular cartilage. J Bone Joint Surg Br 1968; 50: 166-177.

36. Lotke PA, Granda JL. Alterations in the permeability of articular cartilage by proteolytic enzymes. Arthritis Rheum 1972; 15: 302-308.

37. Appleton CT, Pitelka V, Henry J, Beier F. Global analyses of gene expression in early experimental osteoarthritis. Arthritis Rheum 2007; 56: 1854-1868.

38. Buschmann MD, Gluzband YA, Grodzinsky AJ, Hunziker EB. Mechanical compression modulates matrix biosynthesis in chondrocyte/agarose culture. J Cell Sci 1995; 108 (Pt 4): 1497-1508.

39. O'Conor CJ, Leddy HA, Benefield HC, Liedtke WB, Guilak F. TRPV4-mediated mechanotransduction regulates the metabolic response of chondrocytes to dynamic loading. Proc Natl Acad Sci U S A 2014; 111: 1316-1321.

40. Cui Z, Liu K, Wang A, Liu S, Wang F, Li J. Correlation between sialic acid levels in the synovial fluid and the radiographic severity of knee osteoarthritis. Exp Ther Med 2014; 8: 255-259.

41. Kosakai O. [Clinical relevance of sialic acids determination in serum and synovial fluid in orthopaedic disorders]. Rinsho Byori 1991; 39: 197-207.

42. Gobezie R, Kho A, Krastins B, Sarracino DA, Thornhill TS, Chase M, et al. High abundance synovial fluid proteome: distinct profiles in health and osteoarthritis. Arthritis Res Ther 2007; 9: R36.

43. Chavan MM, Kawle PD, Mehta NG. Increased sialylation and defucosylation of plasma proteins are early events in the acute phase response. Glycobiology 2005; 15: 838-848.

44. Browning LM, Krebs JD, Jebb SA. Discrimination ratio analysis of inflammatory markers: implications for the study of inflammation in chronic disease. Metabolism 2004; 53: 899-903.

45. Jay GD, Elsaid KA, Kelly KA, Anderson SC, Zhang L, Teeple E, et al. Prevention of cartilage degeneration and gait asymmetry by lubricin tribosupplementation in the rat following anterior cruciate ligament transection. Arthritis Rheum 2012; 64: 1162-1171.

46. Carlson AK, Rawle RA, Wallace CW, Brooks EG, Adams E, Greenwood MC, et al. Characterization of synovial fluid metabolomic phenotypes of cartilage morphological changes associated with osteoarthritis. Osteoarthritis Cartilage 2019; 27: 1174-1184.

47. Bar-Or D, Rael LT, Thomas GW, Brody EN. Inflammatory Pathways in Knee Osteoarthritis: Potential Targets for Treatment. Curr Rheumatol Rev 2015; 11: 50-58.

48. Bianchi ME. DAMPs, PAMPs and alarmins: all we need to know about danger. J Leukoc Biol 2007; 81: 1-5.

49. Wang P, Zhu F, Lee NH, Konstantopoulos K. Shear-induced interleukin-6 synthesis in chondrocytes: roles of E prostanoid (EP) 2 and EP3 in cAMP/protein kinase A- and PI3-K/Akt-dependent NF-kappaB activation. J Biol Chem 2010; 285: 24793-24804.

50. Wang P, Guan PP, Guo C, Zhu F, Konstantopoulos K, Wang ZY. Fluid shear stress-induced osteoarthritis: roles of cyclooxygenase-2 and its metabolic products in inducing the expression of proinflammatory cytokines and matrix metalloproteinases. FASEB J 2013; 27: 4664-4677.

51. Attur M, Al-Mussawir HE, Patel J, Kitay A, Dave M, Palmer G, et al. Prostaglandin E2 exerts catabolic effects in osteoarthritis cartilage: evidence for signaling via the EP4 receptor. J Immunol 2008; 181: 5082-5088.

52. Wu S, De Luca F. Role of cholesterol in the regulation of growth plate chondrogenesis and longitudinal bone growth. J Biol Chem 2004; 279: 4642-4647.

53. Gkretsi V, Simopoulou T, Tsezou A. Lipid metabolism and osteoarthritis: lessons from atherosclerosis. Prog Lipid Res 2011; 50: 133-140.

54. Bernstein P, Sticht C, Jacobi A, Liebers C, Manthey S, Stiehler M. Expression pattern differences between osteoarthritic chondrocytes and mesenchymal stem cells during chondrogenic differentiation. Osteoarthritis Cartilage 2010; 18: 1596-1607.

55. Aguilar A, Wu S, De Luca F. P450 oxidoreductase expressed in rat chondrocytes modulates chondrogenesis via cholesterol- and Indian Hedgehog-dependent mechanisms. Endocrinology 2009; 150: 2732-2739.

56. Lippiello L, Walsh T, Fienhold M. The association of lipid abnormalities with tissue pathology in human osteoarthritic articular cartilage. Metabolism 1991; 40: 571-576.

57. Zhai G. Alteration of Metabolic Pathways in Osteoarthritis. Metabolites 2019; 9.

58. Tootsi K, Kals J, Zilmer M, Paapstel K, Ottas A, Martson A. Medium- and long-chain acylcarnitines are associated with osteoarthritis severity and arterial stiffness in end-stage osteoarthritis patients: a case-control study. Int J Rheum Dis 2018; 21: 1211-1218.

59. Zheng L, Zhang Z, Sheng P, Mobasheri A. The role of metabolism in chondrocyte dysfunction and the progression of osteoarthritis. Ageing Res Rev 2021; 66: 101249.

60. Maneiro E, Martin MA, de Andres MC, Lopez-Armada MJ, Fernandez-Sueiro JL, del Hoyo P, et al. Mitochondrial respiratory activity is altered in osteoarthritic human articular chondrocytes. Arthritis Rheum 2003; 48: 700-708.

61. Anderson JR, Chokesuwattanaskul S, Phelan MM, Welting TJM, Lian LY, Peffers MJ, et al. (1)H NMR Metabolomics Identifies Underlying Inflammatory Pathology in Osteoarthritis and Rheumatoid Arthritis Synovial Joints. J Proteome Res 2018; 17: 3780-3790.

62. Adams SB, Jr., Setton LA, Kensicki E, Bolognesi MP, Toth AP, Nettles DL. Global metabolic profiling of human osteoarthritic synovium. Osteoarthritis Cartilage 2012; 20: 64-67.

63. Tetlow LC, Woolley DE. Histamine stimulates the proliferation of human articular chondrocytes in vitro and is expressed by chondrocytes in osteoarthritic cartilage. Ann Rheum Dis 2003; 62: 991-994.

64. Tetlow LC, Woolley DE. Histamine, histamine receptors (H1 and H2), and histidine decarboxylase expression by chondrocytes of osteoarthritic cartilage: an immunohistochemical study. Rheumatol Int 2005; 26: 173-178.

65. Yang G, Zhang H, Chen T, Zhu W, Ding S, Xu K, et al. Metabolic analysis of osteoarthritis subchondral bone based on UPLC/Q-TOF-MS. Anal Bioanal Chem 2016; 408: 4275-4286.

66. Maher AD, Coles C, White J, Bateman JF, Fuller ES, Burkhardt D, et al. 1H NMR spectroscopy of serum reveals unique metabolic fingerprints associated with subtypes of surgically induced osteoarthritis in sheep. J Proteome Res 2012; 11: 4261-4268.

67. Okun JG, Kolker S, Schulze A, Kohlmuller D, Olgemoller K, Lindner M, et al. A method for quantitative acylcarnitine profiling in human skin fibroblasts using unlabelled palmitic acid: diagnosis of fatty acid oxidation disorders and differentiation between biochemical phenotypes of MCAD deficiency. Biochim Biophys Acta 2002; 1584: 91-98.

68. Hugle T, Kovacs H, Heijnen IA, Daikeler T, Baisch U, Hicks JM, et al. Synovial fluid metabolomics in different forms of arthritis assessed by nuclear magnetic resonance spectroscopy. Clin Exp Rheumatol 2012; 30: 240-245.

CONCLUDING REMARKS

Since the age of three, I have been an active volunteer at St John's Lutheran Ministries Nursing Home. My aunt, the activities director for all residents, would always let me tag along with her no matter the activity whether that was for a wild game of bingo, delivering Christmas grams in an elf costume, or wheeling residents to and from meals. Some of my first memories are at this nursing home, surrounded by other's grandmas and grandpas that became my own. They taught me how to tie my shoes, sing nursery rhymes, how to play bingo, and most importantly, to always be a kid at heart no matter your age. Because of St John's Lutheran Ministries Nursing Home, I have always had such a deep love and care for the aging population. As I grew up, this love was further fostered where I continued to volunteer and never stopped playing bingo.

At Carroll College, I majored in Health Sciences and Public Health and would visit the residents during Christmas, Spring break, and over summer break I became a licensed certified nursing assistant (CNA) through the nursing home's program. This is when my badge changed from 'volunteer' to 'CNA' on wing 4, a skilled nursing unit. Residents under my care ranged from fully mobile, wheelchair, and bed bound, with few on hospice or palliative care. During my junior year of college, I started as a night-shift CNA on the surgical floor at a local hospital. Most of my patients were at the hospital for musculoskeletal related surgeries. On a typical night shift, I cared for patient X who is a 48-year-old white male, avid downhill skier, with OA. Next on my list is Patient Y who is a 75-year-old Hispanic female with numerous grandchildren, and unfortunately, has a fresh knee replacement due to OA. As I moved down my list of patients under my care, individuals ranged from mid-thirties to early nineties, varying mobility, and different races. Shared goals for all my patients, whether at the hospital or nursing home, was to make them feel cared for

while promoting a safe environment for movement whether that was within hours of surgery or going from the bathroom to bed.

Combined, these experiences as a volunteer and care provider for older individuals facing musculoskeletal diseases, such as OA, truly inspire me and my research rooted in improving the lives of the many grandmas and grandpas I cared for or simply played bingo that became family to me. In both the nursing home and hospital settings, it is evident that current treatment, intervention, and prevention measures are severely lacking. As a research field, OA has been extensively investigated, yet minimal progress has been made at the level of improving patient lives. As a field, we lack (1) optimal and improved treatment beyond total joint replacements, (2) biomarkers for early detection and drug development, and (3) a comprehensive understanding of the complex interactions of OA risk factors and musculoskeletal tissues. As a member of the scientific community who has directly cared for OA individuals, we must do better – for the sake of current and future patients. To advance OA research and improve the lives of those many OA individuals I took care of, my dissertation research was rooted in using mass spectrometry-based approaches to (1) characterize OA phenotypes and endotypes, and (2) explore OA pathogenesis through the lens of disease-associated risk factors. This research and overall approach were novel to the field of OA, enhancing our understanding of the diverse metabolic landscape of OA. My goal was to catalyze biomarker discovery and validation, as well as improve preventative measures to stop OA in its tracks.

In my dissertation, the first area of research examined OA phenotypes and endotypes of OA were generated to elucidate disease-associated mechanisms and shed light on metabolic perturbations that are associated with disease progression. Specifically, Chapters 3 and 4 unveiled

cellular mechanisms associated with disease – such as matrix, amino acid, lipid, and vitamin metabolic pathways – and metabolic indicators of disease, like cervonyl carnitine, which was higher among OA individuals compared to healthy. A notable metabolic theme that was repeatedly detected was lipid metabolism. It has been well-established that healthy cartilage utilizes both glucose and lipid as biofuels, however, OA cartilage has been shown to primarily use lipids. This "metabolic switch" temporarily supports cartilage, but over time, this leads to eventual cartilage breakdown. My work demonstrates that central to this "metabolic switch" is the carnitine shuttle, which was found to be higher in OA cartilage compared to healthy cartilage. The detection of this pathway, along with cervonyl carnitine, supports the notion of perturbed energy metabolism in end-stage OA and warrants further investigation. Future studies should further validate this "metabolic switch" in cartilage and determine if this metabolic activity is detected beyond cartilage in circulatory fluids such as serum and synovial fluid.

The second area of research I examined as described in Chapters 5-8 relates to disease-associated risk factors across tissues and fluids including synovial fluid and serum were investigated. OA is not a "one-size-fits-all" disease, and this is evident when we think about the many individuals effected by OA in our lives. Each person is unique possessing different fingerprints, eye, hair, and skin color. As much they are all visually distinct, their joints exhibit equally unique physiological and metabolic characteristics. Moreover, they present differently symptomatic where we've seen patient X, male, high BMI, with no prior injuries come in with no pain but with severe grade IV OA, whereas patient Y, female, average BMI, and is young but has terrible pain, reduced mobility, and only grade III OA. Thus, our phenotypes and endotypes of OA should account for patient diversity and everyone's own OA risk factors.

To begin investigating and delineating OA phenotypes and endotypes considering patient-specific risk factors, Chapters 5 and 6 explored the effects of injury and sex on multiple tissues, at different length scales, and in human and mouse models. The goals of these chapters were to identify injury-associated pathways, biomarkers, screening targets, and enhance our understanding of the acute metabolic response following injury. Moreover, females are more likely to be injured and experience more severe OA later in life, thus, sex-associated pathways and metabolites were examined in depth. Notably, in Chapter 5 participant sex also was shown to influence the synovial fluid metabolome, both generally within injury types. Therefore, males and females who sustained the same injury were very metabolically different from each other at the synovial fluid level.

Again, cervonyl carnitine concentration differed between male and female participants. We hypothesized that males and females rely on different metabolic pools and mechanisms – such as AMPK activation by estrogen – to meet energy demands post-injury. Cervonyl carnitine emerged as a recurrent finding across multiple studies, exhibiting distinct patterns in various tissues and contexts. In Chapter 3, despite a near-significant p-value ($p = 0.06$), cervonyl carnitine was higher in grade IV cartilage compared to III and was significantly higher in OA cartilage compared to healthy in Chapter 4. This metabolite was detected in studies of Chapter 5. However, it was found in synovial fluid post-injury with sexually dimorphic regulation. Detection of cervonyl carnitine in OA cartilage and in synovial fluid post-injury highlights its potential as a marker that can be monitored over time to oversee joint health and oxidation and predict the onset of OA considering sex. This warrants further investigation into cervonyl carnitine as a potential biomarker or druggable target.

Collectively, these chapters provide a mosaic of OA metabolism, capturing the unique fingerprints –phenotypes and endotypes – of individual patients and their disease status alongside specific risk factors. Disease- and risk factor-associated metabolic themes that were detected across multiple studies mapped to matrix, amino acid, lipid, and vitamin metabolic pathways warrant further investigation into how metabolic regulation and activity changes, or is altered, as disease progresses. Moreover, sex-associated metabolic activity mapped to glycosaminoglycan degradation and the metabolite cervonyl carnitine. Combined, this dissertation provides strong evidence supporting the use of mass spectrometry-based techniques and that these tools can be added to our "orthopedic toolbox" that we as a field use to investigate diseases such as OA. As a field, we urgently need improved treatment, screening, and prevention measures, and I believe multi-omic approaches will catalyze the future of OA to positively influence patients overall.

So, you may be asking – what comes next in this line of research? I would pursue large-scale studies and perform metabolomic analyses of circulatory fluids – including synovial fluid, plasma, and urine – alongside patient data encompassing risk factor, outcomes, radiographic imaging, and clinical assessments to ultimately refine these "OA fingerprints" across time ranging from months to years. With this approach, we will gain insight into the trajectory of disease, how it is influenced by risk factors, and varies patient to patient. Moreover, this will foster patient-centered medical treatment which holds promise for optimizing patient care, ensuring that treatment strategies are tailored to the individual rather than adopting a generic "one-size-fits-all" approach. This will unveil avenues for identifying prognostic, diagnostic, and preventative biomarkers, as well first-in-class therapeutic targets to mitigate, halt, or reverse OA progression. As a young scientist at the forefront, I say no more. We owe our family, friends, and the many

patients and residents I cared better solutions and treatments. Together, as a scientific community, we can improve all the lives of those who face OA daily, regardless of sex, gender, race, weight, socioeconomic status, and background.

REFERENCES CITED

Abdelrazig S, Ortori CA, Doherty M, Valdes AM, Chapman V, Barrett DA. Metabolic signatures of osteoarthritis in urine using liquid chromatography-high resolution tandem mass spectrometry. Metabolomics 2021; 17: 29.

Adams SB, Jr., Setton LA, Kensicki E, Bolognesi MP, Toth AP, Nettles DL. Global metabolic profiling of human osteoarthritic synovium. Osteoarthritis Cartilage 2012; 20: 64-67.

Adeva-Andany MM, Calvo-Castro I, Fernandez-Fernandez C, Donapetry-Garcia C, Pedre-Pineiro AM. Significance of l-carnitine for human health. IUBMB Life 2017; 69: 578-594.

Aguilar A, Wu S, De Luca F. P450 oxidoreductase expressed in rat chondrocytes modulates chondrogenesis via cholesterol- and Indian Hedgehog-dependent mechanisms. Endocrinology 2009; 150: 2732-2739.

Ahn JK, Kim S, Hwang J, Kim J, Kim KH, Cha HS. GC/TOF-MS-based metabolomic profiling in cultured fibroblast-like synoviocytes from rheumatoid arthritis. Joint Bone Spine 2016; 83: 707-713.

Aichler M, Walch A. MALDI Imaging mass spectrometry: current frontiers and perspectives in pathology research and practice. Lab Invest 2015; 95: 422-431.

Akasaka H, Yoshida H, Takizawa H, Hanawa N, Tobisawa T, Tanaka M, et al. The impact of elevation of serum uric acid level on the natural history of glomerular filtration rate (GFR) and its sex difference. Nephrol Dial Transplant 2014; 29: 1932-1939.

Alekos NS, Moorer MC, Riddle RC. Dual Effects of Lipid Metabolism on Osteoblast Function. Front Endocrinol (Lausanne) 2020; 11: 578194.

Alturfan AA, Uslu E, Alturfan EE, Hatemi G, Fresko I, Kokoglu E. Increased serum sialic acid levels in primary osteoarthritis and inactive rheumatoid arthritis. Tohoku J Exp Med 2007; 213: 241-248.

Amstalden van Hove ER, Smith DF, Heeren RM. A concise review of mass spectrometry imaging. J Chromatogr A 2010; 1217: 3946-3954.

Anandacoomarasamy A, Fransen M, March L. Obesity and the musculoskeletal system. Curr Opin Rheumatol 2009; 21: 71-77.

Anderson GP. Endotyping asthma: new insights into key pathogenic mechanisms in a complex, heterogeneous disease. Lancet 2008; 372: 1107-1119.

Anderson JR, Chokesuwattanaskul S, Phelan MM, Welting TJM, Lian LY, Peffers MJ, et al. (1)H NMR Metabolomics Identifies Underlying Inflammatory Pathology in Osteoarthritis and Rheumatoid Arthritis Synovial Joints. J Proteome Res 2018; 17: 3780-3790.

Anderson MJ, Diko S, Baehr LM, Baar K, Bodine SC, Christiansen BA. Contribution of mechanical unloading to trabecular bone loss following non-invasive knee injury in mice. J Orthop Res 2016; 34: 1680-1687.

Antonacci JM, Schmidt TA, Serventi LA, Cai MZ, Shu YL, Schumacher BL, et al. Effects of equine joint injury on boundary lubrication of articular cartilage by synovial fluid: role of hyaluronan. Arthritis Rheum 2012; 64: 2917-2926.

Appleton CT, Pitelka V, Henry J, Beier F. Global analyses of gene expression in early experimental osteoarthritis. Arthritis Rheum 2007; 56: 1854-1868.

Ardern CL, Taylor NF, Feller JA, Webster KE. Fifty-five per cent return to competitive sport following anterior cruciate ligament reconstruction surgery: an updated systematic review and meta-analysis including aspects of physical functioning and contextual factors. Br J Sports Med 2014; 48: 1543-1552.

Attur M, Al-Mussawir HE, Patel J, Kitay A, Dave M, Palmer G, et al. Prostaglandin E2 exerts catabolic effects in osteoarthritis cartilage: evidence for signaling via the EP4 receptor. J Immunol 2008; 181: 5082-5088.

Attur M, Krasnokutsky S, Statnikov A, Samuels J, Li Z, Friese O, et al. Low-grade inflammation in symptomatic knee osteoarthritis: prognostic value of inflammatory plasma lipids and peripheral blood leukocyte biomarkers. Arthritis Rheumatol 2015; 67: 2905-2915.

Ayral X, Pickering EH, Woodworth TG, Mackillop N, Dougados M. Synovitis: a potential predictive factor of structural progression of medial tibiofemoral knee osteoarthritis -- results of a 1 year longitudinal arthroscopic study in 422 patients. Osteoarthritis Cartilage 2005; 13: 361-367.

Bae WC, Payanal MM, Chen AC, Hsieh-Bonassera ND, Ballard BL, Lotz MK, et al. Topographic Patterns of Cartilage Lesions in Knee Osteoarthritis. Cartilage 2010; 1: 10-19.

Bagga D, Wang L, Farias-Eisner R, Glaspy JA, Reddy ST. Differential effects of prostaglandin derived from omega-6 and omega-3 polyunsaturated fatty acids on COX-2 expression and IL-6 secretion. Proc Natl Acad Sci U S A 2003; 100: 1751-1756.

Baghban F, Hosseinzadeh M, Mozaffari-Khosravi H, Dehghan A, Fallahzadeh H. The effect of L-Carnitine supplementation on clinical symptoms, C-reactive protein and malondialdehyde in obese women with knee osteoarthritis: a double blind randomized controlled trial. BMC Musculoskelet Disord 2021; 22: 195.

Baker KR, Matthan NR, Lichtenstein AH, Niu J, Guermazi A, Roemer F, et al. Association of plasma n-6 and n-3 polyunsaturated fatty acids with synovitis in the knee: the MOST study. Osteoarthritis Cartilage 2012; 20: 382-387.

Bar-Or D, Rael LT, Thomas GW, Brody EN. Inflammatory Pathways in Knee Osteoarthritis: Potential Targets for Treatment. Curr Rheumatol Rev 2015; 11: 50-58.

Barbour KE, Helmick CG, Boring M, Brady TJ. Vital Signs: Prevalence of Doctor-Diagnosed Arthritis and Arthritis-Attributable Activity Limitation - United States, 2013-2015. MMWR Morb Mortal Wkly Rep 2017; 66: 246-253.

Barnett SC, Murray MM, Flannery SW, Team BT, Menghini D, Fleming BC, et al. ACL Size, but Not Signal Intensity, Is Influenced by Sex, Body Size, and Knee Anatomy. Orthop J Sports Med 2021; 9: 23259671211063836.

Bartlett SJ, Ling SM, Mayo NE, Scott SC, Bingham CO, 3rd. Identifying common trajectories of joint space narrowing over two years in knee osteoarthritis. Arthritis Care Res (Hoboken) 2011; 63: 1722-1728.

Bastiaansen-Jenniskens YM, Siawash M, van de Lest CH, Verhaar JA, Kloppenburg M, Zuurmond AM, et al. Monounsaturated and Saturated, but Not n-6 Polyunsaturated Fatty Acids Decrease Cartilage Destruction under Inflammatory Conditions: A Preliminary Study. Cartilage 2013; 4: 321-328.

Beery AK, Zucker I. Sex bias in neuroscience and biomedical research. Neurosci Biobehav Rev 2011; 35: 565-572.

Bentley BS, Hill RV. Assessing macroscopic and microscopic indicators of osteoarthritis in the distal interphalangeal joints: a cadaveric study. Clin Anat 2007; 20: 799-807.

Bernstein P, Sticht C, Jacobi A, Liebers C, Manthey S, Stiehler M. Expression pattern differences between osteoarthritic chondrocytes and mesenchymal stem cells during chondrogenic differentiation. Osteoarthritis Cartilage 2010; 18: 1596-1607.

Bianchi ME. DAMPs, PAMPs and alarmins: all we need to know about danger. J Leukoc Biol 2007; 81: 1-5.

Bitton R. The economic burden of osteoarthritis. Am J Manag Care 2009; 15: S230-235.

Blain EJ. Involvement of the cytoskeletal elements in articular cartilage homeostasis and pathology. Int J Exp Pathol 2009; 90: 1-15.

Blaker CL, Ashton DM, Doran N, Little CB, Clarke EC. Sex- and injury-based differences in knee biomechanics in mouse models of post-traumatic osteoarthritis. J Biomech 2021; 114: 110152.

Blanco FJ, Lopez-Armada MJ, Maneiro E. Mitochondrial dysfunction in osteoarthritis. Mitochondrion 2004; 4: 715-728.

Blanco FJ, Rego I, Ruiz-Romero C. The role of mitochondria in osteoarthritis. Nat Rev Rheumatol 2011; 7: 161-169.

Boyan BD, Hart DA, Enoka RM, Nicolella DP, Resnick E, Berkley KJ, et al. Hormonal modulation of connective tissue homeostasis and sex differences in risk for osteoarthritis of the knee. Biol Sex Differ 2013; 4: 3.

Boyan BD, Tosi LL, Coutts RD, Enoka RM, Hart DA, Nicolella DP, et al. Addressing the gaps: sex differences in osteoarthritis of the knee. Biol Sex Differ 2013; 4: 4.

Brahmachary PP, Welhaven HD, June RK. Metabolomic Profiling to Understand Chondrocyte Metabolism. Methods Mol Biol 2023; 2598: 141-156.

Bricca A, Juhl CB, Grodzinsky AJ, Roos EM. Impact of a daily exercise dose on knee joint cartilage - a systematic review and meta-analysis of randomized controlled trials in healthy animals. Osteoarthritis Cartilage 2017; 25: 1223-1237.

Bricca A, Struglics A, Larsson S, Steultjens M, Juhl CB, Roos EM. Impact of Exercise Therapy on Molecular Biomarkers Related to Cartilage and Inflammation in Individuals at Risk of, or With Established, Knee Osteoarthritis: A Systematic Review and Meta-Analysis of Randomized Controlled Trials. Arthritis Care Res (Hoboken) 2019; 71: 1504-1515.

Brophy RH, Silvers HJ, Mandelbaum BR. Anterior cruciate ligament injuries: etiology and prevention. Sports Med Arthrosc Rev 2010; 18: 2-11.

Brouwers H, von Hegedus J, Toes R, Kloppenburg M, Ioan-Facsinay A. Lipid mediators of inflammation in rheumatoid arthritis and osteoarthritis. Best Pract Res Clin Rheumatol 2015; 29: 741-755.

Brown TD, Johnston RC, Saltzman CL, Marsh JL, Buckwalter JA. Posttraumatic osteoarthritis: a first estimate of incidence, prevalence, and burden of disease. J Orthop Trauma 2006; 20: 739-744.

Browning LM, Krebs JD, Jebb SA. Discrimination ratio analysis of inflammatory markers: implications for the study of inflammation in chronic disease. Metabolism 2004; 53: 899-903.

Bruder AM, Culvenor AG, King MG, Haberfield M, Roughead EA, Mastwyk J, et al. Let's talk about sex (and gender) after ACL injury: a systematic review and meta-analysis of self-reported activity and knee-related outcomes. Br J Sports Med 2023; 57: 602-610.

Bruyere O, Cooper C, Arden N, Branco J, Brandi ML, Herrero-Beaumont G, et al. Can we identify patients with high risk of osteoarthritis progression who will respond to treatment? A focus on epidemiology and phenotype of osteoarthritis. Drugs Aging 2015; 32: 179-187.

Buescher JM, Moco S, Sauer U, Zamboni N. Ultrahigh performance liquid chromatography-tandem mass spectrometry method for fast and robust quantification of anionic and aromatic metabolites. Anal Chem 2010; 82: 4403-4412.

Burns R, Graney MJ, Lummus AC, Nichols LO, Martindale-Adams J. Differences of self-reported osteoarthritis disability and race. J Natl Med Assoc 2007; 99: 1046-1051.

Buschmann MD, Gluzband YA, Grodzinsky AJ, Hunziker EB. Mechanical compression modulates matrix biosynthesis in chondrocyte/agarose culture. J Cell Sci 1995; 108 (Pt 4): 1497-1508.

Buschmann MD, Gluzband YA, Grodzinsky AJ, Kimura JH, Hunziker EB. Chondrocytes in agarose culture synthesize a mechanically functional extracellular matrix. J Orthop Res 1992; 10: 745-758.

Caprioli RM, Farmer TB, Gile J. Molecular imaging of biological samples: localization of peptides and proteins using MALDI-TOF MS. Anal Chem 1997; 69: 4751-4760.

Carlo MD, Jr., Loeser RF. Increased oxidative stress with aging reduces chondrocyte survival: correlation with intracellular glutathione levels. Arthritis Rheum 2003; 48: 3419-3430.

Carlson AK, Rawle RA, Adams E, Greenwood MC, Bothner B, June RK. Application of global metabolomic profiling of synovial fluid for osteoarthritis biomarkers. Biochem Biophys Res Commun 2018; 499: 182-188.

Carlson AK, Rawle RA, Wallace CW, Adams E, Greenwood MC, Bothner B, et al. Global metabolomic profiling of human synovial fluid for rheumatoid arthritis biomarkers. Clin Exp Rheumatol 2019; 37: 393-399.

Carlson AK, Rawle RA, Wallace CW, Brooks EG, Adams E, Greenwood MC, et al. Characterization of synovial fluid metabolomic phenotypes of cartilage morphological changes associated with osteoarthritis. Osteoarthritis Cartilage 2019; 27: 1174-1184.

Casadonte R, Kriegsmann M, Zweynert F, Friedrich K, Baretton G, Otto M, et al. Imaging mass spectrometry to discriminate breast from pancreatic cancer metastasis in formalin-fixed paraffin-embedded tissues. Proteomics 2014; 14: 956-964.

Castro-Perez JM, Kamphorst J, DeGroot J, Lafeber F, Goshawk J, Yu K, et al. Comprehensive LC-MS E lipidomic analysis using a shotgun approach and its application to biomarker detection and identification in osteoarthritis patients. J Proteome Res 2010; 9: 2377-2389.

Cerqueira E, Marinho DA, Neiva HP, Lourenco O. Inflammatory Effects of High and Moderate Intensity Exercise-A Systematic Review. Front Physiol 2019; 10: 1550.

Chan DD, Cai L, Butz KD, Nauman EA, Dickerson DA, Jonkers I, et al. Functional MRI can detect changes in intratissue strains in a full thickness and critical sized ovine cartilage defect model. J Biomech 2018; 66: 18-25.

Chan DD, Cai L, Butz KD, Trippel SB, Nauman EA, Neu CP. In vivo articular cartilage deformation: noninvasive quantification of intratissue strain during joint contact in the human knee. Sci Rep 2016; 6: 19220.

Chavan MM, Kawle PD, Mehta NG. Increased sialylation and defucosylation of plasma proteins are early events in the acute phase response. Glycobiology 2005; 15: 838-848.

Chiba K, Nango N, Kubota S, Okazaki N, Taguchi K, Osaki M, et al. Relationship between microstructure and degree of mineralization in subchondral bone of osteoarthritis: a synchrotron radiation microCT study. J Bone Miner Res 2012; 27: 1511-1517.

Christiansen BA, Anderson MJ, Lee CA, Williams JC, Yik JH, Haudenschild DR. Musculoskeletal changes following non-invasive knee injury using a novel mouse model of post-traumatic osteoarthritis. Osteoarthritis Cartilage 2012; 20: 773-782.

Christiansen BA, Guilak F, Lockwood KA, Olson SA, Pitsillides AA, Sandell LJ, et al. Non-invasive mouse models of post-traumatic osteoarthritis. Osteoarthritis Cartilage 2015; 23: 1627-1638.

Cicuttini FM, Spector TD. Genetics of osteoarthritis. Ann Rheum Dis 1996; 55: 665-667.

Cillero-Pastor B, Eijkel G, Kiss A, Blanco FJ, Heeren RM. Time-of-flight secondary ion mass spectrometry-based molecular distribution distinguishing healthy and osteoarthritic human cartilage. Anal Chem 2012; 84: 8909-8916.

Cillero-Pastor B, Eijkel GB, Blanco FJ, Heeren RM. Protein classification and distribution in osteoarthritic human synovial tissue by matrix-assisted laser desorption ionization mass spectrometry imaging. Anal Bioanal Chem 2015; 407: 2213-2222.

Cillero-Pastor B, Eijkel GB, Kiss A, Blanco FJ, Heeren RM. Matrix-assisted laser desorption ionization-imaging mass spectrometry: a new methodology to study human osteoarthritic cartilage. Arthritis Rheum 2013; 65: 710-720.

Cinque ME, Dornan GJ, Chahla J, Moatshe G, LaPrade RF. High Rates of Osteoarthritis Develop After Anterior Cruciate Ligament Surgery: An Analysis of 4108 Patients. Am J Sports Med 2018; 46: 2011-2019.

Coleman MC, Ramakrishnan PS, Brouillette MJ, Martin JA. Injurious Loading of Articular Cartilage Compromises Chondrocyte Respiratory Function. Arthritis Rheumatol 2016; 68: 662-671.

Collins JA, Wood ST, Nelson KJ, Rowe MA, Carlson CS, Chubinskaya S, et al. Oxidative Stress Promotes Peroxiredoxin Hyperoxidation and Attenuates Pro-survival Signaling in Aging Chondrocytes. J Biol Chem 2016; 291: 6641-6654.

Collins JE, Katz JN, Dervan EE, Losina E. Trajectories and risk profiles of pain in persons with radiographic, symptomatic knee osteoarthritis: data from the osteoarthritis initiative. Osteoarthritis Cartilage 2014; 22: 622-630.

Corciulo C, Cronstein BN. Signaling of the Purinergic System in the Joint. Front Pharmacol 2019; 10: 1591.

Cravatt BF, Prospero-Garcia O, Siuzdak G, Gilula NB, Henriksen SJ, Boger DL, et al. Chemical characterization of a family of brain lipids that induce sleep. Science 1995; 268: 1506-1509.

Creamer P, Lethbridge-Cejku M, Hochberg MC. Determinants of pain severity in knee osteoarthritis: effect of demographic and psychosocial variables using 3 pain measures. J Rheumatol 1999; 26: 1785-1792.

Cross M, Smith E, Hoy D, Nolte S, Ackerman I, Fransen M, et al. The global burden of hip and knee osteoarthritis: estimates from the global burden of disease 2010 study. Ann Rheum Dis 2014; 73: 1323-1330.

Croucher LJ, Crawford A, Hatton PV, Russell RG, Buttle DJ. Extracellular ATP and UTP stimulate cartilage proteoglycan and collagen accumulation in bovine articular chondrocyte pellet cultures. Biochim Biophys Acta 2000; 1502: 297-306.

Cui N, Hu M, Khalil RA. Biochemical and Biological Attributes of Matrix Metalloproteinases. Prog Mol Biol Transl Sci 2017; 147: 1-73.

Cui Z, Liu K, Wang A, Liu S, Wang F, Li J. Correlation between sialic acid levels in the synovial fluid and the radiographic severity of knee osteoarthritis. Exp Ther Med 2014; 8: 255-259.

Dalmao-Fernandez A, Lund J, Hermida-Gomez T, Vazquez-Mosquera ME, Rego-Perez I, Blanco FJ, et al. Impaired Metabolic Flexibility in the Osteoarthritis Process: A Study on Transmitochondrial Cybrids. Cells 2020; 9.

Dambrova M, Makrecka-Kuka M, Kuka J, Vilskersts R, Nordberg D, Attwood MM, et al. Acylcarnitines: Nomenclature, Biomarkers, Therapeutic Potential, Drug Targets, and Clinical Trials. Pharmacol Rev 2022; 74: 506-551.

Damyanovich AZ, Avery L, Staples JR, Marshall KW. (1)H NMR metabolic profiling of synovial fluid from patients with anterior cruciate ligament tears and hemarthrosis. Osteoarthritis Cartilage 2023; 31: 1066-1077.

Datta HK, Ng WF, Walker JA, Tuck SP, Varanasi SS. The cell biology of bone metabolism. J Clin Pathol 2008; 61: 577-587.

Davies MR, Ribeiro LR, Downey-Jones M, Needham MR, Oakley C, Wardale J. Ligands for retinoic acid receptors are elevated in osteoarthritis and may contribute to pathologic processes in the osteoarthritic joint. Arthritis Rheum 2009; 60: 1722-1732.

Decker B, Mc KB, Mc GW, Slocumb CH. Comparative distribution of proteins and glycoproteins of serum and synovial fluid. Arthritis Rheum 1959; 2: 162-177.

Demissie S, Cupples LA, Myers R, Aliabadi P, Levy D, Felson DT. Genome scan for quantity of hand osteoarthritis: the Framingham Study. Arthritis Rheum 2002; 46: 946-952.

Deveza LA, Nelson AE, Loeser RF. Phenotypes of osteoarthritis: current state and future implications. Clin Exp Rheumatol 2019; 37 Suppl 120: 64-72.

Di Virgilio F, Adinolfi E. Extracellular purines, purinergic receptors and tumor growth. Oncogene 2017; 36: 293-303.

Dillon CF, Rasch EK, Gu Q, Hirsch R. Prevalence of knee osteoarthritis in the United States: arthritis data from the Third National Health and Nutrition Examination Survey 1991-94. J Rheumatol 2006; 33: 2271-2279.

Ding KH, Cain M, Davis M, Bergson C, McGee-Lawrence M, Perkins C, et al. Amino acids as signaling molecules modulating bone turnover. Bone 2018; 115: 15-24.

Dragojevic J, Logar DB, Komadina R, Marc J. Osteoblastogenesis and adipogenesis are higher in osteoarthritic than in osteoporotic bone tissue. Arch Med Res 2011; 42: 392-397.

Dudley E, Yousef M, Wang Y, Griffiths WJ. Targeted metabolomics and mass spectrometry. Adv Protein Chem Struct Biol 2010; 80: 45-83.

Elliott RJ, Gardner DL. Changes with age in the glycosaminoglycans of human articular cartilage. Ann Rheum Dis 1979; 38: 371-377.

Esen E, Lee SY, Wice BM, Long F. PTH Promotes Bone Anabolism by Stimulating Aerobic Glycolysis via IGF Signaling. J Bone Miner Res 2015; 30: 1959-1968.

Eveque-Mourroux MR, Emans PJ, Boonen A, Claes BSR, Bouwman FG, Heeren RMA, et al. Heterogeneity of Lipid and Protein Cartilage Profiles Associated with Human Osteoarthritis with or without Type 2 Diabetes Mellitus. J Proteome Res 2021; 20: 2973-2982.

Faber SC, Eckstein F, Lukasz S, Muhlbauer R, Hohe J, Englmeier KH, et al. Gender differences in knee joint cartilage thickness, volume and articular surface areas: assessment with quantitative three-dimensional MR imaging. Skeletal Radiol 2001; 30: 144-150.

Felson DT, Lawrence RC, Dieppe PA, Hirsch R, Helmick CG, Jordan JM, et al. Osteoarthritis: new insights. Part 1: the disease and its risk factors. Ann Intern Med 2000; 133: 635-646.

Fernandes JC, Martel-Pelletier J, Pelletier JP. The role of cytokines in osteoarthritis pathophysiology. Biorheology 2002; 39: 237-246.

Fernandez-Moreno M, Rego I, Carreira-Garcia V, Blanco FJ. Genetics in osteoarthritis. Curr Genomics 2008; 9: 542-547.

Figenschau Y, Knutsen G, Shahazeydi S, Johansen O, Sveinbjornsson B. Human articular chondrocytes express functional leptin receptors. Biochem Biophys Res Commun 2001; 287: 190-197.

Findlay DM, Atkins GJ. Osteoblast-chondrocyte interactions in osteoarthritis. Curr Osteoporos Rep 2014; 12: 127-134.

Flannery CR, Little CB, Caterson B, Hughes CE. Effects of culture conditions and exposure to catabolic stimulators (IL-1 and retinoic acid) on the expression of matrix metalloproteinases (MMPs) and disintegrin metalloproteinases (ADAMs) by articular cartilage chondrocytes. Matrix Biol 1999; 18: 225-237.

Fontaine KR, Haaz S, Bartlett SJ. Are overweight and obese adults with arthritis being advised to lose weight? J Clin Rheumatol 2007; 13: 12-15.

Fraser JR, Laurent TC, Laurent UB. Hyaluronan: its nature, distribution, functions and turnover. J Intern Med 1997; 242: 27-33.

Frikha-Benayed D, Basta-Pljakic J, Majeska RJ, Schaffler MB. Regional differences in oxidative metabolism and mitochondrial activity among cortical bone osteocytes. Bone 2016; 90: 15-22.

Gandhi N, Qadeer AS, Meher A, Rachel J, Patra A, John J, et al. Costs and models used in the economic analysis of Total Knee Replacement (TKR): A systematic review. PLoS One 2023; 18: e0280371.

Garnero P, Rousseau JC, Delmas PD. Molecular basis and clinical use of biochemical markers of bone, cartilage, and synovium in joint diseases. Arthritis Rheum 2000; 43: 953-968.

George J, Gautam D, Devasenapathy N, Malhotra R. Is It Worth Delaying Total Knee Replacement as Late as Possible? A Cost-Effectiveness Analysis Using a Markov Model in the Indian Setting. Value Health Reg Issues 2021; 24: 173-180.

Gheita AA, Gheita TA, Kenawy SA. The potential role of B5: A stitch in time and switch in cytokine. Phytother Res 2020; 34: 306-314.

Gieger C, Geistlinger L, Altmaier E, Hrabe de Angelis M, Kronenberg F, Meitinger T, et al. Genetics meets metabolomics: a genome-wide association study of metabolite profiles in human serum. PLoS Genet 2008; 4: e1000282.

Gillespie PG, Muller U. Mechanotransduction by hair cells: models, molecules, and mechanisms. Cell 2009; 139: 33-44.

Gilroy DW, Newson J, Sawmynaden P, Willoughby DA, Croxtall JD. A novel role for phospholipase A2 isoforms in the checkpoint control of acute inflammation. FASEB J 2004; 18: 489-498.

Giugliano DN, Solomon JL. ACL tears in female athletes. Phys Med Rehabil Clin N Am 2007; 18: 417-438, viii.

Gkretsi V, Simopoulou T, Tsezou A. Lipid metabolism and osteoarthritis: lessons from atherosclerosis. Prog Lipid Res 2011; 50: 133-140.

Glatz JF, Luiken JJ, Bonen A. Membrane fatty acid transporters as regulators of lipid metabolism: implications for metabolic disease. Physiol Rev 2010; 90: 367-417.

Gleeson M, Bishop NC, Stensel DJ, Lindley MR, Mastana SS, Nimmo MA. The anti-inflammatory effects of exercise: mechanisms and implications for the prevention and treatment of disease. Nat Rev Immunol 2011; 11: 607-615.

Gobezie R, Kho A, Krastins B, Sarracino DA, Thornhill TS, Chase M, et al. High abundance synovial fluid proteome: distinct profiles in health and osteoarthritis. Arthritis Res Ther 2007; 9: R36.

Gold GE, Cicuttini F, Crema MD, Eckstein F, Guermazi A, Kijowski R, et al. OARSI Clinical Trials Recommendations: Hip imaging in clinical trials in osteoarthritis. Osteoarthritis Cartilage 2015; 23: 716-731.

Goldring MB, Birkhead J, Sandell LJ, Kimura T, Krane SM. Interleukin 1 suppresses expression of cartilage-specific types II and IX collagens and increases types I and III collagens in human chondrocytes. J Clin Invest 1988; 82: 2026-2037.

Goldring MB. Articular cartilage degradation in osteoarthritis. HSS J 2012; 8: 7-9.

Good CJ, Neumann EK, Butrico CE, Cassat JE, Caprioli RM, Spraggins JM. High Spatial Resolution MALDI Imaging Mass Spectrometry of Fresh-Frozen Bone. Anal Chem 2022; 94: 3165-3172.

Gottlob CA, Baker CL, Jr., Pellissier JM, Colvin L. Cost effectiveness of anterior cruciate ligament reconstruction in young adults. Clin Orthop Relat Res 1999: 272-282.

Gratal P, Lamuedra A, Medina JP, Bermejo-Alvarez I, Largo R, Herrero-Beaumont G, et al. Purinergic System Signaling in Metainflammation-Associated Osteoarthritis. Front Med (Lausanne) 2020; 7: 506.

Gray ML, Pizzanelli AM, Grodzinsky AJ, Lee RC. Mechanical and physiochemical determinants of the chondrocyte biosynthetic response. J Orthop Res 1988; 6: 777-792.

Gray ML, Pizzanelli AM, Lee RC, Grodzinsky AJ, Swann DA. Kinetics of the chondrocyte biosynthetic response to compressive load and release. Biochim Biophys Acta 1989; 991: 415-425.

Griffin LY, Albohm MJ, Arendt EA, Bahr R, Beynnon BD, Demaio M, et al. Understanding and preventing noncontact anterior cruciate ligament injuries: a review of the Hunt Valley II meeting, January 2005. Am J Sports Med 2006; 34: 1512-1532.

Guilak F, Fermor B, Keefe FJ, Kraus VB, Olson SA, Pisetsky DS, et al. The role of biomechanics and inflammation in cartilage injury and repair. Clin Orthop Relat Res 2004: 17-26.

Guilak F. Biomechanical factors in osteoarthritis. Best Pract Res Clin Rheumatol 2011; 25: 815-823.

Guntur AR, Le PT, Farber CR, Rosen CJ. Bioenergetics during calvarial osteoblast differentiation reflect strain differences in bone mass. Endocrinology 2014; 155: 1589-1595.

Hahn AK, Wallace CW, Welhaven HD, Brooks E, McAlpine M, Christiansen BA, et al. The microbiome mediates epiphyseal bone loss and metabolomic changes after acute joint trauma in mice. Osteoarthritis Cartilage 2021; 29: 882-893.

Harris MD, Anderson AE, Henak CR, Ellis BJ, Peters CL, Weiss JA. Finite element prediction of cartilage contact stresses in normal human hips. J Orthop Res 2012; 30: 1133-1139.

Hayashi D, Roemer FW, Guermazi A. Imaging for osteoarthritis. Ann Phys Rehabil Med 2016; 59: 161-169.

Heidari B. Knee osteoarthritis prevalence, risk factors, pathogenesis and features: Part I. Caspian J Intern Med 2011; 2: 205-212.

Henak CR, Ateshian GA, Weiss JA. Finite element prediction of transchondral stress and strain in the human hip. J Biomech Eng 2014; 136: 021021.

Hewett TE, Myer GD, Ford KR. Anterior cruciate ligament injuries in female athletes: Part 1, mechanisms and risk factors. Am J Sports Med 2006; 34: 299-311.

Hillenkamp F, Karas M, Beavis RC, Chait BT. Matrix-assisted laser desorption/ionization mass spectrometry of biopolymers. Anal Chem 1991; 63: 1193A-1203A.

Hislop BD, Devine C, June RK, Heveran CM. Subchondral bone structure and synovial fluid metabolism are altered in injured and contralateral limbs 7 days after non-invasive joint injury in skeletally-mature C57BL/6 mice. Osteoarthritis Cartilage 2022.

Hitt K, Shurman JR, 2nd, Greene K, McCarthy J, Moskal J, Hoeman T, et al. Anthropometric measurements of the human knee: correlation to the sizing of current knee arthroplasty systems. J Bone Joint Surg Am 2003; 85-A Suppl 4: 115-122.

Hjertquist SO, Lemperg R. Identification and concentration of the glycosaminoglycans of human articular cartilage in relation to age and osteoarthritis. Calcif Tissue Res 1972; 10: 223-237.

Hla T, Dannenberg AJ. Sphingolipid signaling in metabolic disorders. Cell Metab 2012; 16: 420-434.

Ho CS, Lam CW, Chan MH, Cheung RC, Law LK, Lit LC, et al. Electrospray ionisation mass spectrometry: principles and clinical applications. Clin Biochem Rev 2003; 24: 3-12.

Holland WL, Brozinick JT, Wang LP, Hawkins ED, Sargent KM, Liu Y, et al. Inhibition of ceramide synthesis ameliorates glucocorticoid-, saturated-fat-, and obesity-induced insulin resistance. Cell Metab 2007; 5: 167-179.

Hootman JM, Helmick CG, Barbour KE, Theis KA, Boring MA. Updated Projected Prevalence of Self-Reported Doctor-Diagnosed Arthritis and Arthritis-Attributable Activity Limitation Among US Adults, 2015-2040. Arthritis Rheumatol 2016; 68: 1582-1587.

Hootman JM, Helmick CG. Projections of US prevalence of arthritis and associated activity limitations. Arthritis Rheum 2006; 54: 226-229.

Horning EC, Horning MG. Metabolic profiles: gas-phase methods for analysis of metabolites. Clin Chem 1971; 17: 802-809.

Hoult DI, Busby SJ, Gadian DG, Radda GK, Richards RE, Seeley PJ. Observation of tissue metabolites using 31P nuclear magnetic resonance. Nature 1974; 252: 285-287.

Hu Y, Wu Q, Qiao Y, Zhang P, Dai W, Tao H, et al. Disturbances in Metabolic Pathways and the Identification of a Potential Biomarker Panel for Early Cartilage Degeneration in a Rabbit Anterior Cruciate Ligament Transection Model. Cartilage 2021; 13: 1376S-1387S.

Hugle T, Kovacs H, Heijnen IA, Daikeler T, Baisch U, Hicks JM, et al. Synovial fluid metabolomics in different forms of arthritis assessed by nuclear magnetic resonance spectroscopy. Clin Exp Rheumatol 2012; 30: 240-245.

Hunter DJ, Gerstenfeld L, Bishop G, Davis AD, Mason ZD, Einhorn TA, et al. Bone marrow lesions from osteoarthritis knees are characterized by sclerotic bone that is less well mineralized. Arthritis Res Ther 2009; 11: R11.

Igari T, Tsuchizawa M, Shimamura T. Alteration of tryptophan metabolism in the synovial fluid of patients with rheumatoid arthritis and osteoarthritis. Tohoku J Exp Med 1987; 153: 79-86.

Ingram JG, Fields SK, Yard EE, Comstock RD. Epidemiology of knee injuries among boys and girls in US high school athletics. Am J Sports Med 2008; 36: 1116-1122.

Ingvarsson T, Stefansson SE, Gulcher JR, Jonsson HH, Jonsson H, Frigge ML, et al. A large Icelandic family with early osteoarthritis of the hip associated with a susceptibility locus on chromosome 16p. Arthritis Rheum 2001; 44: 2548-2555.

Ioan-Facsinay A, Kloppenburg M. Bioactive lipids in osteoarthritis: risk or benefit? Curr Opin Rheumatol 2018; 30: 108-113.

Jaalouk DE, Lammerding J. Mechanotransduction gone awry. Nat Rev Mol Cell Biol 2009; 10: 63-73.

Jay GD, Elsaid KA, Kelly KA, Anderson SC, Zhang L, Teeple E, et al. Prevention of cartilage degeneration and gait asymmetry by lubricin tribosupplementation in the rat following anterior cruciate ligament transection. Arthritis Rheum 2012; 64: 1162-1171.

Jay GD, Torres JR, Warman ML, Laderer MC, Breuer KS. The role of lubricin in the mechanical behavior of synovial fluid. Proc Natl Acad Sci U S A 2007; 104: 6194-6199.

Jewett MC, Hofmann G, Nielsen J. Fungal metabolite analysis in genomics and phenomics. Curr Opin Biotechnol 2006; 17: 191-197.

Jones HW, Jr., McKusick VA, Harper PS, Wuu KD. George Otto Gey. (1899-1970). The HeLa cell and a reappraisal of its origin. Obstet Gynecol 1971; 38: 945-949.

Jonsson P, Bruce SJ, Moritz T, Trygg J, Sjostrom M, Plumb R, et al. Extraction, interpretation and validation of information for comparing samples in metabolic LC/MS data sets. Analyst 2005; 130: 701-707.

Jordan JM, Helmick CG, Renner JB, Luta G, Dragomir AD, Woodard J, et al. Prevalence of knee symptoms and radiographic and symptomatic knee osteoarthritis in African Americans and Caucasians: the Johnston County Osteoarthritis Project. J Rheumatol 2007; 34: 172-180.

June RK, Liu-Bryan R, Long F, Griffin TM. Emerging role of metabolic signaling in synovial joint remodeling and osteoarthritis. J Orthop Res 2016; 34: 2048-2058.

Jutila AA, Zignego DL, Hwang BK, Hilmer JK, Hamerly T, Minor CA, et al. Candidate mediators of chondrocyte mechanotransduction via targeted and untargeted metabolomic measurements. Arch Biochem Biophys 2014; 545: 116-123.

Jutila AA, Zignego DL, Schell WJ, June RK. Encapsulation of chondrocytes in high-stiffness agarose microenvironments for in vitro modeling of osteoarthritis mechanotransduction. Ann Biomed Eng 2015; 43: 1132-1144.

Kang KY, Lee SH, Jung SM, Park SH, Jung BH, Ju JH. Downregulation of Tryptophan-related Metabolomic Profile in Rheumatoid Arthritis Synovial Fluid. J Rheumatol 2015; 42: 2003-2011.

Kaprio J, Kujala UM, Peltonen L, Koskenvuo M. Genetic liability to osteoarthritis may be greater in women than men. BMJ 1996; 313: 232.

Karas M, Kruger R. Ion formation in MALDI: the cluster ionization mechanism. Chem Rev 2003; 103: 427-440.

Karsdal MA, Bihlet A, Byrjalsen I, Alexandersen P, Ladel C, Michaels M, et al. OA phenotypes, rather than disease stage, drive structural progression--identification of structural progressors from 2 phase III randomized clinical studies with symptomatic knee OA. Osteoarthritis Cartilage 2015; 23: 550-558.

Karsenty G. Convergence between bone and energy homeostases: leptin regulation of bone mass. Cell Metab 2006; 4: 341-348.

Katz JN, Arant KR, Loeser RF. Diagnosis and Treatment of Hip and Knee Osteoarthritis: A Review. JAMA 2021; 325: 568-578.

Kawamoto T, Kawamoto K. Preparation of thin frozen sections from nonfixed and undecalcified hard tissues using Kawamot's film method (2012). Methods Mol Biol 2014; 1130: 149-164.

Kellgren JH, Lawrence JS. Radiological assessment of osteo-arthrosis. Ann Rheum Dis 1957; 16: 494-502.

Kessner D, Chambers M, Burke R, Agus D, Mallick P. ProteoWizard: open source software for rapid proteomics tools development. Bioinformatics 2008; 24: 2534-2536.

Kevorkova O, Martineau C, Martin-Falstrault L, Sanchez-Dardon J, Brissette L, Moreau R. Low-bone-mass phenotype of deficient mice for the cluster of differentiation 36 (CD36). PLoS One 2013; 8: e77701.

Kim S, Hwang J, Kim J, Ahn JK, Cha HS, Kim KH. Metabolite profiles of synovial fluid change with the radiographic severity of knee osteoarthritis. Joint Bone Spine 2017; 84: 605-610.

Kim S, Hwang J, Kim J, Lee SH, Cheong YE, Lee S, et al. Metabolic discrimination of synovial fluid between rheumatoid arthritis and osteoarthritis using gas chromatography/time-of-flight mass spectrometry. Metabolomics 2022; 18: 48.

Kim S, Hwang J, Xuan J, Jung YH, Cha HS, Kim KH. Global metabolite profiling of synovial fluid for the specific diagnosis of rheumatoid arthritis from other inflammatory arthritis. PLoS One 2014; 9: e97501.

King LK, March L, Anandacoomarasamy A. Obesity & osteoarthritis. Indian J Med Res 2013; 138: 185-193.

Kinney RC, Schwartz Z, Week K, Lotz MK, Boyan BD. Human articular chondrocytes exhibit sexual dimorphism in their responses to 17beta-estradiol. Osteoarthritis Cartilage 2005; 13: 330-337.

Kohn MD, Sassoon AA, Fernando ND. Classifications in Brief: Kellgren-Lawrence Classification of Osteoarthritis. Clin Orthop Relat Res 2016; 474: 1886-1893.

Koolpe M, Pearson D, Benton HP. Expression of both P1 and P2 purine receptor genes by human articular chondrocytes and profile of ligand-mediated prostaglandin E2 release. Arthritis Rheum 1999; 42: 258-267.

Kosakai O. [Clinical relevance of sialic acids determination in serum and synovial fluid in orthopaedic disorders]. Rinsho Byori 1991; 39: 197-207.

Kosinska MK, Liebisch G, Lochnit G, Wilhelm J, Klein H, Kaesser U, et al. A lipidomic study of phospholipid classes and species in human synovial fluid. Arthritis Rheum 2013; 65: 2323-2333.

Kosinska MK, Ludwig TE, Liebisch G, Zhang R, Siebert HC, Wilhelm J, et al. Articular Joint Lubricants during Osteoarthritis and Rheumatoid Arthritis Display Altered Levels and Molecular Species. PLoS One 2015; 10: e0125192.

Kulkarni P, Deshpande S, Koppikar S, Patil S, Ingale D, Harsulkar A. Glycosaminoglycan measured from synovial fluid serves as a useful indicator for progression of Osteoarthritis and complements Kellgren-Lawrence Score. BBA Clin 2016; 6: 1-4.

Kumagai H, Sacktor B, Filburn CR. Purinergic regulation of cytosolic calcium and phosphoinositide metabolism in rat osteoblast-like osteosarcoma cells. J Bone Miner Res 1991; 6: 697-708.

Lane RS, Fu Y, Matsuzaki S, Kinter M, Humphries KM, Griffin TM. Mitochondrial respiration and redox coupling in articular chondrocytes. Arthritis Res Ther 2015; 17: 54.

Lawrence T, Willoughby DA, Gilroy DW. Anti-inflammatory lipid mediators and insights into the resolution of inflammation. Nat Rev Immunol 2002; 2: 787-795.

Lee YJ, Lee EB, Kwon YE, Lee JJ, Cho WS, Kim HA, et al. Effect of estrogen on the expression of matrix metalloproteinase (MMP)-1, MMP-3, and MMP-13 and tissue inhibitor of metalloproternase-1 in osteoarthritis chondrocytes. Rheumatol Int 2003; 23: 282-288.

Leimer EM, Tanenbaum LM, Nettles DL, Bell RD, Easley ME, Setton LA, et al. Amino Acid Profile of Synovial Fluid Following Intra-articular Ankle Fracture. Foot Ankle Int 2018; 39: 1169-1177.

Leonardi R, Jackowski S. Biosynthesis of Pantothenic Acid and Coenzyme A. EcoSal Plus 2007; 2.

Leong A. Sexual dimorphism of the pelvic architecture: a struggling response to destructive and parsimonious forces by natural & mate selection. Mcgill J Med 2006; 9: 61-66.

Lerner RA, Siuzdak G, Prospero-Garcia O, Henriksen SJ, Boger DL, Cravatt BF. Cerebrodiene: a brain lipid isolated from sleep-deprived cats. Proc Natl Acad Sci U S A 1994; 91: 9505-9508.

Li B, Lee WC, Song C, Ye L, Abel ED, Long F. Both aerobic glycolysis and mitochondrial respiration are required for osteoclast differentiation. FASEB J 2020; 34: 11058-11067.

Li Y, Xiao W, Luo W, Zeng C, Deng Z, Ren W, et al. Alterations of amino acid metabolism in osteoarthritis: its implications for nutrition and health. Amino Acids 2016; 48: 907-914.

Lippiello L, Walsh T, Fienhold M. The association of lipid abnormalities with tissue pathology in human osteoarthritic articular cartilage. Metabolism 1991; 40: 571-576.

Little CB, Hunter DJ. Post-traumatic osteoarthritis: from mouse models to clinical trials. Nat Rev Rheumatol 2013; 9: 485-497.

Lockwood KA, Chu BT, Anderson MJ, Haudenschild DR, Christiansen BA. Comparison of loading rate-dependent injury modes in a murine model of post-traumatic osteoarthritis. J Orthop Res 2014; 32: 79-88.

Loeser RF, Goldring SR, Scanzello CR, Goldring MB. Osteoarthritis: a disease of the joint as an organ. Arthritis Rheum 2012; 64: 1697-1707.

Loeser RF, Pathmasiri W, Sumner SJ, McRitchie S, Beavers D, Saxena P, et al. Association of urinary metabolites with radiographic progression of knee osteoarthritis in overweight and obese adults: an exploratory study. Osteoarthritis Cartilage 2016; 24: 1479-1486.

Loeser RF. The Role of Aging in the Development of Osteoarthritis. Trans Am Clin Climatol Assoc 2017; 128: 44-54.

Lohmander LS, Englund PM, Dahl LL, Roos EM. The long-term consequence of anterior cruciate ligament and meniscus injuries: osteoarthritis. Am J Sports Med 2007; 35: 1756-1769.

Long F. Glucose metabolism in skeletal cells. Bone Rep 2022; 17: 101640.

Long H, Liu Q, Yin H, Wang K, Diao N, Zhang Y, et al. Prevalence trends of site-specific osteoarthritis from 1990 to 2019: findings from the Global Burden of Disease Study 2019. Arthritis Rheumatol 2022.

Lotke PA, Granda JL. Alterations in the permeability of articular cartilage by proteolytic enzymes. Arthritis Rheum 1972; 15: 302-308.

Loughlin J. Familial inheritance of osteoarthritis: documented family subsets. Clin Orthop Relat Res 2004: S22-25.

Lu B, Driban JB, Xu C, Lapane KL, McAlindon TE, Eaton CB. Dietary Fat Intake and Radiographic Progression of Knee Osteoarthritis: Data From the Osteoarthritis Initiative. Arthritis Care Res (Hoboken) 2017; 69: 368-375.

Luo G, Ducy P, McKee MD, Pinero GJ, Loyer E, Behringer RR, et al. Spontaneous calcification of arteries and cartilage in mice lacking matrix GLA protein. Nature 1997; 386: 78-81.

Maher AD, Coles C, White J, Bateman JF, Fuller ES, Burkhardt D, et al. 1H NMR spectroscopy of serum reveals unique metabolic fingerprints associated with subtypes of surgically induced osteoarthritis in sheep. J Proteome Res 2012; 11: 4261-4268.

Malek Mahdavi A, Mahdavi R, Kolahi S. Effects of l-Carnitine Supplementation on Serum Inflammatory Factors and Matrix Metalloproteinase Enzymes in Females with Knee Osteoarthritis: A Randomized, Double-Blind, Placebo-Controlled Pilot Study. J Am Coll Nutr 2016; 35: 597-603.

Maneiro E, Martin MA, de Andres MC, Lopez-Armada MJ, Fernandez-Sueiro JL, del Hoyo P, et al. Mitochondrial respiratory activity is altered in osteoarthritic human articular chondrocytes. Arthritis Rheum 2003; 48: 700-708.

Mankin HJ, Lippiello L. Biochemical and metabolic abnormalities in articular cartilage from osteo-arthritic human hips. J Bone Joint Surg Am 1970; 52: 424-434.

Mansouri R, Jouan Y, Hay E, Blin-Wakkach C, Frain M, Ostertag A, et al. Osteoblastic heparan sulfate glycosaminoglycans control bone remodeling by regulating Wnt signaling and the crosstalk between bone surface and marrow cells. Cell Death Dis 2017; 8: e2902.

Maroudas A, Bullough P, Swanson SA, Freeman MA. The permeability of articular cartilage. J Bone Joint Surg Br 1968; 50: 166-177.

Maruotti N, Corrado A, Cantatore FP. Osteoblast role in osteoarthritis pathogenesis. J Cell Physiol 2017; 232: 2957-2963.

Mathiessen A, Conaghan PG. Synovitis in osteoarthritis: current understanding with therapeutic implications. Arthritis Res Ther 2017; 19: 18.

McCutchen CN, Zignego DL, June RK. Metabolic responses induced by compression of chondrocytes in variable-stiffness microenvironments. J Biomech 2017; 64: 49-58.

Mengshol JA, Vincenti MP, Coon CI, Barchowsky A, Brinckerhoff CE. Interleukin-1 induction of collagenase 3 (matrix metalloproteinase 13) gene expression in chondrocytes requires p38, c-Jun N-terminal kinase, and nuclear factor kappaB: differential regulation of collagenase 1 and collagenase 3. Arthritis Rheum 2000; 43: 801-811.

Merrill AH, Jr. Sphingolipid and glycosphingolipid metabolic pathways in the era of sphingolipidomics. Chem Rev 2011; 111: 6387-6422.

Mesiha M, Zurakowski D, Soriano J, Nielson JH, Zarins B, Murray MM. Pathologic characteristics of the torn human meniscus. Am J Sports Med 2007; 35: 103-112.

Messier SP, Legault C, Mihalko S, Miller GD, Loeser RF, DeVita P, et al. The Intensive Diet and Exercise for Arthritis (IDEA) trial: design and rationale. BMC Musculoskelet Disord 2009; 10: 93.

Messier SP, Loeser RF, Miller GD, Morgan TM, Rejeski WJ, Sevick MA, et al. Exercise and dietary weight loss in overweight and obese older adults with knee osteoarthritis: the Arthritis, Diet, and Activity Promotion Trial. Arthritis Rheum 2004; 50: 1501-1510.

Messier SP, Mihalko SL, Legault C, Miller GD, Nicklas BJ, DeVita P, et al. Effects of intensive diet and exercise on knee joint loads, inflammation, and clinical outcomes among overweight and obese adults with knee osteoarthritis: the IDEA randomized clinical trial. JAMA 2013; 310: 1263-1273.

Mickiewicz B, Heard BJ, Chau JK, Chung M, Hart DA, Shrive NG, et al. Metabolic profiling of synovial fluid in a unilateral ovine model of anterior cruciate ligament reconstruction of the knee suggests biomarkers for early osteoarthritis. J Orthop Res 2015; 33: 71-77.

Miller VM. In pursuit of scientific excellence: sex matters. Adv Physiol Educ 2012; 36: 83-84.

Mingorance C, Rodriguez-Rodriguez R, Justo ML, Herrera MD, de Sotomayor MA. Pharmacological effects and clinical applications of propionyl-L-carnitine. Nutr Rev 2011; 69: 279-290.

Misra D, Booth SL, Tolstykh I, Felson DT, Nevitt MC, Lewis CE, et al. Vitamin K deficiency is associated with incident knee osteoarthritis. Am J Med 2013; 126: 243-248.

Moholdt T, Parr EB, Devlin BL, Debik J, Giskeodegard G, Hawley JA. The effect of morning vs evening exercise training on glycaemic control and serum metabolites in overweight/obese men: a randomised trial. Diabetologia 2021; 64: 2061-2076.

Morris SM, Jr. Arginine: beyond protein. Am J Clin Nutr 2006; 83: 508S-512S.

Mumford SL, Dasharathy SS, Pollack AZ, Perkins NJ, Mattison DR, Cole SR, et al. Serum uric acid in relation to endogenous reproductive hormones during the menstrual cycle: findings from the BioCycle study. Hum Reprod 2013; 28: 1853-1862.

Murphy NJ, Eyles JP, Hunter DJ. Hip Osteoarthritis: Etiopathogenesis and Implications for Management. Adv Ther 2016; 33: 1921-1946.

Mustonen AM, Nieminen P. Fatty Acids and Oxylipins in Osteoarthritis and Rheumatoid Arthritis-a Complex Field with Significant Potential for Future Treatments. Curr Rheumatol Rep 2021; 23: 41.

Nelson AE, Renner JB, Schwartz TA, Kraus VB, Helmick CG, Jordan JM. Differences in multijoint radiographic osteoarthritis phenotypes among African Americans and Caucasians: the Johnston County Osteoarthritis project. Arthritis Rheum 2011; 63: 3843-3852.

Nelson KA, Daniels GJ, Fournie JW, Hemmer MJ. Optimization of whole-body zebrafish sectioning methods for mass spectrometry imaging. J Biomol Tech 2013; 24: 119-127.

Neogi T. The epidemiology and impact of pain in osteoarthritis. Osteoarthritis Cartilage 2013; 21: 1145-1153.

Nicholson JK, Connelly J, Lindon JC, Holmes E. Metabonomics: a platform for studying drug toxicity and gene function. Nat Rev Drug Discov 2002; 1: 153-161.

Nieminen P, Hamalainen W, Savinainen J, Lehtonen M, Lehtiniemi S, Rinta-Paavola J, et al. Metabolomics of Synovial Fluid and Infrapatellar Fat Pad in Patients with Osteoarthritis or Rheumatoid Arthritis. Inflammation 2022; 45: 1101-1117.

Norris JL, Caprioli RM. Analysis of tissue specimens by matrix-assisted laser desorption/ionization imaging mass spectrometry in biological and clinical research. Chem Rev 2013; 113: 2309-2342.

O'Connor MI. Sex differences in osteoarthritis of the hip and knee. J Am Acad Orthop Surg 2007; 15 Suppl 1: S22-25.

O'Conor CJ, Leddy HA, Benefield HC, Liedtke WB, Guilak F. TRPV4-mediated mechanotransduction regulates the metabolic response of chondrocytes to dynamic loading. Proc Natl Acad Sci U S A 2014; 111: 1316-1321.

Ohnishi A, Osaki T, Matahira Y, Tsuka T, Imagawa T, Okamoto Y, et al. Correlation of plasma amino acid concentrations and chondroprotective effects of glucosamine and fish collagen peptide on the development of osteoarthritis. J Vet Med Sci 2013; 75: 497-502.

Oiestad BE, Engebretsen L, Storheim K, Risberg MA. Knee osteoarthritis after anterior cruciate ligament injury: a systematic review. Am J Sports Med 2009; 37: 1434-1443.

Okun JG, Kolker S, Schulze A, Kohlmuller D, Olgemoller K, Lindner M, et al. A method for quantitative acylcarnitine profiling in human skin fibroblasts using unlabelled palmitic acid: diagnosis of fatty acid oxidation disorders and differentiation between biochemical phenotypes of MCAD deficiency. Biochim Biophys Acta 2002; 1584: 91-98

Oliveria SA, Felson DT, Cirillo PA, Reed JI, Walker AM. Body weight, body mass index, and incident symptomatic osteoarthritis of the hand, hip, and knee. Epidemiology 1999; 10: 161-166.

Oliviero F, Lo Nigro A, Bernardi D, Giunco S, Baldo G, Scanu A, et al. A comparative study of serum and synovial fluid lipoprotein levels in patients with various arthritides. Clin Chim Acta 2012; 413: 303-307.

Oosthuyse T, Bosch AN. The effect of the menstrual cycle on exercise metabolism: implications for exercise performance in eumenorrhoeic women. Sports Med 2010; 40: 207-227.

Orr AW, Helmke BP, Blackman BR, Schwartz MA. Mechanisms of mechanotransduction. Dev Cell 2006; 10: 11-20.

Paluch EK, Nelson CM, Biais N, Fabry B, Moeller J, Pruitt BL, et al. Mechanotransduction: use the force(s). BMC Biol 2015; 13: 47.

Palumbo C, Ferretti M. The Osteocyte: From "Prisoner" to "Orchestrator". J Funct Morphol Kinesiol 2021; 6.

Pan J, Wang B, Li W, Zhou X, Scherr T, Yang Y, et al. Elevated cross-talk between subchondral bone and cartilage in osteoarthritic joints. Bone 2012; 51: 212-217.

Pang Z, Zhou G, Ewald J, Chang L, Hacariz O, Basu N, et al. Using MetaboAnalyst 5.0 for LC-HRMS spectra processing, multi-omics integration and covariate adjustment of global metabolomics data. Nat Protoc 2022; 17: 1735-1761.

Park S, Baek IJ, Ryu JH, Chun CH, Jin EJ. PPARalpha-ACOT12 axis is responsible for maintaining cartilage homeostasis through modulating de novo lipogenesis. Nat Commun 2022; 13: 3.

Parmelee PA, Harralson TL, McPherron JA, DeCoster J, Schumacher HR. Pain, disability, and depression in osteoarthritis: effects of race and sex. J Aging Health 2012; 24: 168-187.

Patti GJ, Yanes O, Siuzdak G. Innovation: Metabolomics: the apogee of the omics trilogy. Nat Rev Mol Cell Biol 2012; 13: 263-269.

Pedersen BK, Saltin B. Evidence for prescribing exercise as therapy in chronic disease. Scand J Med Sci Sports 2006; 16 Suppl 1: 3-63.

Peffers MJ, Cillero-Pastor B, Eijkel GB, Clegg PD, Heeren RM. Matrix assisted laser desorption ionization mass spectrometry imaging identifies markers of ageing and osteoarthritic cartilage. Arthritis Res Ther 2014; 16: R110.

Pereira H, Caridade SG, Frias AM, Silva-Correia J, Pereira DR, Cengiz IF, et al. Biomechanical and cellular segmental characterization of human meniscus: building the basis for Tissue Engineering therapies. Osteoarthritis Cartilage 2014; 22: 1271-1281.

Peters AE, Akhtar R, Comerford EJ, Bates KT. The effect of ageing and osteoarthritis on the mechanical properties of cartilage and bone in the human knee joint. Sci Rep 2018; 8: 5931.

Petersen AM, Pedersen BK. The anti-inflammatory effect of exercise. J Appl Physiol (1985) 2005; 98: 1154-1162.

Pinto-Cardoso R, Pereira-Costa F, Pedro Faria J, Bandarrinha P, Bessa-Andres C, Correia-de-Sa P, et al. Adenosinergic signalling in chondrogenesis and cartilage homeostasis: Friend or foe? Biochem Pharmacol 2020; 174: 113784.

Plotnikoff R, Karunamuni N, Lytvyak E, Penfold C, Schopflocher D, Imayama I, et al. Osteoarthritis prevalence and modifiable factors: a population study. BMC Public Health 2015; 15: 1195.

Poilvache PL, Insall JN, Scuderi GR, Font-Rodriguez DE. Rotational landmarks and sizing of the distal femur in total knee arthroplasty. Clin Orthop Relat Res 1996: 35-46.

Pornprasertsuk S, Duarte WR, Mochida Y, Yamauchi M. Overexpression of lysyl hydroxylase-2b leads to defective collagen fibrillogenesis and matrix mineralization. J Bone Miner Res 2005; 20: 81-87.

Poulet B, Staines KA. New developments in osteoarthritis and cartilage biology. Curr Opin Pharmacol 2016; 28: 8-13.

Pousinis P, Gowler PRW, Burston JJ, Ortori CA, Chapman V, Barrett DA. Lipidomic identification of plasma lipids associated with pain behaviour and pathology in a mouse model of osteoarthritis. Metabolomics 2020; 16: 32.

Pratta MA, Yao W, Decicco C, Tortorella MD, Liu RQ, Copeland RA, et al. Aggrecan protects cartilage collagen from proteolytic cleavage. J Biol Chem 2003; 278: 45539-45545.

Price PA, Williamson MK, Haba T, Dell RB, Jee WS. Excessive mineralization with growth plate closure in rats on chronic warfarin treatment. Proc Natl Acad Sci U S A 1982; 79: 7734-7738.

Purdom T, Kravitz L, Dokladny K, Mermier C. Understanding the factors that effect maximal fat oxidation. J Int Soc Sports Nutr 2018; 15: 3.

Racunica TL, Teichtahl AJ, Wang Y, Wluka AE, English DR, Giles GG, et al. Effect of physical activity on articular knee joint structures in community-based adults. Arthritis Rheum 2007; 57: 1261-1268.

Reyes AM, Katz JN. Racial/Ethnic and Socioeconomic Disparities in Osteoarthritis Management. Rheum Dis Clin North Am 2021; 47: 21-40.

Richardson DW, Dodge GR. Effects of interleukin-1beta and tumor necrosis factor-alpha on expression of matrix-related genes by cultured equine articular chondrocytes. Am J Vet Res 2000; 61: 624-630.

Rocha B, Cillero-Pastor B, Ruiz-Romero C, Paine MRL, Canete JD, Heeren RMA, et al. Identification of a distinct lipidomic profile in the osteoarthritic synovial membrane by mass spectrometry imaging. Osteoarthritis Cartilage 2021; 29: 750-761.

Rockel JS, Kapoor M. The Metabolome and Osteoarthritis: Possible Contributions to Symptoms and Pathology. Metabolites 2018; 8.

Rumney RM, Wang N, Agrawal A, Gartland A. Purinergic signalling in bone. Front Endocrinol (Lausanne) 2012; 3: 116.

Sah RL, Doong JY, Grodzinsky AJ, Plaas AH, Sandy JD. Effects of compression on the loss of newly synthesized proteoglycans and proteins from cartilage explants. Arch Biochem Biophys 1991; 286: 20-29.

Sah RL, Grodzinsky AJ, Plaas AH, Sandy JD. Effects of tissue compression on the hyaluronate-binding properties of newly synthesized proteoglycans in cartilage explants. Biochem J 1990; 267: 803-808.

Saito M, Marumo K. Collagen cross-links as a determinant of bone quality: a possible explanation for bone fragility in aging, osteoporosis, and diabetes mellitus. Osteoporos Int 2010; 21: 195-214.

Salinas D, Minor CA, Carlson RP, McCutchen CN, Mumey BM, June RK. Combining Targeted Metabolomic Data with a Model of Glucose Metabolism: Toward Progress in Chondrocyte Mechanotransduction. PLoS One 2017; 12: e0168326.

Salinas D, Mumey BM, June RK. Physiological dynamic compression regulates central energy metabolism in primary human chondrocytes. Biomech Model Mechanobiol 2019; 18: 69-77.

Sanchez-Adams J, Leddy HA, McNulty AL, O'Conor CJ, Guilak F. The mechanobiology of articular cartilage: bearing the burden of osteoarthritis. Curr Rheumatol Rep 2014; 16: 451.

Sanghi D, Mishra A, Sharma AC, Raj S, Mishra R, Kumari R, et al. Elucidation of dietary risk factors in osteoarthritis knee-a case-control study. J Am Coll Nutr 2015; 34: 15-20.

Sarma AV, Powell GL, LaBerge M. Phospholipid composition of articular cartilage boundary lubricant. J Orthop Res 2001; 19: 671-676.

Schilling K, Brown E, Zhang X. NAD(P)H autofluorescence lifetime imaging enables single cell analyses of cellular metabolism of osteoblasts in vitro and in vivo via two-photon microscopy. Bone 2022; 154: 116257.

Schmidt TA, Gastelum NS, Nguyen QT, Schumacher BL, Sah RL. Boundary lubrication of articular cartilage: role of synovial fluid constituents. Arthritis Rheum 2007; 56: 882-891.

Schofl C, Cuthbertson KS, Walsh CA, Mayne C, Cobbold P, von zur Muhlen A, et al. Evidence for P2-purinoceptors on human osteoblast-like cells. J Bone Miner Res 1992; 7: 485-491.

Schwarz IM, Hills BA. Surface-active phospholipid as the lubricating component of lubricin. Br J Rheumatol 1998; 37: 21-26.

Seeley EH, Caprioli RM. Molecular imaging of proteins in tissues by mass spectrometry. Proc Natl Acad Sci U S A 2008; 105: 18126-18131.

Seifer DR, Furman BD, Guilak F, Olson SA, Brooks SC, 3rd, Kraus VB. Novel synovial fluid recovery method allows for quantification of a marker of arthritis in mice. Osteoarthritis Cartilage 2008; 16: 1532-1538.

Seito N, Yamashita T, Tsukuda Y, Matsui Y, Urita A, Onodera T, et al. Interruption of glycosphingolipid synthesis enhances osteoarthritis development in mice. Arthritis Rheum 2012; 64: 2579-2588.

Sekar S, Shafie SR, Prasadam I, Crawford R, Panchal SK, Brown L, et al. Saturated fatty acids induce development of both metabolic syndrome and osteoarthritis in rats. Sci Rep 2017; 7: 46457.

Sellam J, Berenbaum F. Is osteoarthritis a metabolic disease? Joint Bone Spine 2013; 80: 568-573.

Setton LA, Mow VC, Muller FJ, Pita JC, Howell DS. Mechanical behavior and biochemical composition of canine knee cartilage following periods of joint disuse and disuse with remobilization. Osteoarthritis Cartilage 1997; 5: 1-16.

Shah K, McCormack CE, Bradbury NA. Do you know the sex of your cells? Am J Physiol Cell Physiol 2014; 306: C3-18.

Shanmugaraj N, Rutten T, Svatos A, Schnurbusch T, Mock HP. Fast and Reproducible Matrix Deposition for MALDI Mass Spectrometry Imaging with Improved Glass Sublimation Setup. J Am Soc Mass Spectrom 2023; 34: 513-517.

Shea MK, Kritchevsky SB, Hsu FC, Nevitt M, Booth SL, Kwoh CK, et al. The association between vitamin K status and knee osteoarthritis features in older adults: the Health, Aging and Body Composition Study. Osteoarthritis Cartilage 2015; 23: 370-378.

Shet K, Siddiqui SM, Yoshihara H, Kurhanewicz J, Ries M, Li X. High-resolution magic angle spinning NMR spectroscopy of human osteoarthritic cartilage. NMR Biomed 2012; 25: 538-544.

Siddiqui A, Ceppi P. A non-proliferative role of pyrimidine metabolism in cancer. Mol Metab 2020; 35: 100962.

Simopoulou T, Malizos KN, Iliopoulos D, Stefanou N, Papatheodorou L, Ioannou M, et al. Differential expression of leptin and leptin's receptor isoform (Ob-Rb) mRNA between advanced and minimally affected osteoarthritic cartilage; effect on cartilage metabolism. Osteoarthritis Cartilage 2007; 15: 872-883.

Sinusas K. Osteoarthritis: diagnosis and treatment. Am Fam Physician 2012; 85: 49-56.

Sitton NG, Dixon JS, Bird HA, Wright V. Serum and synovial fluid histidine: a comparison in rheumatoid arthritis and osteoarthritis. Rheumatol Int 1986; 6: 251-254.

Siuzdak G. The Expanding Role of Mass Spectrometry in Biotechnology. 2nd Edition Edition, MCC Press 2006.

Skou ST, Roos E, Laursen M, Arendt-Nielsen L, Rasmussen S, Simonsen O, et al. Cost-effectiveness of total knee replacement in addition to non-surgical treatment: a 2-year outcome from a randomised trial in secondary care in Denmark. BMJ Open 2020; 10: e033495.

Slauterbeck JR, Kousa P, Clifton BC, Naud S, Tourville TW, Johnson RJ, et al. Geographic mapping of meniscus and cartilage lesions associated with anterior cruciate ligament injuries. J Bone Joint Surg Am 2009; 91: 2094-2103.

Sluzalska KD, Liebisch G, Lochnit G, Ishaque B, Hackstein H, Schmitz G, et al. Interleukin-1beta affects the phospholipid biosynthesis of fibroblast-like synoviocytes from human osteoarthritic knee joints. Osteoarthritis Cartilage 2017; 25: 1890-1899.

Smith CA, O'Maille G, Want EJ, Qin C, Trauger SA, Brandon TR, et al. METLIN: a metabolite mass spectral database. Ther Drug Monit 2005; 27: 747-751.

Smith CA, Want EJ, O'Maille G, Abagyan R, Siuzdak G. XCMS: processing mass spectrometry data for metabolite profiling using nonlinear peak alignment, matching, and identification. Anal Chem 2006; 78: 779-787.

Smith MD. The normal synovium. Open Rheumatol J 2011; 5: 100-106.

Smith RL, Carter DR, Schurman DJ. Pressure and shear differentially alter human articular chondrocyte metabolism: a review. Clin Orthop Relat Res 2004: S89-95.

Smith RL, Soeters MR, Wust RCI, Houtkooper RH. Metabolic Flexibility as an Adaptation to Energy Resources and Requirements in Health and Disease. Endocr Rev 2018; 39: 489-517.

Sohn DH, Sokolove J, Sharpe O, Erhart JC, Chandra PE, Lahey LJ, et al. Plasma proteins present in osteoarthritic synovial fluid can stimulate cytokine production via Toll-like receptor 4. Arthritis Res Ther 2012; 14: R7.

Sokoloff L. Natural history of degenerative joint disease in small laboratory animals. I. Pathological anatomy of degenerative joint disease in mice. AMA Arch Pathol 1956; 62: 118-128.

Song J, Chang HJ, Tirodkar M, Chang RW, Manheim LM, Dunlop DD. Racial/ethnic differences in activities of daily living disability in older adults with arthritis: a longitudinal study. Arthritis Rheum 2007; 57: 1058-1066.

Sonnery-Cottet B, Bazille C, Hulet C, Colombet P, Cucurulo T, Panisset JC, et al. Histological features of the ACL remnant in partial tears. Knee 2014; 21: 1009-1013.

Sophia Fox AJ, Bedi A, Rodeo SA. The basic science of articular cartilage: structure, composition, and function. Sports Health 2009; 1: 461-468.

Spector TD, MacGregor AJ. Risk factors for osteoarthritis: genetics. Osteoarthritis Cartilage 2004; 12 Suppl A: S39-44.

Srikanth VK, Fryer JL, Zhai G, Winzenberg TM, Hosmer D, Jones G. A meta-analysis of sex differences prevalence, incidence and severity of osteoarthritis. Osteoarthritis Cartilage 2005; 13: 769-781.

Steinberg GR, Macaulay SL, Febbraio MA, Kemp BE. AMP-activated protein kinase--the fat controller of the energy railroad. Can J Physiol Pharmacol 2006; 84: 655-665.

Strimbu K, Tavel JA. What are biomarkers? Curr Opin HIV AIDS 2010; 5: 463-466.

Surapaneni KM, Venkataramana G. Status of lipid peroxidation, glutathione, ascorbic acid, vitamin E and antioxidant enzymes in patients with osteoarthritis. Indian J Med Sci 2007; 61: 9-14.

Surowiec I, Arlestig L, Rantapaa-Dahlqvist S, Trygg J. Metabolite and Lipid Profiling of Biobank Plasma Samples Collected Prior to Onset of Rheumatoid Arthritis. PLoS One 2016; 11: e0164196.

Swann DA, Radin EL, Nazimiec M, Weisser PA, Curran N, Lewinnek G. Role of hyaluronic acid in joint lubrication. Ann Rheum Dis 1974; 33: 318-326.

Tan SH, Lau BP, Khin LW, Lingaraj K. The Importance of Patient Sex in the Outcomes of Anterior Cruciate Ligament Reconstructions: A Systematic Review and Meta-analysis. Am J Sports Med 2016; 44: 242-254.

Teranishi R, Mon TR, Robinson AB, Cary P, Pauling L. Gas chromatography of volatiles from breath and urine. Anal Chem 1972; 44: 18-20.

Tetlow LC, Woolley DE. Histamine stimulates the proliferation of human articular chondrocytes in vitro and is expressed by chondrocytes in osteoarthritic cartilage. Ann Rheum Dis 2003; 62: 991-994.

Tetlow LC, Woolley DE. Histamine, histamine receptors (H1 and H2), and histidine decarboxylase expression by chondrocytes of osteoarthritic cartilage: an immunohistochemical study. Rheumatol Int 2005; 26: 173-178.

Teufel S, Hartmann C. Wnt-signaling in skeletal development. Curr Top Dev Biol 2019; 133: 235-279.

Thomas AC, Hubbard-Turner T, Wikstrom EA, Palmieri-Smith RM. Epidemiology of Posttraumatic Osteoarthritis. J Athl Train 2017; 52: 491-496.

Thonar EJ, Masuda K, Hauselmann HJ, Uebelhart D, Lenz ME, Manicourt DH. Keratan sulfate in body fluids in joint disease. Acta Orthop Scand Suppl 1995; 266: 103-106.

Tootsi K, Kals J, Zilmer M, Paapstel K, Ottas A, Martson A. Medium- and long-chain acylcarnitines are associated with osteoarthritis severity and arterial stiffness in end-stage osteoarthritis patients: a case-control study. Int J Rheum Dis 2018; 21: 1211-1218.

Tootsi K, Vilba K, Martson A, Kals J, Paapstel K, Zilmer M. Metabolomic Signature of Amino Acids, Biogenic Amines and Lipids in Blood Serum of Patients with Severe Osteoarthritis. Metabolites 2020; 10.

Tortorella MD, Burn TC, Pratta MA, Abbaszade I, Hollis JM, Liu R, et al. Purification and cloning of aggrecanase-1: a member of the ADAMTS family of proteins. Science 1999; 284: 1664-1666.

Tzafetas M, Mitra A, Paraskevaidi M, Bodai Z, Kalliala I, Bowden S, et al. The intelligent knife (iKnife) and its intraoperative diagnostic advantage for the treatment of cervical disease. Proc Natl Acad Sci U S A 2020; 117: 7338-7346.

Underhill TM, Weston AD. Retinoids and their receptors in skeletal development. Microsc Res Tech 1998; 43: 137-155.

Van de Vyver A, Clockaerts S, van de Lest CHA, Wei W, Verhaar J, Van Osch G, et al. Synovial Fluid Fatty Acid Profiles Differ between Osteoarthritis and Healthy Patients. Cartilage 2020; 11: 473-478.

Varani K, De Mattei M, Vincenzi F, Gessi S, Merighi S, Pellati A, et al. Characterization of adenosine receptors in bovine chondrocytes and fibroblast-like synoviocytes exposed to low frequency low energy pulsed electromagnetic fields. Osteoarthritis Cartilage 2008; 16: 292-304.

Vaughn IA, Terry EL, Bartley EJ, Schaefer N, Fillingim RB. Racial-Ethnic Differences in Osteoarthritis Pain and Disability: A Meta-Analysis. J Pain 2019; 20: 629-644.

Verma RP, Hansch C. Matrix metalloproteinases (MMPs): chemical-biological functions and (Q)SARs. Bioorg Med Chem 2007; 15: 2223-2268.

Verzijl N, DeGroot J, Ben ZC, Brau-Benjamin O, Maroudas A, Bank RA, et al. Crosslinking by advanced glycation end products increases the stiffness of the collagen network in human articular cartilage: a possible mechanism through which age is a risk factor for osteoarthritis. Arthritis Rheum 2002; 46: 114-123.

Villalvilla A, Gomez R, Largo R, Herrero-Beaumont G. Lipid transport and metabolism in healthy and osteoarthritic cartilage. Int J Mol Sci 2013; 14: 20793-20808.

Vina ER, Kwoh CK. Epidemiology of osteoarthritis: literature update. Curr Opin Rheumatol 2018; 30: 160-167.

Visse R, Nagase H. Matrix metalloproteinases and tissue inhibitors of metalloproteinases: structure, function, and biochemistry. Circ Res 2003; 92: 827-839.

Wallace CW, Hislop B, Hahn AK, Erdogan AE, Brahmachary PP, June RK. Correlations between metabolites in the synovial fluid and serum: A mouse injury study. J Orthop Res 2022.

Wallin R, Schurgers LJ, Loeser RF. Biosynthesis of the vitamin K-dependent matrix Gla protein (MGP) in chondrocytes: a fetuin-MGP protein complex is assembled in vesicles shed from normal but not from osteoarthritic chondrocytes. Osteoarthritis Cartilage 2010; 18: 1096-1103.

Walsh NP, Gleeson M, Shephard RJ, Gleeson M, Woods JA, Bishop NC, et al. Position statement. Part one: Immune function and exercise. Exerc Immunol Rev 2011; 17: 6-63.

Wan Q, Kim SJ, Yokota H, Na S. Differential activation and inhibition of RhoA by fluid flow induced shear stress in chondrocytes. Cell Biol Int 2013; 37: 568-576.

Wang J, Li J, Song D, Ni J, Ding M, Huang J, et al. AMPK: implications in osteoarthritis and therapeutic targets. Am J Transl Res 2020; 12: 7670-7681.

Wang P, Guan PP, Guo C, Zhu F, Konstantopoulos K, Wang ZY. Fluid shear stress-induced osteoarthritis: roles of cyclooxygenase-2 and its metabolic products in inducing the expression of proinflammatory cytokines and matrix metalloproteinases. FASEB J 2013; 27: 4664-4677.

Wang P, Zhu F, Lee NH, Konstantopoulos K. Shear-induced interleukin-6 synthesis in chondrocytes: roles of E prostanoid (EP) 2 and EP3 in cAMP/protein kinase A- and PI3-K/Akt-dependent NF-kappaB activation. J Biol Chem 2010; 285: 24793-24804.

Wang Y, Wei L, Zeng L, He D, Wei X. Nutrition and degeneration of articular cartilage. Knee Surg Sports Traumatol Arthrosc 2013; 21: 1751-1762.

Welhaven HD, McCutchen CN, June RK. Effects of mechanical stimulation on metabolomic profiles of SW1353 chondrocytes: shear and compression. Biol Open 2022; 11.

Welhaven HD, Vahidi G et al. The Cortical Bone Metabolome of C57BL/6J Mice Is Sexually Dimorphic. JBMR Plus 2022; 6.

Welhaven HD, Viles E, Starke J, Wallace C, Bothner B, June RK, et al. Metabolomic profiles of cartilage and bone reflect tissue type, radiography-confirmed osteoarthritis, and spatial location within the joint. Biochem Biophys Res Commun 2024; 703: 149683.

Welhaven HD, Welfley AH, Pershad P, Satalich J, O'Connell R, Bothner B, et al. Metabolic phenotypes reflect patient sex and injury status: A cross-sectional analysis of human synovial fluid. Osteoarthritis Cartilage 2023.

Williams JP, Blair HC, McDonald JM, McKenna MA, Jordan SE, Williford J, et al. Regulation of osteoclastic bone resorption by glucose. Biochem Biophys Res Commun 1997; 235: 646-651.

Wishart DS, Guo A, Oler E, Wang F, Anjum A, Peters H, et al. HMDB 5.0: the Human Metabolome Database for 2022. Nucleic Acids Res 2022; 50: D622-D631.

Wishart DS, Tzur D, Knox C, Eisner R, Guo AC, Young N, et al. HMDB: the Human Metabolome Database. Nucleic Acids Res 2007; 35: D521-526.

Wohlgemuth KJ, Arieta LR, Brewer GJ, Hoselton AL, Gould LM, Smith-Ryan AE. Sex differences and considerations for female specific nutritional strategies: a narrative review. J Int Soc Sports Nutr 2021; 18: 27.

Woolf AD, Pfleger B. Burden of major musculoskeletal conditions. Bull World Health Organ 2003; 81: 646-656.

Wu CL, Jain D, McNeill JN, Little D, Anderson JA, Huebner JL, et al. Dietary fatty acid content regulates wound repair and the pathogenesis of osteoarthritis following joint injury. Ann Rheum Dis 2015; 74: 2076-2083.

Wu CL, Kimmerling KA, Little D, Guilak F. Serum and synovial fluid lipidomic profiles predict obesity-associated osteoarthritis, synovitis, and wound repair. Sci Rep 2017; 7: 44315.

Wu L, Liu H, Li L, Liu H, Cheng Q, Li H, et al. Mitochondrial pathology in osteoarthritic chondrocytes. Curr Drug Targets 2014; 15: 710-719.

Wu P, Holguin N, Silva MJ, Fu M, Liao W, Sandell LJ. Early response of mouse joint tissue to noninvasive knee injury suggests treatment targets. Arthritis Rheumatol 2014; 66: 1256-1265.

Wu S, De Luca F. Role of cholesterol in the regulation of growth plate chondrogenesis and longitudinal bone growth. J Biol Chem 2004; 279: 4642-4647.

Wu WH, Hackett T, Richmond JC. Effects of meniscal and articular surface status on knee stability, function, and symptoms after anterior cruciate ligament reconstruction: a long-term prospective study. Am J Sports Med 2002; 30: 845-850.

Xia J, Wishart DS. Using MetaboAnalyst 3.0 for Comprehensive Metabolomics Data Analysis. Curr Protoc Bioinformatics 2016; 55: 14 10 11-14 10 91.

Xiao JF, Zhou B, Ressom HW. Metabolite identification and quantitation in LC-MS/MS-based metabolomics. Trends Analyt Chem 2012; 32: 1-14.

Xiong B, Yang P, Lin T, Xu J, Xie Y, Guo Y, et al. Changes in hip joint contact stress during a gait cycle based on the individualized modeling method of "gait-musculoskeletal system-finite element". J Orthop Surg Res 2022; 17: 267.

Xu Z, Chen T, Luo J, Ding S, Gao S, Zhang J. Cartilaginous Metabolomic Study Reveals Potential Mechanisms of Osteophyte Formation in Osteoarthritis. J Proteome Res 2017; 16: 1425-1435.

Xue M, Huang N, Luo Y, Yang X, Wang Y, Fang M. Combined Transcriptomics and Metabolomics Identify Regulatory Mechanisms of Porcine Vertebral Chondrocyte Development In Vitro. Int J Mol Sci 2024; 25.

Yamauchi M, Terajima M, Shiiba M. Lysine Hydroxylation and Cross-Linking of Collagen. Methods Mol Biol 2019; 1934: 309-324.

Yang G, Zhang H, Chen T, Zhu W, Ding S, Xu K, et al. Metabolic analysis of osteoarthritis subchondral bone based on UPLC/Q-TOF-MS. Anal Bioanal Chem 2016; 408: 4275-4286.

Yang S, Wang J. Estrogen Activates AMP-Activated Protein Kinase in Human Endothelial Cells via ERbeta/Ca(2+)/Calmodulin-Dependent Protein Kinase Kinase beta Pathway. Cell Biochem Biophys 2015; 72: 701-707.

Yeh CC, Chang SF, Huang TY, Chang HI, Kuo HC, Wu YC, et al. Shear stress modulates macrophage-induced urokinase plasminogen activator expression in human chondrocytes. Arthritis Res Ther 2013; 15: R53.

Yi D, Yu H, Lu K, Ruan C, Ding C, Tong L, et al. AMPK Signaling in Energy Control, Cartilage Biology, and Osteoarthritis. Front Cell Dev Biol 2021; 9: 696602.

Yin J, Ren W, Huang X, Deng J, Li T, Yin Y. Potential Mechanisms Connecting Purine Metabolism and Cancer Therapy. Front Immunol 2018; 9: 1697.

Yuan Z, Liu S, Song W, Liu Y, Bi G, Xie R, et al. Galactose Enhances Chondrogenic Differentiation of ATDC5 and Cartilage Matrix Formation by Chondrocytes. Front Mol Biosci 2022; 9: 850778.

Zeng R, Faccio R, Novack DV. Alternative NF-kappaB Regulates RANKL-Induced Osteoclast Differentiation and Mitochondrial Biogenesis via Independent Mechanisms. J Bone Miner Res 2015; 30: 2287-2299.

Zhai G, Wang-Sattler R, Hart DJ, Arden NK, Hakim AJ, Illig T, et al. Serum branched-chain amino acid to histidine ratio: a novel metabolomic biomarker of knee osteoarthritis. Ann Rheum Dis 2010; 69: 1227-1231.

Zhai G. Alteration of Metabolic Pathways in Osteoarthritis. Metabolites 2019; 9.

Zhang L, Wen C. Osteocyte Dysfunction in Joint Homeostasis and Osteoarthritis. Int J Mol Sci 2021; 22.

Zhang Q, Li H, Zhang Z, Yang F, Chen J. Serum metabolites as potential biomarkers for diagnosis of knee osteoarthritis. Dis Markers 2015; 2015: 684794.

Zhang W, Likhodii S, Aref-Eshghi E, Zhang Y, Harper PE, Randell E, et al. Relationship between blood plasma and synovial fluid metabolite concentrations in patients with osteoarthritis. J Rheumatol 2015; 42: 859-865.

Zhang W, Likhodii S, Zhang Y, Aref-Eshghi E, Harper PE, Randell E, et al. Classification of osteoarthritis phenotypes by metabolomics analysis. BMJ Open 2014; 4: e006286.

Zhang W, Sun G, Likhodii S, Liu M, Aref-Eshghi E, Harper PE, et al. Metabolomic analysis of human plasma reveals that arginine is depleted in knee osteoarthritis patients. Osteoarthritis Cartilage 2016; 24: 827-834.

Zhang Y, Jordan JM. Epidemiology of osteoarthritis. Clin Geriatr Med 2010; 26: 355-369.

Zhang Z, Sui D, Qin H, Li H, Zhang Z. Contact pressure distribution of the hip joint during closed reduction of developmental dysplasia of the hip: a patient-specific finite element analysis. BMC Musculoskelet Disord 2020; 21: 600.

Zheng L, Zhang Z, Sheng P, Mobasheri A. The role of metabolism in chondrocyte dysfunction and the progression of osteoarthritis. Ageing Res Rev 2021; 66: 101249.

Zignego DL, Hilmer JK, Bothner B, Schell WJ, June RK. Primary human chondrocytes respond to compression with phosphoproteomic signatures that include microtubule activation. J Biomech 2019; 97: 109367.

Zignego DL, Hilmer JK, June RK. Mechanotransduction in primary human osteoarthritic chondrocytes is mediated by metabolism of energy, lipids, and amino acids. J Biomech 2015; 48: 4253-4261.

Zignego DL, Jutila AA, Gelbke MK, Gannon DM, June RK. The mechanical microenvironment of high concentration agarose for applying deformation to primary chondrocytes. J Biomech 2014; 47: 2143-2148.

APPENDICES

APPENDIX A

SUPPLEMENTAL MATERIAL FOR CHAPTER 3: METABOLOMIC PROFILES IN OSTEOARTHRITIS: CARTILAGE AND BONE

Supplemental Results

Changes in metabolic profiles correspond to radiography-confirmed grade of OA: Pairwise comparisons

Pairwise comparisons were performed to investigate the metabolomes of samples that differ by tissue and OA grade. First, grade differences within tissue were assessed. HCA of AC grade III vs grade IV samples found that samples clustered within their respective experimental groups (Fig. 3.4 A). PCA showed some overlap between grades, but PLS-DA revealed clear separation of groups (Fig. 3.4 B-C). Fold change analysis identified 266 metabolite features that were expressed in higher concentrations in grade III AC compared to grade IV AC, and 259 metabolite features that were expressed in higher concentrations in grade IV AC compared to grade III AC. Volcano plot analysis identified 192 metabolite features that were significant and had higher concentrations in grade III AC compared to grade IV AC, and 160 metabolite features that were significant and had higher concentrations in grade IV AC compared to grade III AC (Fig. 3.4 E). Next, sub-populations of metabolite features differentially expressed between AC grades identified by fold change and volcano plot analysis underwent pathway enrichment analysis. Metabolite features that were higher in grade III AC compared to grade IV AC mapped to GAG degradation, metabolism of xenobiotics by cytochrome P450, and tryptophan metabolism (Table 3.3, Supplemental Table 3.3). Conversely, metabolite features higher in grade IV AC compared to grade III AC mapped to porphyrin metabolism (Table 3.3, Supplemental Table 3.3).

In a similar way, grade differences within SB samples were studied. HCA displayed clear clustering of grade III and grade IV SB (Fig. 3.5 A). PCA showed minimal overlap of SB samples that differ by grade, whereas PLS-DA displayed clear separation of groups (Fig. 3.5 B-C). To further examine these metabolic differences, fold change and volcano plot analyses were

performed. Fold change analysis identified 310 metabolite features that were expressed in higher concentrations in grade III SB compared to grade IV SB, and 371 metabolite features that were expressed in higher concentrations in grade IV SB compared to grade III SB (Fig. 3.5 D). Next, volcano plot analysis identified 288 metabolite features that were significant and higher in concentration in grade III SB compared to grade IV SB, and 427 metabolite features that were significant and higher in concentration in grade IV SB compared to grade III SB (Fig. 3.5 E). Pathway analyses on the subpopulations identified by these tests revealed both distinct and overlapping pathways between grade III and IV SB. Metabolite features associated with purine metabolism and amino acid metabolism (alanine, aspartate, glutamate) were higher in grade III SB compared to grade IV SB (Table 3.3, Supplemental Table 3.4). Conversely, metabolite features associated with ubiquinone biosynthesis, porphyrin metabolism, and GAG degradation were higher in grade IV SB compared to grade III SB (Table 3.3, Supplemental Table 3.4).

Additionally, tissue differences within the same grade were assessed using the same approach that has been previously described (Supplemental Fig. 3.1 A-E). When comparing grade III AC and SB, differentially expressed metabolite features identified by fold change and volcano plot analysis underwent pathway enrichment analyses (Supplemental Fig. 3.1 D-E). Metabolite features higher in grade III SB compared to grade III AC mapped to amino acid metabolism (alanine, aspartate, glutamate, valine, leucine, isoleucine), aminoacyl-tRNA biosynthesis, and phosphatidylinositol signaling system (Table 3.3, Supplemental Table 3.5). Conversely, metabolite features higher in grade III AC compared to grade III SB mapped to steroid hormone biosynthesis, ubiquinone biosynthesis, N-glycan biosynthesis, porphyrin metabolism, and tryptophan metabolism (Table 3.3, Supplemental Table 3.5). GAG degradation was detected in

both grade III AC and grade III SB (Table 3.3, Supplemental Table 3.5). The same set of analyses were performed to compare grade IV AC and grade IV SB and differentially expressed metabolite features identified by fold change and volcano plot analyses underwent pathway enrichment analyses (Supplemental Fig. 3.1 A-E). Metabolite features that were higher in grade IV AC compared to grade IV SB mapped to arachidonic acid metabolism, the pentose phosphate pathway, galactose metabolism, ubiquinone biosynthesis, glycosphingolipid biosynthesis, and lysine degradation (Table 3.3, Supplemental Table 3.6). Conversely, those higher in grade IV SB compared to grade IV AC mapped to amino acid metabolism (alanine, aspartate, glutamate, valine, leucine, isoleucine, histidine), pyrimidine metabolism, and the TCA cycle (Table 3.3, Supplemental Table 3.6). Overall, the results of pathway enrichment analyses of fold change, volcano plot, and median metabolite intensity heatmaps from pairwise and multigroup comparisons strongly suggest that the metabolic endotypes of OU components reflect OA grade (Table 3.3).

Supplemental Figures

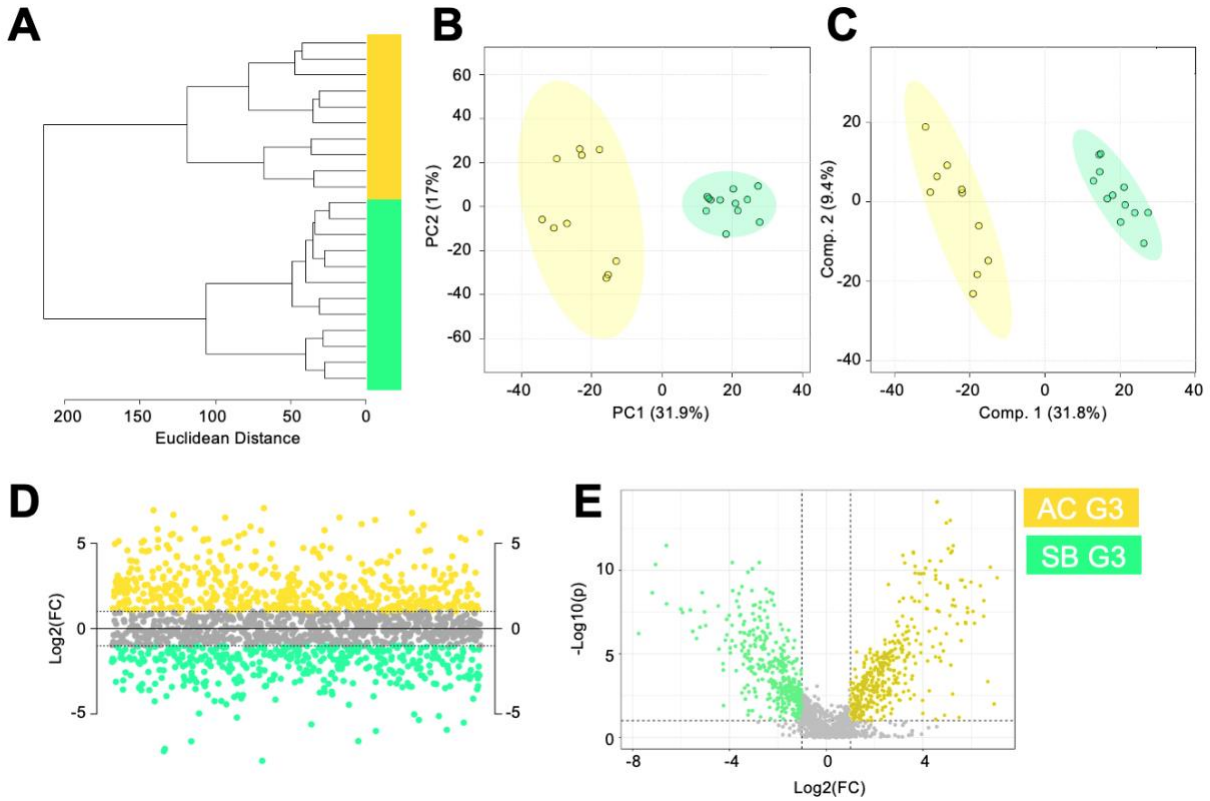

Supplemental Figure 3.1. Metabolic differences exist when comparing osteoarthritis grade III articular cartilage and bone. (A) HCA showcased that the metabolomes of grade III SB and AC are distinct from one another, as shown by complete clustering of AC and SB samples within their respective cohorts. (B) PCA found complete separation between grade III SB and AC. PC1 and PC2 accounted for 48.9% of the variation within the dataset. (C) PLS-DA showed clear separation of grade III SB from AC, with components 1 and 2 accounting for 41.2% of the variation within the dataset. (D) Fold change analysis identified metabolite features that were higher or lower in concentration in grade III AC compared to grade III SB (fold change ratio: AC grade III/SB grade III). Fold change analysis identified 501 metabolite features that were higher in concentration in grade III AC compared to SB with a FC > 2. Conversely, fold change analysis identified 392 metabolite features that were higher in concentration in grade III SB compared to grade III AC with a FC < -2. (E) Volcano plot analysis identified 411 metabolite features higher in grade III AC compared to grade III SB that had a FC > 2 and a p-value less than 0.05, whereas 369 metabolite features were higher in grade III SB compared to grade III AC that had a FC < -2 and a p-value less than 0.05. The colors in A-F correspond to: grade III subchondral bone – green, grade III articular cartilage – yellow. Subchondral bone = SB. Articular cartilage = AC.

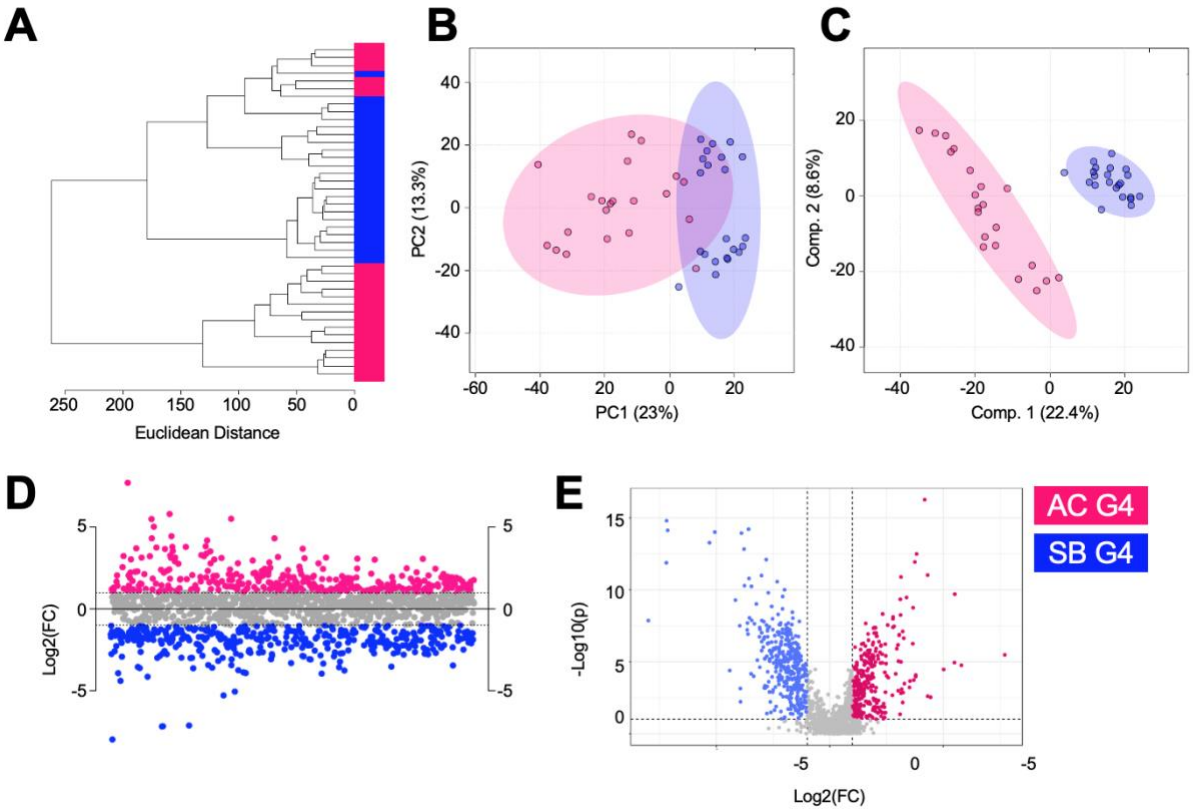

Supplemental Figure 3.2. Osteoarthritis grade IV articular cartilage and subchondral bone have distinct metabolic endotypes. (A) HCA showcased that the metabolomes of grade IV SB and AC are distinct from one another, as shown by correct clustering of most AC and SB samples within their respective cohorts. (B) PCA showed separation between grade III SB and AC, with minor overlap. PC1 and PC2 accounted for 36.3% of the variation within the dataset. (C) PLS-DA showed clear separation of grade IV SB from AC, with components 1 and 2 accounting for 31% of the variation. (D) Fold change analysis identified metabolite features that were higher or lower in concentration in grade IV AC compared to grade IV SB (fold change ratio: AC grade IV/SB grade IV. Fold change analysis identified 348 metabolite features that were higher in concentration in grade IV AC compared to SB with a FC > 2. Conversely, fold change analysis identified 400 metabolite features that were higher in concentration in grade IV SB compared to grade IV AC with a FC < -2. (E) Volcano plot analysis identified 291 metabolite features higher in grade IV AC compared to grade IV SB that had a FC > 2 and a p-value less than 0.05, whereas 382 metabolite features were higher in grade IV SB compared to grade IV AC that had a FC < -2 and a p-value less than 0.05. The colors in A-F correspond to: grade IV subchondral bone – blue, grade IV articular cartilage – pink. Subchondral bone = SB. Articular cartilage = AC.

Supplemental Tables

Supplemental Table 3.1. All metabolite features with a fold change > 2 from all pairwise comparisons including articular cartilage and subchondral bone, grades III and IV articular cartilage, grades III and IV subchondral bone, grade III articular cartilage and subchondral bone, and grade IV articular cartilage and subchondral bone.

Supplemental Table 3.2. All metabolic pathways outputted from MetaboAnalyst when comparing articular cartilage and subchondral bone using fold change and volcano plot analyses.

Supplemental Table 3.3. All metabolic pathways outputted from MetaboAnalyst when comparing grade III and IV articular cartilage and grade III and IV subchondral bone using median metabolite intensity heatmap analysis.

Supplemental Table 3.4. All metabolic pathways outputted from MetaboAnalyst when comparing grade III and IV articular cartilage using fold change and volcano plot analyses.

Supplemental Table 3.5. All metabolic pathways outputted from MetaboAnalyst when comparing grade III and IV subchondral bone using fold change and volcano plot analyses.

Supplemental Table 3.6. All metabolic pathways outputted from MetaboAnalyst when comparing grade III articular cartilage and grade III subchondral bone using fold change and volcano plot analyses.

Supplemental Table 3.7. All metabolic pathways outputted from MetaboAnalyst when comparing grade IV articular cartilage and grade IV subchondral bone using fold change and volcano plot analyses.

Supplemental Table 3.8. All metabolic pathways outputted from MetaboAnalyst when comparing grade III and IV articular cartilage quadrants 1-4 using median metabolite intensity heatmap analysis.

Supplemental Table 3.9. All metabolic pathways outputted from MetaboAnalyst when comparing grade III and IV subchondral bone quadrants 1-4 using median metabolite intensity heatmap analysis.

APPENDIX B

SUPPLEMENTAL MATERIAL FOR CHAPTER 4: METABOLOMIC PROFILES OF OSTEOARTHRITIS AND HEALTHY CARTILAGE ARE DISTINCT

Supplemental Figures

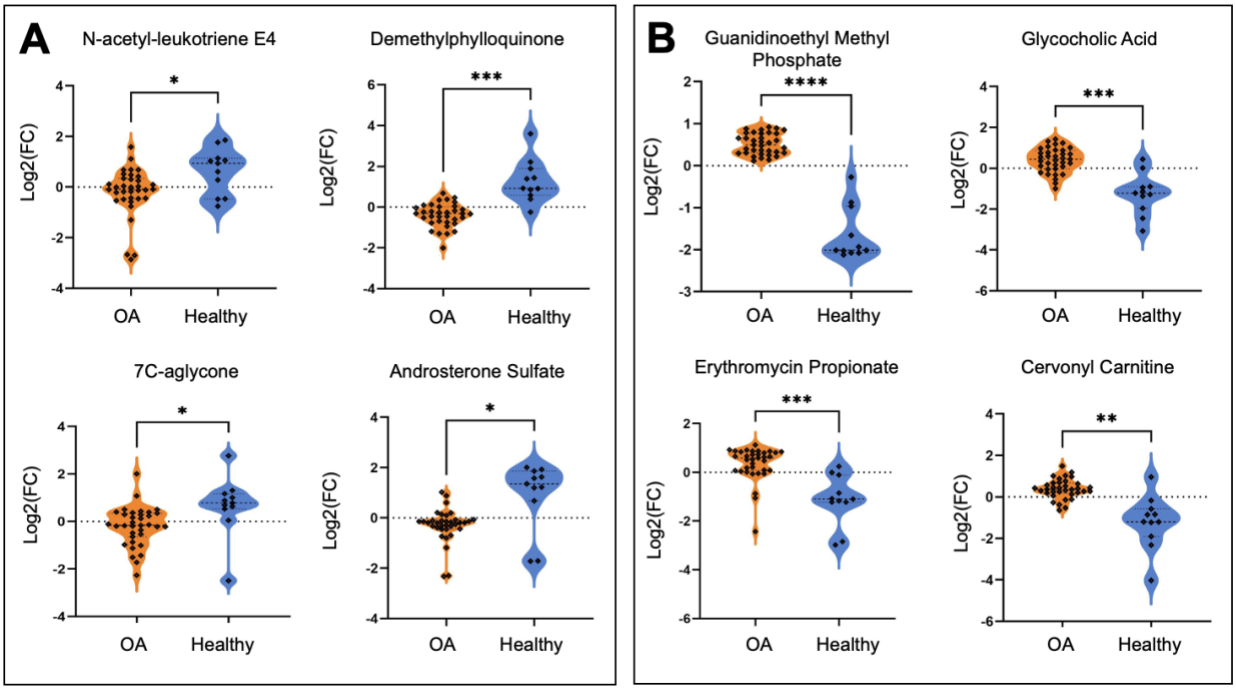

Supplemental Figure 4.1. Identified metabolites differ in abundance between healthy and osteoarthritic cartilage. (A) Metabolites – N-acetyl-leukotriene E4, demethylphylloquinone, 7C-aglycone, androsterone sulfate – are higher in abundance in healthy cartilage compared to osteoarthritic cartilage. (B) Conversely, metabolites - guanidinoethyl methyl phosphate, glycocholic acid, erythromycin propionate, cervonyl carnitine – are higher in abundance in cartilage from individuals with osteoarthritis compared to healthy cartilage. Mass-to-charge intensities of interest were normalized and used to generate plots. To correct for multiple comparisons, FDR p-value corrections were performed and were less than < 0.05. Moreover, Welch's t-tests were performed for each identified metabolite. Orange = osteoarthritis. Blue = healthy. **** = $p < 0.0001$, *** $p < 0.0002$, ** $p < 0.001$, * = $p < 0.05$.

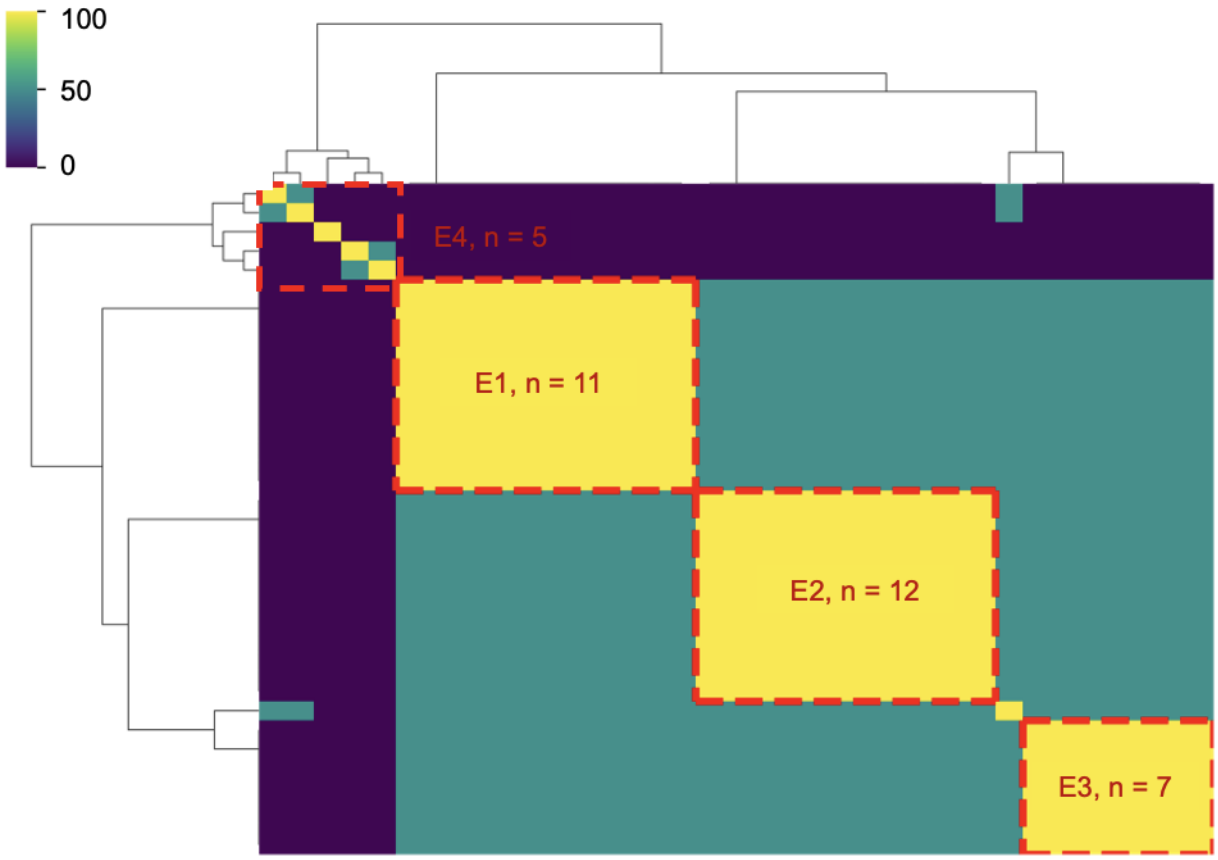

Supplemental Figure 4.2. Ensemble clustering of osteoarthritis participants revealed distinct metabolic endotypes. By employing ensemble clustering of all osteoarthritis participants based on metabolomic data, four unique endotypes were revealed. Specifically, endotype one (E1) is composed of n = 11 participants. Moreover, endotype two (E2), three (E3), and four (E4) are composed of n = 12, n = 7, and n = 5, respectively. Scale bar represents the percentage (%) of time participants cluster together.

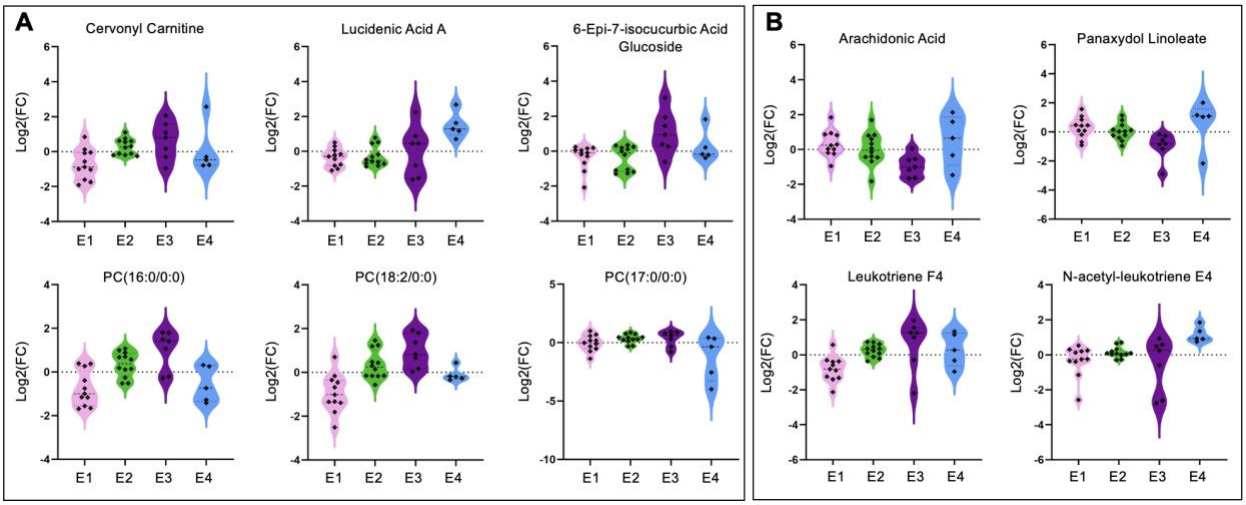

Supplemental Figure 4.3. Identified metabolites differ in abundance across osteoarthritis endotypes. (A) Lipid and lipid-like identified metabolites that are differentially regulated across osteoarthritis endotypes. (B) Identified metabolites that differ in abundance across endotypes and are associated with arachidonic acid metabolism and leukotriene metabolism. Mass-to-charge intensities of interest were normalized and used to generate plots. To correct for multiple comparisons, FDR p-value corrections were performed and were less than < 0.05. Moreover, Welch's t-tests were performed for each identified metabolite. Endotype colors correspond to: pink – Endotype 1; green – Endotype 2; purple – Endotype 3; blue – Endotype 4.

Supplemental Tables

Supplemental Table 4.1. Participant information including donor number, assigned anonymous identifier, age, sex, and osteoarthritis endotype group.

Supplemental Table 4.2. All metabolic pathways determined from MetaboAnalyst when comparing healthy and diseased cartilage using volcano plot analyses. Populations of metabolite features are defined on Figure 4.1C.

Supplemental Table 4.3. Putatively identified metabolites that differ in abundance between healthy and diseased cartilage distinguished by volcano plot analysis. Identifications were made by performing liquid chromatography tandem mass spectrometry (LC-MS/MS). For all identified, information includes observed and theoretical mass-to-charge ratios, parts per million (ppm) error, accepted compound ID and description, adduct, chemical formula, total score out of 100, and fragmentation score. Identifications with error greater than 20 ppm, total score < 60, and a fragmentation score < 12 were excluded.

Supplemental Table 4.4. Putatively identified metabolites that differ in abundance between healthy and diseased cartilage distinguished by t-test analysis. Identifications were made by performing liquid chromatography tandem mass spectrometry (LC-MS/MS). For all identified, information includes observed and theoretical mass-to-charge ratios, parts per million (ppm) error, accepted compound ID and description, adduct, chemical formula, total score out of 100, and fragmentation score. Identifications with error greater than 20 ppm, total score < 60, and a fragmentation score < 12 were excluded.

Supplemental Table 4.5. Putatively identified metabolites that differ in abundance between osteoarthritis endotype groups distinguished by ANOVA analysis. Identifications were made by performing liquid chromatography tandem mass spectrometry (LC-MS/MS). For all identified, information includes observed and theoretical mass-to-charge ratios, parts per million (ppm) error, accepted compound ID and description, adduct, chemical formula, total score out of 100, and fragmentation score. Identifications with error greater than 20 ppm, total score < 60, and a fragmentation score < 12 were excluded. All metabolite features with an FDR-corrected p-value > 0.05 distinguished by ANOVA when comparing all four osteoarthritis groups.

Supplemental Table 4.6. All metabolic pathways determined from MetaboAnalyst when comparing osteoarthritis endotypes using median metabolite intensity heatmap analysis. Clusters defined on Figure 4.2E.

Supplementary Table 4.7. Raw data from XCMS.

APPENDIX C

SUPPLEMENTAL MATERIAL FOR CHAPTER 5: PATIENT SEX & INJURY ALTER SYNOVIAL FLUID METABOLOME

Supplemental Methods

Synovial Fluid metabolite extraction protocol

In total, 100 µL of participant SF samples were aliquoted, centrifuged at 500 x g for 5 minutes at 4°C to remove cells and debris, and precipitated with 500 µL of 4:1 methanol:H_2O. Samples were vortexed for 1 minute then stored at -20°C for 5 minutes. This process was repeated 5 times, then samples were stored at -20°C overnight. The following day, samples were pelleted by centrifugation at 16,100 x g for 10 minutes at 4°C. Supernatants were harvested and dried via vacuum concentration to evaporate solvent and isolate metabolites. To further extract SF metabolites, dried samples were resuspended with 250 µL of 1:1 acetonitrile:water. Again, precipitated SF samples were vortexed for 1 minute then stored at -20°C for 5 minutes. Next, samples were centrifuged at 16,100 x g for 10 minutes at 4°C and supernatants were transferred to new Eppendorf vials for vacuum concentration. The remaining dried samples were resuspended with 50 µL of 1:1 acetonitrile:water for LC-MS analysis. At this time, two pooled samples were generated by randomly selecting 5 µL of extracted SF from 10 participants. Two quality control samples were created, one containing only mass spectrometry grade water and another that underwent metabolite extraction using only the solvents.

Liquid chromatography-mass spectrometry

All samples, participant SF, pooled, and quality control samples, were analyzed using an Acquity UPLC plus coupled through an electrospray ionization source to a Waters Synapt XS. Metabolites were separated using a Cogent Diamond Hydride HILIC column (150 x 2.1 mm) at a flow rate of 0.400 µL/min. Solvents used were 95% water 5% acetonitrile with 0.1% formic acid

(solvent A) and 95% acetonitrile 5% water with 0.1% formic acid (solvent B). The 19-minute elution gradient consisted of 95 to 25% solvent B over 12 minutes, and each run began with 2 minutes of wash. Quality control blanks were injected periodically throughout the overall run to minimize spectral drift and assess LC-MS performance. Participant SF samples underwent standard MS1. Liquid chromatography tandem mass spectrometry (LC-MS/MS) was performed on pooled samples with a constant high energy ramp of 30-50V.

Global metabolomic profiling: statistics and pathway enrichment analyses

LC-MS data consisting of mass-to-charge ratios (m/z values), relative metabolite abundance, and retention times were processed using MSConvert and XCMS. Next, metabolites with a median intensity value of zero across all samples were removed from the analysis. To correct for non-normal distributions, all data underwent interquartile range normalization, were log-transformed, and autoscaled (mean-centered and divided by standard deviation of each variable).

To statistically analyze samples and visualize dissimilarities in metabolomic profiles between males and females with different injuries, previously established analysis pipelines were used and then executed in MetaboAnalyst. Specifically, principal component analysis (PCA) and partial least squares-discriminant analysis (PLS-DA) were used to visualize the presence, or absence, of overlap between participant derived-SF metabolic phenotypes. Variable Importance in Projection (VIP) Scores, an extension of PLS-DA where metabolite features are scored based on their contribution to discriminating between cohorts, were also considered to better understand metabolic shifts induced by different injury types among male and female participants. Fold change, a relative quantification technique, was used to measure the relative change of a given

metabolite feature concentration between groups. Volcano plot, an extension of a fold change analysis, was used to assess significance and magnitude of change. Together, both analyses were employed to visualize and identify populations of metabolite features that are differentially regulated between groups. Heatmap analyses were performed to distinguish clusters of co-regulated metabolite features for pathway enrichment analyses using MetaboAnalyst's Functional Analysis feature. This module employs the *mummichog* algorithm which analyzes the inputted metabolite features to predict networks of functional activity and derive biological relevance. Pathway library Human MFN was reference to match metabolite features to putatively identified metabolites (mass tolerance: 5 ppm, positive mode). Significance was determined using an FDR-corrected significance level of $p < 0.05$ decided on *a priori*.

To identify metabolite features using LC-MS/MS data, Progenesis QI (Nonlinear Dynamics, Newcastle, UK) was utilized. All MS1 and MS2 centroided data was imported, peak picked, and aligned. The Human Metabolome Database (HMDB) was utilized to compare acquired and theoretical fragmentation for identification purposes. Identifications found were then crosschecked by retention time and fragmentation score. For a metabolite identity to be accepted, metabolites must receive a Progenesis score greater than 60/100 and a fragmentation score greater than 12. The three properties that contributed to these scores and percentages were mass error, isotope distribution similarity, and retention time error. Parts per million (ppm) error was calculated between MS1 and MS^E data, and identifications with error > 20 ppm were excluded. Identities made were compared to metabolite features of interest. To correct for multiple comparisons, FDR p-value corrections for identified metabolites were performed.

Supplemental Figures

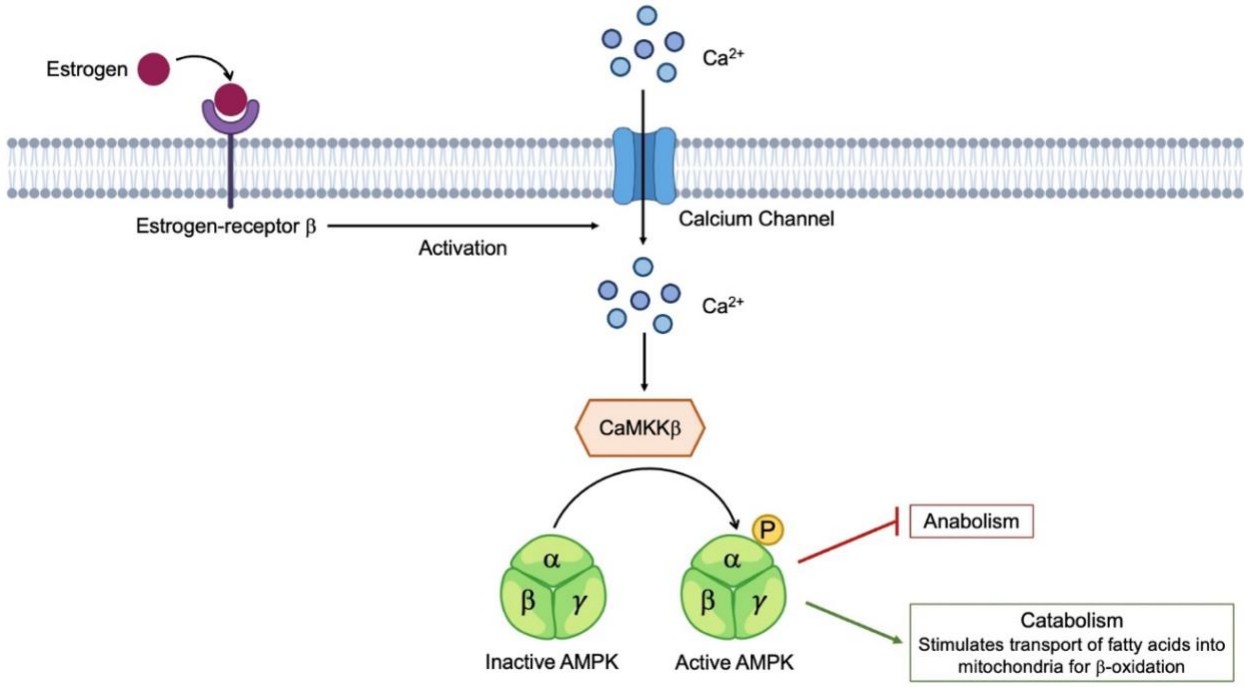

Supplementary Figure 5.1. Proposed mechanism of AMPK activation by estrogen.

Supplemental Tables

Supplemental Table 5.1. Participant information for all participants including BMI, age, sex, time between injury and repair (days), reason for knee arthroscopy repair, and injury pathology assignment.

Supplemental Table 5.2. Identified putative metabolites that differ in abundance between injury pathology and have a variable importance in projection score greater than 2 identified by liquid chromatography tandem mass spectrometry (LC-MS/MS). For all identified putative metabolites provided information includes observed mass-to-charge ratios, theoretical mass-to-charge ratios from Progenesis, ppm error, accepted human metabolome database compound identification number, accepted description, adduct, chemical formula, total score, and fragmentation score. Identifications with error > 20 ppm, overall score < 60, and fragmentation score < 12 were excluded.

Supplemental Table 5.3. All metabolic pathways determined from MetaboAnalyst when comparing participants with different injury pathologies (Ligament, Meniscal, Ligament and Meniscal injuries) using median metabolite intensity heatmap analysis. Clusters defined on Figure 5.3B. No statistically significant pathways were detected in cluster 4.

Supplemental Table 5.4. Identified putative metabolites that differ in abundance between male and female participants identified by liquid chromatography tandem mass spectrometry (LC-MS/MS). For all identified putative metabolites provided information includes observed mass-to-charge ratios, theoretical mass-to-charge ratios from Progenesis, ppm error, accepted human metabolome database compound identification number, accepted description, adduct, chemical formula, total score, and fragmentation score. Identifications with error > 20 ppm, overall score < 60, and fragmentation score < 12 were excluded.

APPENDIX D

SUPPLEMENTAL MATERIAL FOR CHAPTER 6: METABOLIC SIGNATURES PERTURBED BY INJURY IN MICE

Supplemental Results

Differences in Metabolomic Profiles Correspond to Injury Status of Joints: Pairwise Comparisons

To elucidate the systemic response following joints injury across injured, contralateral, and naïve whole joint and synovial fluid samples, PLS-DA, fold change, and volcano plot analyses were performed. Within whole joints, when comparing injured and naïve joints (Supplemental Figure 6.3 A), naïve and contralateral joints (Supplemental Figure 6.3 B), and injured and contralateral joints (Supplemental Figure 6.3 C) using PLS-DA some overlap is observed. However, overlap may be present due to each mouse in the study contributing both joints. Collectively, it is evident that the whole joint metabolome is influenced by injury suggesting a systemic response is produced in both injured and contralateral joints.

Further examination of these metabolic differences between joints, fold change analysis was performed to distinguish populations of metabolite features driving these detected differences between injured and naïve joints (Supplemental Figure 6.3 D), naïve and contralateral joints (Supplemental Figure 6.3 E), and injured and contralateral joints (Supplemental Figure 6.3 F). Populations were subjected to pathway analyses revealing numerous differentially regulated pathways across pairwise comparisons. Sphingolipid metabolism and alanine, aspartate, and glutamate metabolism were consistently highest in injured joints. Tryptophan metabolism was consistently detected in contralateral joints, whereas various amino acid pathways (lysine, arginine, proline) were consistently detected in naïve joints. In total, 16 significant pathways were detected between injured and naïve joints, 12 between contralateral and naïve joints, and 11 between injured and contralateral joints (Supplemental Table 6.2). Volcano plot analyses were

performed to distinguish metabolite features that had a p-value < 0.05 and a fold change < 2. These metabolite features were then matched against putative identifications made using LC-MS/MS.

In a similar way, SF from injured, contralateral, and naïve joints were analyzed to elucidate if a systemic response is seen in this tissue type. PLS-DA analysis of SF samples displays minimal overlap between naïve and injured SF (Supplemental Fig. 6.4 A), naïve and contralateral SF (Supplemental Fig. 6.4 B), and injured and contralateral SF (Supplemental Fig. 6.4 C) suggesting that the SF metabolome reflects injury status and injury causes shifts in metabolism in both injured and contralateral SF. Next, fold change analyses were performed to distinguish populations of metabolite features driving these differences, then features were subjected to pathway analyses to unveil biological pathways (Supplemental Table 6.3). Various amino acid pathways (alanine, proline, alanine, aspartate, glutamate, lysine, arginine, tyrosine, phenylalanine), glycerophospholipid metabolism, and glutathione metabolism were consistently higher in injured SF. Notably, glutathione metabolism was higher in contralateral SF compared to naive SF. Glycine, serine, and threonine metabolism as well as glyoxylate and dicarboxylate metabolism were highest in contralateral SF compared to naïve and injured SF. Biosynthesis of unsaturated fatty acids and terpenoid backbone biosynthesis were highest in naïve SF compared to injured and contralateral SF. In total, 23 significant pathways were detected between injured and naïve SF, 20 between contralateral and naïve SF, and 17 between injured and contralateral SF (Supplemental Table 6.1). Volcano plot analyses were performed to distinguish SF-derived metabolite features that had a p-value < 0.05 and a fold change < 2. These metabolite features were then matched against putative identifications made using LC-MS/MS.

Supplemental Figures

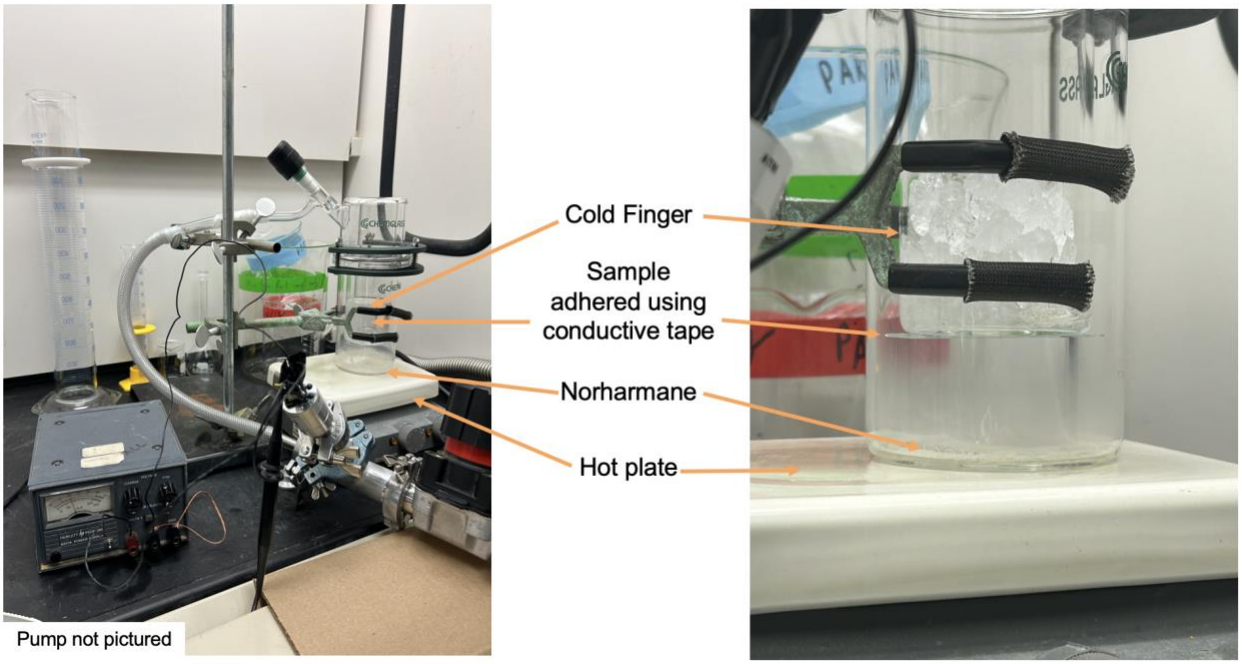

Supplemental Figure 6.1. Sublimation apparatus used to uniformly coat whole joints with matrix. Components of the sublimation apparatus include the cold finger, hot plate, glass condenser and sleeve, O-ring seal, and vacuum pump (not pictured).

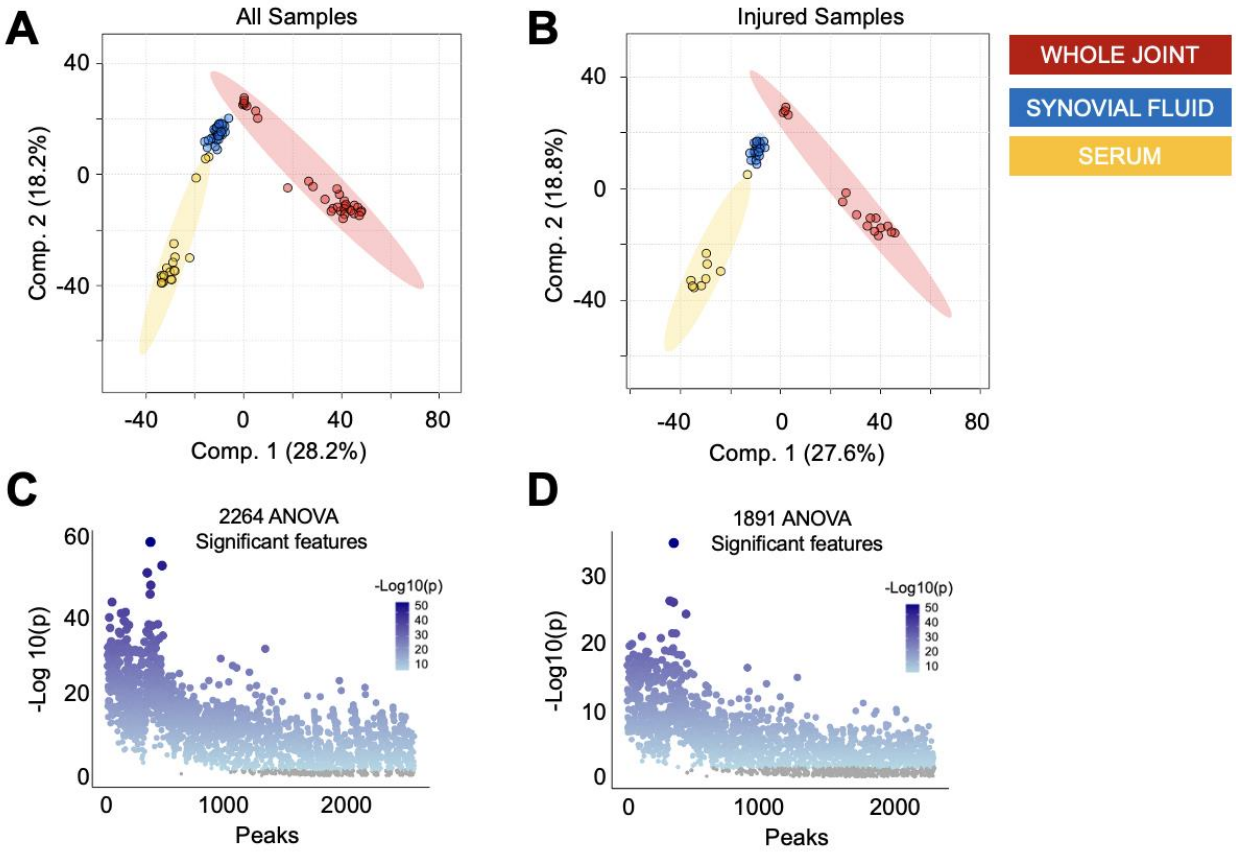

Supplemental Figure 6.2. The metabolome is distinct for whole joints, synovial fluid, and serum. Partial Least Squares-Discriminant Analysis (PLS-DA) of (A) all samples and (B) only samples from injured mice displays clear separation of whole joints, synovial fluid, and serum suggesting the metabolome of each tissue is substantially distinct from others. (C) ANOVA analysis identified 2,264 metabolite features that were significantly dysregulated across samples from all three tissue types. (D) When comparing samples from injured mice only, ANOVA analysis identified 1,891 significantly dysregulated features across tissue types. Colors in A-B correspond to: red = whole joint, blue = synovial fluid, yellow = serum.

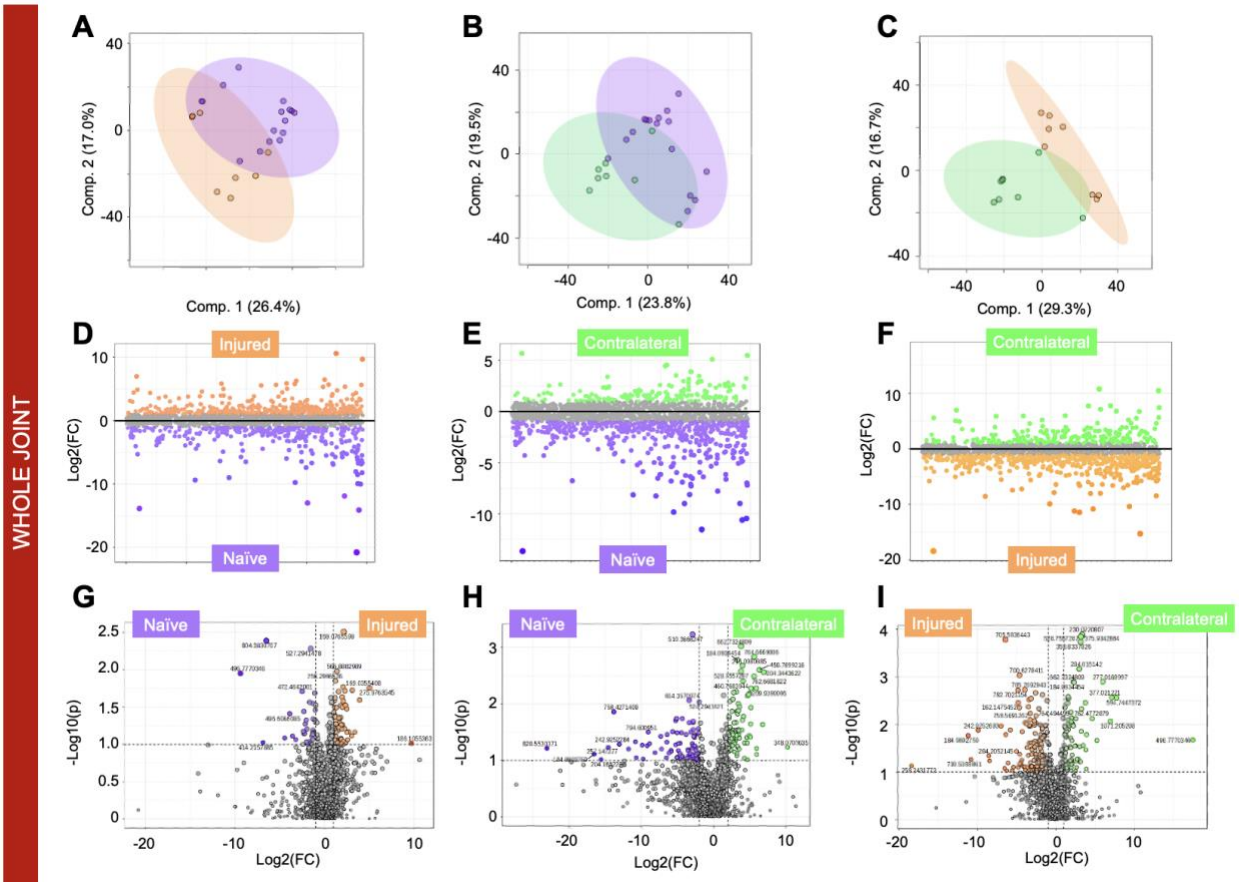

Supplemental Figure 6.3. Metabolomic profiles from injured, contralateral, and naïve whole joints are distinct. (A-C) Partial Least Squares-Discriminant Analysis (PLS-DA) finds some overlap between (A) injured and naïve, (B) naïve and contralateral, and (C) injured and contralateral whole joints. (D-F) Fold change analysis distinguished populations of metabolite features driving separation of metabolomic profiles. (D) Specifically, 427 and 310 metabolite features were highest in injured and naïve whole joints, respectively. (E) 182 and 496 metabolite features were highest in contralateral and naïve whole joints, respectively. (F) 236 and 571 features were highest in contralateral and injured whole joints, respectively. (G-I) To further examine metabolic differences associated with injury status across whole joints, volcano plot analysis was performed and identified numerous metabolite features that had a fold change > 2, a p-value < 0.05, and were differentially regulated between injured and naïve (G, n = 97), contralateral and naive (H, n = 179), and contralateral and injured whole joints (I, n = 268). The colors in A-I correspond to: purple = naïve whole joint, orange = injured whole joint, green = contralateral whole joint.

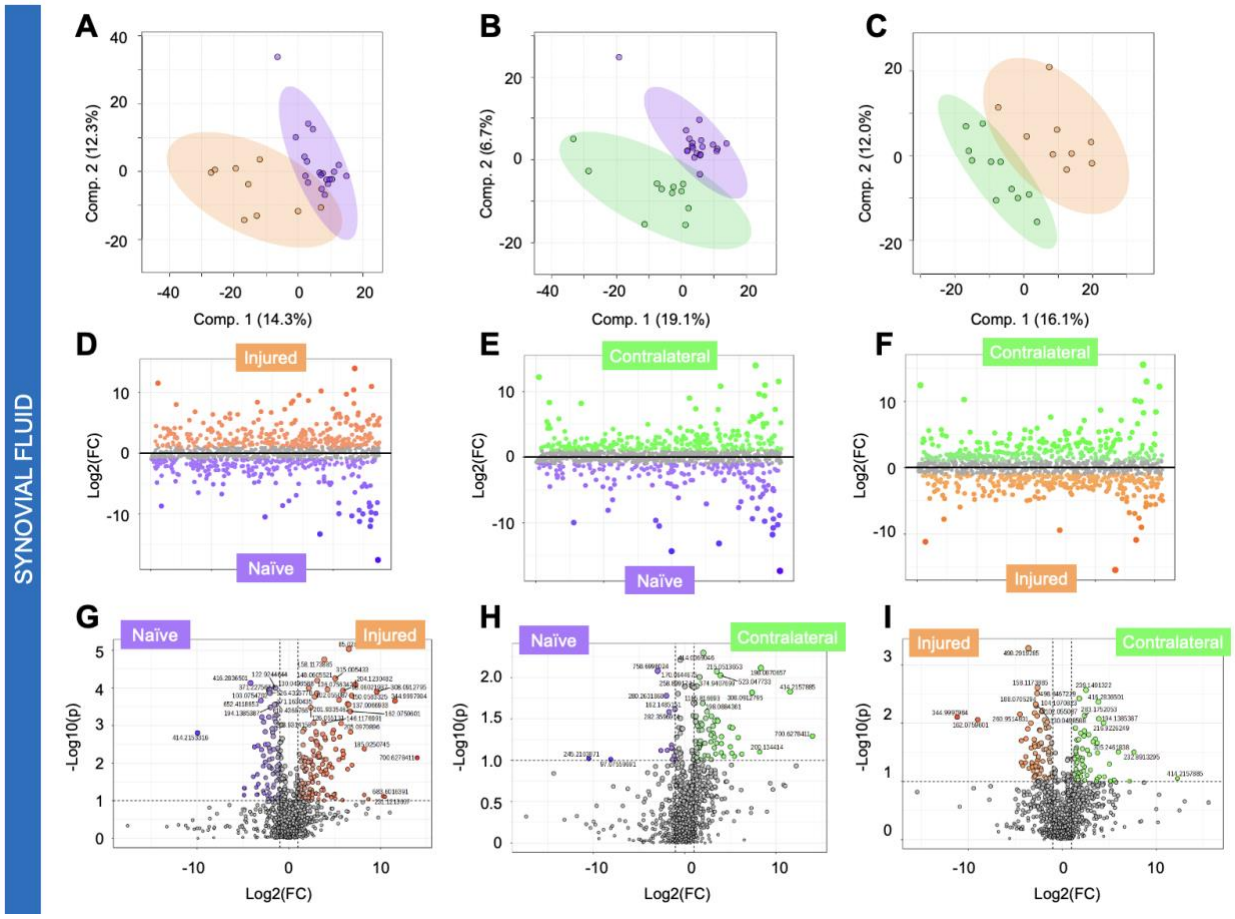

Supplemental Figure 6.4. Synovial fluid metabolome differs across injured, contralateral, and naïve limbs. (A-C) Partial Least Squares-Discriminant Analysis (PLS-DA) finds some overlap between (A) injured and naïve, (B) naïve and contralateral, and (C) injured and contralateral synovial fluid. (D-F) Fold change analysis distinguished populations of metabolite features driving separation of metabolomic profiles. (D) Specifically, 318 and 253 metabolite features were highest in injured and naïve synovial fluid, respectively. (E) 269 and 178 metabolite features were highest in contralateral and naïve synovial fluid, respectively. (F) 303 and 291 features were highest in contralateral and injured synovial fluid, respectively. (G-I) To further examine metabolic differences associated with injury status across whole joints, volcano plot analysis was performed and identified numerous metabolite features that had a fold change > 2, a p-value < 0.05, and were differentially regulated between injured and naïve (G, n = 59), contralateral and naive (H, n = 81), and contralateral and injured synovial fluid (I, n = 140). The colors in A-I correspond to: purple = naïve synovial fluid, orange = injured synovial fluid, green = contralateral synovial fluid.

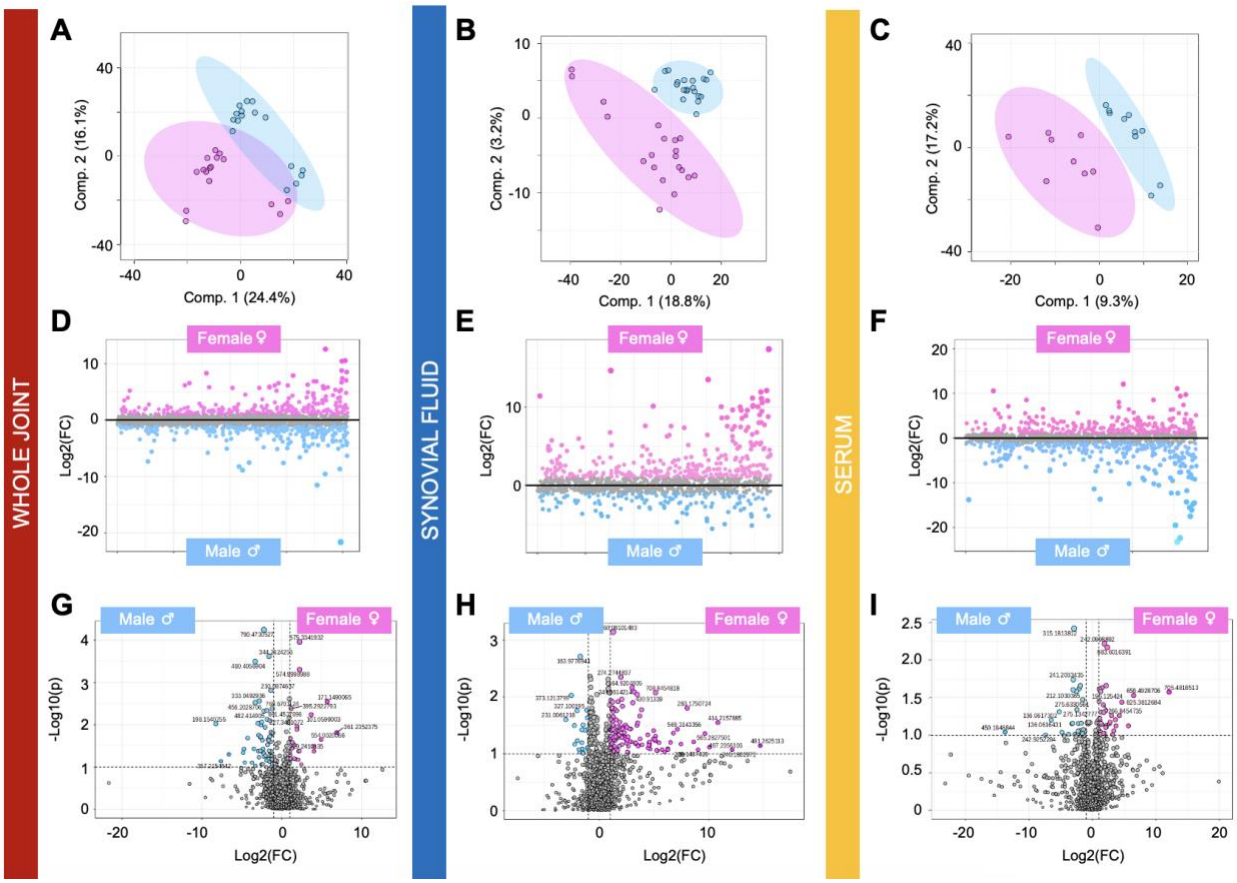

Supplemental Figure 6.5. Sexual dimorphic patterns are detected across whole joints, synovial fluid, and serum from injured and naïve mice. (A-C) Partial Least Squares-Discriminant Analysis (PLS-DA) finds (A) minimal overlap of male and female whole joints, while (B) synovial fluid and (C) serum from males and females perfectly clusters apart from each other. (D-F) Fold change analysis distinguished populations of metabolite features driving separation of male and female metabolomic profiles. (D) Specifically, 253 and 314 metabolite features were highest in female and male whole joints, respectively. (E) 334 and 137 metabolite features were highest in female and male synovial fluid, respectively. (F) 267 and 315 features were highest in female and male serum, respectively. (G-I) To further examine metabolic differences associated with sex across tissue types, volcano plot analysis was performed and identified numerous metabolite features that had a fold change > 2, a p-value < 0.05, and were differentially regulated between male and female whole joints (G, n = 90), synovial fluid (H, n = 159), and serum (I, n = 63). The colors in A-I correspond to: pink = females, blue = males, red = whole joint, blue = synovial fluid, yellow = serum.

Supplemental Tables

Supplemental Table 6.1. Liquid chromatography tandem mass spectrometry (LC-MS/MS).derived putative metabolite identifications that differ between male and female injured mice across tissues (serum, synovial fluid, whole joints), and limbs (injured, contralateral, naïve). Provided information for putative identifications includes observed and theoretical mass-to-charge ratios (m/z), parts per million (ppm) error, compound identification, accepted description/name, adduct information, chemical formula, and scores (total, fragmentation). Identifications with an error > 10 ppm, overall score < 65, and fragmentation score < 30 were excluded.

Supplemental Table 6.2. Differentially regulated pathways, identified by MetaboAnalyst, when comparing injured, contralateral, and naïve whole joints using fold change analysis.

Supplemental Table 6.3. Differentially regulated pathways, identified by MetaboAnalyst, when comparing synovial fluid from injured, contralateral, and naïve limbs using fold change analysis.

Supplemental Table 6.4. Differentially regulated pathways, identified by MetaboAnalyst, when comparing whole joints obtained from male and female injured and naïve mice using fold change analysis.

Supplemental Table 6.5. Differentially regulated pathways, identified by MetaboAnalyst, when comparing synovial fluid from male and female injured and naïve mice using fold change analysis.

Supplemental Table 6.6. Differentially regulated pathways, identified by MetaboAnalyst, when comparing serum from injured, contralateral, and naïve limbs using fold change analysis.

APPENDIX E

SUPPLEMENTAL MATERIAL FOR CHAPTER 7: WEIGHT LOSS INTERVENTION AND SEX-ASSOCIATED METABOLOMIC PROFILES

Supplemental Figures

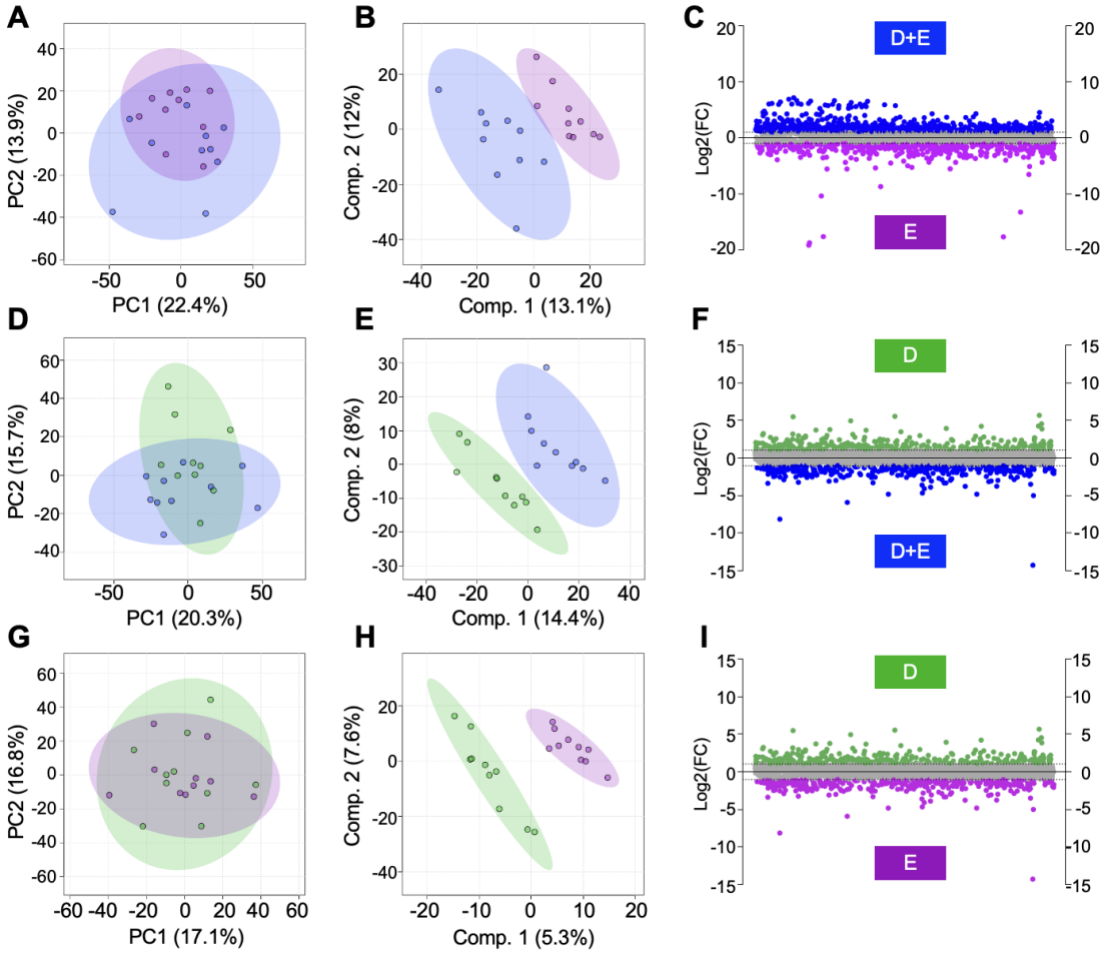

Supplemental Fig. 7.1. Pairwise comparison unveils intervention-associated metabolic patterns. (A) Principal component analysis and (B) partial least squares-discriminant analysis were applied to visualize the metabolome of D+E and E participants after 18-months of intervention. (C) Fold change analysis identified 760 metabolite features that had a FC > 2 and were higher in abundance in D+E participants. Conversely, 429 had a FC < -2 and were higher in abundance in E participants. Similarly, (D) PCA displayed some overlap, whereas (E) PLS-DA displayed clear separation of D+E and D participants. (F) Fold change analysis was applied to examine metabolic differences associated with D+E and D participants. This same suite of analyses was applied to investigate metabolic differences between E and D participants (G-I). Populations of metabolite features distinguished by fold change analyses were then subjected to functional pathway enrichment analyses to pinpoint biological pathways. Collectively, it is evident that the serum metabolome is influenced by intervention type, and differences in metabolic patterns reflect intervention status. The colors in A-I correspond to: green – diet (D); purple – exercise (E); blue – diet and exercise (D+E).

Supplemental Tables

Supplemental Table 7.1. Participant information for all participants including assigned intervention, weight and BMI data at baseline, 6-months, and 18-months, as well as calculated percentage of weight lost and BMI reduction.

Supplemental Table 7.2. Metabolic pathways determined from MetaboAnalyst when comparing participants from different intervention groups using fold change analysis.

Supplemental Table 7.3. Overlapping pathways identified by both fold change analysis and median heatmap analysis.

Supplemental Table 7.4. Putatively identified metabolites that differ in abundance between IDEA participants considering intervention group and sex. Populations of metabolite features distinguished by fold change analyses investigating both factors were investigated and compared to identifications that were made by using LC-MS/MS. Numerous metabolites were distinguished in both fold change analyses investigating both intervention and sex, while a handful of metabolites were either intervention- or sex-associated only. For those identified, metabolite information includes observed and theoretical mass-to-charge ratios, parts per million (ppm) error, compound identifier from either chemspider or HMDB, compound description, chemical formula, total score out of 100, as well as fragmentation score. Metabolites with a ppm error greater than 20 ppm, total score < 60, and a fragmentation score < 20 were excluded from the analysis.

Supplemental Table 7.5. Metabolic pathways determined from MetaboAnalyst when comparing male and female participants within their respective intervention groups using fold change analysis.

APPENDIX F

SUPPLEMENTAL MATERIAL FOR CHAPTER 8: MECHANICAL STIMULATION OF CHONDROCYTES

Supplemental Methods

Statistical Analysis for Untargeted Metabolomic Profiling

Univariate, supervised, and unsupervised multivariate analyses were used to visualize and narrow the dataset. The unsupervised multivariate statistical analyses that were utilized were hierarchical cluster analysis (HCA) and principal component analysis (PCA). HCA is used to visualize metabolomic profiles, identify sub-groups of sample sets, and determine differences between experimental groups. PCA linearly transforms and reduces the high dimensionality dataset into latent variables – specifically principal components (PCs) – to explain the variability in the dataset. Each PC is a combination of metabolite features that contributed most to the clustering of samples.

To further visualize the dataset and identify specific differences between cohorts, we used partial least-squares discriminant analysis (PLS-DA), variable importance in projection scores (VIP) and volcano plot analysis. PLS-DA is similar to PCA but is a supervised statistical analysis that is utilized to seek out differences between cohorts and reveal metabolites that are contributing to the separation between cohorts. PLS-DA is especially useful to this study because it assigns variable importance in projection (VIP) scores to metabolites that are the most important in discriminating between cohorts. Volcano plot analysis was also utilized to identify significantly upregulated and downregulated metabolites with a significance level of 0.05 and false discovery rate (FDR) corrections were applied to correct for multiple comparisons. Specific metabolite features of interest identified by VIP scores and volcano plot analysis were then matched to metabolite identities and metabolic pathways using MetaboAnalyst.

Supplemental Figures

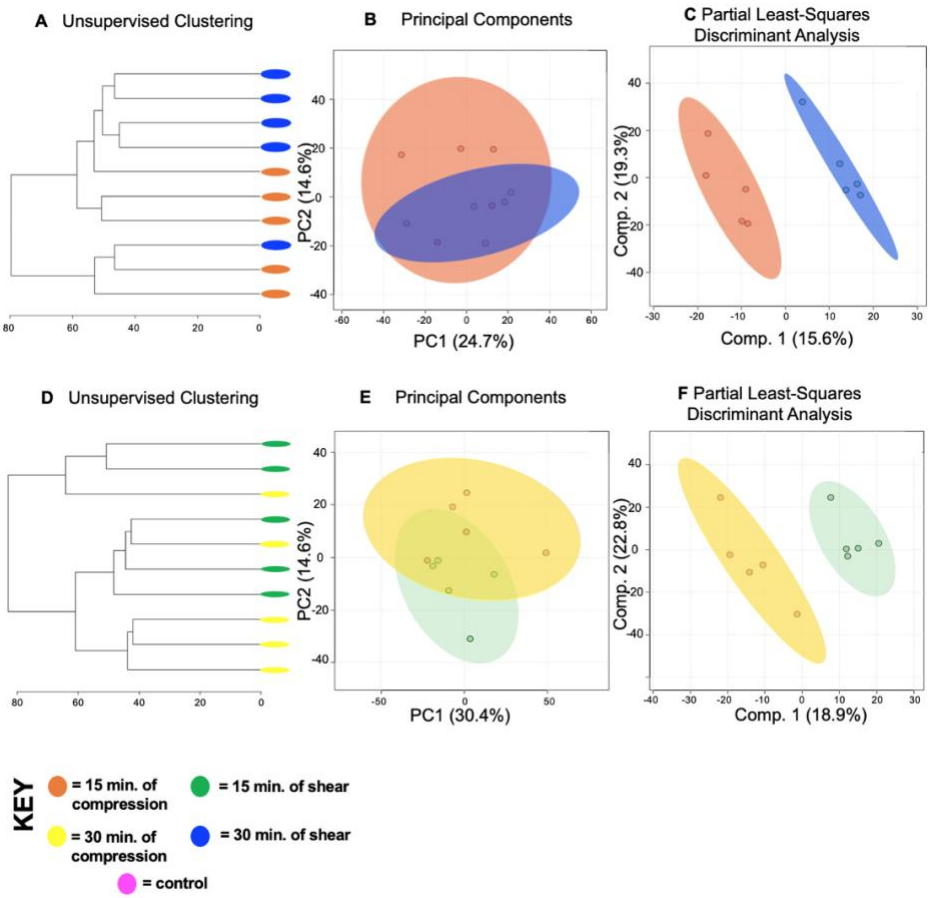

Supplementary Figure 8.1. Metabolic profiles of differing forces with different exposure times vary. Metabolomic profiles of chondrocytes exposed to 15 minutes of compression and 30 minutes of shear forces display distinct metabolomic profiles (A). Samples exposed to different forces for differing amounts of time somewhat separate into clusters by HCA as illustrated in the dendrogram. (B) PCA displays clear clustering of samples within their respective cohorts: chondrocytes exposed to compression for 15 minutes (orange) and chondrocytes exposed to shear forces for 30 minutes (blue). PCA is shown as a scatterplot of the first two PCs (PC1 and PC2), which account for 24.7% and 14.6% of the overall variation in the dataset respectively. (C) PLS-DA finds clear separation between samples. PLS-DA is visualized as a scatterplot of the top two components, which account for 15.6% and 19.3% of the overall variation in the dataset. Additionally, metabolomic profiles of chondrocytes exposed to 30 minutes of compression and 15 minutes of shear force are distinct from each other. (D) HCA illustrates that groups somewhat separate. (E) PCA displays overlap of samples between chondrocytes exposed to different forces and exposure times. PC1 and PC2 account for 30.4% and 14.6% of the overall variation in the dataset respectively. (F) PLS-DA finds clear separation between samples. The two components account for 18.9% and 22.8% of variation in the dataset.